Effect of coal matrix swelling on enhanced coalbed methane production

A field and laboratory study

Frank van Bergen

The front cover shows the RECOPOL site during winter times.

Faculteit der Geowetenschappen

The research reported in this thesis was carried out under the program *Earth Materials: properties and processes* of the Vening Meinesz Research School of Geodynamics (VMSG) and was part of the Utrecht Centre of Geosciences (UCG). The project was funded by the Dutch national research program CATO on CO_2 capture, transport and storage, with co-funding through CATO from the Netherlands Organisation for Applied Scientific Research TNO and Shell International Exploration and Production.

The research was carried out at:
Experimental Rock Deformation Laboratory
Faculty of Geoscience
Utrecht University
Budapestlaan 4
3584 CD Utrecht
The Netherlands

www.geo.uu.nl
www.ucgeo.nl

Printed by: proefschriftmaken.nl

ISBN/EAN: 978-90-5744-176-9

Effect of coal matrix swelling on enhanced coalbed methane production

A field and laboratory study

Het effect van kool matrix zwelling op gestimuleerde productie van koolbedmethaan

Een veld- en laboratorium-studie

(met een samenvatting in het Nederlands)

Proefschrift

ter verkrijging van de graad van doctor aan de Universiteit Utrecht op gezag van de rector magnificus, prof.dr. J.C. Stoof, ingevolge het besluit van het college voor promoties in het openbaar te verdedigen op vrijdag 27 november 2009 des middags te 12.45 uur

door

Frank van Bergen

geboren op 11 februari 1974, te Woerden

Promotor:
Prof.dr. C. Spiers

Co-promotor:
Dr. C. Peach

Reading committee:

- Prof.dr. J. Bruining, Delft University of Technology
- Prof.dr. S. Durucan, Imperial College London
- Prof.dr. S. Harpalani, Southern Illinois University
- Dr. Bernhard M. Krooss, RWTH Aachen University
- Prof.dr. Pawel Krzystolik, Central Mining Institute

Contents

Chapter 1

Introduction

Frank van Bergen

Large parts of this chapter have been previously published in the following paper:
Van Bergen, F., Pagnier, H.J.M. & Van Tongeren, P.C.H. (2007). Peat, coal and coalbed methane. In: T.E. Wong, D.A.J. Batjes and J. De Jager (Editors), Geology of the Netherlands. Royal Netherlands Academy of Arts and Sciences, Amsterdam, pp. 265-282.

1.1 Background and broad aims

Since the industrial revolution, the world has relied on coal for a large portion of its energy demand. It is likely that this reliance will continue for several decades to come (IEA, 2008). Coal is initially deposited as peat, which is formed under anoxic conditions in swamps, marshes or fens where organic matter derived from decaying vegetation is produced faster than it is decomposed by biochemical processes. Compositional and petrophysical differences between coals depend on depositional and biological variations, as well as on different degrees of maturation or coalification. With increasing pressure and temperature during burial, peat changes with time into brown coal, then into bituminous coal, and finally into anthracite (Fig. 1.1).

During this process, hydrocarbons are generated biogenically and thermogenically, and are expelled. Expelled gas can migrate into overlying or neighbouring strata and eventually accumulate in reservoirs. For example, the Upper Carboniferous coal deposits, which underlie most of the Netherlands, are the main source rock for the nation's natural gas accumulations, including the giant Groningen field with its initial recoverable gas reserves, mainly methane, of ca. 2700×10^9 m^3 (De Jager and Geluk, 2007). However, part of the generated methane is not expelled but is retained within the coal itself as "coalbed methane".

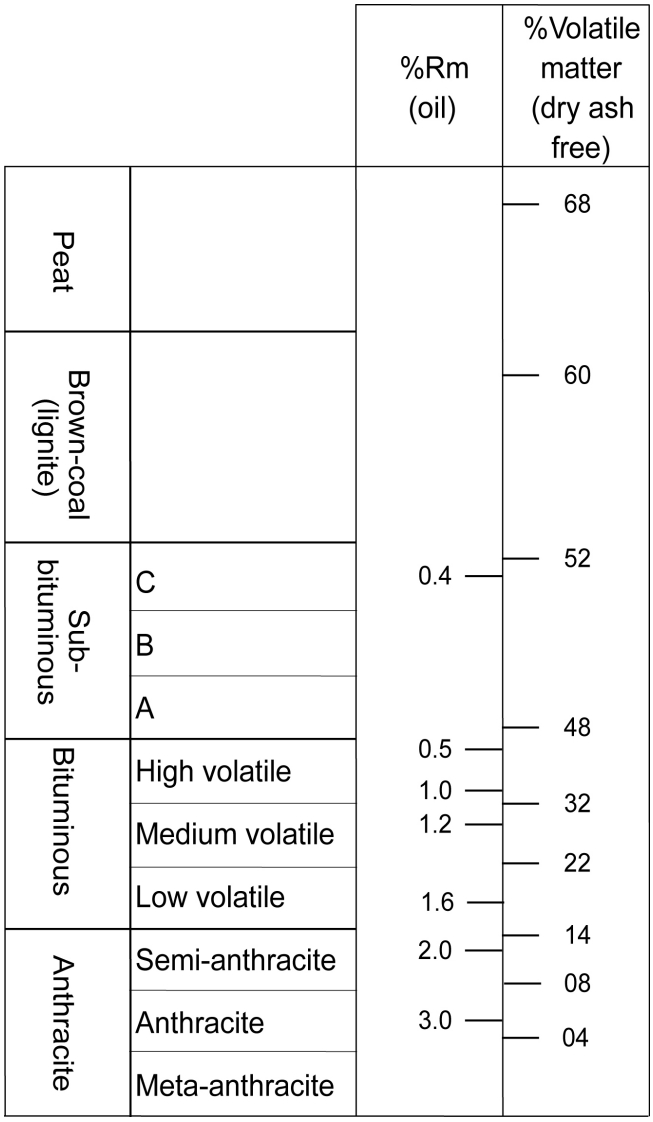

Figure 1.1: Overview of the ASTM (American Society for Testing and Materials) coal rank classification (after Stach *et al*. (1982) and Taylor *et al*. (1998)). The stage of coalification is indicated by the rank of the coal, most commonly expressed in percentage vitrinite reflectance (%Rm) or in percentage of volatile matter (dry ash free). Coalification is the progressive change in composition and structure of peat deposits, and any other carbon components within sediments, during burial, as a result of the interrelated physical, chemical and biological processes that operate (Levine, 1993).

Since the 1970's, interest has grown in extracting coalbed methane and using it as fuel. More recently, attention has broadened to the possibility of enhancing production of coalbed methane by injection of carbon dioxide (CO_2) to displace stored methane. This has the additional advantage that the injected CO_2 adsorbs strongly to the coal and can thus be stored underground. However, this process of ECBM production leads to complex swelling effects in the coal that may inhibit gas production (e.g. Day *et al*. (2008), Karacan (2007), Kelemen and Kwiatek (2009), Majewska *et al*. (2009), Mazumder *et al*. (2006b), Mazumder and Wolf (2008), Pone *et al*. (2009), Robertson and Christiansen (2005a)). This thesis is concerned with the interpretation of observations from the RECOPOL ECBM field test through understanding gained from dedicated laboratory experiments.

1.2 Coalbed Methane

Coalbed methane, or CBM, is the natural gas that is retained in coal in the subsurface. It is known as mine gas, or coal mine methane, in the mining industry, where it is dangerous due to its explosive nature. Due to a concerted effort by the United States government, and by private organisations, to demonstrate commercial production, the coalbed-methane industry in the United States has grown from a little-known, high-cost operation in the 1970's to a competitive, main stream natural-gas producer (Ayers Jr., 2002; Saulsberry, 1996), notably in the Cretaceous San Juan Basin in New Mexico and Colorado and the Black Warrior Basin in Alabama (e.g. Pashin and McIntyre (2003)).

Many European countries possess important coal resources, which are not suitable for conventional mining because of economic or technical reasons. The Carboniferous coal deposits in western Europe show many similarities to those of the Black Warrior Basin, which like its European counterparts is also a Variscan foredeep basin (Pashin, 1998). During the 1990's, interest in CBM accordingly grew rapidly in Europe. Fails (1996) compared the coalbed-methane potential of five Variscan-foredeep coal basins in Germany and Great Britain with the Black Warrior Basin. Compared with the Black Warrior Basin, the European foredeep basins tend to contain much thicker coal-bearing sequences with more numerous coal beds and greater net coal thickness, suggesting significant CBM potential when unmined (e.g. Eastern Ruhr Basin in Germany). However, CBM production in Europe appears to be sub-economic so-far, because production performance depends on other factors than high net coal thickness. Significantly, no correlation is found between coal thickness and production performance in the Black Warrior Basin (Pashin and Hinkle, 1997). Indeed, the most productive wells in the Black Warrior Basin are located in relatively thin coal (Pashin *et al*., 2004; Pashin and Hinkle, 1997). Rather, the critical factors that control coal gas producibility are hydrodynamics (i.e. the ability to dewater the seams), depositional setting, coal distribution, tectonic and structural setting, coal rank and gas generation potential, permeability, and gas content (Scott, 2002).
Hydrodynamic phenomena strongly affect CBM producibility and include both the

basinward movement of meteoric water, which is important for ongoing biogenic gas production, as well as the migration of fluids from deeper in the basin (Scott, 2002). Coal beds are the source and reservoir for methane, so that their widespread occurrence within a basin is critical to establishing a significant coalbed methane resource (Scott, 2002). In addition, sufficient gas should be generated through time from the coal, either through thermogenic or biogenic processes. Thermogenic gas generation is strongly linked to burial depth, and therefore to the tectonic history of the basin. The structural setting of the basin is, amongst other factors, important in determining the continuity of coal seams. In tectonically active areas, coal seams were often buried deeper during their geological history than at present. This paleo-burial depth affects present-day reservoir properties, such as porosity and permeability, through the influence of irreversible compaction effects during burial.

The reservoir properties of coal beds are far more complex than those of conventional gas reservoirs such as sandstone. Permeability in coal beds is determined by its fracture or so-called cleat system, which is in turn largely controlled by the tectonic/structural regime (Scott, 2002). Permeability is thus strongly dependent on present-day in-situ stress state. High normal stresses orthogonal to face cleats will lower permeability, whereas high stresses oriented parallel to the dominant or face cleat orientations may enhance permeability (Scott, 2002). Additionally, precipitation of authigenic material may reduce permeability (Pitman *et al.*, 2003; Scott, 2002). The most highly productive CBM wells in the U.S. have permeabilities ranging between 0.5 and 100 mDarcy (Scott, 2002). Because permeability decreases with increasing depth, CBM production may be limited to depths less than 1500 to 1800 m (McCants *et al.*, 2001; McKee *et al.*, 1988; Scott, 2002). On the other hand, permeability that is too high may have a negative impact on economic production because it results in high water production (Scott, 2002).
Most of the gaseous components present in coal ($>$ 90% methane) are adsorbed on the microstructure of the microporous coal matrix, while the gas content of larger, water-filled pores and of the cleat system is minimal. The gas-sorption capacity of coal is generally found to depend on pressure, temperature and coal characteristics (Bustin and Clarkson, 1998). The relationship between pressure and sorption capacity appears to follow a pressure-dependent Langmuir isotherm. This isotherm displays a hyperbolic increase of the gas-sorption capacity with increasing pressure, until a saturation value is reached above 20 MPa (Fig. 1.2). This behaviour is believed to correspond to monolayer adsorption, whereby the maximum adsorption capacity represents a completely saturated surface along which the monolayer approaches liquid density (Yee *et al.*, 1993). The methane content calculated with the Langmuir isotherm consequently represents the maximum that coal seams can contain at in-situ, reservoir pressure. On the other hand, with increasing temperature, the gas-sorption capacity of coal shows a decrease that is reported to be linear (e.g. Kim (1977); Levy *et al.* (1997); Bustin & Clarkson (1998)). Consequently, the opposing effects of increasing pressure and temperature, with increasing depth, result in a maximum in gas-sorption capacity at a given depth (Fig. 1.2; Van Bergen *et al.* (2007)). Initially, down to 2000 m, pressure will have the largest effect, below that depth, tem-

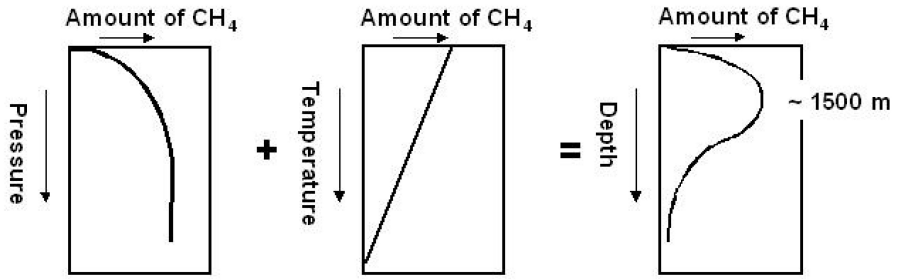

Figure 1.2: Effects of increasing pressure, temperature and depth on the amount of methane adsorbed on coal deposits in nature, assuming a normal geothermal gradient and hydrostatic pressure gradient, as found in the Carboniferous of the Ruhr Basin in Germany (Freudenberg *et al*., 1996). This figure shows a lineair decrease (after Kim (1977); Levy *et al*. (1997); Bustin & Clarkson (1998)).

perature is likely to become dominant. For typical geotherms of 30°C, the maximum gas sorption capacity is expected to occur generally around a depth of 1500 m.

Coal characteristics that affect sorption capacity are maceral composition, rank, ash content and moisture content. The role of maceral composition in determining sorption capacity is complex, and may be related to the pore structure of the macerals (e.g. Ettinger *et al*. (1966); Clarkson and Bustin (1996); Gamson *et al*. (1996); Crosdale *et al*. (1998); Lamberson & Bustin (1993); Levine *et al*. (1993); Beamish & Gamson (1993); Crosdale & Beamish (1993)). Some authors report poor or zero correlation between sorption capacity and maceral composition (Bustin and Clarkson, 1998; Faiz *et al*., 1992; Laxminarayana and Crosdale, 1999). Coal rank is generally considered to be the main parameter determining the methane adsorption capacity of coal (Ryan, 1992), although this correlation has also been questioned (Bustin and Clarkson, 1998). Nevertheless, others have found an increase in sorption capacity with coal rank (e.g. Eddy *et al*. (1982); Yee *et al*. (1993), Laxminarayana & Crosdale (1999)), or a U-shaped relationship (e.g. Moffat & Weale (1955); Patching & Mikhal (1986); Laxminarayana and Crosdale(1999); Durucan *et al*.(2009)), which may be related to pore structure development with rank (Levine, 1993). The ash or clastic/clay mineral content of the coal is generally considered to act as a simple non-sorbing dilutent, thereby reducing storage capacity proportionally (e.g. Bustin and Clarkson (1998); Laxminarayana and Crosdale (1999)), although recent research indicates that shales also have gas storage potential (Busch *et al*., 2008). Moisture present in coal has, in general, a negative effect on sorption capacity (e.g. Joubert *et al*. (1974), Seewald and Klein (1986); Yalcin and Durucan (1991), Levine *et al*. (1993); Levy *et al*. (1997); Bustin and Clarkson (1998); Mavor *et al*. (1990); Lama and Bodziony (1996)). This is because it competes for adsorption sites on the coal surface and may block access of gas to the microporosity (Bustin and Clarkson, 1998; Laxminarayana and Crosdale, 1999; Yee *et al*., 1993).

Coals are often found to be undersaturated with methane, i.e. their gas content as de-

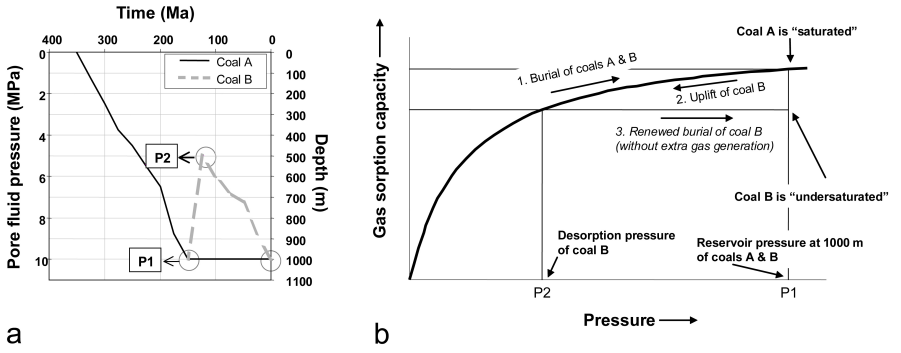

Figure 1.3: The effect of burial history on the gas content of the coal under atural conditions, as determined from desorption test on freshly recovered core or cutting material. Coal A and Bboth represent coal deposited during the Carboniferous. (a) Coals A and B were buried to depths of 1000 m. While coal A remained at that depth, coal B experienced a phase of uplift, after which it was reburied to 1000 m. (b) During the uplift phase, coal B released some of its adsorbed methane. Assuming no renewed gas charge, coal B will not adsorb more methane during reburial, and hence becomes undersaturated (adapted from McElhiney *et al*.(1993)).

termined from desorption test on freshly recovered core or cutting material, is lower than expected for reservoir temperature and pressure conditions on the basis of laboratory measured isotherms. Such undersaturation may reflect uplift, possibly resulting in degassing of the coal beds, as reported for the Upper Silesian Coal Basin in Poland (McCants *et al*., 2001). Degassing probably occurred in the Ruhr Basin in Germany too (Freudenberg *et al*., 1996). This means that the burial history of a given area has to be taken into account when the in-situ gas content of coal is estimated on the basis of the adsorption isotherm, to correct for a possible degassing (Van Bergen *et al*., 2000; Van Bergen *et al*., 2007). Methane undersaturation can also be caused by the thermal history of the coal. The sorption capacity increases with decreasing temperature, which can be the result of decreasing basinal heat flow in time or due to a decrease in temperature during uplift (Scott *et al*. (1994); Fig. 1.3).

The global volume of CBM is estimated to be of the order of 83-263$\times 10^{12}$ m^3 (Boyer II and Qingzhao, 1998). In the U.S., CBM has developed into a competitive industry that in the year 2000 constituted more than 20,000 wells in more than a dozen basins, providing 8.8% of U.S. reserves and 9.2% of U.S. dry gas production (Ayers Jr., 2002). Since 2000, the CBM industry expanded further , both in the U.S. and other countries, notably Canada, Australia and China.

1.3 Enhanced Coalbed Methane production

The Kyoto protocol of 1997, in which many countries, including all members of the European Union, committed themselves to reduce their CO_2 emissions, opened new

possibilities for use of subsurface coal seams. Carbon capture and storage (CCS) is considered to be a key technology, in addition to other measures like increasing energy efficiency and increasing the use of renewables, to reduce emissions of CO_2 into the atmosphere. One of the options for underground storage is to store CO_2 in subsurface coal beds. Gas adsorption on coal has proven stable over long periods of geological time, and the risk of future CO_2 release is considered low. Injected CO_2 adsorbs at a near-liquid density firmly on the coal and replaces adsorbed CH_4. This released methane can be produced while injecting CO_2, with reduced production time and improved recovery compared to standard coalbed methane production. This technique is therefore referred to as enhanced coalbed methane (ECBM) and has attracted much interest as a potential clean energy technology. Other benefits of the technology are that coal seams can be exploited that are not minable, and that decentralised generation of energy in remote areas near coal basins can minimise the costs of energy transportation.

Early laboratory experiments have indicated that, based on measured adsorption isotherms, for two sequestered CO_2 molecules one CH_4 molecule is released (e.g. Puri & Yee (1990); Stevenson *et al*. (1991)). An exchange ratio of CO_2 over CH_4 higher than unity implies that, in areas rich in coal, ECBM-burning power plants could be developed which emit less CO_2 per unit of energy produced than conventional plants, possibly even zero (Gunter *et al*., 1997), making this technology an exceptionally clean source of energy. However, since the early adsorption studies (Puri & Yee (1990); Stevenson *et al*. (1991)), the value of the exchange ratio has been controversial in literature. Several authors have presented different values for exchange ratios, influenced mostly by pressure and rank. At high pressures, in particular at experimental conditions where the CO_2 is likely to be supercritical, the exchange ratio of CO_2 for CH_4 could be higher, e.g. experimental data at 12 MPa, which is equivalent to 1200 m at hydrostatic pressure, indicate that it could be up to 5:1 (Hall *et al*., 1994). Pashin *et al*. (2004) showed that the exchange ratio ranges from 2:1 in medium volatile bituminous coal to 5:1 in high volatile A bituminous coal at a pressure of 2.4 MPa. These observations have been partly confirmed under laboratory conditions for Westphalian coal samples, with CO_2:CH_4 exchange ratio varying between 1.2:1 and 6.3:1 (Krooss *et al*., 2002; Van Bergen *et al*., 2000; Wolf *et al*., 1999). For low rank coals, the exchange ratio can even be higher, exceeding 20 at lignite rank (Burruss, 2003). However, Busch *et al*. (2003) found that under certain conditions the exchange ratio is even less than 1, implying preferential CH_4 sorption.

It should be emphasized that the exchange ratio as described above is based on adsorption isotherm measurements in the laboratory. Theoretically, CO_2 injection can increase coalbed methane recovery by up to 100% (Stevens *et al*., 1999). However, it is very likely that factors other than sorption capacity will control the eventual exchange of CO_2 for CH_4 under in-situ conditions. For example, the increase in recovery of CBM due to injection of CO_2 in the Black Warrior Basin is estimated to be over 20% because of the saturation state of the coal (Pashin *et al*., 2004). Another factor probably controlling exchange is the ability of the coal to transport CO_2, CH_4 and

water into and out of the coal.

1.4 Scope of this thesis

Despite the perceived advantages of ECBM, it must be emphasized that, because of the uncertainties outlined above, CO_2 storage in coalbeds, and associated CBM recovery, is not yet a well-established, mature technology. Although several theoretical studies have illustrated the potential of the process, only a few demonstration sites have been initiated world-wide, for example in the U.S., Canada, Japan and China. Demonstrations are essential to test the applicability of the technique under field conditions. The first part of this thesis therefore reports the results of the first field test conducted in Europe, i.e. the RECOPOL field in the Upper Silesian Coal Basin in southern Poland. The observations made in this field test led to the conclusion that the transport properties of coal, both cleat permeability and coal matrix diffusion, are key for the success of ECBM production. This is because most of the ECBM demonstration sites operated to date show permeability reduction in the accessed coal seam, which is generally considered to be caused by swelling of the coal as the result of CO_2 injection. The second part of the thesis is therefore dedicated to the investigation of factors that influence the swelling behaviour of coal, such as coal type, moisture content, stress, and stress history.

1.5 Specific objectives

On the basis of the previous studies mentioned above, a number of specific research questions have been identified and are addressed in this thesis. These are as follows:

1. What conclusions can we draw from the measurements made in the RECOPOL field, on variables such as injectivity with time, gas production rate, and gas composition, about the processes taking place in the coal reservoir which determine the overall performance of the ECBM field test? This is addressed in Chapters 2 and 3.

2. Can we verify the development of swelling in coal matrix blocks, as opposed to bulk coal samples? See Chapter 4 for description of the methodology applied and the results.

3. Can we develop a diffusion model that explains and reproduces the development of swelling with time observed in coal matrix samples? See Chapter 5 for the model and the modelling results.

4. What is the effect of water on the magnitude and rate of swelling of coal matrix samples that are exposed to CO_2 and CH_4? This is addressed in Chapters 4 and 5.

5. Are there differences between various coal types (subbituminous, bituminous and anthracitic coal) in the magnitude and rate of swelling of developed by coal matrix samples? See Chapter 5 for this evaluation.

6. What is the effect of applied stress on the development of stress-strain by coal matrix grains? This is described in Chapter 6.

7. Can we verify the interpretation of the field observations by the results of the laboratory experiments conducted? This is discussed in Chapter 7.

Acknowledgements

This introduction is largely based on the publication by Van Bergen *et al*. (2007). The Royal Netherlands Academy of Arts and Sciences is acknowledged for granting the permission to reprint parts of this publication. Co-authors of this paper, Henk Pagnier and Peter van Tongeren, are acknowledged for their contributions. The editors of the volume where the paper was published, Dick Batjes, Jan de Jager and Theo Wong, are thanked for their valuable suggestions. Jack Pashin from the Geological Survey of Alabama and Dierk Juch from the Geologische Dienst NRW are gratefully acknowledged for the review of the paper.

Chapter 2

Field experiment of enhanced coalbed methane - CO_2 in the Upper Silesian Basin of Poland

Frank van Bergen, Henk Pagnier & Pawel Krzystolik

This chapter was published as:
Van Bergen, F., Pagnier, H. & Krzystolik, P. (2006). Field experiment of enhanced coalbed methane-CO_2 in the upper Silesian basin of Poland. Environm. Geosc. 13, 201-224.

Abstract

A field experiment of CO_2 storage in underground coal seams with simultaneous (enhanced) production of coalbed methane production was set-up and performed in the Upper Silesian Coal Basin in Poland. The main aim of this project was to investigate the technical and economic feasibility of this type of CO_2 storage under European conditions. An existing coalbed methane well was cleaned up, repaired and put back into production in May 2004 to establish a baseline production. A new injection well was drilled 150 m (492 ft) away from the production well. This distance was chosen to establish a breakthrough of the injected CO_2 into the production well, in order to learn as much as possible from the operations. Initial injection of CO_2 took place in August 2004 in three seams of Carboniferous age in the depth interval between 900 and 1250 m (3117 and 4101 ft). Several actions were taken to establish continuous injection, which was eventually reached in April 2005 after stimulation of the reservoir by a frac job. In May 2005, approximately 12-15 tonnes per day were injected in continuous operations. Compared to baseline production, the production of methane increased significantly due to the injection activities. Recovery of methane was, however, low which is probably related to low diffusion rates into and out of the coal. Nevertheless, a total of 692 tonnes

of CO_2 are stored in the reservoir, most likely due to adsorption of CO_2 on the coal. The results provide good hope for successful future upscaling of the operations although further research is required. The realization of an on-shore pilot for CO_2 storage can possibly help to overcome start-up barriers of future CO_2 storage initiatives in Europe.

Key words: CBM; ECBM; field demonstration; carbon dioxide

2.1 Introduction

Reducing carbon dioxide (CO_2) emissions in order to control the overall levels of CO_2 in the atmosphere has become an international priority in the wake of the Kyoto protocol. Despite all past and ongoing efforts put into the development of sustainable energy supplies, the world still depends heavily on fossil fuels and will continue to do so for years to come. For this reason, technology options are required that will allow for the continued use of fossil fuels without substantial emissions of CO_2. Subsurface storage of CO_2 in underground coal seams is considered as one promising perspective. This type of storage is anticipated to be combined with the production of coalbed methane (CBM). In conventional CBM production, gas is released from the coal by pumping water from the reservoir, thereby reducing hydrostatic pressure. Because gas production rates per CBM well may be several orders of magnitude lower than natural gas wells, a relatively large number of wells is required. It is expected that the production rates of such CBM wells and the amount of methane recovered from the coal seams can be enhanced by simultaneous injection of CO_2 in the coal seams in nearby wells (therefore the term Enhanced Coalbed Methane production, or ECBM). The injected CO_2 is expected to be retained by the reservoir and is therefore stored in the subsurface. It must be emphasized that this technique is not yet a well-established and mature technology, and, therefore, implies some inevitable uncertainties and risks.

Although several theoretical studies illustrated the potential of the process, pilot projects are required in order to gain necessary practical experience. In general, the research window for projects on subsurface CO_2 storage has slowly but surely shifted from desk studies to demonstrations. A few experimental CO_2-ECBM field sites have been implemented worldwide to date. A micro-pilot field test was set-up in Alberta, Canada (Gunter *et al.*, 1997; Gunter *et al.*, 1998), a similar test was recently performed in China, a two-well test is ongoing in Japan, while the world's first large-scale ECBM pilot using CO_2 injection was operated in the San Juan Basin in New Mexico, U.S.A. (Erickson and Jensen, 2001; Gunter *et al.*, 1998; Reeves and Schoeling, 2001; Schoeling and McGovern, 2000). This paper gives an overview of some of the results obtained in the first European field demonstration in Poland, following earlier reports on this project (Pagnier *et al.*, 2005a; Pagnier *et al.*, 2005b; Van Bergen *et al.*, 2003a; Van Bergen *et al.*, 2003b).

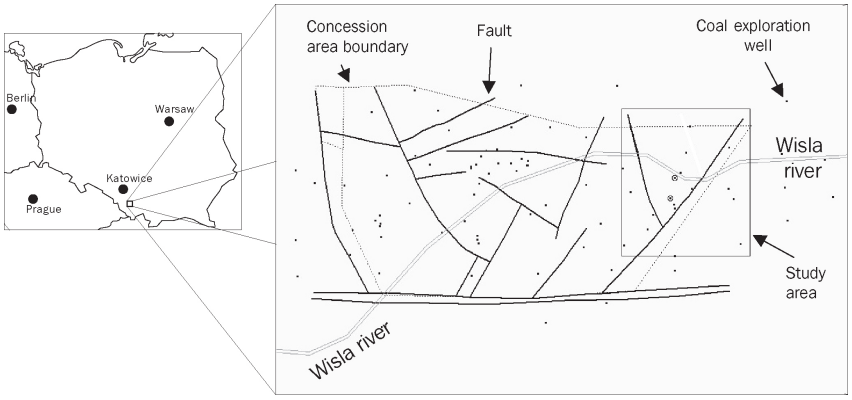

Figure 2.1: Location of the site in the Upper Silesian Coal basin. The existing CBM wells and the new injection well are indicated with the small circles.

The main goal of this project is to demonstrate, in the Upper Silesian Coal Basin (USCB) in Poland, that CO_2 injection in coal under European conditions (i.e. geological, technical and economical) is feasible. This basin was selected as the most suitable coal basin in Europe for the application of ECBM (Stevens *et al.*, 1999; Wong *et al.*, 2001). It is the largest coal basin in Poland and one of the largest in Europe, and has more favorable coalbed properties (i.e., thicker seams, higher permeability, fair gas contents) compared to other European coal basins. Exploration and production of coalbed methane was undertaken in the basin in the 1990's. The main aim of this conventional CBM production was the recovery of gas, which proved to be uneconomical. In ECBM operations there is a focus on both methane recovery and CO_2-storage, which has the potential to make these kinds of operations economically feasible in the future.

2.2 Site characterization

2.2.1 Location

The USCB is located in the south of Poland, north of the Carpathian mountains and west of the city of Krakow. The location of the pilot site in the village Kaniow, about 40 km south of Katowice (Fig. 2.1), was selected at an early stage of the project. The selected site is located within the concession of the Silesia mine, which has been in operation for decades. Two wells were in place, 375 m apart, which were used to produce CBM for a short period of time in the second half of the 1990s. In the summer 2003 a new injection well (MS-3) was drilled in-between the existing wells.

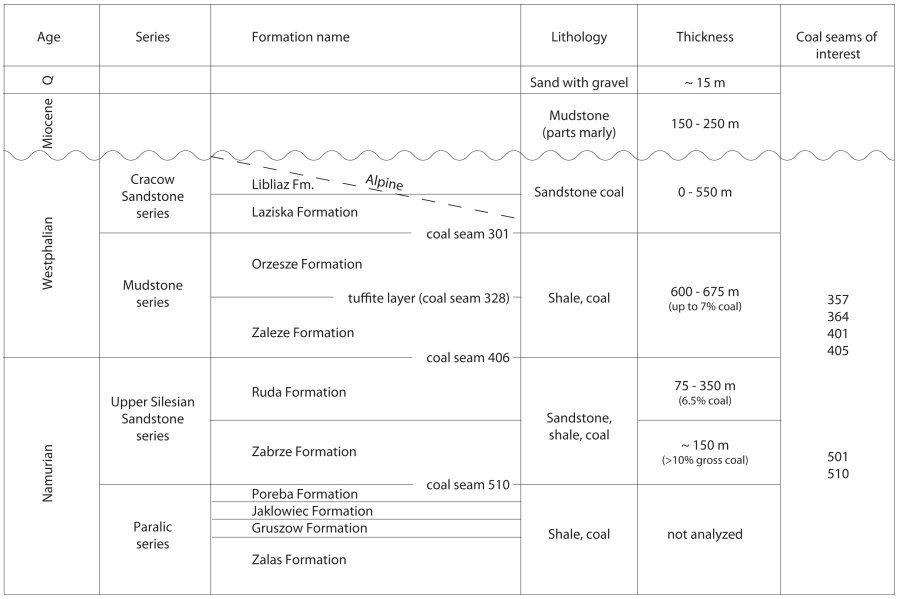

Figure 2.2: Overview of the stratigraphic succession in the area of the pilot site and surrounding area, based on well evaluations and after McCants *et al*. (2001).

2.2.2 Geology

The coal-bearing deposits in the USCB were deposited in an intermontane basin during the Carboniferous and have a total thickness of at least 1000 m (3280 ft) in the area. The deposits within the interval of interest (between 950-1250 m or 3117 and 4101 ft) are of Late Namurian to Early Westphalian age (Fig. 2.2). Coal seams occur throughout the entire depth interval. The Late Namurian succession, approximately 75 to 125 m (246 to 410 ft) thick, consists of sandstone-dominated to claystone-dominated fluvio-deltaics. The overlying 125 to 200 m (410 to 656 ft) thick succession of Early Westphalian age is dominated by claystones. The majority of the sandstone bodies are between 5 and 8 m (16.4 and 26.2 ft) thick, and their distribution suggests that they were deposited along syn-sedimentary faults (Fig. 2.3). Some of these bodies cut into underlying coal seams, thereby destroying the lateral continuity of the coal. This indicates that there was tectonic activity during deposition of these sediments. In general, the faults with a north-south orientation in the area are related to Carboniferous tectonic events.

The tectonic history of the area, and of the entire USCB, is complex, especially compared to commercial coalbed methane basins in the U.S.A. (McCants *et al*., 2001). Periods of active tectonic periods have alternated with periods of relative inactivity, as is for example indicated by the upward decrease in the abundance of sandstone bodies. This likely indicates a period of relative low tectonic activity. The area of

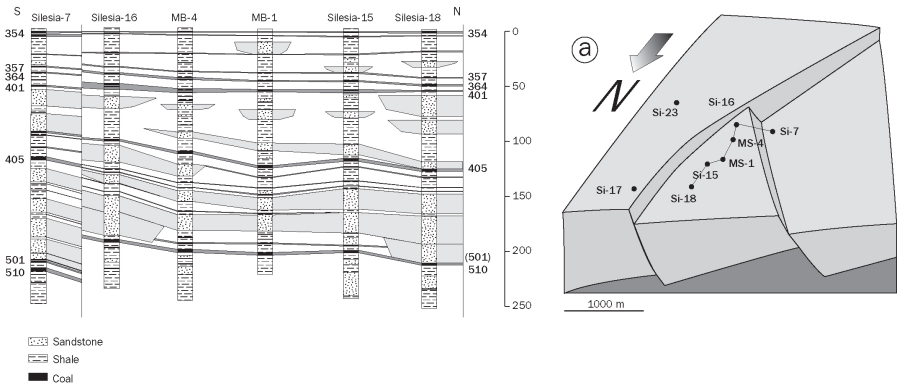

Figure 2.3: Stratigraphic cross section (N-S) of the site through 6 wells using coal seam 354 as datum. Identification and correlation of the coal seams is based on experience from the Silesia mine. Thickness variations across fault between Silesia 7 and Silesia 16 well indicate synsedimentary tectonic movement.

interest within the USCB is mainly characterized by fault block tectonics. The pilot site is located on a large block that was upthrusted during the Alpine orogeny. In general, faults with an east-west orientation can be attributed to this event. The fault block is triangular and wedged between a hangingwall block in the west and a footwall block in the east. The bounding faults have a NE-SW and a NW-SE orientation (Fig. 2.1 and Fig. 2.3). These faults are pre-Miocene and were already active in the Carboniferous. Experience from the coal mines suggests a sealing character of these intra-Carboniferous faults (L. Wǎtor, pers. comm., 2002). The major E-W fault zone to the south, bordering the upthrusted block, is still active. There are no faults detected inside the block; coal seams are therefore expected to be continuous within the bounding faults. However, the possibility of the occurrence of smaller (sub-seismic) faults can not be excluded. The thickness of the overburden in the area is about 250 m, mainly consisting of shale deposits of Miocene age that uncomformably and disconcordantly overly the Carboniferous deposits (Fig. 2.2). Local mining experience showed that the Miocene shales are sealing and are not in hydrological contact with the Carboniferous (Wǎtor, pers. comm., 2002; Z. Adamaszek, pers. comm., 2002).

2.3 Coal characteristics and gas content

Within the area 6 main coal seams are present in the depth interval of interest (950-1250 m; 3117 - 4101 ft), varying in thickness between 1 and 3.5 m (3.3 and 11.5 ft). Multiple thinner seams are occur in-between these main seams. From a sedimentological point of view, the top three coal seams (seams 357, 364, and 401) are more likely to be continuous than the lower seams because of the absence of large sand bodies. These seams are positioned within a 20 m (65.6 ft) thick package of alternat-

Table 2.1: Characterization of the coal seams of wells MS-1, MS-4 and MS-3. The data of the seams in wells MS-1 and MS-4 are based on historical information. No information was available for seams 364, 405 and 501 in well MS-1. No information was available for seams in MS-4, except for seam 510. The data from the seams in well MS-3 were analyzed within the scope of this study. The abbreviation n.a. means not analyzed.

Well name	Coal seam	Sample	Core length	R_o	Maceral comp.				Moisture		Ash	V.M.	Chemical composition				
									as received	inherent	as received	dry ash free	dry ash free				
					V	L	I	M					C	H	N	S	O
		no.	cm		%	%	%	%	%	%	%	%	%	%	%	%	%
MS-1	356	1	60	0.82	62	9	24	5	1.85		10.44	34.67	83.1			0.5	
	357	1	100	0.81	72	7	15	7	1.77		6.62	33.68	82.5			0.7	
	401	1	135	0.85	54	6	21	19	1.35		17.14	32.87	82.5			0.5	
	401	2	40	0.84	49	14	32	5	1.41		6.65	34.43	84.3			0.5	
	510	1	250	0.91	38	11	45	6	n.a.		n.a.	n.a.	n.a.			n.a.	
MS-4	510	1	260	0.90	56	6	35	3	n.a.		n.a.	n.a.	n.a.			n.a.	
MS-3	357	1	70	0.84 ± 0.04	80	7	8	5	3.51	2.28	4.08	36.15	84.0	5.0	1.5	1.0	8.5
	364	1	60	0.80 ± 0.05	48	11	30	11	3.66	2.02	5.34	33.43	84.7	4.8	1.5	0.7	8.3
		4	45	n.a.	n.a.				8.00		4.25	n.a.					
		2	27	0.84 ± 0.04	30	1	15	54	4.65	2.39	58.97	-	70.1	11.7	1.1	1.8	15.3
		3	28	0.83 ± 0.04	86	7	5	2	3.34	2.35	2.55	35.08	84.9	5.1	1.6	0.8	7.7
	401	1	100	0.80 ± 0.03	53	11	23	13	3.73	1.95	9.96	34.50	84.5	4.6	1.5	0.9	8.5
		2	40	0.81 ± 0.03	50	2	6	42	4.33	1.87	42.66	-	76.2	6.5	1.1	2.8	13.4
	405	1	80	0.88 ± 0.06	14	13	66	7	3.52	1.70	3.58	24.60	87.3	4.0	1.4	0.4	6.8
				0.87 ± 0.04	27	6	61	6	4.25	1.78	8.00	24.38	86.7	4.4	1.4	0.4	7.1
		2	30	0.83 ± 0.03	39	12	45	4	2.54	1.51	4.07	32.76	85.4	5.4	1.4	0.5	7.3

ing shale and coal layers, and the risks of leakage of the injected CO_2 to other strata is considered to be low. Seam 405 is also positioned between shale layers, but the chance of connectivity to an adjacent sandstone body is higher.

The differences in maceral composition between the coal seams are large. For example, compositional analysis of the samples taken from seam 405 in the new injection well showed a very high content of inertinite and relatively low content of vitrinite. The other seams of interest have much higher vitrinite content. Also, the differences in mineral matter content can vary significantly between the coal seams (Tab. 2.1; Fig. 2.4). The coal is high-volatile bituminous with a vitrinite reflectance of about 0.8-0.85%Rr.

During the course of the geological history of the area, the coal seams were buried deeper in the past than they are at present times (McCants *et al.*, 2001). This resulted in relatively low to moderate permeability (1 - 2 mD), declining gradually with depth (McCants *et al.*, 2001). The in-situ permeability of the coal seams was assessed in September 2003 by a well test directly after the perforation of the casing. The permeability of the coal seams 364 and 401 was in the lower range ($\sim$ 0.4 - 1.5 mD) of the regional variation (1 - 2 mD). The permeability of seam 405 was very low ($\sim$ 0.01 - 0.05 mD), which is possibly related to the composition of this seam (Fig. 2.4). The permeability of the coal is, given the cleat system, likely to be anisotropic. The cleat system

of the coal, as measured in the Silesia mine, has two main directions (15 and 105). The orientation of 105 is assumed to be the open direction, based on observations in the nearby Silesia mine. However, extrapolation of this orientation is not straightforward, since orientations of open cleats can vary significantly on a local scale. No preferred orientation of the joints or cleats could be established by evaluation of the caliper log data.

Exploration activities for CBM showed that the gas content in the USCB is often relatively low, mainly as a result of degassing through faults during uplift phases (Kędzior, 2002; Kotas, 1994; McCants *et al.*, 2001). This resulted in under-saturated coals because there was no new generation of gas after the last uplift phase. Due to the undersaturation of the coal, the free gas in the cleat system of the coal will be very limited. Also, the gas content of the sandstone intervals will be relatively low because the majority of these intervals are connected to the coal seams.

During the drilling of the MS-3 well a total of 9 core and 29 cutting samples were collected for desorption tests. Correction for lost gas was applied, although the amounts of lost gas were limited because desorption rates are very low. Desorption tests took several months, probably due to low diffusion rates, and the amount of residual gas was high, especially for the cores (Fig. 2.5). Still, the total gas content of the cores was up to 10 m^3/ton (dry ash free, i.e., corrected for moisture and mineral content of the coal), indicating that the total amount of gas in place is fairly good. The gas from canister tests from the wells MS-1, MS-4, and MS-3 showed CH_4 concentrations of usually 95% or higher, with some percentages of N_2 (0.5-3%) and CO_2 (1-3%) and traces of other gases.

2.4 Pilot operations

Several well configurations were considered during the first phase of the project. It was decided, mainly due to budgetary constraints, to develop the test with one production well and one new injection well. The operational activities on the pilot site took place during a period of 13 months from May 2004 to June 2005. Three periods could be distinguished in this time: 1) baseline production before injection, 2) injection and production before stimulation of the reservoir, and 3) injection and production after stimulation of the reservoir. Stimulation was performed by means of a frac job in April 2005.

2.4.1 Baseline CBM production (May 2004 to August 2004)

In order to evaluate possible effects of CO_2 injection, it is mandatory to establish the initial, or baseline, conditions that existed before the start of the injection operations. Evaluation of historical data from 1996 shows a peak production of the MS-4 well of ca. 100 m^3/d (3,531 cf/d) after circa 20 days of production declining to 60 m^3/d

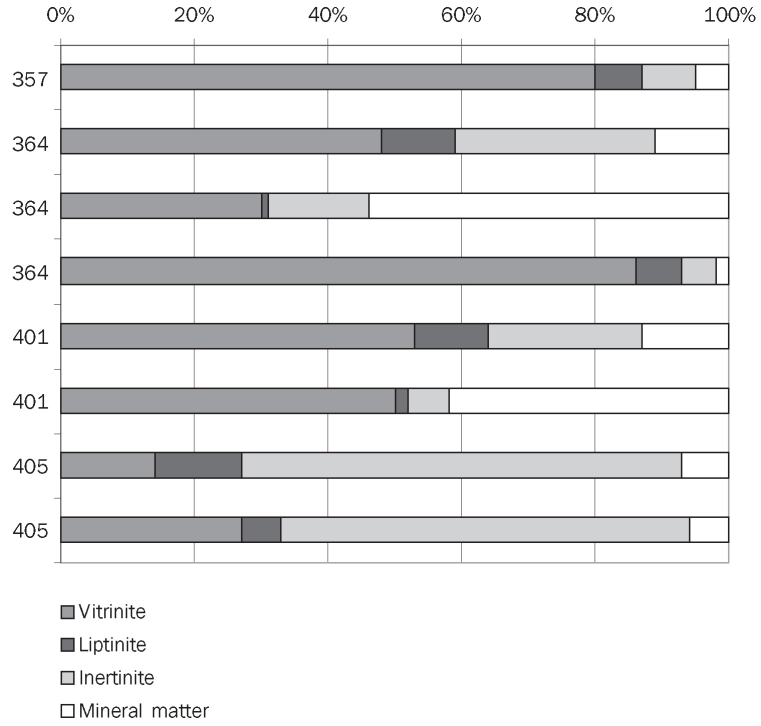

Figure 2.4: Composition of coal samples from cores of the main coal seams drilled by the MS-3 well. It was attempted to take complete cores of coal seams 357, 364, 401 and 405 for canister desorption tests prior to compositional tests. However, the recovered cores were not completely intact, resulting in cores of 27 to 100 cm (0.9 to 3.3 ft) length. Seam 357 could be recovered in one piece, while other seams were recovered in two, three or four pieces. Sample 3 of seam 364 was not analyzed; distance between bottom of core piece 2 and top of core piece 4 is 65 cm (2.1 ft). Seam 401 is in fact composed of several thinner seams with intercalated shale layers, the distance between bottom of core piece 1 and top of core piece 2 is 470 cm (15.4 ft). The high content of mineral matter demonstrates the presence of the shale layers in the seam. The second compositional analysis of the first core of seam 405 (Tab. 2.1) are not plotted.

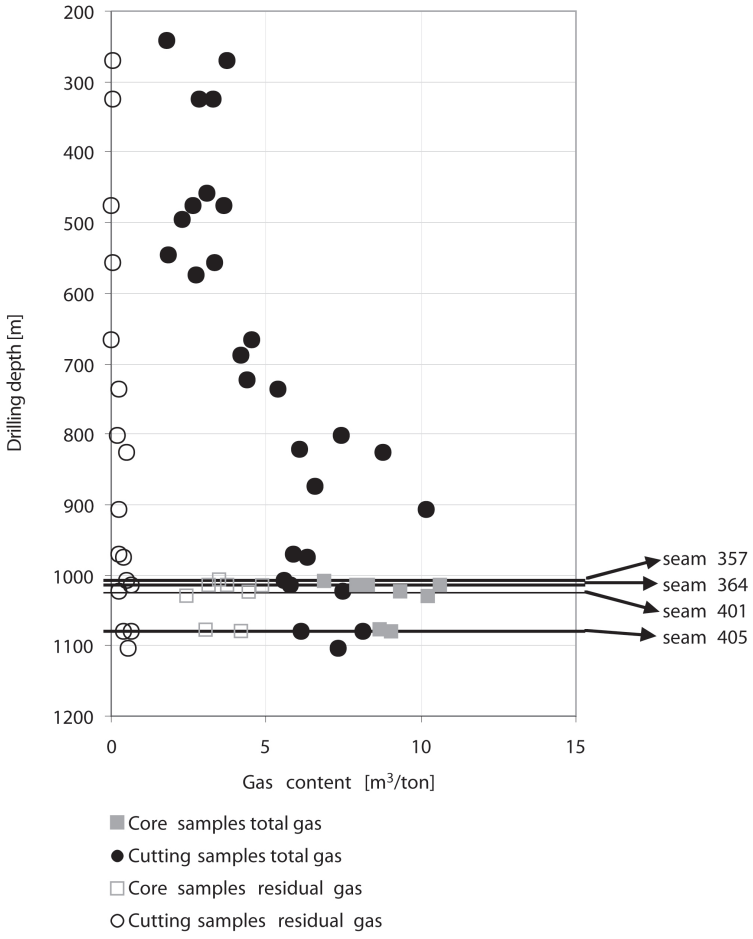

Figure 2.5: Gas content from desorption tests of cuttings and cores from the MS-3 well.

Figure 2.6: Picture of the MS-4 production well and pump. The gas is flared (left), while the water is transported by truck to a disposal site.

(2,119 cf/d) after 60 days. These figures represent the cumulative production figures of the 357, 364, 401, 405, 501 and 510 seams. Of these seams, only the seams 364, 405 and 510 were stimulated by fracturing.
The existing coalbed methane production well (MS-4) was cleaned and repaired (Fig. 2.6). An initial reservoir pressure of 9.0 MPa (1,305 psi) was determined and the water level in the MS-4 was measured at ca. 170 m (558 ft) below surface, comparable to the level in the MS-3 well. This indicates that the reservoir pressure in the well is hydrostatic towards the top of the Carboniferous, confirming that the Miocene is not in hydrological communication with the underlying Carboniferous. In order to eliminate the contribution of the 501 and 510 seams, that were not drilled by the MS-3 well, a bridge plug was placed in the MS-4 well between seams 405 and 501. The well was put back into production at the end of May 2004 with varying pump intervals.

During the first month gas production rates varied, because the pump frequency optimum still had to be established. After this first month, production rates were approximately 40 m^3/d (1,413 cf/d) in the beginning and declining towards approximately 30 m^3/d (1,059 cf/d), where they appeared to stabilize. This trend appears to be a continuation of the historical trend described above, given that the amounts are slightly less because seams 501 and 510 are isolated by the bridge plug. Analysis of the produced gas showed that it was composed of approximately 97% CH_4, 1.5 - 2% CO_2, and small amounts of other gases. This composition was comparable to the composition of the gas from the canisters. Water production has, after varying production in the start-up phase, declined since the start to approximately 1-2 m^3/d (35.3 - 70.6 cf/d; Fig. 2.7).

The composition of the produced water was analyzed on a regular basis before the start of the injection to establish baseline conditions and its natural variation. The data before the start of the pumping were taken at irregular intervals with very low

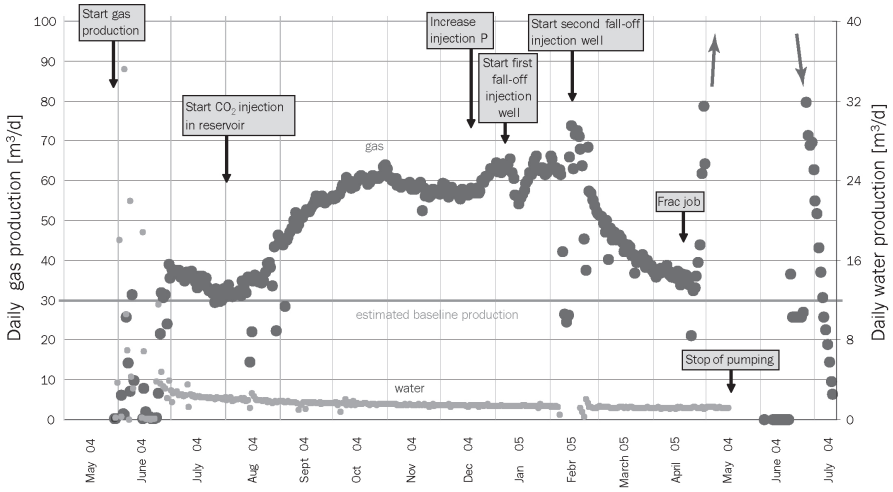

Figure 2.7: Gas production from MS-4 well between May 2004 and April 2005.

amounts of water produced. Therefore, the analyzed fluid sampled before and directly after June 2004 was highly influenced by the operations for testing and repair of the MS-4 well (Fig. 2.8). These data show significantly higher amounts of iron and manganese ions, indicating the influence of the steel casing of the well on the composition of the reservoir water. Also, the lower concentration of bicarbonate (HCO_3^-) suggests that the water experienced some degassing of (natural) CO_2 as a result of the lower pressures during the earlier production. It took until July 2004 to produce reservoir water that was not influenced by the earlier activities, providing the actual baseline conditions of the formation water. The baseline data, after the start of the pump, show that the water is highly saline (approximately 140 kg/m^3 or 3.96 kg/cf).

2.4.2 CO_2 injection and CBM production (August 2004 to March 2005)

Site preparation

The new injection well (MS-3) was drilled 150 m (492 ft) north (downdip) of the existing MS-4 production well (Fig. 2.9) to a depth of 1120 m (3,675 ft). The location of the well was defined by numerical modeling in the development phase of the project in order to establish a breakthrough of the CO_2 in the production well, within the project lifetime (maximum of 18 months of experimental operations) and with the available CO_2 (1,000 to 1,500 tonnes). The cemented casing was perforated in three zones, which included the coal seams 364, 401 and 405, over a cumulative thickness of about 6 m (19.7 ft; figures 2.10 and 2.11). The CO_2 is stored at the site in liquid form in containers (Fig. 2.12). A high-pressure CO_2 pump unit with heaters was in-

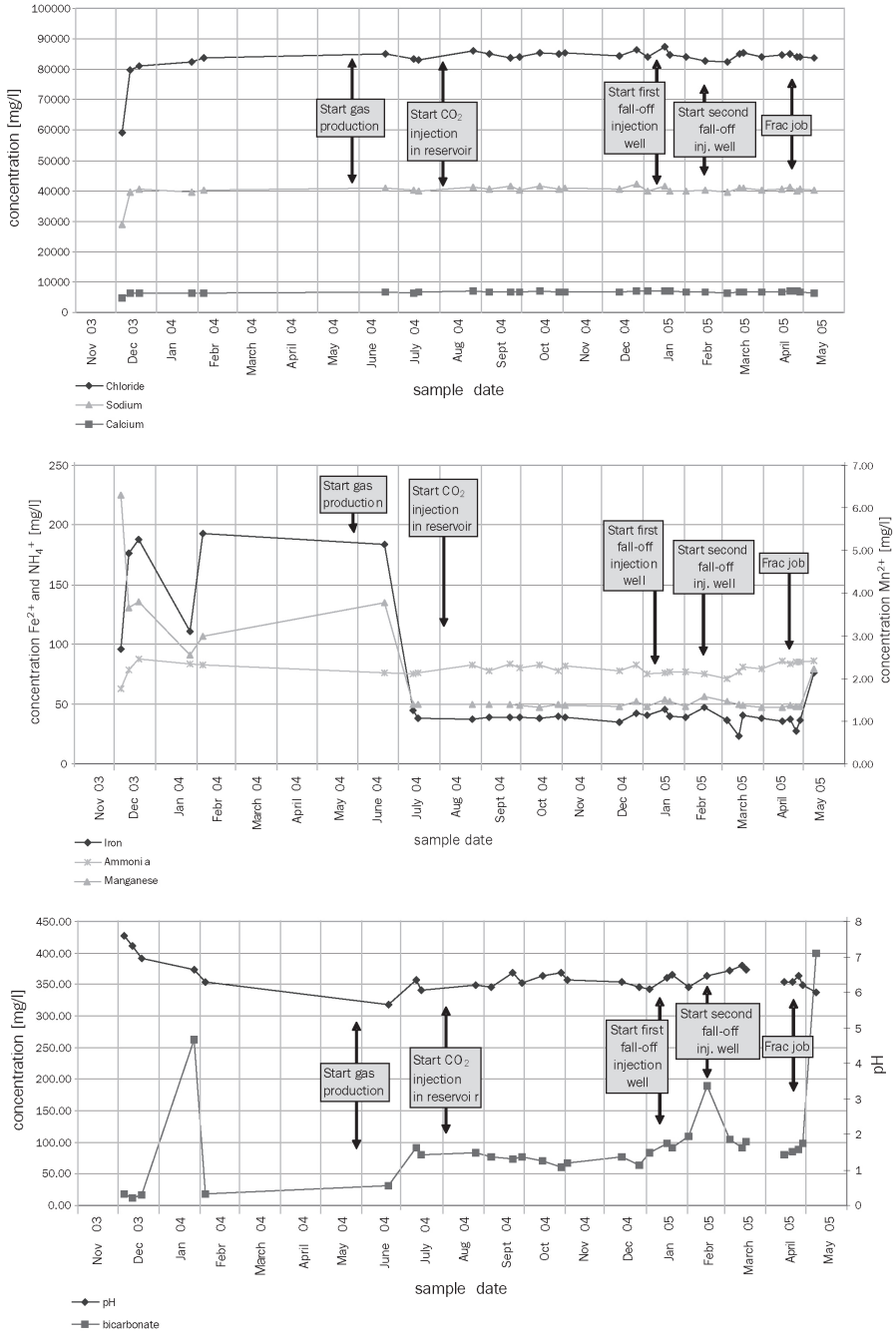

Figure 2.8: Composition of the produced water of the MS-4 well.

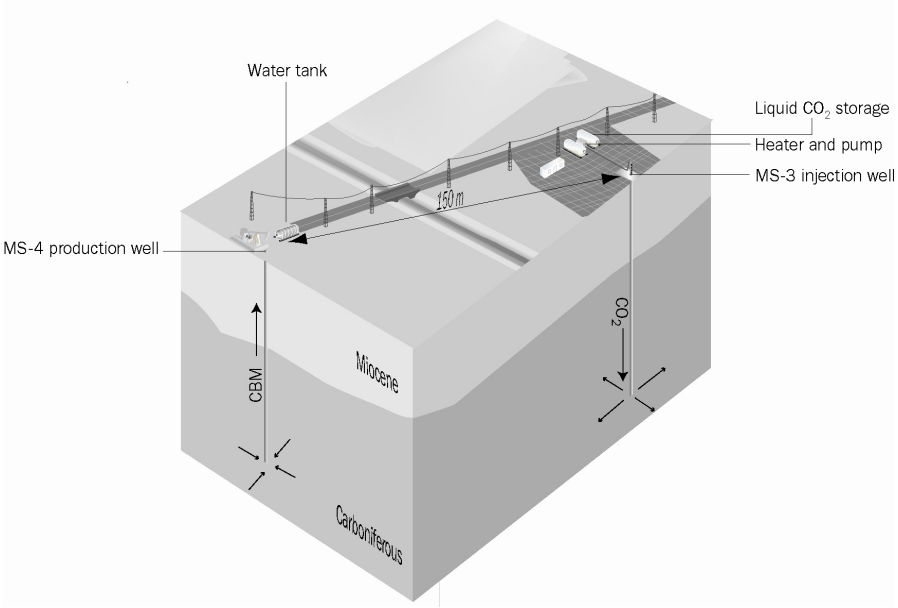

Figure 2.9: Design of field experiment. The boundary between the Carboniferous and the Miocene cover is schematically indicated.

stalled to be able to prevent frost in the injection line, wellhead and tubing. The pressure and temperature conditions in the water-filled injection well were determined at 1,000 m (3,281ft) before injection at 8.6 MPa (1,247 psi) and 39.5°C (103.1 °F), respectively. Also, the initial equilibrium water level in the tubing was established at 146 m (479 ft) below surface. The CO_2 flow during injection, casing pressure, tubing pressure and tubing temperature are registered digitally at 15 seconds time intervals. The time intervals were changed during specific injection periods or during longer periods of operational standstill.

CO_2 injection

First injection tests with water took place at the beginning of July 2004. Liquid CO_2 from an industrial source was injected for the first time at the beginning of August 2004. From the start, it was not possible to maintain continuous injection. Required injection pressures with the applied injection rates (ca. 10 l/min or 0.01 m^3/min or 0.35 cf/min) appeared higher than initially anticipated. The injection of CO_2 was therefore realized by intermittent pumping up to 9 MPa (1,305 psi) at the well head, followed by a fall off period. In the second half of December, adaptation of the injection equipment allowed higher injection pressures up to 14 MPa (2,031 psi) at the wellhead. Still, no continuous injection could be established. The injection was es-

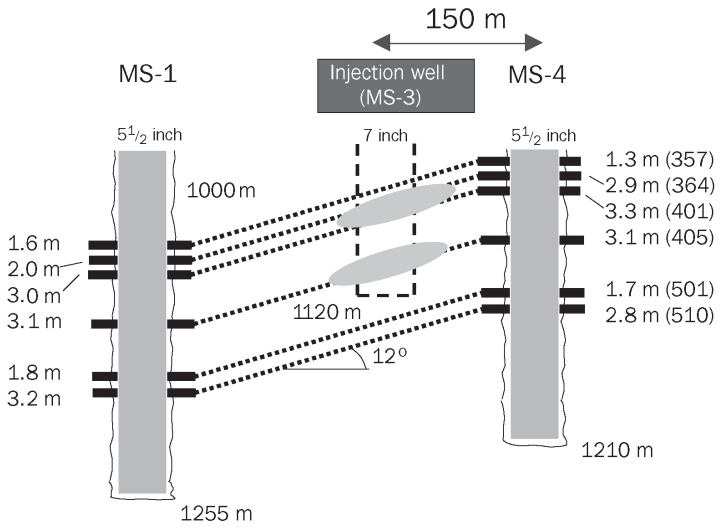

Figure 2.10: Correlation and thickness of target coal seams for CO_2 sequestration at the RECOPOL pilot site.

timated at approximately 1-1.3 ton per day in the build-up/fall-off cycles. Between mid-February to March 2005 injection stopped in order to have a long fall-off period to be able to determine the permeability. Evaluation of wellhead pressure and temperature data during the pressure build-up and fall-off of the intermittent injection periods, taking into account phase behavior and density changes of the CO_2, showed that the build-up time is decreasing and the fall-off time is increasing in time (figures 2.13 and 2.14). Additionally, the steep fall-off in the beginning of the curve during start-up (with water downhole) has disappeared in November and December. Both observations indicate a reduced permeability in time.

Downhole pressure-temperature gauges were installed during several periods during the project (June 28-July 5, 2004; August 2 - 10, 2004; December 16, 2004 - January 11, 2005; February 8 - March 1, 2005; March 2 - 22, 2005; and June 21 - 30, 2005). The downhole data can be correlated very well to the wellhead data, by taking into consideration the density variation with depth due to phase behavior. The data showed that the CO_2 is in supercritical phase at in situ bottom hole temperature (relatively constant at approximately 40°C) and the pressure conditions (varying between 8,6 and 24,5 MPa (1,247 and 3,553 psi) during operations), but its density and the viscosity are variable during the pressure fall-off period. This phase behavior of the CO_2 in the well complicated the interpretation with the available software, which is currently not designed to handle this. Despite the difficulties in the interpretation, the data clearly showed that the permeability of the coal seams decreased in time. Since well damage (e.g., blocked perforations) is unlikely, the reduced injectivity is presumably the result of swelling of the coal after contact with the CO_2. Addition-

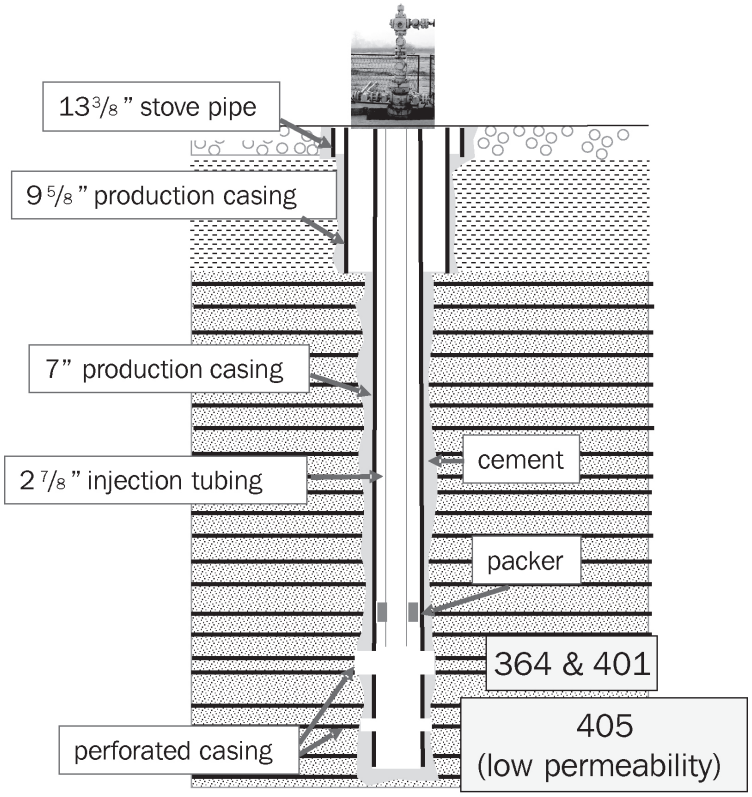

Figure 2.11: Well lay-out of the 1120 m (3,675 ft) deep injection well (MS-3). The well was completed with a 0.18 m (7 inch) casing. The casing was cemented and the cement job was checked by running a cement bond log. There are three perforation intervals at 1012, 1022, and 1076 m (3320, 3353, and 3530 ft). These intervals correspond with the seam 364 (over a total of 1.8 m or 5.9 ft), the seam 401 (over a total of 2.6 m or 8.5 ft), and the seam 405 (over a total of 2.0 m or 6.6 ft). The perforation density was 16.4 shots/m (5 shots/ft) under an angle of 60° with a penetration depth of 0.767 m (30.18 inch). In October 2003 the x-mas tree and downhole equipment were installed, consisting of a 0.073 m (2 $^{7}/_{8}$ inch) injection tubing of 1010 m (3314 ft) length and a 0.18 m (7 inch) packer at 975 m (3199 ft). Coal seams occur throughout the Laziska, Orzesze, and Ruda Formations. The coal seams indicated in this picture (other than the 364, 401 and 405) are for illustration only and do not represent actual position of the seams.

ally, it was observed that there were no indications of fracturing. This is remarkable, because bottom hole pressures that were reached during injection (with a maximum of 24.5 MPa) were higher than the originally estimated fracture pressure of the coal. This indicates a change in reservoir properties.

Gas production

The gas production from the MS-4 well was rising (Fig. 2.7) in the course of August 2004, several days after the start of the injection of CO_2 in the MS-3 well. This increase in production rate directly after the start of the injection is surprising, given the distance between the wells. This increase can be an effect of the conventional production, but its appearance directly after the start of the injection seems too coincidental. Since there were no indications of breakthrough of the CO_2 at this time (see below), the most likely explanation is an effect of pressure. Because of a pressure reduction around the production well due to production of water, gas has desorbed from the coal surface into the cleats. On the other hand, reservoir pressure was increased around the injection well due to the injection. Therefore, a pressure gradient is created between the wells that pushes the gas in the cleats towards the MS-4 production well. The total amount of desorbed gas was limited due to the undersaturation of the coal, and production decreased in November and December. Nevertheless, the production rates are significantly higher than the baseline rates, indicating that more gas is released than can be explained by conventional production. Therefore, it seems likely that exchange reactions between the CH_4 and the CO_2 are taking place, delivering coalbed gas to the production well. The expected dependency of exchange reactions on pressure is yet unclear. Therefore, given the pressure gradient between the wells, it is not clear where these exchange reactions take place: all along the pathway or only at those positions with optimal pressure conditions. A clear connectivity between the wells is shown by the response of the production rates on the changes in the injection rates, with increasing rates after increase of injection pressures and decrease in production when there was no injection. However, it is still unclear how this can be related to the adsorption behavior at the coal surface: the inverse relation was expected (adsorption capacity increases at higher pressure, thus higher pressure, more adsorption, lower production). Probably, diffusion time is more important than pressure, as shown by the increase of the production rate after a period of standstill of the pump. By giving the system time to exchange and desorb, more gas is released from the coal surface. This is an indication that the exchange of CO_2 for CH_4 might be dependent on transport into (and out of) the matrix.

In order to establish the breakthrough of the injected CO_2 in the production well the composition of the produced gas was monitored (Fig. 2.15). From November 2004 onwards, a slow rise in the CO_2 content in the production gas above the baseline was observed (maximum 10%) which could be attributed to the injected CO_2. During the fall-off period in the second half of February, the CO_2 content in the gas decreased to approximately 3%, still higher than the baseline content. The observations above indicate, in addition to the observations in the production rates, a clear response of

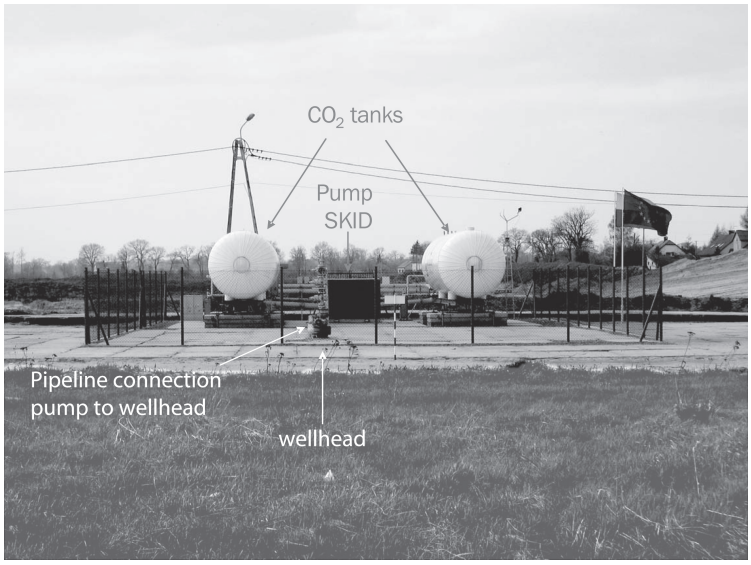

Figure 2.12: Picture of the well site of the injection operations.

the production well on the injection activities.

Investigation of the isotope signature of the gas shows that the $\delta^{13}C$ of the carbon dioxide in the gas of the baseline production was slightly negative to positive (-0.3 to 7.6 ‰). This represents the naturally occurring CO_2 in the coal seams, most likely resulting from thermogenic generation. The $\delta^{13}C$ of the injected CO_2 was distinctly different (-48.0 to -45.3 ‰). The values of the baseline production and of the carbon dioxide in the tank can be considered as the end members of a mixing blend: the closer the measured value gets to the value of the tank, the more it will consist of injected CO_2. The isotope signature of the production gas is relatively stable until at least mid-October 2004 (Fig. 2.16), indicating that a breakthrough of the injected CO_2 before this time is not probable. Based on the decreasing $\delta^{13}C$ of the CO_2, first breakthrough of the CO_2 likely occurred between mid-October 2004 and December 2004. This corresponds to the results of the composition of the produced gas. The value of $\delta^{13}C(CO_2)$ decreased further until mid-February 2005, indicating that the part of injected CO_2 of the total was increasing. The stop of the injection during the fall-off period resulted almost instantly in a decrease in $\delta^{13}C(CO_2)$ of the production gas. This could be explained by fractionation of $\delta^{13}C$ in the adsorption process.

The composition of the water remained relatively stable until December 2004 (Fig. 2.8). From December onwards, the bicarbonate content of the water was steadily rising. This is likely to be related to the contact between the formation water and the injected CO_2. There is no indication that the formation water is becoming more acidic

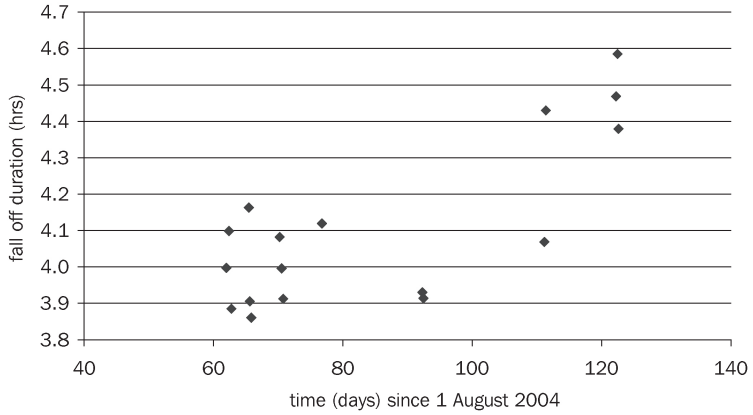

Figure 2.13: Variation of the duration of pressure fall-offs (between 9.0 and 7.1 MPa) from the start of the injection. These data are derived from well head data.

(lower pH) from December onwards, as could be expected on the basis of the carbonate equilibrium reactions. This is probably due to the high salinity of the water, giving it a high buffering potential. There are no indications for mineral dissolution. Based on the increase of bicarbonate, there is an apparent breakthrough from the beginning of December onwards, somewhat later than indicated by the gas composition and by the gas isotope signature. This can be explained by the higher mobility of the CO_2 as a gas compared to CO_2 in solution.

2.4.3 CO_2 injection and CBM production after reservoir stimulation (March 2005 to June 2005)

CO_2 injection after reservoir stimulation by "mini-frac" job

Because the permeability of the coal seams decreased over time and injection rates were lower than expected, it was decided to stimulate the reservoir by performing a mini-frac job without proppant. This mini-frac job was was intended to open the cleat system by applying high flow rates of fluid (water) into the reservoir. It was anticipated that if the cleat system was opened once, it would, even without proppant, remain sufficiently open to allow continuous injection at a wellhead injection pressure of approximately 14 MPa (2,031 psi). However, the injectivity of CO_2 at lower pressures was very low after the mini-frac: it was reduced from approximately 1 t/d to approximately 0.1 t/d in discontinuous injection. This was due to the presence of water in the well that was difficult to displace by CO_2 with a lower density.

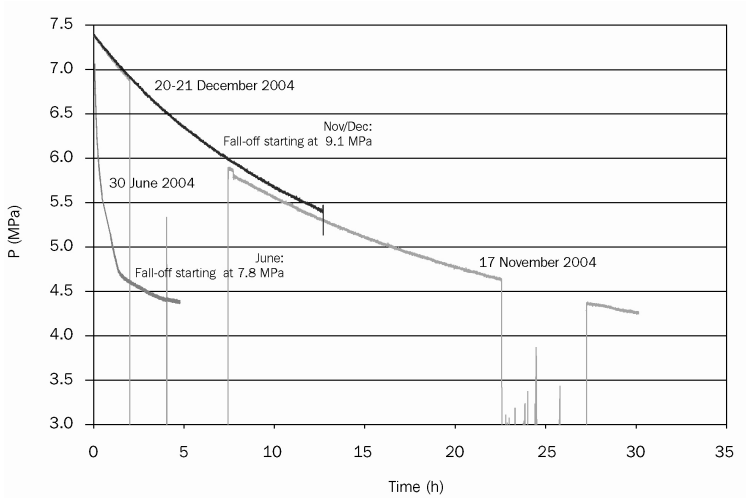

Figure 2.14: Comparison of pressure fall-offs in time at different stages of the project. Time is considered 0 at the stop of injection and subsequent closure of the wellhead valves. These data are derived from well head data.

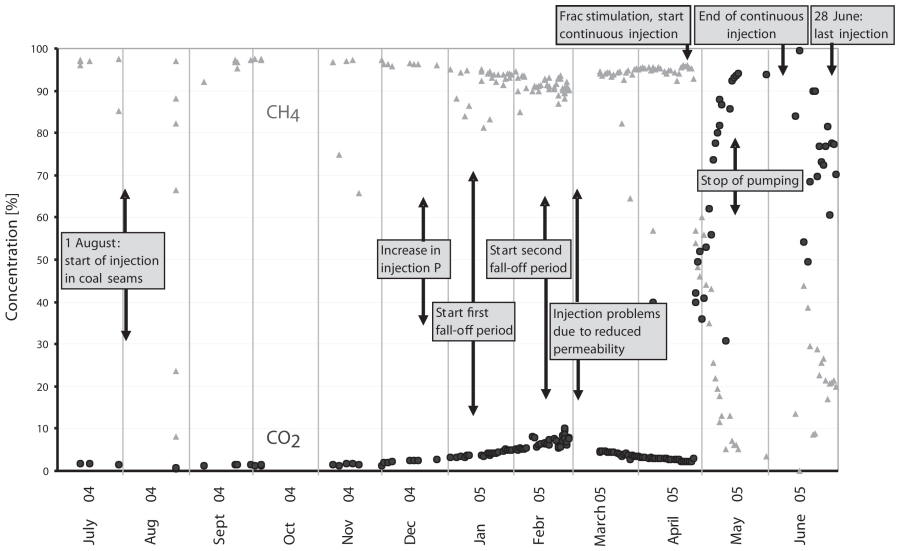

Figure 2.15: Composition of the production gas of the MS-4 well.

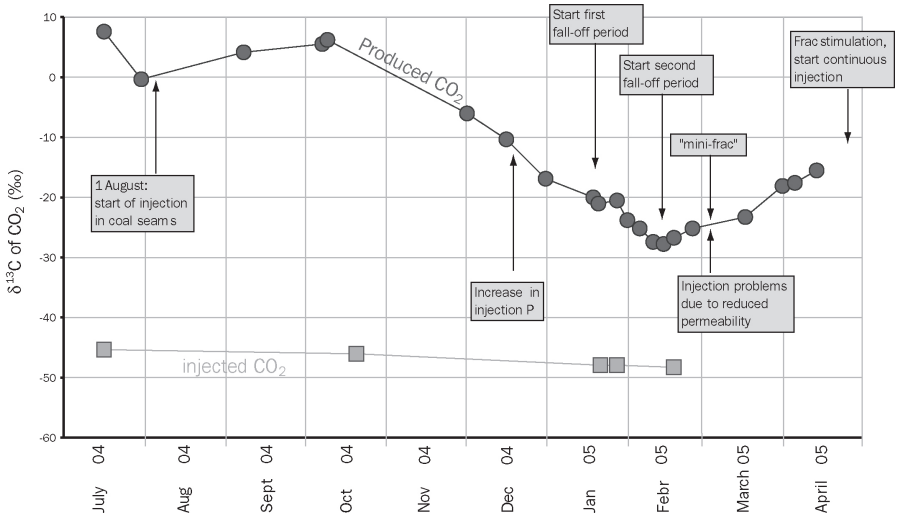

Figure 2.16: Values of $\delta^{13}C$ CO_2 (‰) determined before and after CO_2 injection.

CO_2 injection after reservoir stimulation by frac job

Because of the low injectivity rates after the mini-frac, the reservoir was fracced with a sand proppant on the April 20, 2005. The fracture pressure was significantly higher than could be anticipated on the basis of earlier tests. After opening of the cleat system, approximately 3 m^3 (106 cf) of proppant could be injected into the reservoir. After flushing with water, the well was further cleaned with nitrogen (flushing for 2 h) with a coiled tubing unit. This unit was also used to inject nitrogen until a wellhead pressure of approximately 19 MPa (2,756 psi) was reached after 1 hour. After shut-in of the well an initial fall-off was observed of the nitrogen-filled well before the nitrogen was released until a wellhead pressure of approximately 10 MPa (1450 psi) was reached.

Restarting of the CO_2 injection showed a slow increase of the wellhead pressure until stabilization at approximately 14.3 MPa (2074 psi) during continuous injection (Fig. 2.17). In the following days, there were several periods of standstill of the injection, due to operational activities and the arrangements for CO_2 supply. Continuous injection could be established between the 4^{th} of May and the 3^{rd} of June 2005 (Fig. 2.18). During the periods of continuous injection from April to early June, approximately 12-15 tonnes of CO_2 were injected per day. Until the end of June, injection took place in intervals of variable duration because CO_2 was temporarily unavailable. In the second half of June, continuous injection could only be reached by reducing the flow rate. However, this could only be maintained for a limited period.

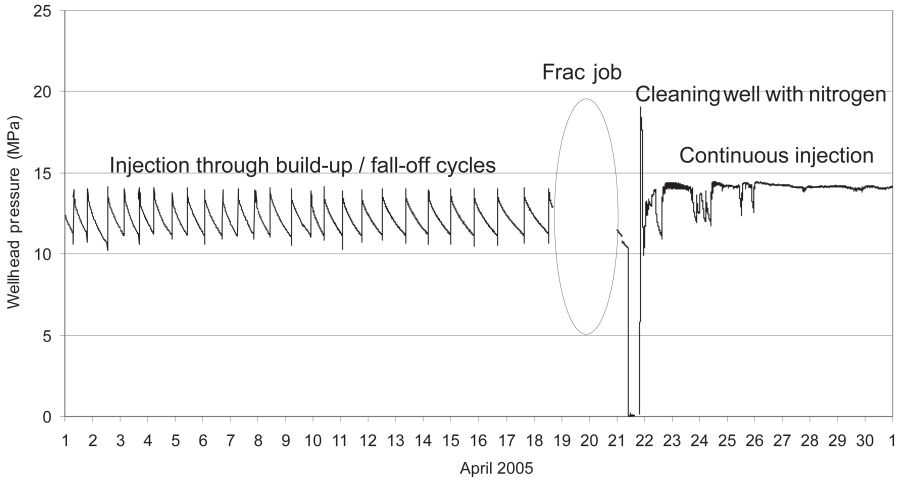

Figure 2.17: Pressure at the injection wellhead, showing the intermittent injection before the frac job and the continuous injection after the frac job.

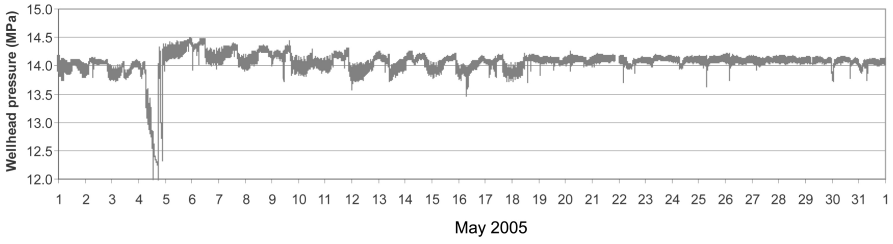

Figure 2.18: Pressure at the injection wellhead, showing the continuous injection after May 4, 2005.

The establishment of continuous injection showed that the frac job was successful, and that even a small amount of proppant is sufficient to open the cleat system around the wellbore. However, this is not a fixed situation. The stabilization pressure at the wellhead, where continuous injection was reached, increased after each period of standstill in the last week of April. This indicates that the reservoir becomes tighter, probably related to swelling of the coal. During the period of continuous injection, the stabilization pressure slightly decreased. This shows that the dynamics of the reservoir, i.e., the swelling, becomes less pronounced. At this stage, it seemed that the conditions in the reservoir were stabilized. However, in June 2005 the stabilization pressure at the wellhead increased again after each period of standstill. This shows that the coal has not ceased to be reactive, probably because pristine coal comes into contact with the CO_2 during periods of standstill. Again, this indicates that the performance of the operations depends on the time that is given to the system to equilibrate, thus the diffusive transport of the gases in the coal.

Gas production after reservoir stimulation by "Mini-frac" job

The production rates of the MS-4 well were declining since mid-February 2005, probably because the injection in the MS-3 well stopped (Fig. 2.7). The CO_2 concentration in the production gas since mid-February decreased further to 2.2% in mid-April, nearly to the baseline level (Fig. 2.15). The observed shift in $\delta^{13}C$ of the carbon dioxide in the production gas from mid-February onwards was continuing in March and April 2005, again coinciding with decreasing production rates (Fig. 2.16). In the produced water, the trend of decreasing bicarbonate concentration continued until it was back to the baseline level (Fig. 2.8). These observations indicate that the coal acts a sink for the CO_2 during a period of relative inactivity, probably due to adsorption on the coal surface.

Gas production after reservoir stimulation by frac job

The gas production increased rapidly one week after stimulation of the injection well. Between the April 28 and May 14, the daily production rates increased from approximately 40 m^3/d (1413 cf/d) up to more than 700 m^3/d (24,720 cf /d). Because of the high production rates in the second week of May 2005, coal fines were released from the seams and damaged the downhole pump. For this reason, pump activity and water production ceased after May 14, 2005. Analysis of the coal fines showed that, based on their coalification rank and composition, they are most likely resulting from the upper seams rather than the lower 405 seam (Fig. 2.19). Gas will thus be mainly produced from the upper seams, which is in agreement with the low permeability of the 405 seam. Gas production was continued, even without pumping, after May 14, 2005, because of the overpressure in the reservoir. Maximum gas production reached approximately 1350 m^3/d (47,675 cf/d) just at the end of May 2005. After pumping stopped, the water level in the well steadily rose to a depth of 240 m (787 ft) on the June 1, 2005 (Fig. 2.20). On this date the well was shut-in and the pressure rise was observed, showing stabilization at 5 MPa at the wellhead after circa 1.5 days. A sec-

ond shut-in test, between June 6 and 16, 2005, showed a lower stabilization pressure of approximately 2.2 MPa (319 psi) after one week. The water level in the well on the June 17 was measured at a depth of 480 m (1575 ft), indicating a downhole pressure at 1050 m (3445 ft) of approximately 8.5 MPa (1233 psi). This is close to the original reservoir pressure. In the second half of June 2005, there was a rapid decrease of production rates. Production rates increased occasionally in response to the interval injections. In combination with decreased production rates, this pressure response indicates the uptake of CO_2 in the reservoir since the end of continuous injection, most likely due to adsorption on the coal.

From March 2005 onwards, there was continuous measurement of the produced gas composition after the installation of a digital infra red analyzer, with a data registry every 15 seconds. The concentration of methane in the production gas dropped significantly one week after the frac job (Fig. 2.21). This coincided with an increase in CO_2 concentration. The gas composition data from samples do not show signs of nitrogen. In May 2005 there was, except for a small increase around the May 5, a general decrease of CH_4 concentration until it stabilized around 3-4% in mid-May 2005 (Fig. 2.22). After the shut-in tests in June 2005, the content of methane in the gas increased up to nearly 50%. At the end of June, this decreased to a stable level of approximately 20% (Fig. 2.23). Again, this shows that in order for exchange reactions to take place, sufficient time is required. Diffusion rates into and out of the coal appear to be the critical factors.

Samples of the produced gas that were taken in May 2005 show a value of $\delta^{13}C$ of the CO_2 that is comparable to the value of the CO_2 in the containers prior to injection (Fig. 2.16). This clearly indicates that almost all of the produced CO_2 originated from the injection and that the percentage of natural CO_2 was very low at this time. Analysis of the composition of the water shows a rapid increase in bicarbonate content, especially in the first weeks of May 2005 (Fig. 2.8). Again, this shows the clear interference between the injection and production well and a breakthrough of the CO_2. Similar to the earlier observations, the breakthrough of the CO_2 in solution is later than that of the gas. Iron and manganese ion concentrations also show a slight increase in May 2005. This could indicate corrosion of the casing or well equipment as a result of the contact with CO_2. However, the pH of the water is relatively stable at a value of about 6.

2.5 Discussion

Several months of injection showed that injection without stimulation is difficult under the local field conditions. It was expected that a small additional pressure above the reservoir pressure would be sufficient to establish continuous injection, but this was clearly not the case. The injection pressures required were nearly twice the reservoir pressure. Apparently, this was the result of a decrease in permeability of the

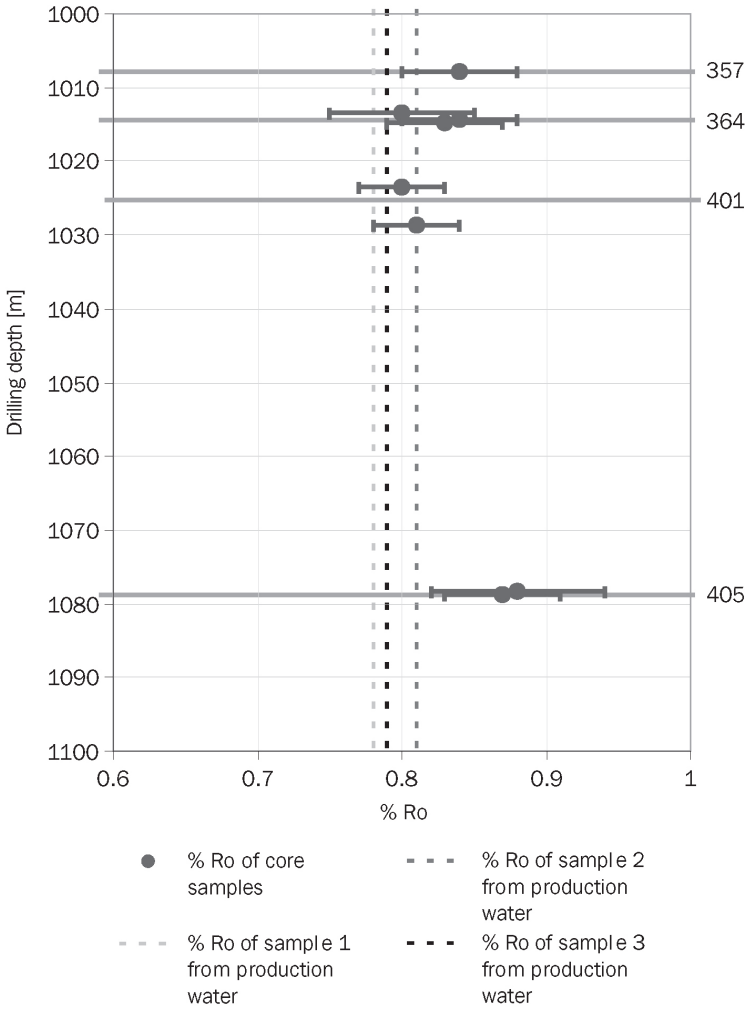

Figure 2.19: Vitrinite reflectance of seams 364, 401 and 405, and vitrinite reflectance of the coal fines that were produced by the MS-4 production well. The latter are corresponding to the values of the upper seams (364 and 401).

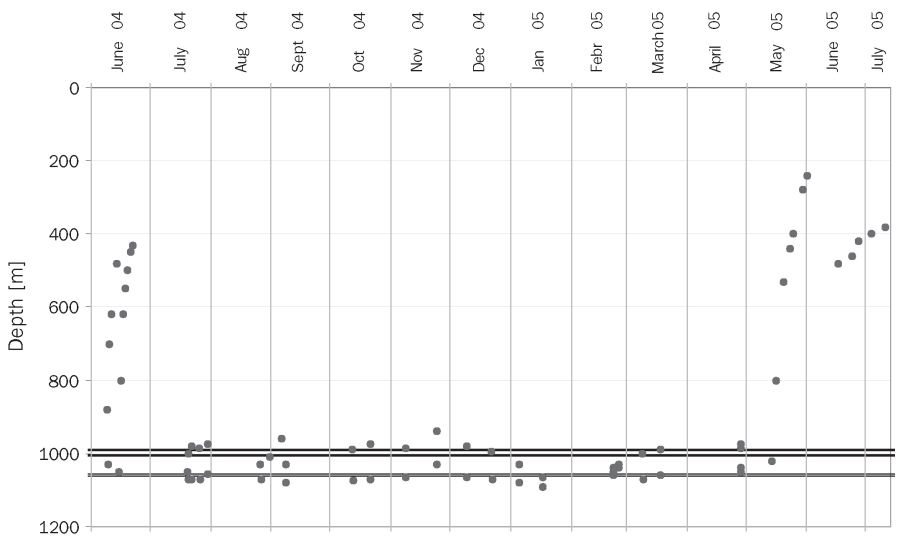

Figure 2.20: Water level in the MS-4 production well.

reservoir during injection, most likely due to swelling of the coal. These observations are in line with the observations in Canada and the United States (Reeves, 2003; Reeves *et al.*, 2003; Van der Meer and Fokker, 2003). Experiments on cores have shown that coal swelling can indeed cause a significant decrease in permeability (Mazumder *et al.*, 2006a). In November 2004 an unexpected early breakthrough of the injected CO_2 occurred in the production well. This breakthrough was unexpected for the following reasons: 1) the high permeability cleats are oriented perpendicular to the flow line between the wells; 2) numerical modeling indicated that the injected volume until November 2004 was insufficient to result in breakthrough; 3) CO_2 was expected to be adsorbed by the coal; 4) CO_2 injection was expected to result in a reduction in permeability. Conclusively, the observations show that it is very difficult to get the CO_2 into the reservoir, but that once it is injected, it is able to flow relatively fast towards the production well. Transport through high permeability streaks (small sand channels, fractures) is unlikely, because by far the most of the CO_2 remains in the reservoir (see below). The most plausible explanation is swelling of the coal, creating a very low permeability zone around the injection well, while the permeability is higher outside this zone. The frac job was able to connect the wellbore compartment with the zone of higher permeability, explaining the increase of injection rates after the frac job. However, once the system is given time to diffuse and re-equilibrate, the zone of low permeability is extending, as is shown by the increase in stabilization pressure in April and June 2005.

Another observation is the apparent change of the frac pressure of the coal seams. The frac pressure was determined during the well testing in advance of the operations, i.e., before the coal had been in contact with the CO_2. During the mini-frac job and

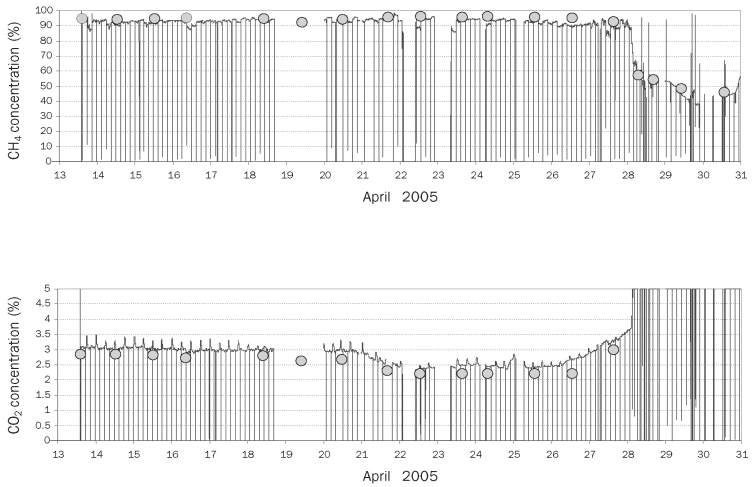

Figure 2.21: Composition of the production gas (CH_4 top graph, CO_2 bottom graph) of the MS-4 well at the end of April 2005, as measured with the IR analyzer (lines) and via gas samples (dots). The analyzer was able to measure CH_4 between 0 and 100%, and CO_2 between 0 and 25%. The results of the analyzer are in good agreement with the laboratory analyses of the samples.

the frac job, i.e., after the coal had been in contact with the CO_2, it appeared that the fracture pressure was significantly increased. This is an indication that the coal changed under the influence of the CO_2. One of the changes, and an explanation of the increased fracture pressure, could be that the coal has become more plastic or "rubbery", as was suggested by others (Larsen, 2004).

2.5.1 Enhancement effect

The total maximum amount of gas that could have been produced by conventional production between August 1, 2004, and April 28, 2005, is estimated at ca. 8,100 m^3

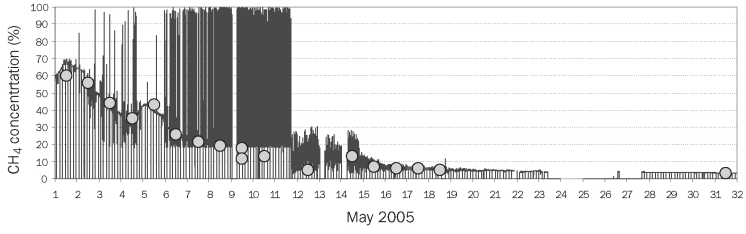

Figure 2.22: CH_4 content of the production gas of the MS-4 well in May 2005, as measured with the IR analyzer (lines) and via gas samples (dots). The peaks are probably related to automatic calibration of the analyzer.

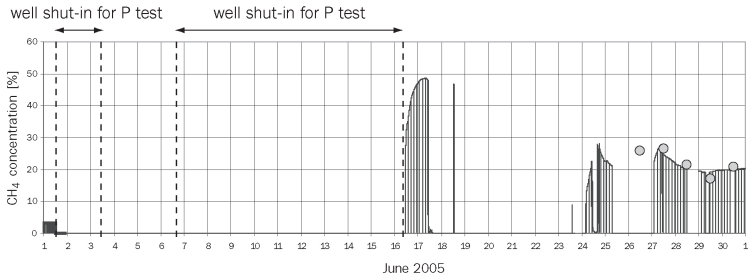

Figure 2.23: CH_4 content of the production gas of the MS-4 well in June 2005, as measured with the IR analyzer.

(286,049 cf), assuming a baseline production of 30 m^3/d (1059 cf/d). The actual production of methane amounted up to 13,900 m^3 (490,874 cf), thus an increase of ca. 70%. The baseline production after the frac job is estimated to have been approximately 1,100 m^3 (38,846 cf), while actual methane production amounted up to 1,700 m^3 (60,035 cf). This is an increase of ca. 55%. The absolute amounts of CH_4 that were produced are significantly higher than the projected baseline production with conventional production (Fig. 2.24). It can therefore be concluded that the injection activities had a positive effect on the gas recovery within the project lifetime, probably due to exchange reactions. However, the role of pressure in relation to the adsorption behavior and the exchange reaction is still unclear. The enhancement factor is decreasing as a result of the higher injection rates after the frac job, i.e., while the frac job helps in getting the CO_2 into the reservoir and is good from the storage point of view, it actually decreases the amount of methane produced. A probable explanation is that at higher injection rates the time for exchange and adsorption reactions is decreased. The contact time between the coal and the CO_2 was higher before the frac job, allowing diffusion of the gas into and out of the coal matrix. Despite the enhancement the produced amounts and the recovery factor are very low, probably due to the low diffusion in the coal as shown by the desorption tests. However, it must be emphasized that high production rates were not the primary goal of this project. Only a limited number (3) of coal seams were completed because of the research character of the project.

2.5.2 CO_2 storage

In total approximately 760 tonnes of CO_2 were injected between August 2004 and the end of June 2005 (Fig. 2.25). The amount of the injected CO_2 that was produced back by the MS-4 production well, mainly after the frac job, was estimated to amount up to 68 metric tonnes (75 short tonnes). The amount of produced CO_2 was much lower (ca. 9%) than the amount of injected CO_2, indicating a clear sink of approximately 692 metric tonnes (763 short tonnes) or CO_2 in the reservoir. This sink was confirmed by the rapid decrease of production rates after continuous injection stopped in June 2005. Shut-in tests of the production well in June 2005 and measurements of the

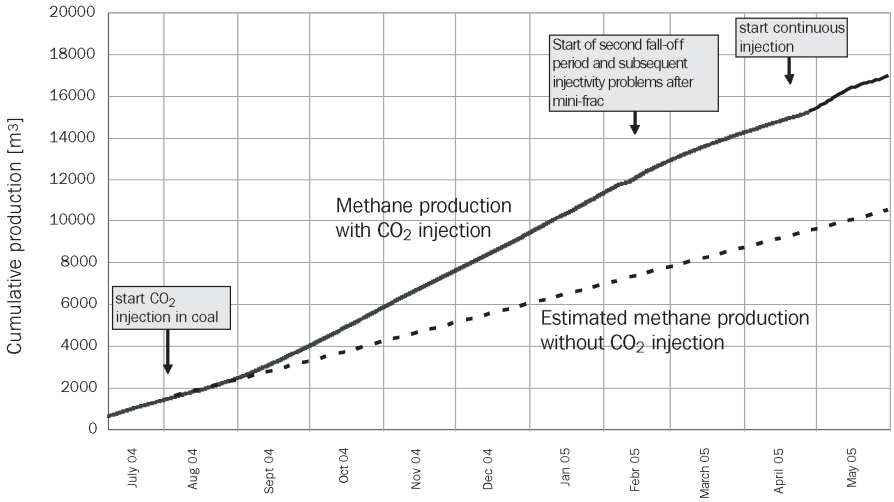

Figure 2.24: Cumulative amount of produced methane in time in the RECOPOL project. The positive effect of the injection activities on the gas production is clearly visible once compared to the projected baseline production.

water level in June 2005 showed that the reservoir pressure around the production well was slightly increased compared to the initial pressure but was returning to its equilibrium level. This also seems to confirm that around the production well adsorption of CO_2 is taking place. However, pressure fall-off of the injection well after the stop of the injections appears to be very slow. Possibly, this is an indication of compartmentalization of the reservoir.

2.6 Conclusions

Conclusively, the consortium showed that it was possible to set up the first on-shore CO_2 storage pilot in Europe and to handle all soft issues (permits, contracts, opposition, etc.) related to this kind of innovative projects. The lessons learned in this operation can possibly help to overcome start-up barriers of future CO_2 storage initiatives in Europe. Advances were made in the understanding of the process that allows improvements in the dedicated numerical simulators. Enhancement of methane production was proven, although the underlying process is not fully understood. Further field experiments and laboratory studies should be undertaken to gain further knowledge of the processes involved. The permeability of the coal remains a critical factor, even though it is shown that the injectivity in low permeability coal could be increased to substantial rates. The injected amounts provide a good basis for a future upscaling of the operations. It is expected that in the Upper Silesian basin locations can be found with higher permeability, thicker seams and higher gas content, providing a better prospectivity for gas production. With the experiences of this

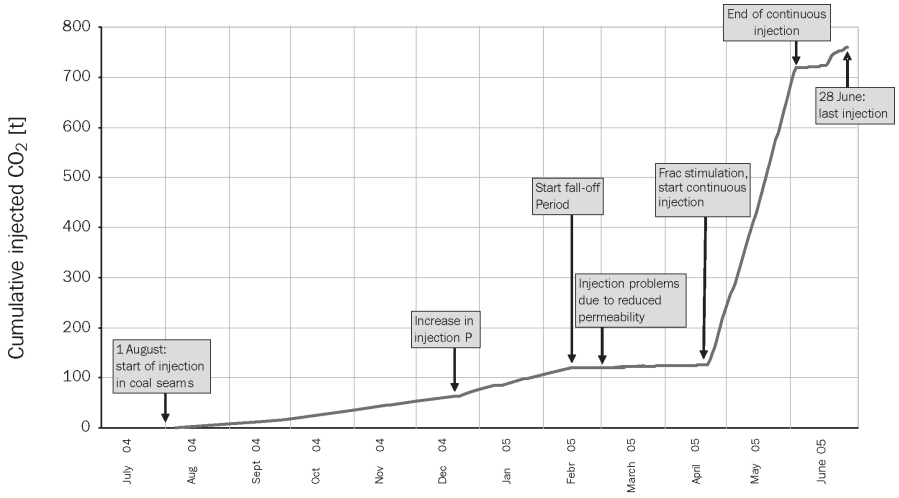

Figure 2.25: Cumulative amount of injected CO2 in time in the RECOPOL project.

project, field optimization can be performed to enhance production in future sites. Since the process appears to be diffusion-controlled, an optimum distance should be chosen between the wells that guarantees sufficient contact time between the injected CO_2 and the in situ coal. Other well completions, such as horizontal or "fishbone" drilling, need to be researched to assess their impact on injectivity and productivity. To enhance the recovery factor even further, dedicated operational schemes, with varying injection and production intervals, should be planned. Operational flexibility in the applied pressure and flow rates is highly recommended to manage the swelling effects.

Acknowledgements

The American Association of Petroleum Geologists is acknowledged for granting the permission to reprint this publication. The European Commission is acknowledged for funding and support of this project executed under the programme ENERGY, ENVIRONMENT AND SUSTAINABLE DEVELOPMENT (contract no. ENK-CT-2001-00539). Shell International, JCoal, the Federal Region of Wallonie (through the Faculté Polytechnique de Mons) and the Polish and Dutch governments (via Novem) are thanked for their support. RECOPOL is carried by an international consortium of research institutes, universities and industrial partners, who are all acknowledged for their contributions and financial support for this study. Consortium members are: Central Mining Institute, Delft University of Technology, Aachen University of Technology, Air Liquide, DBI Gas- und Umwelttechnik GmbH, Gaz de France, Institut Français du Pétrole, International Energy Agency Greenhouse Gas R & D Programme, CSIRO, Gazonor and ARI. Bart Jura, Jacek Skiba and Zbigniew Kobiela

(Central Mining Institute) and Guillaume De-Smedt, Paul Wentink and Vladimir Hasanov (Air Liquide) and Dan Bossie-Codreanu (Institut Français du Pétrole) are acknowledged for their efforts on the field activities. Bert van der Meer, Eric Kreft and Erik Simmelink are thanked for their involvement in the work and discussions of the project and its activities. Cees Geel and Frank van den Belt are acknowledged for their contribution to the geological work. Jerzy Hadro is thanked for his contributions in the drilling and the desorption tests and for his general advice. Metanel S.A. is acknowledged for providing the concession of the site and Mr. Z. Adamaszek and staff for support during the project. We thank Pablo Tejera-Cuesta, Fred van der Bas and Jos Maas (Shell) for their support and advice on the frac job. Prof. Kotarba is acknowledged for the isotope analyses.

Chapter 3

Production of gas from coal seams in the Upper Silesian Coal Basin in Poland in the post-injection period of an ECBM pilot site

Frank van Bergen, Pawel Krzystolik, Niels van Wageningen, Henk Pagnier, Bartlomiej Jura, Jacek Skiba, Pascal Winthaegen & Zbigniew Kobiela

This chapter was published as:
Van Bergen, F., Krzystolik, P.,Van Wageningen, N., Pagnier, H., Jura, B.,Skiba, J., Winthaegen, P. & Kobiela, Z. (2009). Production of gas from coal seams in the Upper Silesian Coal Basin in Poland in the post-injection period of an ECBM pilot site, International Journal of Coal Geology, 77(1-2): 175-187

Abstract

A pilot site for CO_2 storage in coal seams was set-up in the Upper Silesian Coal Basin in Poland in the scope of the RECOPOL project, funded by the European Commission. About 760 tonnes CO_2 were injected into the reservoir from August 2004 to June 2005. Breakthrough of the injected CO_2 was established, which resulted in the production of about 10% of the injected CO_2 in this period. This paper reports on activities performed under the European Commission project MOVECBM that aimed at the assessment of the storage performance of the reservoir in the follow-up period, i.e. whether the injected CO_2 was adsorbed onto

the coal or whether it was still present as free gas in the pore space. The injection well was used for this purpose, as the production well had to be abandoned for permitting reasons. Several operational periods can be defined between the last injection in June 2005 and the abandonment of the well in October 2007. In the first period the well was shut-in to observe the pressure fall-off, from about 15.0 MPa at the wellhead after the last injection until about 4.5 MPa at the end of 2005. This pressure fall-off curve showed that the reservoir permeability was very low. This seemed to confirm the observed swelling of the coal during the injection period. In the first months of 2006 the pressure at the wellhead was decreased by releasing gas in a controlled way. The amount and composition of the gas were measured. As a result of the pressure reduction, the well flooded with water. A production pump was placed on the former injection well, enabling active production from the coal from March to September 2007. Results of these operations showed that whereas the gas production rates were as expected based on the experience with the production well, the water production was remarkably low. This could be related to permeability issues or, alternatively, indicate a drying effect of the CO_2 in the reservoir. Further, the gas composition showed a predominance of CO_2 over CH_4 during the gas release that changed gradually into a predominance of CH_4 over CO_2 during the production phase. Although stabilization was not reached within the given production period, the composition approached a 60% methane, 40% CO_2 ratio. This indicates that the exchange of these gases is more complex than often envisaged. After removal of the pump the well was filled with water, which ceased the gas release. This indicates that the pressure in the reservoir was back to its original, hydrostatic, state. As the total volume of CO_2 produced was only a fraction of the amount that was injected, it can be concluded that the CO_2 was taken up by the coal and is currently adsorbed. This gives confidence in the long-term stability of the injected CO_2.

Key words: carbon dioxide; swelling; production; injection

3.1 Introduction

Storage of carbon dioxide (CO_2) in coal seams in the underground is considered to be one of the options to reduce the emissions of this greenhouse gas into the atmosphere. The coal gas (coalbed methane, or CBM) that these coal seams naturally contain can be produced in advance of the injection of CO_2 or simultaneously. As the injected CO_2 may enhance the release of the CBM from the internal surface of the coal, the additional revenues from the gas may reduce some of the costs for injection. This principle has been the subject of many studies in recent years and have led to the development of several field sites around the world (e.g. in Alberta, Canada (Gunter *et al*., 1997; 1998), in Shanxi, China (Wong *et al*., 2007), in Hokkaido, Japan (Yamaguchi *et al*., 2005; 2007), in the San Juan Basin in New Mexico, U.S.A. (Gunter *et al*., 1998; Erickson and Jensen, 2001; Reeves and Schoeling, 2001; Schoeling and McGovern, 2000), and in the Upper Silesian Coal Basin, Poland. The results of the injection and production of this latter European pilot site were reported extensively before (Van Bergen *et al*., 2006). This paper reports on the activities and results that were undertaken at the field site in the follow-up period after the injection. The aim of this work was to assess the storage performance of the reservoir, i.e. whether the injected CO_2 was adsorbed onto the coal or whether it was still present as free gas in the pore space.

In order to provide the background for the interpretations that are presented in this paper, the following summary is presented on the basis of the paper by Van Bergen *et al*. (2006). The ECBM pilot site is located in the Upper Silesian Coal Basin (USCB) in Poland. This basin was selected as the most suitable coal basin in Europe for the application of ECBM (Stevens *et al*., 1999; Wong *et al*., 2001). The Carboniferous coal-bearing deposits in the USCB have a total thickness of at least 1000 m in the area. Coal seams with thicknesses between 1 and 3.5 m occur throughout the entire depth interval in further sand- to claystone dominated sedimentary sequence. Locally, coal seams occur with thicknesses up to 30 m. Synsedimentary tectonics resulted in faults with a north-south orientation that are expected to be sealing. The pilot site is located on a large block that was upthrusted during the Alpine orogeny. The thickness of the overburden in the area is about 250 m, mainly consisting of sealing shale deposits of Miocene age that uncomformably and disconcordantly overly the Carboniferous deposits. The high-volatile bituminous coal (vitrinite reflectance ~ 0.8-0.85%Rr) varies significantly in maceral composition, but is mainly vitrinite dominated. Permeability is different per individual seam: the upper two seams had a value in the lower range (~ 0.4 - 1.5 mD) of the regional variation (1 - 2 mD), whereas the permeability of the deepest seam was very low (~ 0.01 - 0.05 mD). Reservoir simulations indicated a permeability in the order of 1 mD for matching the water production. Total gas content of the cores was up to 10 m^3/ton (dry ash free, i.e., corrected for moisture and mineral content of the coal), with CH_4 concentrations of usually 95% or higher, with some percentages of N_2 (0.5-3%) and CO_2 (1-3%) and traces of other gases. Desorption tests, however, took several months and showed very slow diffusion out of the coal matrix. An existing coalbed methane well, remnant of CBM exploration and production activities undertaken in the 1990's, was cleaned up, repaired and put back into production in May 2004 to establish a baseline production. A new injection well (the MS-3 well) was drilled 150 m away from the production well (the MS-4 well). Initial injection of CO_2 took place in August 2004 in three seams of Pennsylvanian age in the depth interval between 1000 and 1100 m (Fig. 3.1). Several actions were taken to establish continuous injection. This appeared not to be possible because the injectivity was decreasing in time, probably due to swelling of the coal. Continuous injection was eventually reached in April 2005 after stimulation of the reservoir by a hydraulic fracture treatment. In this effort 3000 kg of sand particles with a range of diameters between 0.39 and 0.85 mm, i.e. particles that will pass through a 20 mesh sieve and be retained by a 40 mesh sieve, were injected of which about half was placed in the created fracture. A fall-off test before the creation of the fracture indicated that the permeability was very poor (0.05 mD). The hydraulic fracture treatment probably removed the skin-effects around the well, as reservoir simulations showed that bottom hole pressure and injection rate after the treatment match with a permeability of 1.3 mD. This value is in the same order as obtained in earlier simulations for the water production. In May 2005, approximately 12-15 tonnes per day were injected in continuous operations. About 760 tonnes of CO_2 have been injected into the reservoir from August 2004 to June 2005. Breakthrough of the injected CO_2 was established, which resulted in the production of about 10% of the injected CO_2 by the production

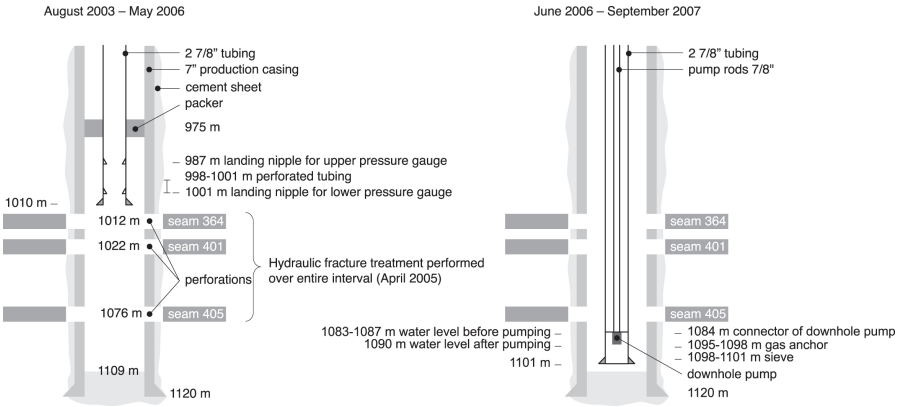

Figure 3.1: Schematic presentation of the well layout of the 1120 m deep well MS-3. The well was completed with a (7 inch) casing. The casing was cemented, and the cement job was checked by running a cement-bond log. Three perforation intervals exist at 1012, 1022, and 1076 m. These intervals correspond to seam 364 (over a total of 1.8 m), seam 401 (over a total of 2.6 m), and seam 405 (over a total of 2.0 m). The perforation density was 16.4 shots/m (5 shots/ft) under an angle of 60° with a penetration depth of 0.767 m (30.18 inch). In October 2003, the Christmas tree and downhole equipment were installed for injection, consisting of a 0.073 m ($2\,^{7}/_{8}$ inch) injection tubing of 1010 m length and a 7 inch packer at 975 m. Landing nipples were installed in the tubing for placement of downhole P-T gauges. In April 2005 a hydraulic fracture treatment was performed with this lay-out, resulting in stimulation of the complete interval below the packer (left picture). In May 2006 the tubing and packer were retrieved and a pump was installed (right picture). This downhole pump (BOLLAND 25-175-RHAM-12-4) was installed on the $^{7}/_{8}$ inch pump rods. The pump was fixed on the connector at the depth of 1084 m. This pump was operated in intervals, also indicated in the picture are the water levels before and after each pump cycle.

well in this period. As such, a total of 692 tonnes of CO_2 were stored in the reservoir. The results of the gas production showed that, although the recovery of methane was still low, the production of methane increased significantly compared to baseline production due to the injection activities.

The first important lesson learned from this field experiment was that injection into these low permeability coal seams is not trivial. It was expected that a high injection pressure would overcome the low injectivity but this appeared not to be the case. There are strong indications that coal is swelling, thereby reducing the permeability, which affected the injectivity even after the reservoir stimulation. Secondly, low diffusion rates into and out of the coal control the overall performance during the injection and production.

This paper reports on the follow-up period of the injection. Several operational periods can be defined between the last injection in June 2005 and the abandonment of the well in October 2007, which are described chronologically below and are repre-

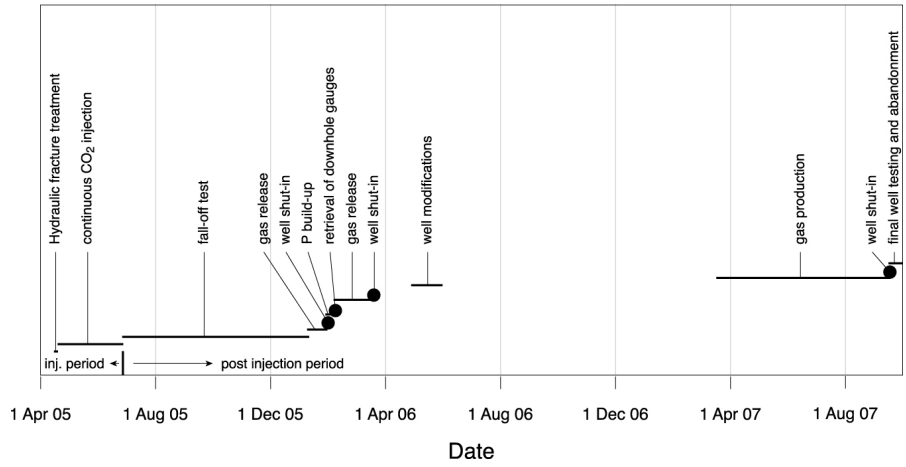

Figure 3.2: Overview of operational activities that are reported in this paper.

sented in Fig. 3.2.

3.2 Operational activities since the last injection of CO_2

3.2.1 Period 1: Pressure fall-off in the MS-3 well (June 28, 2005 to January 10, 2006)

The last injection of CO_2 in the MS-3 well occurred on June 28, 2005. Injection was stopped because of the end of the project funding for field operations. The well was shut-in, by closing the upper valve on the Christmas tree, directly after the last injection at a wellhead pressure of 14.96 MPa. Because downhole memory gauges for registration of pressure and temperature (P-T gauges) were installed on June 21, 2005, a downhole pressure of 24.09 MPa could be measured at 1001 m depth. During the installation of the downhole equipment, the gauges were lowered in several stages, allowing equilibration of pressure and temperature at various depths for 30 minutes. This enabled the derivation of the pressure and temperature gradients in the well. The pressure fall-off was registered downhole until retrieval of the gauges on August 10, 2005, while registration of the wellhead P-T conditions continued until the start of the next period. In July, 2005 the wellhead was not completely tight, which was solved by a wellhead repair on July 20, 2005. Retrieval of the gauges on August 10, 2005 also caused a small pressure drop.

From the beginning of November 2005 modifications on the field equipment were made in order to be able to decrease the pressure at the wellhead (aim of period 2). Waiting for natural depressurization to atmospheric pressure would take too long

because the pressure decline curve was flattening, therefore the pressure had to be decreased by gas release. An atmospheric pressure at the wellhead was required to install the production pump (aim of period 3), because otherwise the injection tubing could not be pulled out of the well. Measurement of pressure, temperature, gas production and composition were considered mandatory during the gas release. For this reason, also downhole pressure-temperature gauges were installed from December 8, 2005 onwards. Several technical problems were encountered in November and December especially related to frost of installations as the gas, comprising mainly of CO_2, was adiabatically expanding. Several tests were undertaken, often followed by modifications to the equipment, until January 11, 2006 (start of period 2).

MS-4 production well

During the first phase of this period the MS-4 production well was still open and it was releasing gas without active pumping. The production rates of the gas and the water were registered manually from a meter during the remaining lifetime of the well. The composition of the produced gas was registered with a digital infrared analyzer, with a data registry every 15 s. Unfortunately, the maximum CO_2 concentration that could be measured was 5% because of the parameter setting of the installed analytical equipment, while the actual concentration was higher. Gas and water samples were taken at a regular basis for laboratory analysis. Gas release at very low rates continued until the final shut-in of the MS-4 well in the second half of July 2005. The MS-4 well was abandoned on September 9, 2005.

3.2.2 Period 2: Decrease of pressure on the MS-3 well through gas release (January 11, 2006 to March 19, 2006)

Following the attempts and modifications of equipment in period 1, the first controlled gas release over a prolonged period could be realized on January 11, 2006. Still, the gas release was associated with freezing of the installation on January 15, 2006 that required a period of defrosting before the start of a new release period. On January 16, 2006 it was possible to establish a continuous gas release without frost problems. This was maintained until the well was shut-in at January 30, 2006 to observe the pressure build-up in the well. On February 7, 2006 the downhole gauges that were installed in December 2005 were retrieved. This was associated with some gas loss. During the retrieval, the gauges were allowed to equilibrate with pressure and temperature for 30 minutes each time at various depths to establish pressure and temperature gradients in the well. The pressure was decreased to atmospheric through gas release on February 8, 2006. Again, frost problems were encountered which were overcome by closing the well and re-opening the well after it reached an ambient temperature level. The gas release was accompanied by first water production, probably due to gas lift in the well. As at this stage water production was not wanted, the well was shut-in temporarily to allow the separation of gas and water in the well. Because the shut-in was performed at the first signs of water production, only a very small amount of water was produced. The release of gas continued from

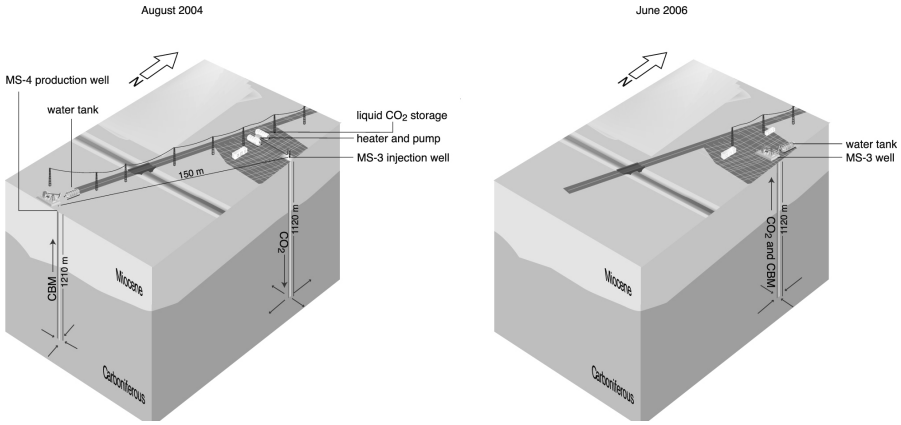

Figure 3.3: Schematic overview of the site lay-out during injection and in Periods 1 to 3 (left) and during production in Period 4 (right). The changes made in the site lay-out before production included the abandonment of the MS-4 production well and the modification of the MS-3 well from injection to production well.

February 8 to March 19, 2006 when the well was shut-in.

During this period the production rate of the gas was registered manually once per hour from a meter. In this period there was, while the water level in the well was rising slowly to the surface, no water production except some associated water of February 8, 2006. The digital infrared analyzer was transferred from the former production well to the MS-3 well, enabling the digital registration of the composition of the gas. The analyzer was adapted to measure CO_2 concentrations in the range of 0-100%. There was also digital registration of wellhead temperature and pressure and of casing pressure with data registry every 15 s. Gas samples were taken at a regular basis for laboratory analysis, also during well shut-in periods.

3.2.3 Period 3: Placement of pump for production of gas from the MS-3 well (20 March 2006 - 20 March 2007)

The well remained shut-in until May 2006. In May 2006 the injection tubing and packer were retrieved from the MS-3 well and the production tubing and pump string were installed. In June 2006 a pump jacket was installed on the MS-3 well, enabling active water pumping and thereby gas production from the coal. The resulting field set-up is schematically shown in Fig. 3.3. After the modifications of the field site the activities ceased until March 2007, with the exception of a limited number of pump tests. Gas and water samples were taken during these pump tests and at a regular basis for laboratory analysis. This period of standstill was caused by regulatory and financial issues that were solved in the first months of 2007.

3.2.4 Period 4: Production of gas from the MS-3 well (March 21, 2007 to September 18, 2007)

Pumping of water and gas from the MS-3 well started on March 21, 2007. Similar to the previous periods there was manual registration of gas and water production rates and digital registration (every 15 s) of the composition of the produced gas, wellhead pressure and temperature. The first production of water was associated with many gas bubbles. This has probably resulted in an erratic registration of the amount of the produced water. The actual amount of water is estimated to be in the order of 12 m^3, slightly more than the well volume. After production of this well volume the water production was very low and it was decided to continue with production intervals. After the first week of production the interval time between active pumping was 3 days. Although in the time between the active production the well was filling up with water, it was ascertained that the water level stayed below the perforations to guarantee continuous gas release. Gas production continued until September 18, 2007. Gas and water samples were taken at a regular basis in the entire period for laboratory analysis.

3.2.5 Period 5: Abandonment (September 19, 2007 to November, 2007)

During the final stage of the field operations several tests were performed to establish whether the perforations in the well were still open. Firstly, the well was filled with water up to the surface. This ceased the gas release, roughly indicating that the pressure in the reservoir was back to its original state. The original state was hydrostatic with respect to the top of the Carboniferous sediments, about 250 m below the surface. The drop of the water level as a result of the expected overpressure in the well was observed as a function of time. Once the water level stabilized, the well was filled again and the test was repeated. This was done several times at the end of September 2007. Secondly, a Drill Stem Test (DST) was performed on the top perforations in October 2007. The MS-3 well was finally abandoned in November 2007.

3.3 Results

3.3.1 Period 1: Pressure fall-off in the MS-3 well (June 28, 2005 to January 10, 2006)

In the first period the well was shut-in to observe the pressure fall-off, from 14.96 MPa at the wellhead after the last injection until about 4.5 MPa at the end of 2005 (Fig. 3.4). It was intended to estimate the reservoir permeability from this pressure fall-off curve, which was considered crucial given the observed swelling of the coal during injection.

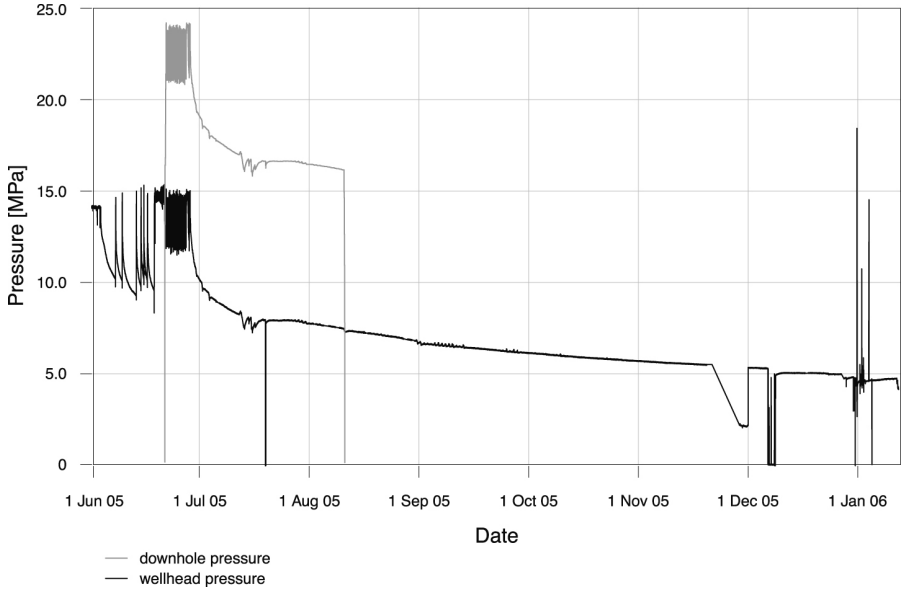

Figure 3.4: Pressure development in time in the MS-3 well in Period 1 (from June 28, 2005 to January 10, 2006). The upper line represents the registration of the downhole pressure from June 21 to August 10, 2006. Registration by the downhole gauges from December 8, 2005 onwards is not represented in this graph. The high peaks that were registered in the wellhead were not registered downhole and were therefore only due to wellhead conditions.

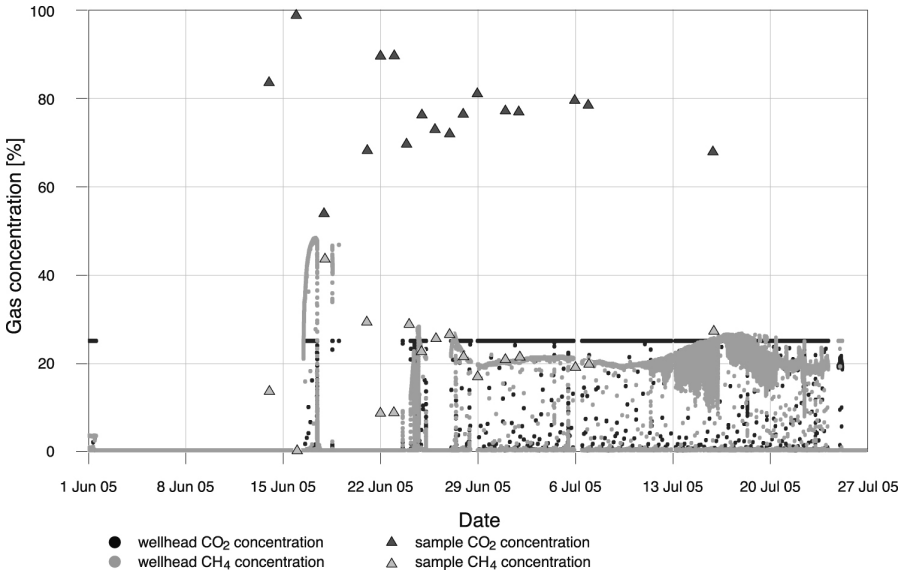

Figure 3.5: Development of gas composition in time in the MS-4 well in June and July, 2005, covering the first part of Period 1 (from June 28, 2005 to January 10, 2006). Note that the instrument could not measure CO_2 concentrations higher than 5% in this period (this was changed for measurements in later periods). Analysis of samples showed CO_2 concentrations of 50% and higher.

Several occasional pressure drops are shown in the fall-off curve, resulting from problems with the wellhead tightness (July 2005), the retrieval and installation of the P-T gauges (August and December 2005), and from the modifications and tests for gas release (November, 2005-January, 2006). Because of these pressure drops in the curve, no permeability could be derived from the curve. However, it can be observed that the pressure decline is extremely slow, which can be an indication of permeability reduction due to swelling.

MS-4 production well

The production rate in the MS-4 well was rapidly decreasing in the last weeks of the production as the downhole pressure was returning to its pre-injection value (Van Bergen *et al.*, 2006). Because pumping ceased from 14 May, 2005 onwards the water was flowing into the well and rising to the surface, thereby slowing down gas production rates. Gas release at very low rates continued until the final shut-in of the MS-4 well in the second half of July 2005. The gas contained about 20% methane at the end of June 2005 (Van Bergen *et al.*, 2006). This concentration increased slightly up to 23% in the second week of July 2005 until final shut-in (Fig. 3.5).

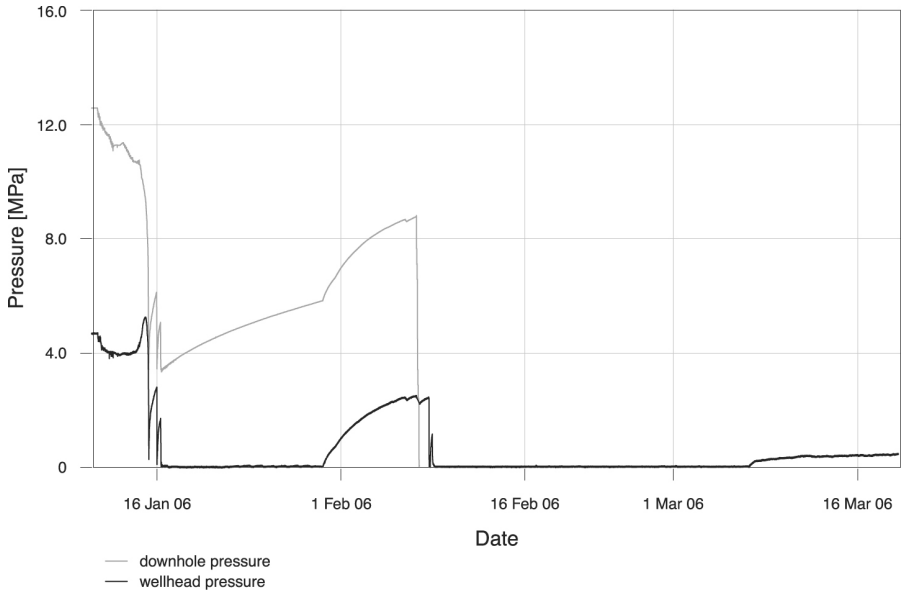

Figure 3.6: Downhole (January 10 to February 7, 2006) and wellhead (January 10 to March 19, 2006) pressure during gas release from MS-3 well in Period 2.

3.3.2 Period 2: Decrease of pressure on the MS-3 well through gas release (January 11, 2006 to March 19, 2006)

Pressure and water level

The first phase of gas release did not show a clear pressure fall-off. The freezing of the installation prevented a continuous gas release. Once this occurred, the well was shut-in and the pressure at the wellhead was increasing rapidly. This pressure, the starting pressure for the next release period, was not stabilized at the time that the installation was defrosted and ready for operation. Because of the gas release, this starting pressure was lower at each period until it was so low that the adiabatic cooling did not result in freezing of the whole installation. This was the case at a starting pressure of 1.73 MPa, which was reached on January 16, 2006.

An increase in pressure at the wellhead was measured on January 15, 2006 that was not observed downhole (Fig. 3.6) and is therefore not related to reservoir pressure. Most likely, this is related to ice development on the wellhead given a local rise in pressure. Once the wellhead pressure stabilized at atmospheric pressure on January 17, 2006 (Fig. 3.6) with ongoing gas production there was no pressure build-up in the system anymore and the measured gas rates represent the gas release rates from the reservoir. From this date onwards the well was open and the pressure increase downhole is due to the inflow of water into the well.

The rise of the water level in the well can be deduced, assuming that the pressure of the gas column is negligible, from the downhole P measurements at 1001 m depth

(Fig. 3.7) with the following formulas.

$$\text{Height of water column [m]} = \frac{\text{Pressure [Pa]}}{(\text{density of water [kg/m}^3] \times \text{gravity [m/s}^2])} \quad (3.1)$$

$$\text{Water level below surface [m]} = 1001 - \text{height of water column [m]} \quad (3.2)$$

This evaluation shows a decreasing inflow rate of water in time. During the shut-in of the well, (January 30 to February 8, 2006) the pressure was building-up as could be observed from both wellhead and downhole pressure measurements. The good correspondence between downhole and wellhead indicates a gas pressure build-up above the water, which is still flowing into the well. The developing gas cap indicates that there is still gas released from the coal seams. The staged retrieval of the P-T memory gauges allowed the estimation of the depth of the water level at 400 m on February 7, 2006. This confirmed the continuous inflow of water during the shut-in period, although at declining rates (Fig. 3.7). Extrapolation of the data in Fig. 3.7 indicates a stabilization pressure in between 6.0 to 8.0 MPa, which approaches the original reservoir pressure in August 2004 of about 8.5 MPa, before injection activities were undertaken (Van Bergen *et al.*, 2006). This implies that the reservoir is returning back to hydrostatic conditions.

Gas production and composition

The gas production rate increased rapidly on January 15, 2006 when the majority of the gas in the well could be released, associated with a large pressure decrease. When the well was depressurized on January 16, 2006 the gas production rates were rapidly declining to about 30-40 m^3 per day. Although these rates are far from being commercial, they were in the same order of magnitude as the production rates of the former MS-4 well. Although comparison is complicated because of the different fracture stimulation of the seams between the MS-3 and MS-4 well, it is an indication that the reservoir conditions in both wells are to some extend analogous. The production rates are declining as the water is rising in the well, thereby hampering further gas release. The well shut-in does not seem to have affected the trend in the production rates (Fig. 3.8).

The very first measurements of gas concentrations showed some gas stratification in the well, indicated by initial high methane concentration in the gas, followed by high carbon dioxide concentration. When all the gas stored in the well was released on January 17, 2006 and the gas from the reservoir was coming to the surface the composition showed a concentration of about 33% methane and 61% carbon dioxide (Fig. 3.9). This concentration of CH_4 is higher than measured in the gas that was produced from the MS-4 well in July 2005. In the week after, the gas composition shows a relatively stable composition of about 40% CH_4 and 60% CO_2 (Fig. 3.9). The

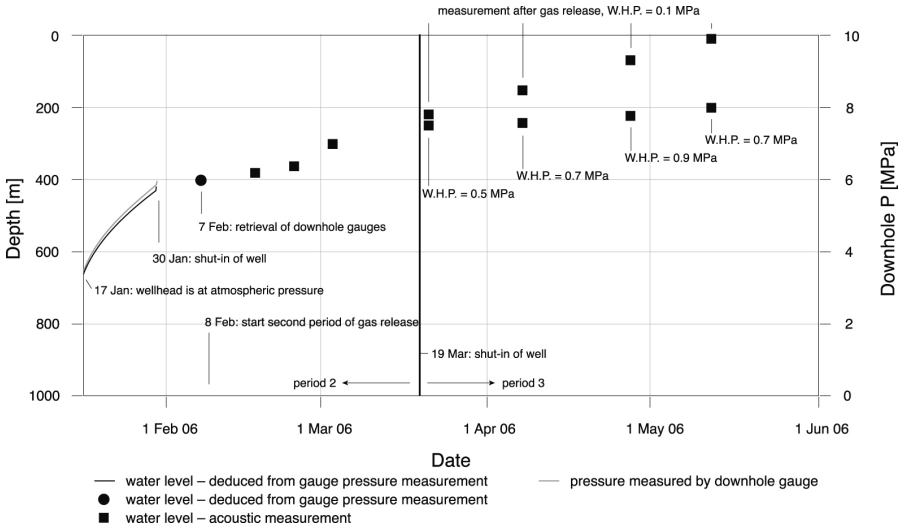

Figure 3.7: Development of water level in the well with time in the period from January 17 (when the wellhead pressure was at atmospheric pressure) to June 1, 2006. The water level in January 2006 was deduced from the measured pressure (also plotted), by assuming a water density of 1050 kg/m^3 and gravity of 9.8 m/s^2. The determination of the water level on February 7 is based on the pressure conditions at several depths as measured during retrieval of the P-T gauges. The Span and Wagner equation of state was used to define the CO_2 density in the gas cap. No water level was deduced from January 30 to February 7, 2006 because in this period the developing gas cap is affecting the pressure measurement, i.e. it can not be assumed that the pressure from the gas in the well is negligible. Measurements of the water level after February 7 were made with an acoustic tool. Measurements in Period 3 are made in two-fold: once when the wellhead is closed and there is a gas pressure and a second time (1-3 h later) when the wellhead is open and at atmospheric pressure. It can be observed that release of gas by opening of the well results in a rise of the water level.

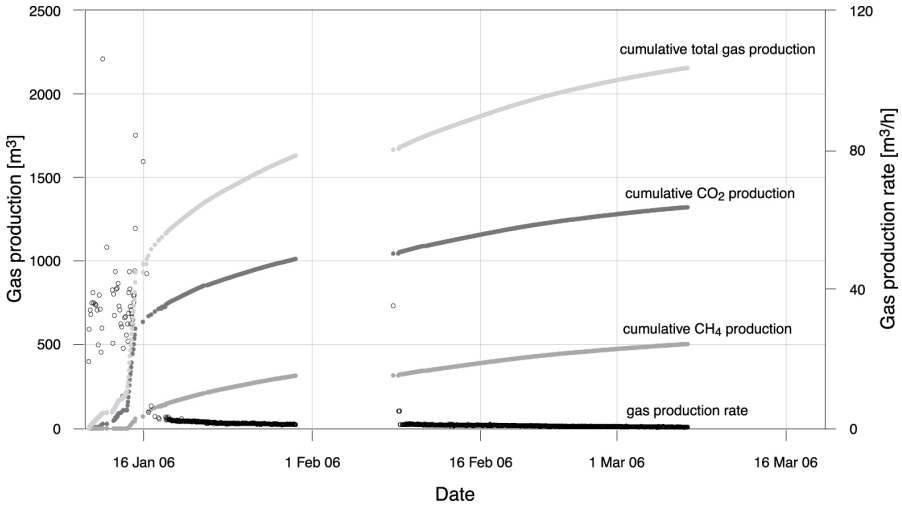

Figure 3.8: Cumulative gas production and production rate in the period from January 10, 2006 to March 19, 2006. Gas production was too low to measure during the last days of this period and is therefore not plotted.

CH_4 concentration appears to increase very slowly until the well shut-in on March 19, 2006 (Fig. 3.9). The well shut-in does not seem to have affected the gas composition, except during the very first phase of gas release on February 8, 2006. The total produced volumes of CO_2 and CH_4 were calculated by multiplying the total gas production by the concentration (Fig. 3.8). This evaluation shows that during the gas release in this period 1322 m^3, or 2.5-3.0 tonnes CO_2 were produced back from the reservoir. Gas production ceased with the shut-in of the well on March 19, 2007 when production rates were low and declining.

3.3.3 Period 3: Placement of pump for production of gas from the MS-3 well (20 March 2006 - 20 March 2007)

During the reconstruction of the well, the well was filled with water up to the surface. This provided an overpressure in the reservoir, ceasing gas production. Gas composition measurements from samples taken at the wellhead from November, 2006 to March, 2007 show an increase in CO_2 concentration and a decrease in CH_4 concentration. It seems more likely that this mirrors the situation in the well during standstill rather than any reservoir conditions. Sampling probably preferentially removes the lighter CH_4 that is concentrated in the wellhead, leaving lower concentrations of CH_4 in later gas samples. It seems unlikely that there is much release of gas from the coal seams into the well, which provides a 1 year soaking period of the gas into the coal during the operational pause.

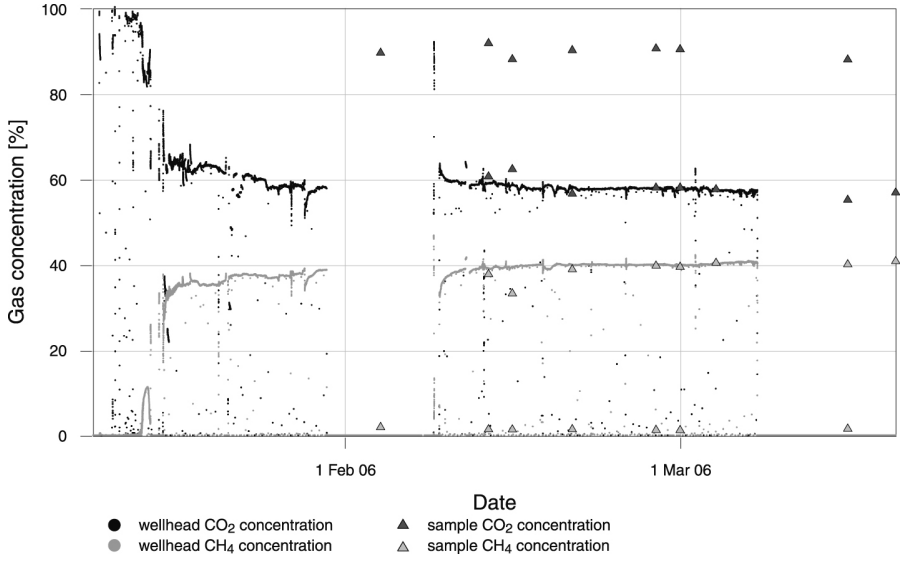

Figure 3.9: CO_2 and CH_4 concentration in the produced gas during gas release in Period 2. Gas composition was measured every 15 seconds by a Siemens Ultramat 23 gas analyzer. In addition, samples were taken and analyzed in the laboratory. At several occasions, two samples were taken within 5 minutes. The samples that are taken first show a high CO_2 and low CH_4 concentration that is different from the analyses of the Siemens analyzer, while the second samples show a composition in agreement with the measurement of the analyzer. Apparently, there is CO_2 enrichment in the first samples that is not representative for the reservoir gas.

3.3.4 Period 4: Production of gas from the MS-3 well (March 21, 2007 to September 18, 2007)

Pressure and water level

With the start of the pumping and the emptying of the well in the first days of operation the pressure in the well was reduced to atmospheric conditions. After the initial phase, the water level was kept below the perforations at all times in this period.

Gas production and composition

The start of the pumping of the well was characterized by a production of a water-gas mixture. This hampered the proper measurement of the gas and water production, probably resulting in a erroneous measurement of the amount of water produced in this first phase. An estimated volume of 12 m^3 seems more likely than the reported 34 m^3. At the time that the water was below the perforations, the active production resulted in gas production rates of about 70 m^3 per day, in the same order of magnitude as in the beginning of the continuous gas release in Period 2 (30-40 m^3 per day in January 2006). The water production, however, was much lower than expected based on the experience with the production well. In the first week the water was produced that filled the well volume. From March 24, 2007 the production rate of water is rapidly decreasing which is associated with the first production of water from the wellbore zone. From this point onwards it was sufficient to operate the pump for about 15 minutes every three days to keep the water level below the lowest perforations. The volume of water produced in these 15 minutes was very low and declining from about 0.10 m^3 at the beginning of April 2007 to about 0.05 m^3 in mid-September 2007. The rate of gas production was declining over the production time (Fig. 3.10).
Further, the gas composition showed a predominance of CO_2 over CH_4 during the gas release that changed gradually into a predominance of CH_4 over CO_2 during the production phase. Although stabilization was not reached within the production period, the composition approached a 60% methane, 40% CO_2 ratio (Fig. 3.11). The cumulative amount of CH_4 and CO_2 produced in this period are 4134 m^3 and 4157 m^3 ($\sim$ 8 tonnes), respectively (Fig. 3.12).

Composition of the produced water

The composition of the original reservoir water could be established with good confidence from the produced water of the MS-4 well (Van Bergen *et al.*, 2006). This reservoir water was highly saline (approximately 140 kg/m^3) and dominated by sodium and chlorine ions. After injection of the CO_2 the pH decreased slightly from about 6.5 to a value of about 6 while the bicarbonate concentration was increasing, up to 400 mg/l in May 2005. These were interpreted as clear indications that the CO_2 was dissolving into the water (Van Bergen *et al.*, 2006).

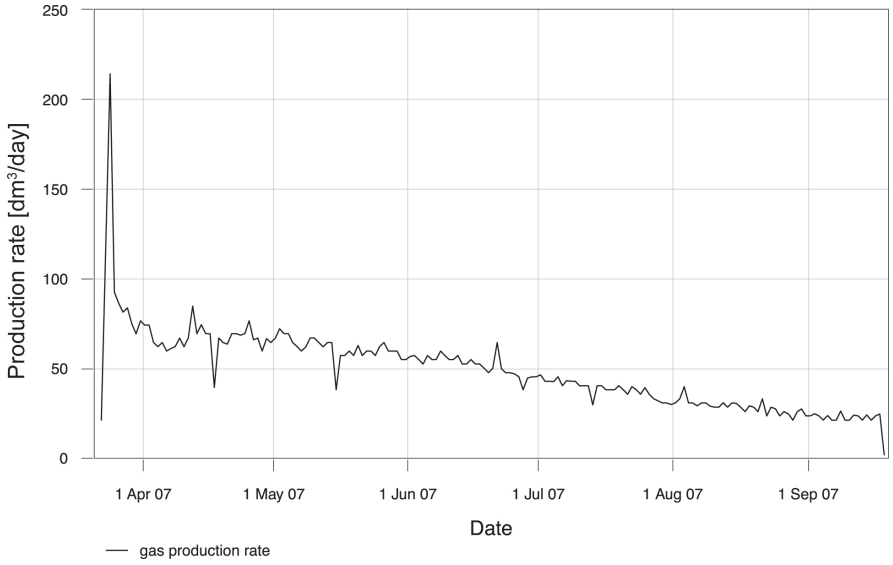

Figure 3.10: Production rate of the gas during Period 4.

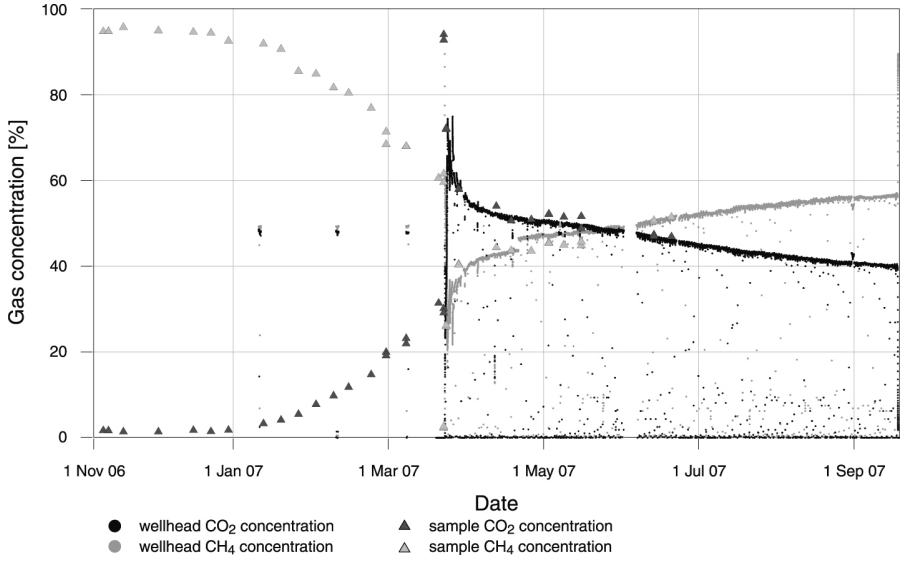

Figure 3.11: Concentration of CH_4 and CO_2 in time in Period 4. Gas composition was measured every 15 seconds by a Siemens Ultramat 23 gas analyzer. In addition, samples were taken and analyzed in the laboratory. Note the high CH_4 concentrations in the samples taken before the active pumping started. This is likely the result of some stratification in the well during standstill of the operations and is not considered to represent the composition of the gas in the reservoir.

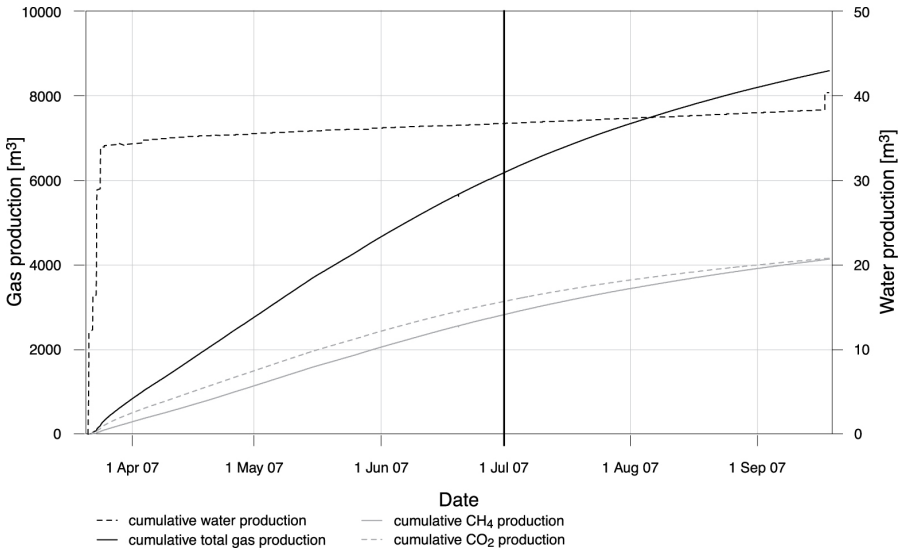

Figure 3.12: Cumulative production of water, total gas, and of CH_4 and CO_2 in time in Period 4. The value for water production in the first phase of the production is probably incorrect. Probably, too high values were measured because of a mixture of water and gas (gas lift) in this phase. An estimated volume of 12 m^3 seems more likely than the reported 34 m^3. July 1, 2007 is, subjectively, indicated as the start of a period where fluids from the reservoir outside a wellbore zone are produced (see discussion).

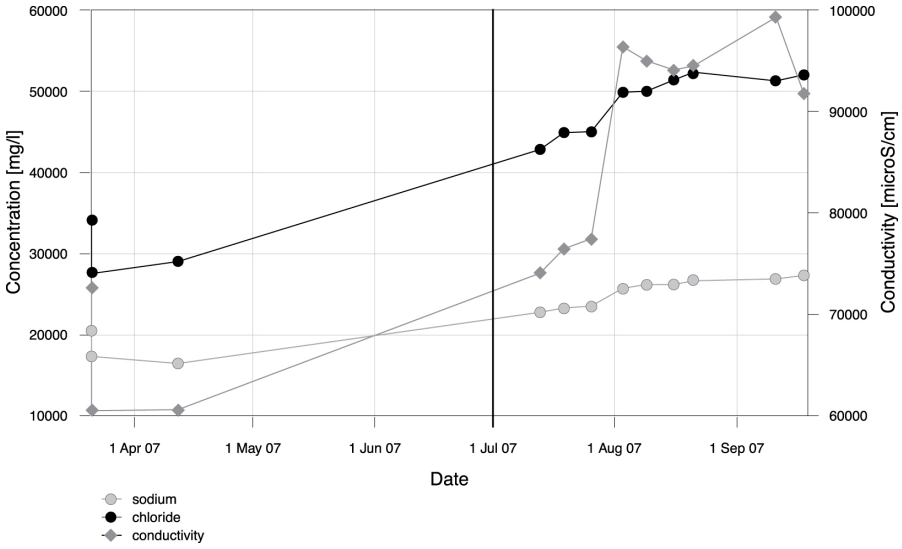

Figure 3.13: Development of concentrations of sodium and chloride in the production water and its conductivity in time. July 1, 2007 is, subjectively, indicated as the start of a period where fluids from the reservoir outside a wellbore zone are produced (see discussion).

The analyses of the samples taken from the water produced in the MS-3 well showed that the salinity was much less (30 kg/m^3) than the original reservoir water, probably due to the use of fresh water during the creation of the fracture in April 2005 (Fig. 3.13). The fracture fluid was pre-mixed using fresh water (no KCl has been added) and included the pH-buffer and polymer breaker. A borate crosslinker was added during pumping. Fracture fluid was injected in two stages: firstly about 20 m^3 were injected without proppant and secondly about 30 m^3 were injected with proppant. Part of the injected fluid was recovered by cleaning of the well using nitrogen with a coiled tubing. The volume of water that remained in the reservoir is therefore less than the amount that was injected during the hydraulic fracture treatment. The fact that this fresh water is still present implies that this water was not replaced by the injection of the CO_2 in the period after the fracture stimulation. This seems to confirm the interpretation of Van Wageningen and Maas (2007) who posed that the early breakthrough of the CO_2 was caused by a gravity override of the CO_2 on top of the water phase. The increase in the salinity indicates a further mixture with reservoir water further away from the well.

The plot of the concentrations of trace elements in time shows that especially the nickel and manganese concentrations are very high in the beginning (Fig. 3.14). This manganese and nickel are likely to be a product of the corrosion of the well. A logging analysis showed that some corrosion ($<$ 1mm) took place in the lower part of the well, without affecting the integrity of the well. From April to July 2006 the concen-

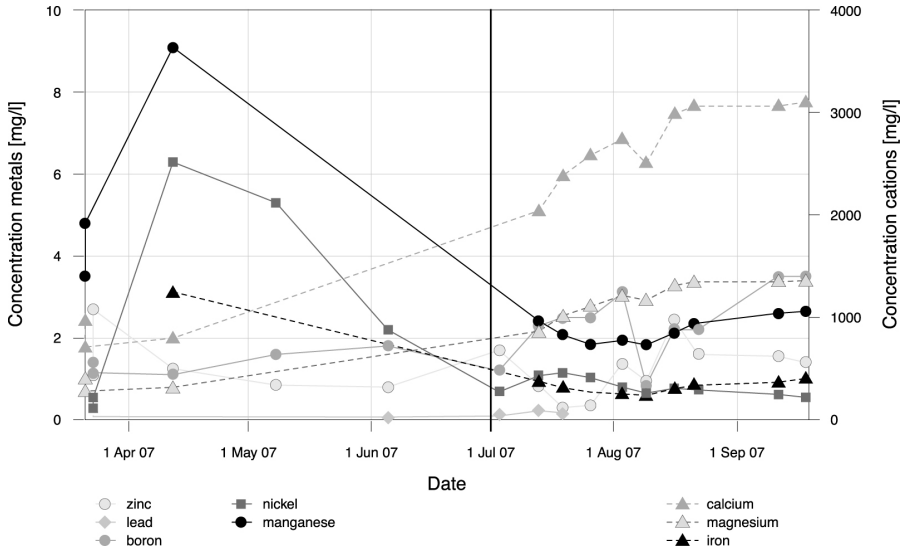

Figure 3.14: Development of concentrations of cations in the production water in time. July 1, 2007 is, subjectively, indicated as the start of a period where fluids from the reservoir outside a wellbore zone are produced (see discussion).

trations of these metals are decreasing until they seem to be back at their background value in the formation water in the course of July 2006. Although no exact date can be indicated where this change occurred exactly, July 1, 2006 is subjectively considered the date from which point onwards water was produced from outside the wellbore zone. The total amount of water produced between March 24, 2007 (when first water from the wellbore zone was produced) and July 1, 2007 is 2.8 m^3.

In the first phase of the production the water shows a high bicarbonate concentration of more than 3000 mg/l, about 50 times higher than the background value (~ 50-70 mg/l) and more than 7 times higher than measured in the production water of the MS-4 well in May 2005. Clearly, some of the CO_2 has dissolved into the water (Fig. 3.15). As expected, there is a correlation between the concentration of bicarbonate and the value of the pH (Fig. 3.15). The drop in pH is, however, not so dramatic which shows the buffering capacity of the highly saline water. The dissolution of minerals into the water as a result of the lower pH seems to have been limited, as there is no pronounced increase of calcium or magnesium concentrations. The pH is increasing during the production, while the bicarbonate concentration is decreasing. The rate of change of the bicarbonate concentration and pH are declining during July 2007, at about the same time that the nickel and manganese were back to their background value (Fig. 3.14).

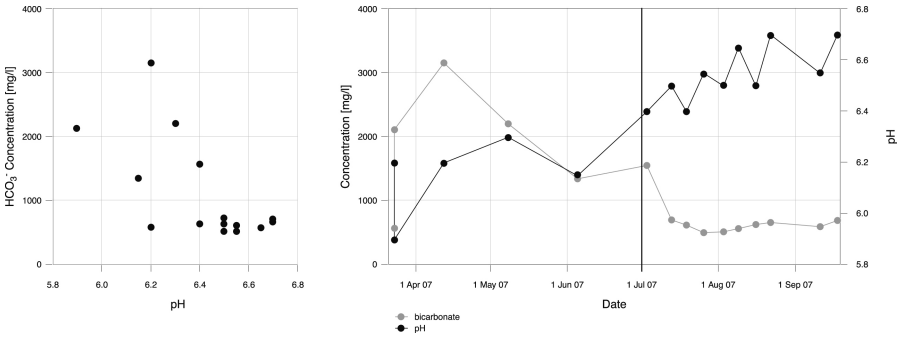

Figure 3.15: Left: pH vs. bicarbonate concentration. Right: development of bicarbonate concentration and pH in time. July 1, 2007 is indicated as a transition between the fluids from a wellbore zone and from the reservoir (see discussion).

3.3.5 Period 5: Abandonment (September 19, 2007 to November, 2007)

Both the test with water and the DST test showed that the perforations were still open and that there is still sufficient permeability in the system to inject some water.

3.4 Discussion

The activities and results during the post-injection period reported in this paper can not be considered independently from those before and during the injection of the CO_2. Coal swelling is considered to have occurred before the hydraulic fracture treatment was executed. The permeability after the creation of the fracture was sufficiently high to allow continuous injection, although at high injection pressure. However, as indicated by Van Bergen *et al*. (2006) this was not a fixed situation. After periods where the continuous injection was temporarily stopped higher injection pressures where required to reach similar injection rates as before the injection pause. This was considered to be an indication that the reservoir becomes tighter, probably related to swelling of the coal (Van Bergen *et al*., 2006). Once continuous injection was established the injection pressure slightly decreased at the same injection rate, indicating that part of the permeability could be recovered. However, subsequent pauses in the injection were again associated with a decrease in injectivity. This seems to be confirmed by the slow fall-off curve of the first period in the post-injection period, indicating a low permeability. Probably, this can be explained by further swelling of the coal. Laboratory experiments on samples from the same coal seam have confirmed that these coals are susceptible to swelling under a CO_2 at in situ pressure and temperature conditions (Mazumder *et al*., 2006a). The rate of water inflow in the MS-3 well during the production period (Period 4) was much lower than could be expected, even considering the low production rates of water in the MS-4 well. This could be explained by the low permeability as a result of the swelling. Nevertheless,

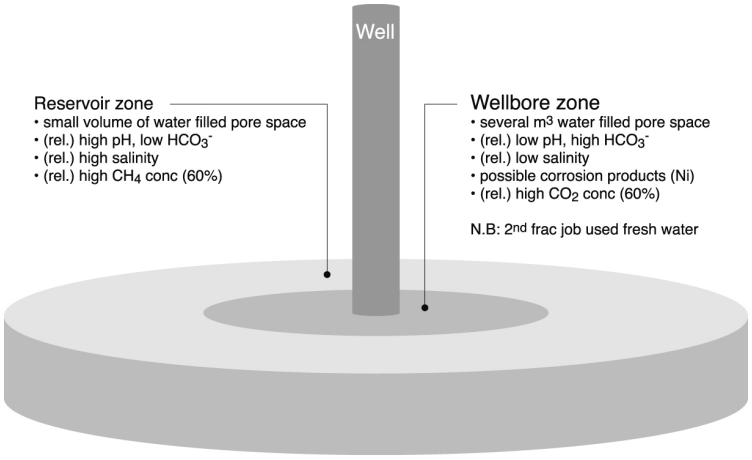

Figure 3.16: Simplified scheme of the anticipated situation.

the gas production rates of the MS-3 well were comparable to the rates measured in the former MS-4 production well, although it must be noted that a quantitative comparison is complicated because of the differences in seam fraccing and well completions. The declining rates of both water and gas could indicate a further closure of the transport system of the coal during the production period. However, it is difficult to distinguish this effect from other processes that may have occurred. The low rates could also be an indication of a drying effect of the CO_2 in the reservoir, as water can dissolve into the CO_2 phase. The CO_2 could also have pushed away the water further away in the reservoir, which is than unable to flow back as the cleats of the coal closed when the pressure in the reservoir decreased.

The reported results indicate a situation where there is a clear change between a wellbore zone and a reservoir zone. The wellbore zone is characterized by a relatively low pH, high bicarbonate concentration and a low salinity. The volume of this zone is difficult to asses given the uncertainties in the water measurements at the start of Period 4, but is expected to be in the order of several m^3. The water in this zone probably contains corrosion products of the well. The gas contains relatively high amounts of CO_2 (60%) compared to methane (40%). The wellbore zone is likely to be the zone that is affected by the frac stimulation as performed in April 2005. The water in the reservoir zone has a relatively high pH, low bicarbonate content, and a high salinity. This seems to suggest that this water has not been in contact with CO_2, but this is considered to be unlikely given the amount of CO_2 that was injected. The buffer capacity of the high saline water is probably a better explanation for this. The gas is richer in CH_4 (60%) than in CO_2 (40%). These observations are schematically visualized in Fig. 3.16.

The results of the gas and water production during period 2 and 3 were different

than was expected. Two scenarios were envisaged before the gas release operations took place. In the first scenario, no CO_2 adsorption would take place. This scenario was thought feasible because of the very low rates of the baseline gas production (Van Bergen *et al.*, 2006). As the desorption tests from the cores indicated very slow diffusion out of the coal cores, it could be expected that diffusion into the coal was also very slow. Since 692 tonnes of CO_2 were still in the reservoir, this would have resulted in an overpressured reservoir. The gas release and production operations would have resulted in the production of almost the total amount of injected CO_2. Clearly, this scenario has not become reality. The pressure fall-off during period 1 indicated (slow) migration of the gas away from the wellbore zone or into the coal. Only 2-3 tonnes of CO_2 were produced back during period 2, and about 8 tonnes during period 4. This indicates that only 1-2% of the injected CO_2 was produced back when the reservoir returned to its initial hydrostatic conditions. The second scenario was the adsorption of CO_2 into the coal where it would exchange with the CH_4 that is present on the internal coal surface, because of its higher affinity for CO_2. This is the process that is generally considered to be responsible for the enhancement of the gas production in ECBM operations. If this process would have taken place, this would have resulted in a clear increase in CH_4 production and content. Instead, the actual results showed a slow stabilization of the composition of the gas, with 40% CO_2 and 60% CH_4 at low production rates. These results suggest that while significant amounts of CO_2 are able to diffuse *into* the coal, there is hardly any diffusion of CH_4 *out of* the coal.

Alternative explanations of the fate of the injected CO_2 have also been considered. Migration of CO_2 into overlying sandstones would have resulted in a higher volume of produced CO_2 when the pressure in the well was lowered. Migration into the overburden is considered unlikely, given the sequence of Pennsylvanian sediments in the overburden with shales and tight sandstones. A monitoring program was setup around the injection site, including soil gas sensors and measurements in a nearby coal mine. The soil gas monitoring did not indicate any changes out of the ordinary in CO_2 concentrations, fluxes or isotope signature. The mine was positioned on the opposite side of the western bounding fault of the tectonic block where the site is located. Analyses of gas samples taken in the mine showed changes in the isotopic signature. However, this change was definitely inconclusive with regard to CO_2 migration through the fault because of other influencing factors in the mine. If the total amount of CO_2 would have migrated through the fault, the change in isotopic signature should have been much more dramatic than the subtle change observed. Another scenario that was considered is dissolution in the water. Although dissolution is proven by the high bicarbonate concentration, the amount of water appears to be too small to contain that much CO_2.

In conclusion, the CO_2 is probably diffused into the coal between June 2005 and March 2007 and is stored in the coal due to adsorption to the coal surface. The CO_2 is strongly fixed to the coal, as pressure release by water production did not result in release of the CO_2. The release of pressure in the reservoir probably added to the

fixation by closing of pores. Also, coal swelling due to the adsorption of CO_2 may have eventually sealed the coal matrix. However, it is unclear why this adsorption was not accompanied by desorption of the CH_4. The presence of CH_4 was clearly identified by the coal cores, although most was residual gas after the canister desorption testing. The stable gas composition indicates that the exchange of the gases is more complex than often envisaged. Clearly, the often reported exchange ratio of 2 molecules of CO_2 for 1 molecule of CH_4 is too simplistic given the results of this field study.

3.5 Conclusions

The activities undertaken in this study have been very useful to learn about operational issues related to ECBM and to acquire a general understanding of processes that operate under in-situ conditions. Several operational problems have been encountered and were solved. Especially, the release and measurements of a high pressure gas with a high CO_2 concentration required caused more effort than originally anticipated. In the course of the operations some modifications had to be made in the original designs, especially because gas and water rates and gas compositions were different than beforehand estimated. On this basis, flexibility in the operational equipment and metering tools is highly recommended.

The results of this study show many features that were unexpected beforehand, indicating that field studies are mandatory, next to theoretical and laboratory work, to comprehend the complexity of the coal-water-CO_2 system The understanding of the in situ processes with regard to matrix diffusion and strain development is crucial in planning an operational phase of any ECBM project. Also, not all observations can be explained from the common theory, demonstrating that the interaction between CO_2 and coal under reservoir conditions is still a research issue. Nevertheless, significant progress is made since the start of the field activities. History matching of the results could improve the understanding of the processes that are taking place in the reservoir. The use of numerical simulators proved to be a strong analytical tool for quantifying some of the effects observed during the injection period (Van Wageningen and Maas, 2007). However, experience from numerical simulations in various software models for the injection period showed that the prediction of the behavior beforehand by numerical models is still difficult. Progress in the understanding of the reservoir processes may help in improving the predictive capabilities of the numerical models.

As the total volume of CO_2 produced was only a fraction of the amount that was injected, it can be concluded that the CO_2 was taken up by the coal and is currently adsorbed. This gives confidence in the long-term stability of the injected CO_2. The direct relation between CO_2 adsorption and CH_4 desorption could not be confirmed in this study. Therefore, the option of injecting CO_2 in a depleted CBM field, thus after active production, without further production should be seriously considered.

In this case, the coal would be used purely as a storage medium. However, it must be emphasized that extrapolation of the results of this study to other locations should be done with care as the reservoir conditions of coal seams vary enormously, even over short distances. Coal in the subsurface still holds a large potential storage medium for CO_2, but the complexity of the system makes the implementation of larger scale projects more complicated than other subsurface options, like depleted gas fields. As such, ECBM is considered a niche option in Europe for those areas where alternatives are not readily available. In other parts of the world, where unminable coal is abundant and there are hardly any alternative options for CO_2 storage ECBM might become crucial in climate friendly energy production. However, it seems vital to have a well-developed CBM industry in place before ECBM can be realized.

Acknowledgements

The European Commission is thanked for funding and support of the RECOPOL and MOVECBM (no. 038967) projects. Shell International, JCoal, the Federal Region of Wallonie (through the Facult Polytechnique de Mons) and the Polish and Dutch governments (via Novem) are thanked for their support to RECOPOL. Shell International, Schlumberger, Air Liquide, Central Mining Institute and TNO are acknowledged for funding and supporting the transition period. We are grateful for the endusers of the MOVECBM project: Electrabel, Carbosulcis and Veolia Environment. The RECOPOL and MOVECBM projects are a team effort, with contributions from all partners of the international consortium. All are acknowledged for their contributions and financial support: Central Mining institute, Delft University of Technology, Aachen University of Technology, Air Liquide, DBI-GUT, Gaz de France, IFP, IEA Greenhouse Gas R & D Programme, CSIRO, GAZONOR, ARI, TNO, Shell International, University of Roma, University of Mons, Utrecht University, SKLCC, OGS, ERICO, OXAND, RIPED, EPS and CUCBM. Maartje Hamers and Mariette Jongen are thanked for their efforts in making the dataplots and figures of this paper. Elsevier is acknowledged for granting permission to reprint this article in the thesis.

Chapter 4

Strain development in unconfined coals exposed to CO_2, CH_4 and Ar: Effect of moisture

Frank van Bergen, Chris Spiers, Geerke Floor & Pieter Bots

This chapter was published as:
Van Bergen, F., Spiers, C., Floor, G. & Bots, P. (2009). Strain development in unconfined coals exposed to CO_2, CH_4 and Ar: Effect of moisture. International Journal of Coal Geology, 77(1-2): 43-53.

Abstract

Field experiments and laboratory studies have shown that swelling of coal takes place upon contact with carbon dioxide at underground pressure and temperature conditions. Understanding this swelling behavior is crucial for predicting the performance of future carbon dioxide sequestration operations in unminable coal seams conducted in association with methane production. Swelling is believed to be related to adsorption on the internal coal surface. Whereas it is well established that moisture influences the sorption capacity of coal, the influence of water on coal swelling is less well-defined. This paper presents the results of laboratory experiments to investigate the effect of moisture on coal swelling in the presence of carbon dioxide, methane and argon. Strain development of an unconfined sample of about 1.0-1.5 mm^3 at 40°C and 8 MPa (and at other pressures) was observed in an optical cell under a microscope as a function of time. Both air dried and moisturized samples were used. Results confirmed different swelling behavior of coal with different substances: carbon dioxide leads to higher strain than methane, while exposure to

argon leads to very little swelling. The experiments on moisturized samples seem to confirm the role of moisture as a competitor to gas molecules for adsorption sites. Adsorption of water could also explain the observed swelling due to water uptake at atmospheric pressure. A re-introduction of carbon dioxide, after intermediate gas release, results in higher strains which indicate a drying effect of the carbon dioxide on the coal. The results of this study show that the role of water can not be ignored if one wants to understand the fundamental processes that are taking place in enhanced coalbed methane operations.

Key words: swelling; carbon dioxide; methane; argon; moisture

4.1 Introduction

Interest in the storage of carbon dioxide (CO_2) in underground coal seams coupled with enhanced coalbed methane production forms a topic of ongoing interest in the energy sector. Several demonstration projects (e.g. in Canada, U.S.A., Poland, Japan and China) have shown the potential of enhanced coalbed methane (ECBM) production, though commercial application still has to be realized. Most of these sites have experienced permeability reduction in the coal seam, sometimes leading to operational difficulties such as reduced injectivity with time. This reduction of permeability is generally considered to be caused by swelling of the coal as the result of CO_2 injection. Understanding and managing the development of swelling with time will be one of the most critical factors determining the success of future ECBM sites. There have accordingly been various laboratory studies of this phenomenon in recent years (e.g. Day *et al*., 2008; Karacan, 2003; Karacan, 2007; Mazumder *et al*., 2006a; Mazumder *et al*., 2006b; Robertson and Christiansen, 2005a). Much has been learned from these studies but the effects of water are not well known. Aside from transport through the cleat system, it was demonstrated that gas transport through the coal matrix can be a key parameter determining the performance of ECBM production in the field (Van Bergen *et al*., 2006). Therefore we focus in this study on the swelling behavior of matrix blocks of coal. We report results on the swelling behavior of unconfined coal exposed to CO_2, methane (CH_4) and argon (Ar) at pressures up to 8.2 MPa and at a temperature of 40°C. These were obtained through microscopic observations performed in an optical cell with the specific purpose of investigating the role of moisture.

4.2 Background

It is well known that many solids show marked swelling as a result of the uptake of a gas, liquid or supercritical fluid (Adamson and Gast, 1997). Coal is one of these solids where ad- or desorption by the matrix may lead to a volumetric response. Matrix shrinkage as a result of gas release has been reported in literature, and is assumed to be related to desorption and as such to the external gas or fluid pressure (e.g. Harpalani and Chen, 1997; Harpalani and Schraufnagel, 1990; Mavor and

Gunter, 2006; Palmer and Mansoori, 1996; Palmer and Mansoori, 1998; St. George and Barakat, 2001). Swelling of coal under gas pressure has been confirmed by several studies (Goodman *et al.*, 2005b; Goodman *et al.*, 2006; Karacan, 2003; Karacan, 2007; Larsen, 2004; Robertson and Christiansen, 2005a). Besides adsorption this swelling effect is also attributed to dissolution into the coal matrix (absorption) associated with structural changes in the coal matrix (Goodman *et al.*, 2005a; Goodman *et al.*, 2005b; Goodman *et al.*, 2006; Karacan, 2003; Larsen, 2004; Mazumder *et al.*, 2006a; Mazumder *et al.*, 2006b; Mazumder *et al.*, 2006c). These changes can be related to observed changes in elastic modulus in coal after fluid treatment (Viete and Ranjith, 2006). Extraction of some hydrocarbons by CO_2 or other fluids may also occur (Kolak and Burruss, 2006).

A larger volumetric change in coal is observed for CO_2 sorption compared to CH_4 sorption. This may reflect a higher sorption affinity (St. George and Barakat, 2001). However, Pan and Connell (2007) report that even when the adsorbed volume of gas or fluid is the same, coal experiences a higher strain in case of CO_2 sorption. This may be due to other effects that may be occurring in parallel with physical gas adsorption.

Less well-known is the relation between water and coal swelling. Coal seams in the subsurface always contain water, because they were originally deposited as peat layers under humid or wet conditions. It takes an advanced coalification stage to drive out all the water from the coal. Three different forms or phases of water can be distinguished in the typical coal matrix material: a) free and capillary water filling macro- to mesopores, b) adsorbed water on the internal surface area of the pores, and c) bound (absorbed) water in the coal structure. It is possible that adsorption of water by the coal matrix and imbibition (i.e. absorption) of water into the solid structure of the coal is associated with a volumetric increase of the coal. This was demonstrated by Walker *et al.* (1988). Day *et al.* (2008) reported slight shrinkage as the result of the loss of moisture. Swelling caused by adsorption of water is never large, due to limited chemical and physical interactions of the coal structure with water. Swelling due to imbibition of water can range from negligible to large, depending on the extent of chemical or physical interaction of the fluid with the coal structure. The main cause of swelling in coal is attributed to the formation of hydrogen bonds between water and by oxygen bearing functional groups, like phenolic carboxyl and hydroxyl groups (Gutierrez-Rodriguez *et al.*, 1984; Nishino, 2001; Prinz and Littke, 2005; Walker *et al.*, 1988). These are also the functional groups where CO_2 adsorption is likely to take place. As such, it can be expected that there will be direct competition for adsorption sites between water and CO_2 molecules, though coverage of micropores by water is only a fraction of that found for CO_2 (Walker *et al.*, 1988). The competition between water and CO_2 molecules may be reflected in the swelling behaviour of moisturized coal samples. This competition will be less between water and CH_4, because this gas tends to bind to other types of adsorption sites (Krooss *et al.*, 2002; Nishino, 2001). There is a need to test different types of coal because the amount of swelling due to water adsorption is related to the rank of the coal (Walker *et al.*, 1988). An under-

standing of the role of water in coal during gas or supercritical CO_2 uptake may be crucial to predict coal swelling in the field.

4.3 Samples

4.3.1 Sample material

Our optical cell enabled us to study the 2-D swelling behavior of small cubical fragments of coal of the order of 1-1.5 mm^3 in volume, as well as similarly sized control samples. The various materials used are described below.

Metal sample for control experiment

A stainless steel sample was used for a control experiment in order to study the influence of the refractive index of CO_2 filling the optical cell and to test the overall procedure. The same conditions and experimental set-up was used as for the testing of coal samples. The cylinder-shaped sample had a diameter of 1.4 mm and a thickness of 0.74 mm.

Bituminous coal

Bituminous coal sample material was taken from seam 364 at a depth of 640-740 m in the Brzeszcze coal mine in the Upper Silesian Basin in Poland. The Brzeszcze mine is located at about 5 km from the ECBM field test reported by Van Bergen *et al*. (2006). The mined coal samples in this basin are of Pennsylvanian (Upper Carboniferous) age (Van Bergen *et al*., 2006). The dominant maceral in the coal is vitrinite (59.8-66.0%), with additional inertinite (26.4 to 30.0%) and liptinite (7.6 to 9.8%) in the bulk coal. The coal samples were taken in bulk and were air dried. Proximate analysis showed about 30% volatile matter, 5-7% ash, 65% fixed carbon, and a moisture content of 2.5-3%. This moisture represents the inherent moisture of the coal, according to the definition by Ward (1984). Ultimate analysis indicated a carbon content of about 75% and a sulphur content of about 0.5 - 0.6%. Vitrinite reflectance is 0.77% $\pm$ 0.05%.

Subbituminous coal

Subbituminous coal sample material was obtained from the Monte Sinni coal mine (Carbosulcis) located in the Sulcis Coal Province in Sardinia, Italy. The composition of the samples used for this study has not been analysed, but this type of coal has been the subject of adsorption studies by Ottiger *et al*. (2006). These authors determined coal composition for their samples to be 49.4% fixed carbon, 41.2% volatile matter, 2.1% ash, and 7.3% moisture. The values should be considered indicative for the samples used in the present study. Vitrinite reflectance was determined to be 0.43% $\pm$ 0.05%, in agreement with the values reported by Dreesen *et al*. (1997), but significantly lower than the rank as determined by Ottiger *et al*. (2006). The subbituminous coal from the Monte Sinni mine is known to have remarkably low moisture

content for coal of this rank. Care should therefore be taken with extrapolation of the results of this study to subbituminous coal samples from other locations.

4.3.2 Sample preparation

The bulk coal samples were first broken into smaller fragments of a few cm^3. From those pieces, small blocks were prepared with a volume of about 1-1.5 mm^3 (~ 1.2-1.4 mm wide and 0.7-0.9 mm height) by sawing into parallel sided plates with a diamond saw. These plates were then cut into cube-like samples with a scalpel. The samples were cut in such a way that the plane of view in the optical cell is perpendicular to the sedimentary layering, i.e. more or less parallel to the face cleats.

Some of the samples were moisturized following the guidelines of the ASTM D1412-04 standard test method. This and similar methods have been widely used for moisturizing coal in previous sorption and related experiments on coals (Krooss *et al.*, 2002; Mavor *et al.*, 1990; Prinz and Littke, 2005). The method exposes coal samples in a dessiccator to a controlled environment with 96% humidity whereby an equilibrium moisture content is reached that is closely similar to natural coalbed moisture content (van Krevelen, 1993). In our application of the method, the ASTM D1412-04 procedure was slightly modified to facilitate the experimental procedure, due to practical restrictions and to suit the sample material. The samples were not shaken in a flask to prevent damage to the coal blocks. To compensate for this, and because the samples are slightly bigger than mentioned in the standard method, the equilibration time in the desiccator was extended (4 days or longer instead of 2 days for bituminous coal and 3 days for lignite; see Tab. 4.1)

4.4 Methodology

4.4.1 Experimental set-up

A see-through high-pressure cell was used for the experiments consisting of a circular stainless steel casing with two opposing Pyrex lenses. EPDM o-rings around the lenses prevent gas leakage. A titanium ring placed coaxially between the lenses, with a thickness of 1.0 mm and an inner diameter of 1.6 mm, acts as a sample holder. Unconfined samples of 1.0 to 1.5 mm^3 placed in the inner space of the ring are able to swell in all directions. Slots in the titanium ring guarantee gas access to the inner space. The cell was connected with a stainless steel tube to a gas supply system. Ar, CO_2 and CH_4 can be used in this system. For CO_2 and CH_4 pressures higher than standard supply cylinder pressures were reached using an argon-backed separator or gas-booster, which enabled pressures over 10.0 MPa to be reached. Ar was introduced into the system directly from the supply cylinder. The cell is heated using embedded elements regulated by an analogue CAL 9900 temperature controller connected to a K-type thermocouple placed against the sample holder. During the full duration of each experiment the cell was placed under a microscope system, a Leica

Table 4.1: Overview of the different strain development experiments performed. All samples are air dried (before moisturizing). The top surface of sample BIT3 was covered by a thin gold layer to test improvement of contrast in the scope image. The thin gold surface cover was assumed to be inert.

Exp. no.	Material	Gas	P(MPa)	T(°C)	Time on P	Comments
Control experiment						
S1	Steel	CO_2	8.0±0.2	40±2	-	
Experiments with air dried coal samples						
BIT1	Bit. coal	Ar	8.0±0.2	40±2	24 h	
BIT2	Bit. coal	CH_4	7.9±0.2	40±2	40 h	Difficult to find recognizable points (low contrast)
BIT3	Bit. coal	CO_2	8.0±0.2	40±2	17 h	Surface with gold layer
BIT4	Bit. coal	CO_2	8.0±0.2	40±2	22 h	
BIT5	Bit. coal	CO_2	8.0±0.2	40±2	24 h	
BIT6	Bit. coal	CO_2 (twice)	8.1±0.1	40±0.5	2*24 h	
BIT7	Bit. coal	CO_2 (multiple)	2.7±0.1 5.3±0.1 8.2±0.1	40±0.5	3*24 h	
SUB1	Subbituminous coal	CO_2	8.1±0.1	40±0.5	24 h	
SUB2	Subbituminous coal	CO_2	8.1±0.1	40±0.5	24 h	
Experiments with moisturized coal samples						
BIT8	Bit. coal, moist	Ar (twice)	8.1±0.1	40±0.5	2*24 h	Moisturizing: 6 days in dessiccator at P=0.05 MPa, T= 30°C
BIT9	Bit. coal, moist	CO_2 (twice)	8.1±0.1	40±0.5	2*24h	Moisturizing: 4 days in dessiccator at P=0.05 MPa, T= 30°C
BIT10	Bit. coal, moist	CO_2 (twice)	8.1±0.1	40±0.5	2*24h	Moisturizing: 5 days in dessiccator at P=0.05 MPa, T= 30°C

DM RC using a 5 times magnification objective lens. A Leica DC300 CCD camera was connected to the microscope and to a computer with the Leica Qwin software to obtain pictures with a resolution of 2088 by 1550 pixels, representing 2.3mm by 1.7mm (1 pixel length ~ 1.1 μm). A routine was developed to take pictures automatically with a time interval of 10 s or more.

4.4.2 Experimental procedure

The pressure and temperature of most experiments were maintained at 8.0 MPa and 40°C, i.e. at values similar to the conditions at the depth of injection (around 1000 m) of the ECBM test in Poland (~ 8.5 MPa and ~ 43°C; Van Bergen *et al*., 2006). Under these conditions CO_2 is in the supercritical phase. P-T records logged during our experiments show that the maximum pressure variation around the chosen value was ± 0.2 MPa and that the temperature varied usually within 0.5°C, and maximally within ± 2°C. This implies a variation on density of the CO_2 in our cell between 250-320 kg/m^3. The density of the other gases used, Ar and CH_4, does not vary significantly under these conditions.

At the start of each experiment the sample was placed in the high pressure cell, which was then heated to ~ 40°C. The gas supply system was flushed with the chosen test gas before connecting to the cell. A photograph was taken of the sample at atmospheric pressure, directly before gas was added to the cell at 8.0 MPa. The samples were then exposed to the Ar, CH_4 or supercritical CO_2 ($scCO_2$) at fixed pressure for at least 17 h, followed by an almost instantaneous pressure decrease to 0.1 MPa achieved by release of the exit valve. The sample was then observed for a further period up to 24 h under these conditions. Digital photographs were made during the entire experiment, using an automatic sampling interval varying between 10 s (for the period immediately after the introduction of the gas) and 30 min (approximately 1 h after release of the gas). At the end of each experiment (i.e. after venting the cell pressure) the final dimensions of the sample were determined and compared to its size before the first addition of the gas (see appendix for data processing procedure).

Three types of experiments were performed (Tab. 4.1). First, control experiments were repeatedly performed with the stainless steel sample under CO_2 pressure to calibrate out any optical effects of the CO_2 refraction index.

Secondly, six air dried samples of the bituminous coal were tested - one with Ar, one with CH_4, and four with CO_2 - and two air dried subbituminous coal samples were tested with CO_2 (Tab. 4.1). In one test (BIT6) the experiment was repeated by means of a second introduction of CO_2 into the cell, following exactly the same procedure, to check the reproducibility of the experiment. One additional test was added to the experimental set that deviated in its pressure and temperature conditions. In this experiment, a seventh bituminous coal sample was first put under a CO_2 pressure of 2.7 MPa for 24 h. This was followed by an increase of the CO_2 pressure to 5.2 MPa, without depressurizing the sample between times. After 24 h at these conditions the

CO_2 pressure was increased to 8.2 MPa. The coal was then, again, maintained under these conditions for 24 h.

Thirdly, experiments were performed on moisturized bituminous coal samples (Tab. 4.1). Before moisturizing, the coal sample was put in the open cell and was photographed at atmospheric pressure and room temperature under the microscope to determine its size. Moisturizing of the sample was done by placing the entire (open) cell into the dessiccator. After moisturizing, the cell was removed from the dessiccator, directly closed by placement of the upper lense, and put under the microscope. A photograph was taken at atmospheric pressure and room temperature to measure the size of the moisturized sample. Directly afterwards scCO_2 was introduced and sample swelling monitored according to the procedure described for the air dried samples. It could not be prevented that in the period (< 1 h) between the retrieval from the humid atmosphere in the dessiccator and the introduction of the gas into the closed cell some of the equilibrium moisture was lost. The loss of moisture of coal with time at room conditions was therefore determined in a separate experiment. This experiment comprised the moisturizing of an aggregate of coal particles of similar size (1-2 mm^3) and subsequent exposure to room conditions, while the loss of moisture with time was measured by weight loss.

One moisturized sample was tested with Ar (eighth bituminous coal sample) and two with CO_2 (ninth and tenth bituminous coal samples; Tab. 4.1). In all tests the experiment was repeated by a second introduction of CO_2 in the cell, following the same procedure, to check the reproducibility of the experiment.

4.4.3 Strain determination

Five points were selected on the digital images that could be well recognized on the photographs taken at different time steps. For the pictures from several time steps the distances between these individual points were measured. Linear strain was determined by comparing the distance between the points, as determined for a certain time step, to the distance measured before the gas or fluid was added. A surface strain was calculated by squaring the average of the measured linear strains. Further details are given in the appendix.

The measurement error of about 0.3% absolute strain, resulting from point recognition on the photographs, is relatively large. The reliability of the lower strain values, such as those induced by Ar, is therefore limited. However, despite the error, the observed trends are obvious and the data fitting is satisfactory for most experiments as indicated by the correlation factor (R).

4.5 Results

The results reported here focus on the trends that can be observed in the strain vs. time data obtained for the various samples and on the two parameters that result from the mathematical fit applied to the data (see Appendix). The first parameter is the maximum surface strain (e_{s-max}). Because this results from a data fit, the observed maximum strain can occasionally be larger than e_{s-max}. The second parameter is the half-saturation time ($t_{1/2}$) which is the required time to reach 50% of e_{s-max}. In the description of our results, an increase in size is referred to as positive strain, a decrease in size as negative strain.

4.5.1 Control experiment

Supercritical CO_2 has a different refractive index than air, which is linearly related to its density (Sun *et al.*, 2003) and therefore depends on the pressure and temperature conditions. Given the conditions in this study, the refractive index will be 1.06-1.07 for a wavelength of 632.8 nm (Besserer and Robinson, 1973; Sun *et al.*, 2003). Evaluation of the digital images obtained in our control experiment did not result in marked changes in the size of the sample on the image, from which it could be concluded that the refractive index did not affect the experimental results significantly. No corrections for the refractive index of CO_2 were therefore required.

4.5.2 Air dried samples

The coal sample that was exposed to Ar did not show any measurable changes in dimensions. The sample that was exposed to CH_4 developed a strain of 0.65% (Fig. 4.1). The data fitting was hampered by the low contrast of the photographs (making the identification of points on the photograph more difficult) and the relatively small strain that developed, which resulted in a low correlation coefficient (Tab. 4.2). After gas release the sample returned to its original size at equilibrium to atmospheric pressure. All samples that were exposed to CO_2 developed strain that varied between 0.94 and 1.81% for bituminous coal (experiments BIT1, BIT2, BIT3, BIT4, BIT5 and BIT6; Fig. 4.2) and between 1.05 and 1.49% for the subbituminous coal (experiments SUB1, SUB2; Fig. 4.3) after the first introduction of the gas. Around 1-5 h are needed to obtain 50% of the maximum swelling. The bituminous coal samples returned close to their original size, but with a slightly negative strain, at equilibrium to atmospheric pressure after gas release, except in experiment BIT6. In this case, the sample was significantly smaller than before the experiment. The subbituminous coal samples showed a significant negative strain (Fig. 4.3).

The second introduction of CO_2 in experiment BIT6 showed a similar maximum strain value as was observed after the first introduction (Tab. 4.2), although it must be noted that this experiment started at a negative strain (compared to its original size). Also, the half saturation time was comparable. The size of the sample was closer to its original size after the second exposure to the gas (Fig. 4.2; Tab. 4.2).

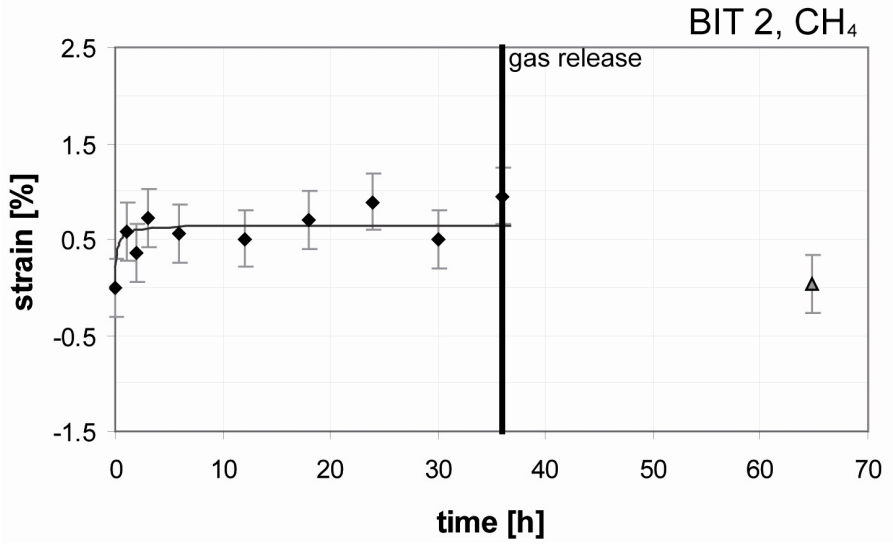

Figure 4.1: Development of strain with time of an air dried bituminous coal sample under CH_4 pressure. The gas is introduced at 0h. The line represents the best fit through the data. The measurement point after equilibration to atmospheric pressure is indicated by the triangle.

The results of the three subsequent CO_2 additions at increasing pressure on the bituminous coal showed an increase in maximum strain with increasing pressure. Strain equilibrium is probably not reached with 2.7 and 8.2 MPa CO_2 pressure within the experimental time. The strain at 8.2 MPa of 2.24% is significantly higher than the maximum strain observed for the experiments that were directly put on a pressure of 8.1 MPa. The sample did not return to its original size once it was back at equilibrium with atmospheric pressure after gas release.

4.5.3 Moisturized samples

The equilibrium moisture content of the bituminous sample was measured to be 4.1% and of the subbituminous coal sample 6.7%. Extrapolation of the curves of moisture loss with time (Fig. 4.4) indicates an inherent moisture content, i.e. moisture remaining after air drying, of 2.8% for the bituminous sample and 5.3% for the subbituminous coal sample. The ratio between surface moisture, which is lost by air drying, and inherent moisture is about 1/2.2 for the bituminous sample and 1/3.5 for the subbituminous coal sample. The evaluation of moisture loss at room conditions showed that within 1 h the bituminous sample loses about 20% and the subbituminous coal sample about 15% of its equilibrium moisture (Fig. 4.4).

Three experiments were performed with moisturized bituminous coal samples. Eval-

Table 4.2: Overview of experimental results. The measurement error is given as an absolute error in the strain value. Experiment BIT3 exhibits the lowest strain for CO_2 of the air dried bituminous coal samples, which may be related to the covering with the gold layer.

Exp.no.	Gas	Comments	**Parameters of data fit**						Measurement error
			e_{s-max}	e_{s-max} -error	$t_{1/2}$	$t_{1/2}$ -error	R	R^2	
S1	CO_2	Measured strain value after experiment: -0.03 %	-	-	-	-	-	-	0.30
BIT1	Ar	Measured strain value after experiment: 0.09 %	-	-	-	-	-	-	0.30
BIT2	CH_4		0.65	0.09	9.56	27.33	0.66	0.43	0.30
BIT3	CO_2		0.94	0.06	110.81	30.51	0.93	0.87	0.30
BIT4	CO_2		1.27	0.05	132.85	22.09	0.98	0.96	0.30
BIT5	CO_2		1.81	0.10	243.26	42.52	0.98	0.96	0.30
BIT6	CO_2	First	1.67	0.05	26.85	5.02	0.96	0.93	0.33
		Second - compared to first starting point	1.68	0.03	31.52	4.04	0.98	0.96	0.33
		Second - compared to second starting point	2.24	0.04	16.60	2.50	0.96	0.93	0.33
BIT7	CO_2	2.7 Mpa	1.35	0.07	310.05	44.09	0.99	0.97	0.26
		5.3 Mpa - compared to final value at 2.7 Mpa (1.11% strain)	0.37	0.03	35.11	15.51	0.86	0.73	0.26
		5.3 Mpa - compared to starting value at 0 Mpa (0% strain)	1.48						
		8.1 Mpa - compared to final value at 5.3 Mpa (1.47% strain)	0.77	0.12	597.17	221.33	0.96	0.92	0.26
		8.1 Mpa - compared to starting value at 0 Mpa (0% strain)	2.24						
SUB1	CO_2		1.05	0.03	36.54	6.20	0.96	0.93	0.25
SUB2	CO_2		1.49	0.04	36.25	4.92	0.98	0.96	0.25
BIT8M	Ar	First	0.28	0.21	743.84	1147.11	0.67	0.45	0.24
		Second - compared to first starting point	0.46	0.04	11.87	7.57	0.44	0.19	0.24
		Second - compared to second starting point	0.50	0.04	11.16	6.34	0.81	0.65	0.24
BIT9M	CO_2	First	1.46	0.07	231.51	35.35	0.98	0.96	0.28
		Second - compared to first starting point	1.14	0.05	117.19	26.10	0.93	0.87	0.28
		Second - compared to second starting point	1.60	0.05	48.86	11.06	0.88	0.77	0.28
BIT10M	CO_2	First	1.20	0.05	53.83	10.87	0.97	0.93	0.32
		Second - compared to first starting point	1.19	0.04	33.20	6.01	0.97	0.94	0.32
		Second - compared to second starting point	1.48	0.04	16.37	2.50	0.96	0.93	0.32

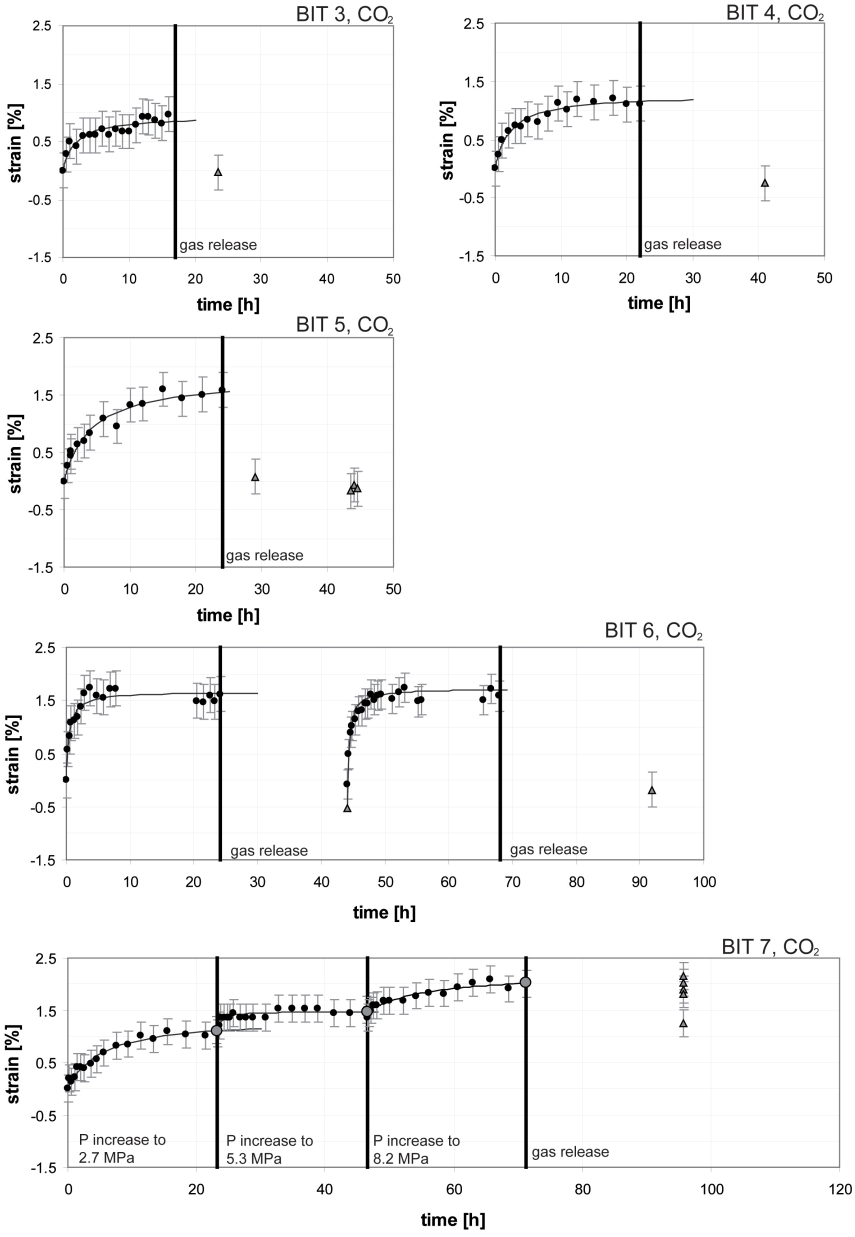

Figure 4.2: Development of strain with time of air dried bituminous coal samples under CO_2 pressure. See Fig. 4.1 for explanation of graphic symbols. In the plot of experiment BIT7 the calculated strain value from the fit is plotted at the time just before gas release (see Fig. A.1), indicated by the grey circle. The gap in the data in experiments BIT6 was caused by temporary failure of the camera or its controlling computer routine, while the experiment itself was not interrupted.

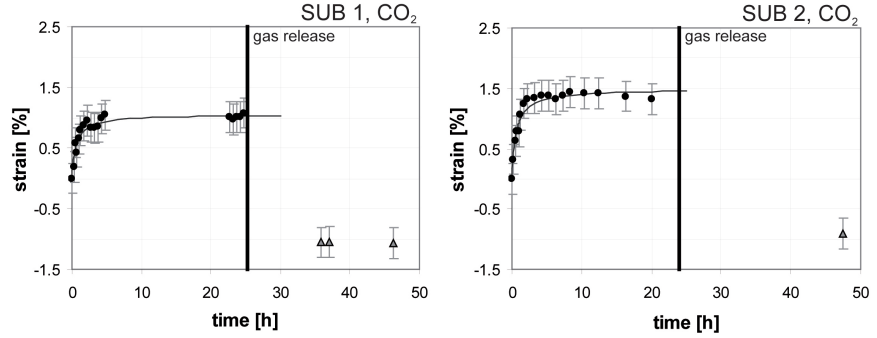

Figure 4.3: Development of strain with time of air dried subbituminous coal samples under CO_2 pressure. See Fig. 4.1 for explanation of graphic symbols. The gap in the data in experiments SUB1 was caused by temporary failure of the camera or its controlling computer routine, while the experiment itself was not interrupted.

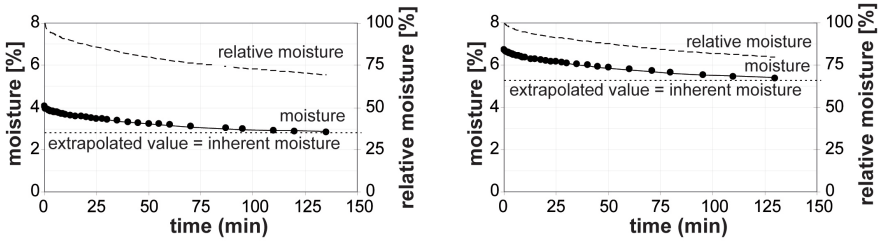

Figure 4.4: Loss of moisture with time of the bituminous coal (left) and the subbituminous coal (right) samples of 1-2 mm^3 particles once exposed to room conditions. The moisture at the beginning of the experiment represents the equilibrium moisture. 0% moisture content represents the moisture content after oven drying at 105 °C, as determined at the end of the experiment.

Table 4.3: Average strain in the bituminous coal samples of the as received coal sample. The dimensions of the sample after moisture equilibration are considered as 0% strain. A negative strain value implies that the coal sample was smaller before than after the moisturizing. The average strain and standard deviation is based on two individual measurements.

Experiment number	Strain (%)	SD
BIT8M	-0.63	0.14
BIT9M	-0.37	0.04
BIT10M	-0.92	0.05

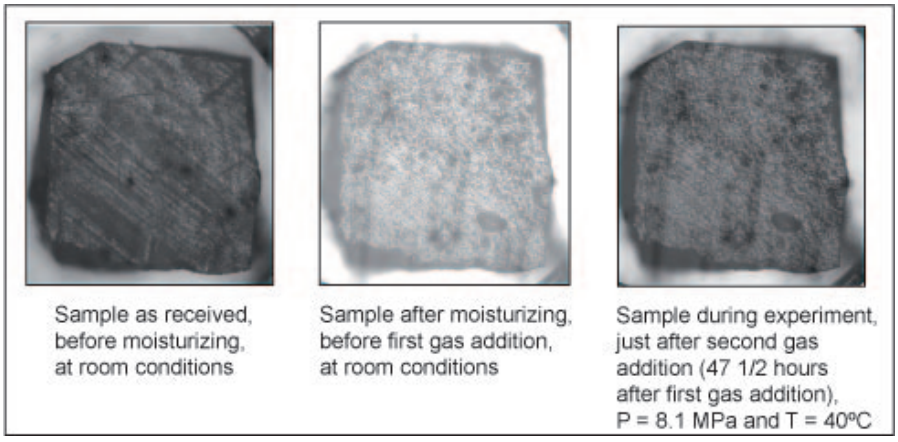

Figure 4.5: Pictures from the coal matrix block during experiment BIT 9M before moisturizing, after moisturizing (before the addition of CO_2), and just after the second addition of CO_2.

uation of the microscope pictures before and after moisturizing showed a clear increase in size in all samples (Tab. 4.3). The moisturizing procedure changed the appearance of the coal markedly (Fig. 4.5), which complicated the recognition of points on the photographs. However, still sufficient points could be recognized for a good evaluation of strain.
The measured strain values during the first addition of Ar in experiment BIT8M are of the same order as the measurement error and are therefore considered to be below the detection limit of the applied method. During the second introduction of Ar there was a development of strain larger than the measurement error (Fig. 4.6; Tab. 4.2). No strain was observed when the sample was back at equilibrium with atmospheric pressure.

The two experiments with CO_2 showed a development in strain of 1.20 and 1.46% during the first stage. Back at atmospheric pressure, both samples showed a decrease in size. The appearance of the coal sample on the photograph taken at this stage is different compared to its appearance on the photograph taken directly before

the start of the experiment (Fig. 4.5). The observed strain during the second stage of exposure to CO_2 was lower (BIT9M) or comparable (BIT10M) to that of the first stage, but markedly higher if the (negative) starting point is taken into consideration (Tab. 4.2). The $t_{1/2}$ was markedly shorter during the second stage compared to the first stage. Neither of the samples returned to their original size at atmospheric pressure at the end of the experiment (Fig. 4.6). Notable is further that experiment BIT9M showed an S-shaped curve in the beginning of the experiment, that was not observed in experiment BIT10M (Fig. 4.6).

4.6 Discussion

There are many reports in literature about the volumetric expansion, or swelling of coal, as an effect of gas or fluid adsorption on the coal. However, few of these observations are based on direct measurements (Day *et al.*, 2008; Robertson and Christiansen, 2005a). This study has established linear strain development by optical observation of coal samples.

Coal is a very heterogeneous material because it is composed of a combination of macerals and mineral matter ("ash"). Different macerals and ash components show different swelling behaviors leading to anisotropy that is additionally related to the orientation of the bedding plane (Day *et al.*, 2008). Karacan (2003) and Karacan and Mitchell (2003) determined that gas adsorption and dissolution is highest for clay minerals and inertinite regions followed by vitrite layers. Due to swelling processes the structure of coal changes significantly; for example several components like clay minerals and inertinite were compressed while vitrite showed the highest degree of swelling due to dissolution of CO_2 (Karacan, 2003; Karacan, 2007).

The linear strain data of the experiment with CH_4 (BIT3) and one experiment with CO_2 (BIT5) were evaluated to get an idea of the anisotropic swelling in our experiments. This evaluation showed that although most lines showed a positive strain there were also negative linear strains measured in the same experiment. This was especially the case for the CH_4 experiment. Although swelling is dominant it can be concluded that in some parts in the coal sample shrinkage takes place simultaneously. Averaging the lines always resulted in a positive strain. The CO_2 experiment showed that expansion parallel to bedding-planes was dominant over the out-of-bedding plane expansion.

In this study, main interest was in the behavior of a matrix block rather than the individual coal components. Anisotropic swelling was therefore not taken into further consideration in this study. The reported strain values resulted from the averaging and squaring of linear strain that was determined in multiple directions (see Appendix). The length over which the linear strains are determined (varying between 0.30 and 0.95 mm) is usually larger than the individual macerals or mineral components, and by averaging the linear strain the effect of differential swelling therefore

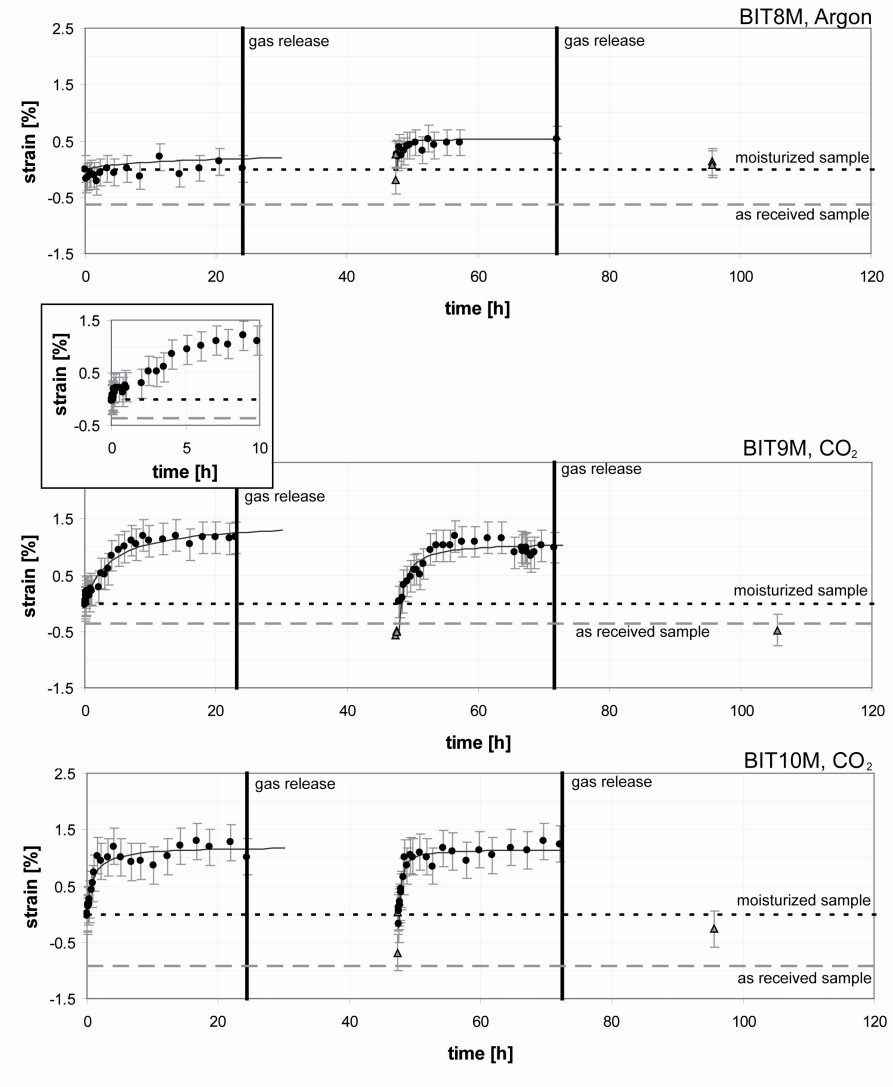

Figure 4.6: Development of strain with time of moisturized bituminous coal samples under CO_2 pressure. See Fig. 4.1 for explanation of graphic symbols. The gap in the data in experiments BIT8M was caused by temporary failure of the camera or its controlling computer routine, while the experiment itself was not interrupted. In experiment BIT9M there was a temporary pressure decrease from 8.1 to 5.1 MPa between 3500 and 3820 min, after which the pressure was restored to 8.1 MPa. An S-shaped curve can be observed in the data of the first 10 h of experiment BIT9M (see inset).

averages out. A good correlations exists between the strain obtained from the linear strain and the overall surface strain (see Appendix). The reported strain values in this study can therefore be considered as a representative 2-D measure for the matrix blocks as a whole.

The purely empirical mathematical equation used to describe the development of strain with time (see Appendix) gave in general a satisfactory fit to the data, as indicated by correlation factors that are higher than 0.85. However, for the CH_4 and Ar exposure the data and resulting fit show large uncertainties (Tab. 4.2). Still, the resulting values for the amount of swelling are considered suitable for comparison.

4.6.1 Relation between adsorption and swelling

As indicated in section 2, swelling of coal is likely to be related to the gas adsorption on the coal surface. The differences in strain response of the coal upon exposure to different gasses and fluids may therefore be related to the differences in the adsorption capacity at defined pressure and temperature conditions as determined by adsorption isotherms. The sample exposed to Ar (BIT1) did not exhibit measurable swelling, because the relatively inert Ar did not adsorb significantly to the coal. The results of the experiments on the air dried samples showed that the swelling (defined by e_{s-max}) was about 1.5 to 2.8 times higher for CO_2 (BIT3-6) than for CH_4 (BIT2). This is in good agreement with the difference between the adsorption capacity of coal for these gases, which is about 2 times higher for CO_2 than for CH_4 (e.g. Hall *et al.*, 1994; Puri and Yee, 1990; Stevenson *et al.*, 1991).

The experiment with the air dried coal at different pressures (BIT7) showed an increase in strain with increasing pressure (Fig. 4.7; Tab. 4.2), also confirming the anticipated relation with adsorption. It must be noted that the strain under 8.2 MPa CO_2 pressure is much larger compared to all other results from previous experiments at comparable conditions. This would suggest that the equilibrium strain is influenced by the pressure history, although the dataset is too limited to draw any firm conclusions here. Because only three pressure steps were investigated, it is not possible to suggest any physical basis for the observed trend. Given the accepted relationship between swelling and adsorption a Langmuirian type seems logical (Levine, 1996). However, extrapolation of the Langmuir relation for adsorption above the supercritical point of CO_2 is not well established (e.g. Krooss *et al.*, 2002). Equally, a linear relationship could explain the correlation between the linear expansion of the solid and the fill pressure of the adsorbed material. This is in certain cases observed where the adsorption of a vapor by a porous solid is involved (Adamson and Gast, 1997). Day *et al.* (2008) observed that swelling was proportional to the amount of CO_2 adsorbed up to a pressure of about 8 MPa.

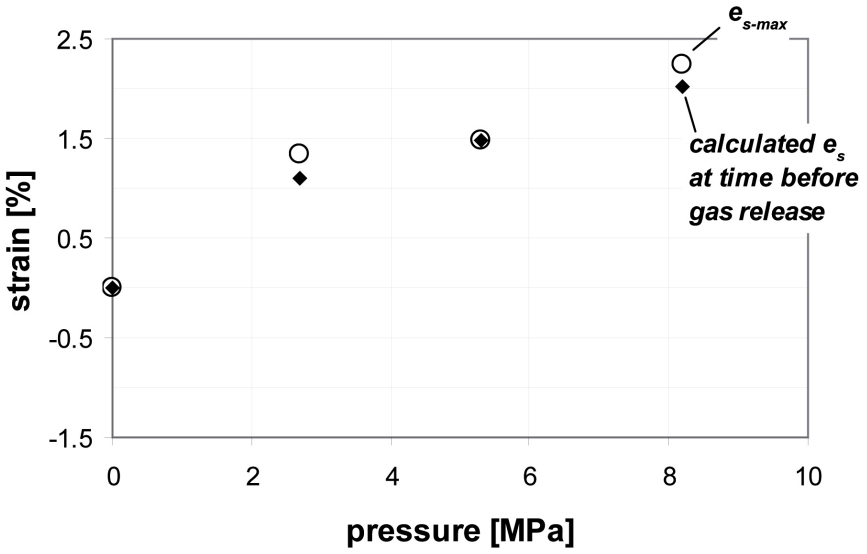

Figure 4.7: Maximum strain values as determined by experiment BIT7 at different pressures (2.7, 5.3 and 8.2 MPa). There is a difference between the e_{s-max}(resulting from the data fit) and the maximum strain calculated for the time just before gas release because equilibrium was not reached within the experimental period at 2.7 and 8.2 MPa.

4.6.2 Role of moisture on the development of strain

This study also showed that coal swells not only as the result of gas uptake but also as the result of water uptake, confirming the observations of Walker *et al*. (1988). In the moisturizing procedure, surface moisture is added to the air dried sample that is only containing inherent moisture. Given the observed relation between the addition of surface moisture and the developed strain, it is expected that this moisture is adsorbed to the coal surface. This makes sense, because measurements of the pore volume containing moisture as a result of the ASTM D1412-04 method by Prinz and Littke (2005) indicated that through this procedure water molecules are able to penetrate micropores ($>$ 0.4 nm). In these micropores adsorption takes place. Smaller pores are not filled, probably due to the formation of clusters of water molecules which are too large to enter these submicropores. The water that is adsorbed on the coal surface will compete with gas for adsorption sites on the coal surface and as such decrease the overall gas adsorption capacity compared to dry coal (Bustin and Clarkson, 1998; Clarkson and Bustin, 2000; Goodman *et al*., 2006; Jahediesfanjani and Civan, 2006; Joubert *et al*., 1974; Krooss *et al*., 2002; Lama and Bodziony, 1996; Laxminarayana and Crosdale, 1999; Levine *et al*., 1993; Levy *et al*., 1997; Mavor *et al*., 1990; Prinz and Littke, 2005; Seewald and Klein, 1986; Yalcin and Durucan, 1991; Yee *et al*., 1993). Based on the results of Walker *et al*. (1988) the coal swelling of the bituminous coal due to water was expected to vary between 1 and 20%. The samples of this study show a strain of 0.3 - 1% as the result of moisturizing. This is smaller compared to the strain induced by CO_2 and CH_4 but still significant.

Given that moisture in coal under natural conditions is generally considered to have a negative effect on gas sorption capacity, it was expected that the moisturized samples would exhibit a markedly lower strain than the air dried samples once exposed to the first introduction of the CO_2. For example, this was inferred by Siemons and Busch (2007) from sorption experiments where CO_2 induced strain in a moisturized sample was less compared to dry samples. This could not be confirmed by the results of this study where the strain values of the moisturized samples (1.20 and 1.46% for the first introduction) are within the range found for air dried samples (0.94 to 1.81%).

However, differences could be observed in the strain values after gas release. The air dried bituminous coal samples in contact with Ar and CH_4 were restored close to original size after equilibration to atmospheric pressure, with strain values of respectively 0.09 and 0.04%. The experiments with the bituminous coal samples in contact with CO_2 all showed negative strain values (-0.03, -0.25, -0.17, and -0.50%; Fig. 4.2). The strain value after the second equilibration to atmospheric pressure in experiment BIT6 was -0.18%. This shrinkage of the sample could be associated with loss of (inherent) moisture from the coal. Drying of the coal is likely to be enhanced by contact with the CO_2 (Goodman *et al*., 2005b; Iwai *et al*., 1998; Iwai *et al*., 2002). Iwai *et al*. (1998) reported that during injection of supercritical CO_2 into a coal sample the amount of water present in the coal matrix decreased by about 60 to 95%. However, not all moisture can be removed by the supercritical CO_2. At low moisture content, the rate of

drying in coals is assumed to be limited by the diffusion of moisture out of the pores of the coal (Iwai *et al.*, 1998). Also, for effectively drying coals by supercritical CO_2, a water film on coal surfaces should first be interrupted (Plug *et al.*, 2006). A change in the wetting phase in the coal matrix as a result of the introduction of CO_2 in the coal-water system under pressure has been reported previously by several authors (Mazumder *et al.*, 2003; Plug *et al.*, 2006; Siemons *et al.*, 2006). It can be assumed that a change in the wettability of the system from water wet to CO_2 wet leads to drying and as such to a probable shrinkage of the coal due to the migration of water out of the coal matrix.

The effect of coal drying on strain is less for the experiments on air dried samples with Ar and CH_4, which is probably due to the much lower solubility of these gases in water (and vice versa). A drying of the coal due to CO_2 would also explain the negative strain values of the subbituminous coal samples (-1.05 and -0.91%) at equilibrium to atmospheric pressure. The drying effect would be higher for subbituminous coal because their (inherent) moisture content is higher.

It was expected that the equilibrium strain of moisturized coal samples after the first gas release would be even more negative. The results of the experiments with Ar showed that the measured strain at atmospheric pressure after the first gas introduction is difficult to detect, with values of -0.20 and 0.25% (Fig. 4.6). However, whereas the strain developed under gas pressure during the first stage is low (near the resolution of the data processing), strain is clearly developed during the second introduction of the gas. This would suggest that some adsorbed moisture is indeed removed, creating adsorption space for some Ar molecules. The developed strain due to the Ar is remarkable, given the low adsorption capacity of coal for Ar. The sample returns close to its original size (equilibrium strain value of 0.08%) after the second stage gas release.

The experiments with CO_2 did show negative equilibrium strain values after the first gas release for the moisturized bituminous coal samples (-0.52 and -0.68%), and also indicate a drying effect of the CO_2. These values are more negative than for the air dried bituminous coal samples, although a value of -0.50% was measured in experiment BIT6. The order of magnitude of the shrinkage is comparable to the swelling as the result of the moisturizing of the sample, suggesting that the CO_2 removes the surface moisture that was added in the sample preparation (Fig. 4.6). In Fig. 4.5 it can be observed that moisture on the surface is removed after the first phase. If the negative strain value is considered as the starting point for the second stage, the e_{s-max} was significantly higher than that of the first stage (1.60 vs. 1.46% and 1.48 vs. 1.20%). This suggests that by removal of some of the moisture additional adsorption sites became available, confirming the competition for the same adsorption sites between water and CO_2 molecules.

Another indication for removal of moisture due to the entrance and release of CO_2 is the much longer time it takes for the moisturized samples to reach half-saturation

compared to the air dried samples. This indicates that, next to the competing role of water for adsorption sites it also influences the transport properties of the matrix blocks. The presence of water, possibly in molecular clusters, is expected to impede the entrance of gas to the pores of the coal and thereby delays the diffusion of the CO_2 into coal (Krooss *et al*., 2002). The observed S-shape in the curve for experiment BIT9M could indicate initial pore blockage (Fig. 4.6). The second introduction shows faster half saturation times, which suggests that pore access is enhanced.

4.6.3 Implications for (E)CBM

The results of this study have confirmed that coal dimensions change due to water uptake or release. The recognition of coal shrinkage as a result of water release could be relevant for regular CBM production when coal seams are dewatered. The observed permeability increase may be the cumulative result of a volume decrease of matrix blocks due to both gas and water desorption from the internal coal surface.

The understanding of the strain development in time can be crucial in the planning and operational phase of any future ECBM project. Swelling of coal under field conditions, as observed in pilot sites (Van Bergen *et al*., 2006), could reduce porosity of the coal seam significantly and in turn reduce permeability resulting in the loss of commercial value of the project. The reported strain values for $scCO_2$ were obtained for unconfined coal samples, whereas under field conditions the coal is experiencing horizontal and vertical stresses. However, the relevance is indicated by the reported strain values (up to 1.8%) which are an order of magnitude higher than the total porosity of the sampled bituminous coal seam (0.02 to 0.16% on the basis of well logs (Krooss *et al*., 2005).

Based on the observed shrinkage of the coal due to drying an alternative injection-production scheme can be developed in which the CBM field is dewatered as much as possible before CO_2 injection. This could also prevent gravity override in the reservoir, which was identified as an operational problem (Van Wageningen and Maas, 2007). In such a scheme, a phased injection of $scCO_2$ might be considered where the first phase of injection may serve as additional drying of the coal. This may resulting in coal matrix shrinkage and permeability increase. Once the coal seam reaches maximum permeability it can be used to store CO_2.

4.7 Conclusions

1. Microscopic observations confirmed that strain develops in unconfined coal samples as a result of introduction of CH_4, $scCO_2$ and water at a pressure of about 8 MPa and a temperature of 40°C.

2. Point (1) confirms that water and gas molecules both compete for adsorption sites.

3. Because adsorption and swelling are related, point (2) implies that swelling will be less for moisturized coals than for dry coals.

4. We recommend that these studies be extended to other coals of different rank and composition. The results of these studies could lead to conclusions on how to improve the access of gas and scCO_2 to pores in a coal matrix.

Acknowledgements

This study was performed under the Dutch CATO project (CO_2 Afvang Transport en Opslag) and under the MOVECBM (contract no. 038967) project funded by the European Commission. Shell International and TNO are acknowledged for co-funding and supporting this study. The laboratory experiments would have been impossible without the technical support of Peter van Krieken and Gert Kastelein, who are gratefully acknowledged. Colin Peach and Sander Hol are thanked for the fruitful discussions in the course of the study. Harry Veld has been very supportive in the petrological analysis of the coal samples. Thanks also go to Xiangmin Zhang for the use of his routine. The Brzeszcze mine (Poland) and Carbosulcis (Italy) are thanked for the provision of samples. Elsevier is acknowledged for granting permission to reprint this article in the thesis.

Chapter 5

Diffusive properties of coal matrix fragments determined from swelling kinetics

Frank van Bergen, Philip Wehrens & Chris Spiers

Abstract

It is well-known that coal swells when exposed to gas or fluid at elevated pressures and temperatures. In this study the development of swelling strain with time is evaluated that is induced by uptake of argon, methane and carbon dioxide. The strain development for block-shaped coal matrix fragments exposed to in coal matrix blocks is measured by using a high-pressure see-through cell under an optical microscope. Experimental results for a subbituminous coal, a bituminous coal and an anthracite have been used for this evaluation, partly taken from earlier work and partly measured and reported here. A finite difference diffusion model was developed and applied, under the assumption that the kinetics of swelling are governed by transport properties of the coal matrix characterized by a single valued, uniform diffusion coefficient (unipore model). The model showed good correspondence with the so-called unipore model solution at the start of the diffusion process and provides a satisfactory fit to the experimental data until equilibrium is reached. Diffusion coefficient values obtained by fitting our model to the data are within the range of previously published literature values, indicating that the swelling experiments can be used to determine transport properties of the coal matrix. Rank effects on diffusion were expected but could not be discerned. However, an effect of moisture on the rate of swelling was found and seems to be larger for bituminous coal than for anthracite, although this cannot be explained at present.

Key words: coal diffusion; swelling; carbon dioxide; methane

5.1 Introduction

In recent years, several field tests have been carried out to investigate the potential of enhanced coalbed methane (ECBM) production through the injection of carbon dioxide (CO_2) into underground coal seams. One of the operational problems identified in such tests is the transport of the injected CO_2 into the coal bed. Transport of the injected CO_2 and displaced fluids through coal is a combination of Darcian flow through interconnected fractures, or cleats, coupled with diffusive transport through the fine scale pore system of the intervening coal matrix. Since Darcian flow through the fractures in coal is relatively well understood (Van Wageningen and Maas, 2007), understanding the behaviour of CO_2, methane (CH_4) and water in the coal matrix, and the impact of these substances on the matrix transport properties of the coal, is key to evaluating the feasibility of ECBM production.

The pore structure of coal matrix material is completely different from that of siliciclastic or carbonate rocks, which generally show a connected network of intergranular pores with dimensions of the order of micrometers to millimeters. Coal matrix material, i.e. excluding the cleats, contains pores at all sizes ranging from 2 nm to 10μm (Melnichenko *et al.*, 2009), although ultramicropores ($<$ 0.4 nm) are also reported (Prinz and Littke, 2005). The largest matrix pores are usually water filled (Levine, 1993).The pore system often shows a bimodal distribution with macropores at the micrometer scale and micropores at the nanometer-scale, i.e. reaching the same order of length scale ($\sim$ 0.5 nm) as the diameter of molecules such as CO_2 and CH_4 (Anderson *et al.*, 1956; Gan *et al.*, 1972; Levine, 1993; Nandi and Walker, 1966; Unsworth *et al.*, 1989; Yi *et al.*, 2009). From a modern, materials science perspective, these two size ranges of pores would best be termed micropores (μm) and nanopores (nm). However, we adhere to the conventional terms macro- ($> 5\times10^{-8}$ m), meso- (2×10^{-9}- 5×10^{-8} m) and micropores (4×10^{-10}- 2×10^{-9} m) in this paper. Most of the gas storage capacity of coal is related to this range of pore structures within the coal matrix (Harpalani and Chen, 1995; Levine, 1993) and especially to the micropores, which make up a large part of the total porosity of the coal matrix and provide most of the surface area available for sorption processes. In subbituminous coal samples, for example, micropores contribute 50 to 60% of the total matrix porosity of 13-25% (Mares *et al.*, 2009). Significantly, the dimensions of the micropores and fine mesopores found in coal matrix material imply that the porosity is intermolecular, as opposed to interparticulate, and is determined by molecular interactions (Levine, 1993). These molecular interactions imply that accessibility of the pore system will depend on the fluid used for its determination (e.g. helium vs. nitrogen vs. CO_2) and therefore that the porosity of coal is not a fixed property.

Transport of gas or fluid through coal is complicated by swelling of the coal due to sorption of gas or fluid molecules in the micropores of the coal matrix material, leading to permeability reduction in the cleats (e.g. Goodman *et al.* (2005); Goodman *et al.* (2006); Karacan (2003); Karacan (2007); Pan and Connell (2007); Robertson and Christiansen (2005b)) and shrinkage due to methane desorption (e.g. Harpalani and

Chen (1997); Harpalani and Schraufnagel (1990); Mavor and Gunter (2006); Palmer and Mansoori (1996); Palmer and Mansoori (1998); St. George and Barakat (2001)). At the same time, contraction of samples exposed to an external gas or fluid pressure occurs due to the increasing hydrostatic confining stress (Kelemen and Kwiatek, 2009; St. George and Barakat, 2001). Nonetheless, since most coals exhibit quite low elastic compressibility (high bulk modulus ~ 2.0 GPa (Pan and Connell, 2007)), volume change is overwhelmingly dominated by the swelling. Conventional poroelastic effects on the coal density and pore structure are expected to have a negligible influence on transport (Yi *et al*., 2009), as they are limited to connected macropores. In line with all this, Siriwardane *et al*. (2009) showed experimentally that the bulk permeability of fractured coal samples decreases significantly as a result of matrix swelling when exposed to carbon dioxide, and hypothesized that tight, fractured coal can become completely impermeable at sufficiently long exposure times. In such cases, transport through the coal will be fully dependent on matrix diffusion. Despite all that is known about the pore structure of coal, however, understanding and quantifying the mechanism and kinetics of transport through coal matrix material remains problematic (Kelemen and Kwiatek, 2009).

This study extends the experiments of Van Bergen *et al*. (2009a), who reported data on time-dependent swelling strain induced by uptake of CO_2, CH_4 and Ar by block-shaped coal matrix fragments. These data are used here for a kinetic evaluation of the rate of swelling (*cf.*Kelemen and Kwiatek (2009)). New experiments are added on subbituminous, bituminous and anthracitic coal matrix fragments. The swelling data obtained are compared, together with our previous measurements, with a simple (numerical) model for swelling controlled by diffusion of CO_2, CH_4 and Ar into a spherical coal particle. Using this model, the diffusion coefficients for CO_2, CH_4 and Ar in our coal sample are estimated. Finally, the dependence of these diffusion coefficients and of strain response upon rank and moisture content are examined.

5.2 Experiments

This study extends the optical cell experiments on matrix fragment swelling described by Van Bergen *et al*. (2009a), by using similar coal samples from Poland (Brzescze) and Italy (Monte Sinni) and by adding new material from S. Wales, U.K (Selar).

5.2.1 Sample material and preparation

The coals used span the rank range from subbituminous (Monte Sinni) to bituminous (Brzescze) to anthracite (Selar). The subbituminous material from the Monte Sinni coal mine in Italy is composed of 49.4% fixed carbon, with 41.2% volatile matter, 2.1% ash, and 7.3% moisture (Ottiger *et al*., 2006). The vitrinite reflectance of this material was determined to be 0.43% $\pm$ 0.05. The bituminous coal from Poland was taken in the form of bulk samples from seam 364 at a depth of 640-740 m in the Brzeszcze coal

mine, located in the Upper Silesian Basin of Poland. These vitrinite-dominated samples of Pennsylvanian age show a vitrinite reflectance of 0.77% $\pm$ 0.05. More details on this material are provided by Van Bergen *et al*. (2009a). The anthracitic sample from the United Kingdom was obtained, through Delft University of Technology, from Selar colliery, located in the South Wales Coalfield. The characteristics of this coal have been reported by Siemons (2007), Siemons and Busch (2007), and Siemons *et al*. (2007). These authors determined the composition of their samples to be 89.27% fixed carbon, 7.9-10.4% volatile matter, 3.9-5.5% ash and 1.3- 1.4% moisture. Vitrinite reflectance was determined to be 2.41%.

The present sample preparation procedure, including moisturizing of some samples, followed that described by Van Bergen *et al*. (2009a). Small matrix blocks with a volume of 1-1.5 mm^3 ($\sim$ 1.2-1.4 mm in lateral dimensions by 0.7-0.9 mm height) were prepared by cleaving from air-dried, bulk coal specimens. The samples were cleaved in such a way that the plane of view in the optical cell was perpendicular to the sedimentary layering, i.e. more or less parallel to the face cleats. Prior to exposure to CO_2, some of the anthracite samples were moisturized following the ASTM D1412-04 standard method, which involves exposure to a controlled environment with 96% relative humidity. However, our samples were allowed longer to equilibrate with the imposed humidity than prescribed by the ASTM method, namely 4 days or more instead of 2-3 days, depending on the type of coal, as laid down in ASTM D1412-04.

5.2.2 Experimental method

Optical swelling measurements were performed on the prepared coal blocks using the same see-through optical cell as described in detail by Van Bergen *et al*. (2009a). This see-through, high-pressure cell consists of a pill-box shaped cylindrical pressure vessel containing a small-volume sample chamber situated between two opposing Pyrex lenses. A titanium ring placed coaxially between the lenses acts as a sample holder. Unconfined samples placed within the ring are free to swell in all directions. The cell is connected to a gas supply system that enables injection of Ar, CO_2 and CH_4 at pressures up to 15.0 MPa, and is heated by PID-controlled heating elements embedded in the vessel body. During the full duration of each experiment, the cell was placed under a Leica DMRX optical microscope system to obtain digital images of the sample automatically, i.e. to monitor changes in its surface dimensions. All experiments were performed at pressures of 8.0 MPa and a temperature of 40°C. We conducted three experiments with subbituminous coal injecting Ar, CH_4 and CO_2, one experiment with bituminous coal and CO_2, and four experiments with anthracitic coal adding Ar, CH_4 and CO_2 (Tab. 5.1). Additionally, one experiment was executed on a pre-moisturized anthracite, exposing this to CO_2. The effect of moisturizing anthracite samples in the initial air-dried condition, before the addition of CO_2, was determined in an independent set of experiments (Tab. 5.2).

At the start of each experiment the sample was placed in the optical cell, which was then heated to 40°C without evacuation. After thermal equilibration, a digital image

was taken of the sample at atmospheric pressure, directly before gas was added to the cell. The samples were then exposed to the Ar, CH_4 or supercritical CO_2 ($scCO_2$) at a fixed pressure of 8.0 MPa, by venting this pressure into the cell from an external reservoir. The full pressure developed almost instantaneously, facilitated by the small volume of the cell. After a period of at least 17 h, the cell was depressurized, again more or less instantaneously, by venting to atmosphere via release of the exit valve. The sample was then observed for a further period of up to 24 h under these conditions. Digital images were acquired during the entire experiment, using an automatic sampling interval varying between 10 s (for the period immediately after the introduction of the gas) and 30 min (from approximately 1 h after release of the gas).

The 2-D surface dimensions of the sample were determined from these images at each stage of the experiment and compared with those measured before the first addition of the gas, using a network of distinctive marker points chosen in the surface of each sample as described by Van Bergen *et al*. (2009a). Significant improvements were made in the accuracy of the strain data compared with our earlier work, due to use of more powerful image manipulation, with improved contrast and white balance, providing better image quality. Measurement error was 0.01-0.04%, taken as an absolute value in the strain value, for 2-D surface strain (e_s), one order of magnitude smaller than the error in our previous experiments. The measurements yielded 2-D strain data versus time, which showed rapid sample expansion towards a saturation or equilibrium value reached after 1-20 hours. A best fit was made to this data using a purely empirical hyperbolic function of the form :

$$e_s = \frac{t \times e_{s-max}}{t + t_{1/2}} \tag{5.1}$$

This yielded two parameters per exposure experiment, namely the maximum 2-D strain attained at equilibrium (e_{s-max}) and the half-saturation time ($t_{1/2}$), which is the time required to reach 50% of e_{s-max}. These parameters are used to describe our data and to compare them with our earlier measurements (Tab. 5.1). For the calibration of the results from the numerical modelling, as described later in this paper, also the maximum volumetric strain at equilibrium (e_{v-max}) was determined (see Tab. 5.1). In one test with subbituminous coal and CO_2 (SUB5), and in the single test performed with moisturized anthracite (ANT5M), the experimental procedure was repeated by means of a second introduction of CO_2 into the cell, to check reproducibility (Tab. 5.1).

Table 5.1: Overview of the results from experiments performed in this study and added experiments performed by Van Bergen *et al.* (2009a), labelled with an #. Experiments coded with SUB were performed on subbituminous coal, with BIT were performed on bituminous coal and with ANT were performed on anthracite. The label M at the end of some experiment codes indicates that the sample was moisturized. Strain of the moisturized samples was taken relative to the sample size after the moisturizing procedure. The measurement error is given as an absolute error in the strain value. Values for maximum surface strain e_{s-max} labelled with * are determined compared to first starting point, those labelled with ** are determined compared to second starting point. The volumetric stain (e_v) was calculated, assuming isotropic material, from mean 1-D strain (e_l) by $e_v = 100\times (3e_l + 3e_l^2 + e_l^3)$, *cf.*Robertson and Christiansen (2005a). Mean 1-D strain follows from surface strain (e_s) via the relation $e_l = ((e_s/100)+1)^{1/2} - 1$. Experimental data resulting from the hyperbolic fit and values of the effective diffusion coefficient D per experiment, are included. The values of D are obtained by fitting the spherical model to the experimental strain data obtained by the see-through high-pressure cell. The lower and the higher value of D are indications of the lower and upper boundaries of the range of diffusion coefficients that provide an acceptable fit to the measured data, as expressed by a correlation coefficient (R_D) higher than 0.9.

Exp. No.	Material	Gas/ Fluid	P	T	Exposure time at pressure P	Meas. error	$t_{1/2}$	$t_{1/2}$-error	Max. surface strain e_{s-max}	Error in e_{s-max}	Max. volume strain e_{v-max}***	R_s	Modelled effective diffusion coefficient D			
			MPa	°C	h	%	min	min	%	%	%		Lower value D ($m^2 s^{-1}$)	R_D	Higher value D ($m^2 s^{-1}$)	R_D
SUB3	Subb. coal	Ar	8.0	40	21.2	0.06	89.36	79.56	0.24	± 0.05	0.36	0.41	5.00E-13	0.47	3.00E-12	0.40
SUB4	Subb. coal	CH_4	8.0	40	22.3	0.03	107.81	43.41	0.20	± 0.02	0.30	0.86	1.50E-13	0.83	3.00E-13	0.84
SUB1#	Subb. coal	CO_2	8.1	40	24.0	0.25	36.54	6.20	1.05	± 0.03	1.58	0.96	1.50E-12	0.87	4.00E-12	0.94
SUB2#	Subb. coal	CO_2	8.1	40	24.0	0.25	36.25	4.92	1.49	± 0.04	2.24	0.98	1.50E-12	0.89	3.00E-12	0.95
SUB5	Subb. coal	CO_2 (twice)	8.0	40	23.7	0.01	80.07	14.43	1.09	± 0.05	1.64	0.97	9.00E-13	0.92	3.00E-12	0.97
					23.8	0.01			1.34*		2.02					
						0.01	45.31	5.40	2.31**	± 0.06	3.48	0.98	1.00E-12	0.93	2.00E-12	0.97
BIT1#	Bit. coal	Ar	8.0	40	24.0	0.30	-	-	-	-	-	-				
BIT2#	Bit. coal	CH_4	7.9	40	40.0	0.30	9.56	27.33	0.65	± 0.09	0.97	0.66	5.00E-13	0.48	3.00E-12	0.33
BIT3#	Bit. coal	CO_2	8.0	40	17.0	0.30	110.81	30.51	0.94	± 0.06	1.41	0.93	8.00E-13	0.91	1.00E-12	0.90
BIT4#	Bit. coal	CO_2	8.0	40	22.0	0.30	132.85	22.09	1.27	± 0.05	1.91	0.98	3.00E-13	0.96	5.00E-13	0.97
BIT5#	Bit. coal	CO_2	8.0	40	24.0	0.30	243.26	42.52	1.81	± 0.10	2.73	0.98	9.00E-14	0.98	1.50E-13	0.98
BIT6#	Bit. coal	CO_2	8.1	40	24.0	0.33	26.85	5.02	1.67	± 0.05	2.51	0.96	1.50E-12	0.90	4.00E-12	0.95
					24.0	0.33	31.52	4.04	1.68*	± 0.03	2.53	0.98				
						0.33	16.60	2.50	2.24**	± 0.04	3.38	0.96	1.50E-12	0.94	3.00E-12	0.98
BIT11	Bit. coal	CO_2	8.0	40	23.3	0.50	97	23.00	1.94	± 0.10	2.92	0.94	5.00E-13	0.90	9.00E-13	0.93
ANT1	Anthracite	Ar	8.0	40	23.8	0.04	51.23	32.43	0.21	± 0.03	0.32	0.71	8.00E-13	0.70	4.00E-12	0.63
ANT2	Anthracite	CH_4	8.0	40	24.0	0.02	-	-	-	-	-	-	-	-	-	-
ANT3	Anthracite	CH_4	8.0	40	23.4	0.02	31.86	8.14	0.43	± 0.02	0.65	0.92	1.00E-12	0.87	2.00E-12	0.87

Continued on next page

Table 5.1 – continued from previous page

Exp. No.	Material	Gas/ Fluid	P	T	Exposure time at pressure P	Meas. error	$t_{1/2}$	$t_{1/2}$-error	Max. surface strain e_{s-max}	Error in e_{s-max}	Max. volume strain e_{v-max}***	R_s	Modelled effective diffusion coefficient D			
			MPa	°C	h	%	min	min	%	%	%		Lower value D ($m^2 s^{-1}$)	R_D	Higher value D ($m^2 s^{-1}$)	R_D
ANT4	Anthracite	CO_2	8.0	40	24.0	0.01	12.05	2.27	1.95	± 0.04	2.94	0.97	3.00E-12	0.97	6.00E-12	0.92
BIT8M#	Bit. coal, moist	Ar	8.1	40	24.0	0.24	743.84	1147.11	0.28	± 0.21	0.42	0.67	-	-	1.00E-13	0.67
					24.0	0.24	11.87	7.57	0.46*	± 0.04	0.69	0.44				
						0.24	11.16	6.34	0.50**	± 0.04	0.75	0.81	2.00E-12	0.43	3.00E-12	0.42
BIT9M#	Bit. coal, moist	CO_2	8.1	40	24.0	0.28	231.51	35.35	1.46	± 0.07	2.20	0.98	3.00E-13	0.97	5.00E-13	0.97
					24.0	0.28	117.19	26.10	1.14*	± 0.05	1.71	0.93				
						0.28	48.86	11.06	1.60**	± 0.05	2.41	0.88	7.00E-13	0.90	2.00E-12	0.93
BIT10M#	Bit. coal, moist	CO_2	8.1	40	24.0	0.32	53.83	10.87	1.20	0.05	1.81	0.97	6.00E-13	0.92	2.00E-12	0.96
					24.0	0.32	33.20	6.01	1.19*	± 0.04	1.79	0.97				
						0.32	16.37	2.50	1.48**	± 0.04	2.23	0.96	2.00E-12	0.95	5.00E-12	0.97
ANT5M	Anthracite, moist	CO_2 (twice)	8.0	40	22.6	0.04	11.64	1.25	1.27	± 0.02	1.91	0.98	5.00E-12	0.98	1.50E-11	0.93
					24.8	1.13*	1.70									
						0.04	2.70	0.52	1.11**	± 0.01	1.67	0.99	5.00E-12	0.75	1.50E-11	0.88

Table 5.2: Surface strain of moist anthracite samples (in percent) compared to their air-dried state, defined as $100\times\ (A_t - A_0)/A_0$, where A_0 is the surface area of the sample before, and A_t the surface area of the sample after the ASTM moisturizing procedure. The digital image of the coal sample was taken within 30 minutes after taking the sample out of the dessicator, to limit loss of moisture. A negative strain value indicates a decrease in size (i.e. shrinkage).

Exp. No	Material	P [MPa]	T [°C]	Humidity [%]	Exposure time [days]	P [MPa]	T	Surface strain [%]
ANT5M	Anthracite	0.05	30	96	~4	atmosph., 0.1	room	-0.39
ANT6M	Anthracite	0.05	30	96	~4	atmosph., 0.1	room	-0.09
ANT7M	Anthracite	0.05	30	96	~4	atmosph., 0.1	room	-0.47
ANT8M	Anthracite	0.05	30	96	~4	atmosph., 0.1	room	-0.66

5.2.3 Experimental results: strain development with time

All air-dry samples plus pre-moisturized sample ANT5M showed swelling upon exposure to added Ar, CH_4 and CO_2, with a gradual approach to equilibrium dimensions (see Figures 5.1 to 5.3). The chosen hyperbolic function provided mostly good fits to the data, as indicated by correlation coefficients (R_s) in the range 0.86-0.99 (Tab. 5.1). Exceptions are a) the experiments with Ar (SUB3 and ANT1), which did show the development of an equilibrium strain but displayed low correlation coefficients of 0.41 and 0.71, and b) experiment ANT2 performed using anthracite and CH_4, which did not show the development of a clear equilibrium strain (Tab. 5.1). In the description of our results that follows, an increase in sample size (i.e. swelling) is specified as a positive strain (e_s)while a decrease in size (i.e. shrinkage) is specified as a negative strain. We structure our description according to the gases added rather than per coal type.

The subbituminous coal sample exposed to Ar (SUB3) developed an equilibrium strain (e_{s-max}) of 0.24%, while the anthracite sample (ANT1) showed an e_{s-max} of 0.21% upon Ar exposure (see Figures 5.1a and 5.3a, plus Tab. 5.1). Half of the swelling was reached within 1 to $1^1/_2$ hours, but the error in this estimate is large due to scatter in the data. After gas release, the strain returned to zero for the subbituminous coal sample while the anthracite showed negative strain values before returning to near-original dimensions (Figures 5.1a and 5.3a).

The samples that were exposed to CH_4 showed an e_{s-max} value of 0.20% for subbituminous coal (SUB4 - Fig. 5.1b) to 0.43% for Anthracite (ANT3 - Fig. 5.3b). The anthracite sample in the second test with CH_4 (ANT2) exhibited an on-going increase in strain and no e_{s-max} value could be retrieved (Fig. 5.3b). The subbituminous coal sample (SUB4) required about $1^3/_4$ hours to reach 50% of its maximum swelling,

whereas ANT3 required about half an hour. SUB4 exhibited a negative strain after gas release, although equilibrium seems not to have been reached, even 20 hours later (Fig. 5.1b). One anthracite sample returned to its original dimensions (ANT2), while the other (ANT3) retained a permanent positive strain of 0.1% (Fig. 5.3b).

The samples that were exposed to CO_2 showed e_{s-max} values of 1.09% for subbituminous coal (SUB5 - Fig. 5.1c, first exposure cycle), 1.94% for bituminous coal (BIT11 - Fig. 5.2), and 1.95% for anthracite (ANT4 - Fig. 5.3c). Both the subbituminous and bituminous coal sample show a value of $t_{1/2}$ of approximately 1 hours. For the anthracite, $t_{1/2}$ is about 12 minutes. Experiment SUB5 showed a distinct, permanent strain of -0.7% after pressure release (first exposure cycle, Fig. 5.1c), whereas ANT4 exhibited a positive strain of 0.65% (Fig. 5.1c). Strain evolution after gas release was not determined for BIT11 (Fig. 5.12). Re-introduction of CO_2 in experiment SUB5 showed a higher maximum strain value (1.34%) than was observed after the first exposure cycle, despite the fact that re-exposure started at a negative strain (Fig. 5.1c). Half of the maximum swelling strain was also reached faster than during the first cycle (Tab. 5.1). After the gas release in the second cycle, the sample returned to its size after the first cycle.

Before pressurization with CO_2, pre-moisturized sample ANT5M showed a negative strain of -0.39% relative to its air-dried state (Tab. 5.2, Fig. 5.1d). The three air-dried anthracite samples that were separately tested also showed shrinkage compared to their original size in the moisturized state (see Tab. 5.2). Although marker point identification in the images was difficult, the shrinking effect was thus identified in all four moisturized samples. The strain developed in pre-moisturized sample ANT5M after first addition of CO_2 was +1.27%, measured relative to the moisturized state (dotted line, Fig. 5.3d). After gas release, the sample shrank to surface dimensions slightly larger than its starting size. The observed strain (1.13%) during the second cycle of exposure to CO_2 was lower relative to the moisturized state than during the first cycle. The sample returned more or less to its starting, moist dimensions after gas release in the second cycle, though our fitting procedure suggests a small, positive, residual strain (Fig. 5.3d).

5.3 A model for time-dependent swelling and comparison with experimental data

While the kinetic parameter $t_{1/2}$ obtained from the empirical hyperbolic function fitted to our data can be used to compare the rates of swelling seen in our different experiments, neither the hyperbolic fit nor $t_{1/2}$ have a physical meaning (van Bergen *et al.*, 2009a). As mentioned before, it is well-established for all coals exposed to CO_2, CH_4, Ar or water, that swelling is related to adsorption on the internal surface area of the coal (e.g. Goodman *et al.* (2005b); Goodman *et al.* (2006); Karacan (2003); Karacan (2007); Robertson and Christiansen (2005a). As such, the kinetics of swelling seen in our samples must depend on the kinetics of gas/fluid transport through the matrix

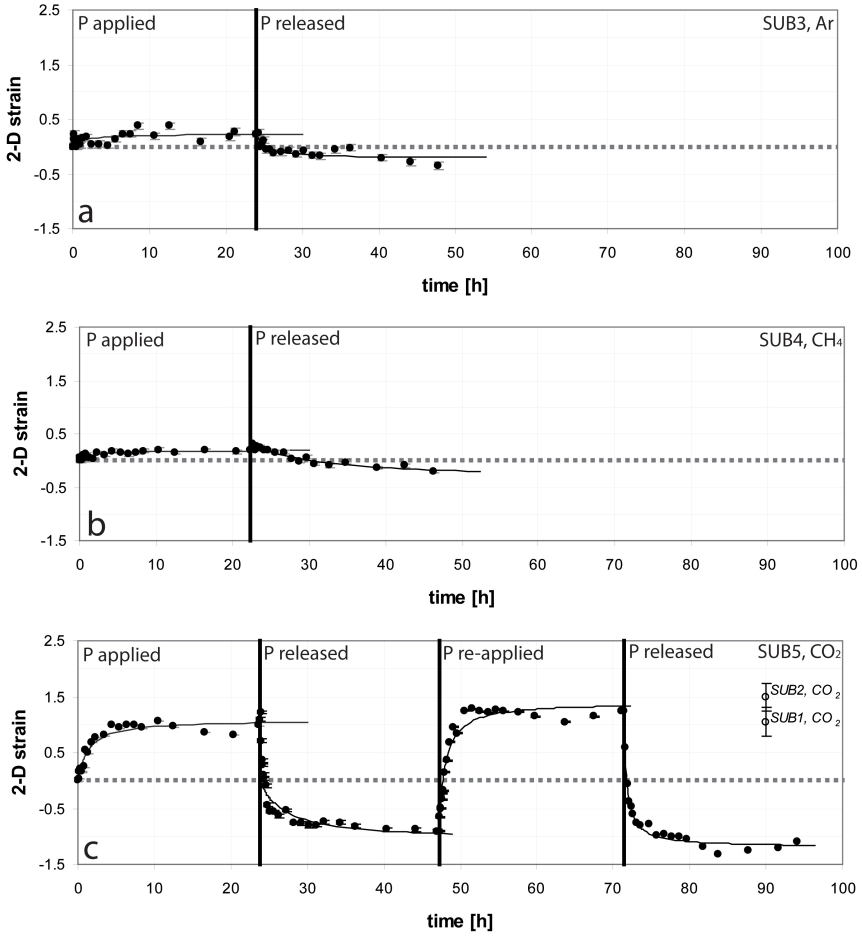

Figure 5.1: Surface strain (e_s) vs. time plot for the swelling experiments performed on subbituminous samples: a) with Ar, b) with CH_4, and c) with CO_2. Experiment SUB5 was repeated in two cycles. The vertical black line indicates the point of pressure release and of re-application in experiment SUB5. The hyperbolic fit made is shown in all graphs. The values determined for e_{s-max} in similar experiments at the same pressure and temperature conditions on subbituminous coal reported by Van Bergen *et al.* (2009a) are plotted for comparison (arbitrarily at 90h - SUB1 and SUB2).

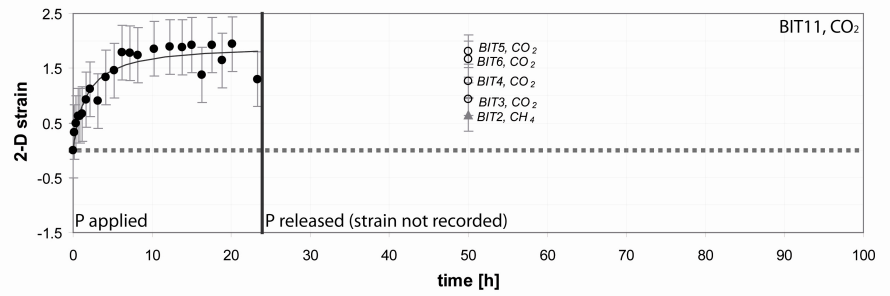

Figure 5.2: Surface strain (e_s) vs. time plot for the experiment on bituminous coal sample BIT11 with added CO_2. The hyperbolic fit is shown. For this experiment, no further measurements were done after gas release. The values determined for e_{s-max} for similar experiments at the same pressure and temperature conditions on bituminous coal reported by Van Bergen *et al.* (2009a) are plotted for comparison (arbitrarily at 50h - BIT2, BIT3, BIT4, BIT5 and BIT6).

pore system and/or on the kinetics of adsorption on the pore surfaces.

The time required for the adsorption step can be considered negligible compared to the time required for transport (e.g. Gruszkiewicz *et al.* (2009)). As indicated by Kelemen and Kwiatek (2009), many kinetics studies dealing with CO_2 and CH_4 adsorption/desorption by coal have accordingly been interpreted within a Fickian diffusion framework assuming a unipore model (Bielicki *et al.*, 1972; Busch *et al.*, 2004; Charrière *et al.*, 2009; Clarkson and Bustin, 1999b; Kissell and Bielicki, 1972; Marecka and Mianowski, 1998; Mavor *et al.*, 1990; Nandi and Walker Jr, 1975; Smith and Williams, 1982; Smith and Williams, 1984), or a bidisperse pore model (Clarkson and Bustin, 1999b; Cui *et al.*, 2004; Shi and Durucan, 2005; Smith and Williams, 1982), i.e. single valued or bimodal pore size distributions. In line with this, the kinetics of swelling of coal will also be governed by Fickian diffusion of gas or fluid into the coal structure , although some authors have interpreted the kinetics of swelling in terms of so-called Case II diffusion, which involves a solvent uptake process whose rate is controlled by relaxation of the macromolecular network structure and is characterized by a sharp front separating the swollen and unswollen regions of the coal (Mazumder *et al.*, 2006a; Otake and Suuberg, 1997).

In the following, we develop a swelling model based on Fickian diffusion and apply it to retrieve quantitative values for matrix diffusion coefficients of the coal samples tested, which are then compared with literature data. We assume that transport in the coal matrix occurs entirely by diffusion and that diffusion can be described by a simple diffusion coefficient, which is equivalent to a unipore model for the pore structure of the coal. In other words, we assume that the pore system of the matrix is homogeneous, with no short-circuit or rapid diffusion paths, so that the bulk diffusion coefficient reflects a single diffusion process through pores of more or less uniform dimensions. The unipore model is better applicable for bright coals, because of their

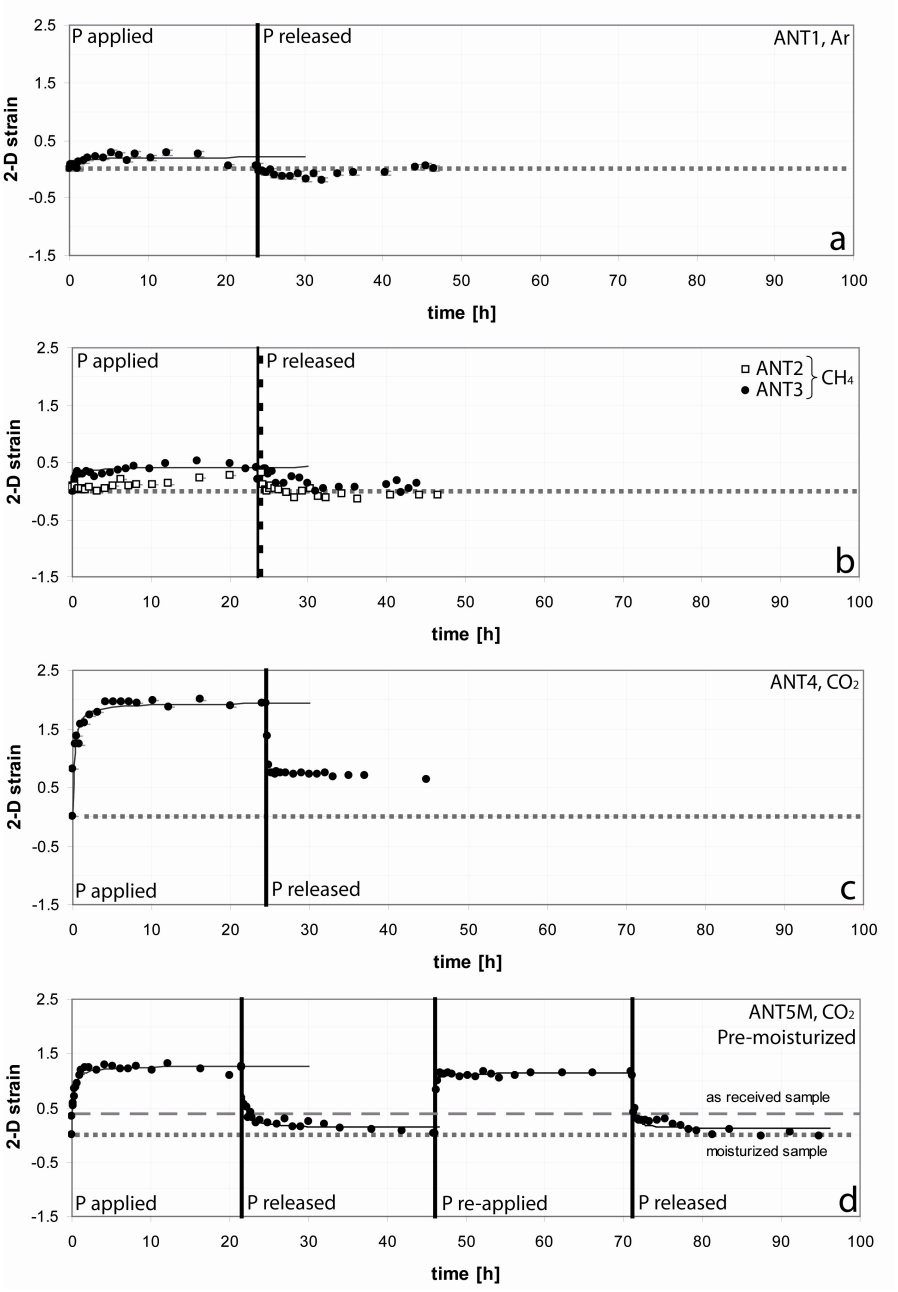

Figure 5.3: Surface strain (e_s) vs. time plot for the experiments on anthracite samples:a) with Ar, b) with CH_4, c) with CO_2, and d) with CO_2 using a pre-moisturized sample. The vertical black line indicates the point of pressure release (or re-introduction in d). The dashed line in b) indicates the point of gas release in ANT2. The hyperbolic fit made is shown in all graphs, except for ANT2 where it could not be determined. In the bottom graph for ANT5M, the dotted line corresponds to the dimensions of the sample after the moisturizing procedure. The strain relative to this reference value, measured before moisturizing (as received), is shown by the dashed line. In this experiment (ANT5M), CO_2 was introduced in two cycles.

uniform micropore structure compared with dull or banded coals, which have a more complicated pore structure (Gamson *et al.*, 1993) and seem to require a bidisperse model (Clarkson and Bustin, 1999b). The unipore approach is considered acceptable for the purpose of the present study because our samples are bright coals. Moreover, application of the unipore Fickian diffusion model (*cf.*Charrière *et al.* (2009); Crosdale and Beamish (1995)) gives a first approximation of diffusion parameters that can be incorporated into existing CBM/ECBM reservoir simulators (Busch *et al.*, 2004; Kelemen and Kwiatek, 2009).

5.3.1 Model formulation

Following the above reasoning, our model focuses on the transport properties of the coal by assuming that adsorption, and thus swelling response, is instantaneous once the diffusing species reaches the adsorption sites. In other words, we assume that the rate controlling step for swelling of our coal particles is diffusion through the coal matrix. We further assume that pressure driven flow does not occur in the matrix particles considered, i.e. transport is diffusion only. We are accordingly treating the uptake of the diffusing species as one of dissolution in the coal. For mathematical tractability, we treat the coal particles as spheres.

Diffusion equations

Transport of gas or fluid from the outer boundary of the sample to its centre is described by Fick's first and second laws, written

$$J = -D\,grad C \quad (Fick's\ first\ law) \tag{5.2}$$

and

$$\frac{\partial C}{\partial t} = D\,div(grad C) \quad (Fick's\ second\ law) \tag{5.3}$$

where J is the diffusion flux (mol/m^{2}s), D is the effective diffusion coefficient (m^2/s) of the diffusing species in the coal matrix, C is its concentration (mol/m^3), and t is time (s). Note that D as defined here is a bulk diffusion coefficient that includes the effects of matrix porosity, tortuosity and intrinsic pore diffusion coefficient.

Chemical potential of the diffusing species

For the present (hydrostatic) problem, whereby the detailed thermodynamic behaviour of the diffusing species within the coal is unknown, it is convenient to specify its thermodynamic state in terms of its chemical potential (μ_f), or partial molar Gibbs free energy. For a given hydrostatic pressure (P) and temperature (T), the chemical potential of a gas or compressible fluid, in a free volume such as that outside our coal samples, is given by the standard relation

$$\mu_f = \int_0^P V\,(P,T)\,dP \tag{5.4}$$

where V is the molar volume of the gas or fluid. Now, the molar volume of the gas or fluid in the void space outside the coal sample in our experiments is given by the appropriate equation of state. Hence, for a given pressure and temperature, Eq. (5.4) plus the equation of state (EOS) gives the chemical potential (μ_{f-max}) of the gas or fluid phase at the outer boundary of the sample. This is easily obtained in practice by numerical integration of Eq. (5.4).

The diffusive transport from the outer boundary of the coal particle to its centre is driven by the internal concentration gradient of the diffusing species according to Eq. (5.2). However, from the theory of solutions, the pointwise concentration (C) of the diffusion species within the coal can be related to its local chemical potential (μ) via the relation;

$$\mu = \mu_0 + RT\,ln\frac{\gamma C}{\gamma_0 C_0} \tag{5.5}$$

where μ_0 is an reference chemical potential at standard conditions, γ_0 is a reference activity coefficient, γ is activity coefficient, C_0 is the reference concentration, R is the universal gas constant, and T is temperature.

At equilibrium, the chemical potential (μ) throughout the coal equals the chemical potential in the gas or fluid (μ_{f-max}) beyond the outer boundary of the coal. If the chemical potential at the outer boundary changes due to a pressure change in the gas or fluid, the concentration and chemical potential inside the coal will evolve accordingly in an attempt to re-establish global equilibrium. This will lead to an evolving chemical potential and concentration profile. The change in chemical potential with concentration, assuming γ is constant, follows from the derivative of Eq. (5.5):

$$\frac{\partial \mu}{\partial C} = \frac{RT\gamma}{\gamma C} = \frac{RT}{C} \tag{5.6}$$

This can now be coupled with Fick's first law (Eq. (5.2)) using the relation

$$gradC = \frac{\partial C}{\partial \mu} \cdot grad\mu = \frac{C}{RT} \cdot grad\mu \tag{5.7}$$

to obtain

$$J = -\frac{DC}{RT} \cdot grad\mu \tag{5.8}$$

which is Fick's first law written in terms of chemical potential gradient.
The advantage of using the chemical potential in this way, compared to concentration, is the avoidance of having to use an EOS to determine the concentration of the diffusing species in the coal from the external (partial) pressure or from the (partial)

pressure in the pore system, and the avoidance of having to assume activity coefficient values. Recent investigations indicate that the EOS is not applicable inside the pore system. For example, Melnichenko *et al*. (2009) report that molecular gas-pore wall interactions inside the porous matrix result in condensing the saturating gas into a liquid, leading to a fluid density of injected CO_2 in pores that is a factor of three to four larger than the density of unconfined or free CO_2 at similar thermodynamic conditions. Further evidence for deviations from the EOS inside the pore system can be deduced from other results of Melnichenko *et al*. (2009) and from those of Radlinski *et al*. (2009). It is for this reason that we treat the problem as one of pure diffusion of a solute into a solid (solvent) medium.

Swelling vs. chemical potential

The above relation (Eq. 5.8) provides a means of calculating the evolution of the chemical potential profile inside a coal particle, as time progresses after exposure to an external gas or fluid pressure. This can be used to determine the evolution of swelling with time, if we can establish a relation between (local) chemical potential and swelling. When global equilibrium is reached in experiments such as those reported here, the final or equilibrium volumetric strain (e_{v-max}) achieved can be related to the chemical potential of the gas/fluid species which must be uniform throughout the system, i.e. equal within and outside the coal sample. Using Eq. (5.4), the swelling vs. pressure data obtained by Van Bergen *et al*. (2009a) provide the basis for such a relation. However, the form of the relation (linear or non-linear) between pressure and swelling strain is not well established, as the discussion in literature about the relation between adsorption and swelling is not yet settled (e.g. (Bustin *et al*., 2008; Cui *et al*., 2007; Harpalani, 2005; Harpalani and Chen, 1995; Kelemen and Kwiatek, 2007; Kelemen and Kwiatek, 2009; Levine, 1996; Majewska *et al*., 2009; Pekot and Reeves, 2002). In this study, a linear relation is assumed between chemical potential and volumetric strain (e_v), following the trend seen in the data presented by Van Bergen *et al*. (2009a). This is accordingly written:

$$e_v = a \cdot \mu_f + b \; or \; \frac{de_v}{d\mu_f} = a \tag{5.9}$$

The slope (a) of this line can be determined for each of the present experiments, on an individual basis, using

$$a = \frac{e_{v-max}}{\Delta\mu_{f-max}} \tag{5.10}$$

where $\Delta\mu_{f-max}$ is the difference between the chemical potential at atmospheric pressure and at the pressure applied in the experiment. Equation (5.9) can then be applied to all points within a given coal particle assuming that adsorption is instantaneous, thus that local equilibrium is attained at all times, and that no mechanical interaction or effect of internal strain gradients occurs within the sample. Using equations (5.8) and (5.9), we now have all that is needed to calculate strain development in a coal particle with time.

Specific application to spherical coal particles

As already mentioned, we assume that our coal particles can be treated as spheres. A spherical diffusion model is commonly used to interpret sorption of gas by coal samples using an analytical solution for unipore diffusion based on the work of Carslaw and Jaeger (1959) and Crank (1975). This will be discussed later.
Our diffusion model assumes that a spherical particle with radius R is exposed instantaneously to a gas or fluid at pressure P. Using spherical coordinates, the radial position from the centre of the sphere is represented by r. In such a situation, it is easily shown that

$$\frac{\partial \mu}{\partial t} = \frac{\partial C}{\partial t} \cdot \frac{RT}{C} = D \left[\frac{\partial^2 \mu}{\partial r^2} + \frac{1}{RT} \cdot \left(\frac{\partial \mu}{\partial r} \right)^2 + \frac{2}{r} \cdot \frac{\partial \mu}{\partial r} \right] \tag{5.11}$$

The solution to this equation for $\mu(r, t)$, coupled with Eq. (5.9) and with the initial condition

$$\mu\,(r, 0) = \mu_I \tag{5.12}$$

and the boundary conditions

$$\left. \frac{\partial \mu}{\partial r} \right|_{r=0} = 0 \tag{5.13}$$

and

$$\mu \Big|_{r=R} = \mu_{f-max} \tag{5.14}$$

gives the evolution of the swelling strain profile $\epsilon_v(r, t)$, assuming no effects of the strain gradient on swelling as mentioned above. Here, μ_I is the initial, uniform value of the chemical potential of the diffusing species in the coal before the experiment starts, and $\epsilon_v(r, t)$ is the pointwise equivalent of e_v.

The total volume change $\Delta V(t)$ and hence volumetric strain of the sample is finally obtained from the sum of the strain in all individual shells of thickness dr, as swelling progresses. The total volumetric strain (e_v) is thus given by

$$e_v\,(t) = \frac{\Delta V\,(t)}{V_0} = \frac{1}{V_0} \int_0^R \epsilon_v\,(r, t)\, 4\pi r^2 dr = \frac{3}{R^3} \int_0^R (a \cdot \mu\,(r, t) + b)\, r^2 dr \tag{5.15}$$

Note that for calculating $\mu(r, t)$ and $\epsilon_v(r, t)$, this approach assumes that r remains constant with time, thereby ignoring the strain development in r. The impact of this assumption on the results for $e_v(t)$ will be negligible, however, as changes in r will be of the order of $e_v/3$ whereby e_v is of the order of 0.3 to 3.5% in our samples (Tab. 5.1).

Numerical implementation

The simplest possible finite difference solution of Eq. (5.11) to yield μ as a function of r and t is now given by

$$\Delta\mu = D\left[\frac{\partial^2\mu}{\partial r^2} + \frac{1}{RT}\cdot\left(\frac{\partial\mu}{\partial r}\right)^2 + \frac{2}{r}\cdot\frac{\partial\mu}{\partial r}\right]\Delta t \tag{5.16}$$

Given the present P-T conditions and range of μ and r values corresponding to our experimental configuration, the second term is negligible as it is more than 1000 times smaller than the third term. Eq. (5.16) is then reduced to

$$\Delta\mu \approx D\left[\frac{\partial^2\mu}{\partial r^2} + \frac{2}{r}\cdot\frac{\partial\mu}{\partial r}\right]\Delta t \;\; which\ is\ equivalent\ to\ \Delta\mu \approx D\left[\frac{1}{r^2}\frac{\partial}{\partial r}\left(r^2\frac{\partial\mu}{\partial r}\right)\right]\Delta t \tag{5.17}$$

whereby the following explicit approximation was used:

$$\frac{\partial}{\partial r}\left(r^2\frac{\partial\mu}{\partial r}\right) \approx \frac{1}{\Delta r}\left(\left(\frac{(r_i + r_{i+1})}{2}\right)^2\cdot\frac{\mu_{i+1}-\mu_i}{\Delta r} - \left(\frac{(r_i + r_{i-1})}{2}\right)^2\cdot\frac{\mu_i-\mu_{i-1}}{\Delta r}\right) \tag{5.18}$$

Substitution of Eq. (5.18) in Eq. (5.17) leads to:

$$\Delta\mu = D\left[\frac{1}{r^2}\frac{1}{\Delta r}\left(\left(\frac{(r_i + r_{i+1})}{2}\right)^2\cdot\frac{\mu_{i+1}-\mu_i}{\Delta r} - \left(\frac{(r_i + r_{i-1})}{2}\right)^2\cdot\frac{\mu_i-\mu_{i-1}}{\Delta r}\right)\right]\Delta t \tag{5.19}$$

which was the actual Euler form used.

A finite difference algorithm programmed in Fortran 95 was used to provide the numerical solution to Eq. (5.19). The explicit approximation given in Eq. (5.19), uses values of the chemical potential in a previous time step (t-1) of neighboring points (r+1 and r-1) in space. At the inner boundary of the model, i.e. the centre of the sample, an artificial additional point was assumed with a similar value for chemical potential as that calculated for the centre. This simulated the boundary condition defined by Eq. (5.13). Any artifacts because of this assumption are limited because of the relatively small volume of the innermost sphere, given a sufficiently large number of distance steps (Δr), in the finite difference calculation. At the outer boundary of the sphere, the chemical potential is fixed, as given by Eqs. (5.4) and (5.14).

Strain development in the concentric shells ($e_{v(s)}$) of the spherical coal particle in time and space was calculated by combining the result of Eq. (5.19) with Eq. (5.9), written as $\Delta e_{v(s)} = a\cdot\Delta\mu$. Explicitly, this was calculated in finite difference form using

$$\Delta e_{v(s)} = a \cdot D \left[\frac{1}{r^2} \frac{1}{\Delta r} \left(\left(\frac{(r_i + r_{i+1})}{2} \right)^2 \cdot \frac{\mu_{i+1} - \mu_i}{\Delta r} - \left(\frac{(r_i + r_{i-1})}{2} \right)^2 \cdot \frac{\mu_i - \mu_{i-1}}{\Delta r} \right) \right] \Delta t \tag{5.20}$$

Finally, the total volumetric strain (in percent) of the particle was calculated as a function of time using Eq. (15) written in the form

$$e_v(t) = \frac{300}{R^3} \sum_{0}^{n} \Delta e_{v(s)} \cdot r^2 \Delta r \tag{5.21}$$

with n being the number of distance steps taken in the model, and by taking

$$\epsilon_v(r, 0) = 0 \tag{5.22}$$

The model results in a bulk strain vs. time plot that can be fitted to the measured data by adjusting the value of the diffusion coefficient D.

5.3.2 Model input

The spherical diffusion model requires various input parameter values in order to run. These include R, μ_f, e_{v-max} and values for parameters a and b of the relation between chemical potential and volumetric strain (Eqs. (5.9) and (5.10)). To simulate each experiment performed, the particle radius (R) was taken as the shortest distance from the edge to the centre of the sample and was measured for each individual sample on the initial image, i.e. taken just before the introduction of the gas or fluid. The chemical potential for Ar, CH_4 and CO_2 in the void space outside the coal at different pressures was determined by combining Eq. (5.4) with the EOS for these gases using the NIST website data for Ar and CH_4 and the Span and Wagner (1996) EOS for CO_2. The initial, uniform value of chemical potential μ_I, i.e. before addition of gas or fluid, was calculated from the partial pressure of each particular gas in air at atmospheric pressure and at 40°C (the constant temperature of the experiments). However, the final calculation of $e_{v(s)}$ and e_v depends only on changes in $\mu(r, t)$ and is hence independent of μ_I. A plot of volumetric strain vs. relative chemical potential (i.e. the difference between μ and μ_I) is shown for a selection of experiments in Fig. 5.4. The equilibrium volumetric strain (e_{v-max}) of each individual experiment was used to determine parameters a and b from Eqs. (5.9) and (5.10). A division of the particle radius into 100 distance steps (Δr) and a time step (Δt) of 0.1 seconds provided stable numerical solutions for all experiments simulated.

5.3.3 Varying the diffusion coefficient to fit the experimental data

Our models were fitted to the volumetric strain data as determined for each experiment individually (Figures 5.1- 5.3) by varying the diffusion coefficient value entered into the numerical model. The resulting curve of swelling vs. time was compared to

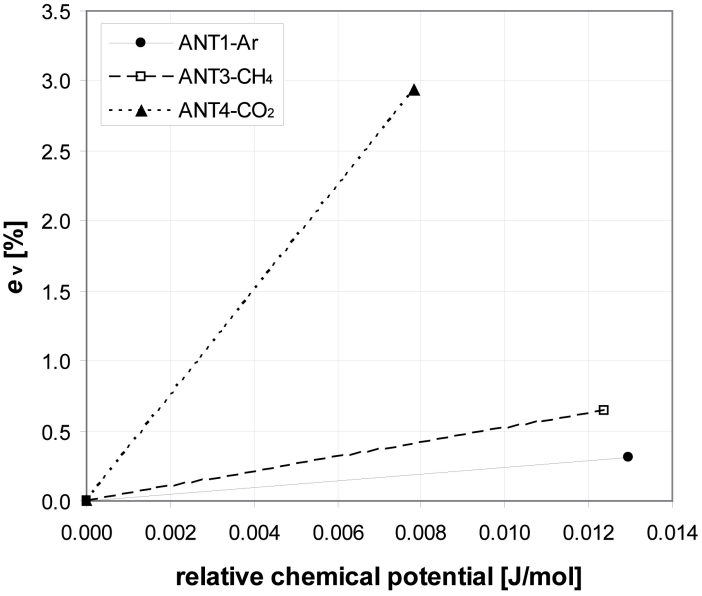

Figure 5.4: Volumetric strain (e_v) vs. the relative chemical potential (μ-μ_I) for anthracite samples. The initial chemical potential (μ_I) was defined from the partial pressure of the particular gas in air at atmospheric pressure and 40°C. At atmospheric pressure, no swelling is assumed. Chemical potential is calculated for the individual experimental pressure (see Tab. 5.1).

the volumetric strain data with time that were calculated from the surface strains that were determined from the experimental results (calculations *cf.*Robertson and Christiansen (2005a), see Tab. 5.1). A number of different values for D were tested and the fit to the data was examined by calculating the correlation coefficient (R_D) between the data, calculated to volumetric strain, at the designated time and the model result at that same time. The lower and the higher value of D, listed in Tab. 5.1, are indications of the lower and upper boundaries of the range of diffusion coefficients that provide an acceptable fit to the measured data, as expressed by a correlation coefficient higher than 0.9. This resulted in lower and higher values of the diffusion coefficient, obtained for each of the present experiments, and for those reported by Van Bergen *et al*. (2009a).

5.4 Discussion

5.4.1 Comparison with analytical approximation and previous diffusion data

As already indicated, unipore spherical diffusion models based on work of Carslaw and Jaeger (1959) and Crank (1975), have been applied to interpret diffusion of gases into coal samples by Charrière *et al.*(2009), Clarkson and Bustin (1999b), Mavor *et al*. (1990), Nandi and Walker (1964), Nandi and Walker (1970), Nelson and Walker (1961), and Smith and Williams (1984). Besides the assumption that the porous solid is spherical, this approach assumes that the solid is interspersed with nonconnecting cylindrical pores of one radius (Smith and Williams, 1984). Under the assumption that adsorption is diffusion controlled and that the concentration (potential) at the surface of the spherical particle is constant, which is an important boundary condition in our experiments, the fraction of gas adsorbed at any time is given by:

$$\frac{M}{M_t} = 1 - \frac{6}{\pi^2}\sum_{n=1}^{\infty}\frac{1}{n^2}exp\left(-\frac{Dn^2\pi^2 t}{r_p^2}\right) \tag{5.23}$$

where M is volume of gas adsorbed, M_t is the maximum volume of gas adsorbed, and r_p is the particle radius. For very short times, or where $\frac{M}{M_t} < 0.5$, the following approximation normally is used:

$$\frac{M}{M_t} \cong \frac{6}{\sqrt{\pi}}\sqrt{\frac{Dt}{r_p^2}} \tag{5.24}$$

Assuming that adsorbed mass and swelling strain are linked in a (near) linear manner, as suggested by the analysis of previous experimental data by Pan and Connell (2007), $\frac{M}{M_t}$ in Eq. (5.24) can be substituted by $\frac{e_v}{e_{v-max}}$, leading to

$$\frac{e_v}{e_{v-max}} \cong \frac{6}{\sqrt{\pi}}\sqrt{\frac{Dt}{r_p^2}} \tag{5.25}$$

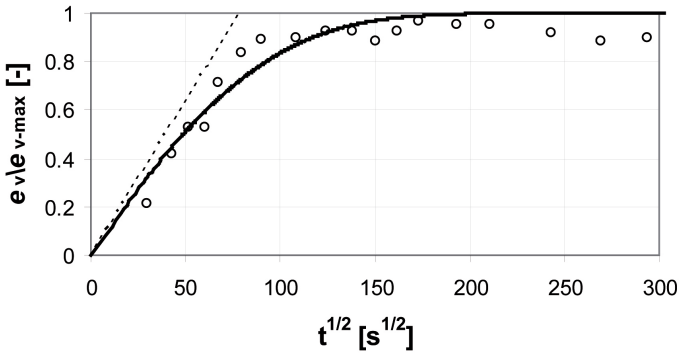

Figure 5.5: Development of e_v/e_{v-max} with time for experiment SUB2, as measured (open circles) and as modelled with the present spherical diffusion model (solid line) and with the approximate relation (dotted line) of Eq. (5.25). For both the spherical model and for the approximation a value for the particle radius of 0.464 mm and a D-value of 3×10^{-12} m^2/s were used.

The validity of this approximation, for very short times, constitutes a major limitation of this approach, because it depends heavily on measurements made directly after the start of the experiment, which may be less accurate, due to effects such as the Joule-Thompson effect (Charrière *et al.*, 2009). The finite difference approach followed in this study is less dependent on these first measurements and provides a fit up to the point at which equilibrium is reached.

Inserting similar values of the diffusion coefficient and the particle radius into both the approximation of Eq. (5.25) and the finite difference model yields very similar results for short times (Fig. 5.5). For longer times, the results given by Eq. (5.25) and the finite difference model deviate, whereby our model follows the data more closely. Comparison between the approximate analytical form (5.25) and the finite difference solution confirms the comment by Smith and Williams (1984) that the total time required for equilibrium is an order of magnitude longer than predicted by Eq. (5.25). This result provides added confidence in the applicability of our finite difference model. However, a more exact numerical calculation would be desirable in future work, incorporating all terms in Eq. (16).

The results given in Tab. 5.1 show that the values determined for the effective diffusion coefficient D using the finite difference model are of the order of 10^{-11} to 10^{-14} m^2/s for CO_2, and of the order of 10^{-12} to 10^{-13} m^2/s for Ar and CH_4. Comparison with literature data is complicated because of the different coal types and different experimental conditions used by different authors. Moreover, values in the literature have been determined by comparing lab data with different finite different models, the approximation of Eq. (5.25), etc. Still, even when considered indicative only, a

comparison shows that the results of our study are within range of the reported values (Tab. 5.3).

Many previous authors found fast and slow diffusion rates through the application of bidisperse models or approximations (e.g. Smith and Williams (1984), Clarkson and Bustin (1999b), Pone *et al*. (2009b)). The slow diffusion observed ($D < 10^{-9}$ m^2/s) is always attributed to micropore transport. Clearly, the values reported in this study are associated with the slow diffusion rates and thus with micropore diffusion. Most probably, our method of preparation of the matrix coal samples resulted, as intended, in the elimination of larger pathways, such as cleats or microfractures (as defined by Gamson *et al*. (1993)). Moreover, these microfractures are less likely to occur in the bright coals used (Clarkson and Bustin, 1999b; Gamson *et al*., 1993). Larger size blocks are likely to contain these cleats or microfractures, and diffusion modeling of such samples could require bidisperse models. This should be taken into account when upscaling to seam transport is required.

5.4.2 Rank dependence of swelling and diffusion rates

In the literature, a U-shaped relation is reported between rank and adsorption (Durucan *et al*., 2009; Laxminarayana and Crosdale, 1999) and between rank and swelling (Durucan *et al*., 2009). This relationship has been explained as reflecting the total porosity of the coal matrix, which also shows a U-shaped relation with rank (Durucan *et al*., 2009; Mares *et al*., 2009; Rodrigues and Lemos de Sousa, 2002). The relatively high porosity, up to 25%, in lower rank coal is mainly due to macroporosity that is dominant in coal with a carbon content less than about 75% (Gan *et al*., 1972), although others report an equal contribution of micro- and macroporosity to the total matrix porosity of low rank coals (Mares *et al*., 2009). At higher rank, high volatile bituminous or higher, the meso- and macroporosity is 1-3 orders of magnitude less than the microporosity (Prinz *et al*., 2004). However, with increasing rank not only macroporosity but also microporosity decrease, resulting in a decrease of total porosity of the matrix, which can fall to 1% or less for bituminous coal (Levine, 1993; Mares *et al*., 2009). Microporosity increases again with further coalification into the anthracite stage, whereas macroporosity remains low (Gan *et al*., 1972). The recovery of total matrix porosity at anthracitic rank is therefore due to an increase of microporosity. The minimum in the total porosity is found at a carbon content in the range of 87 - 92% (Mares *et al*., 2009), corresponding to a vitrinite reflectance value of about 1.25 to 2.40% (Stach *et al*., 1982). Prinz and Littke (2005) report a minimum in the microporosity in the range of 1.2-1.4% vitrinite reflectance.

Because swelling is related to adsorption in the smallest micropores (Melnichenko *et al*., 2009; Radlinski *et al*., 2009), the relation expected between swelling and rank in this study was a U-shaped relation. Such a relation (with a minimum around 1.1-1.3% vitrinite reflectance) was found by Siemons and Busch (2007), based on volumetric changes interpreted from adsorption studies. However, the spread in the data of e_{s-max} vs. rank is too large to lead to any conclusions in this context (Fig. 5.6), also

Table 5.3: Literature values of diffusion coefficients in coal. Only an indicative comparison between the studies can be done as coal type and experimental conditions vary. As r_p can only be approximated, some authors choose to report values for $D/{r_p}^2$ (indicated by an *), which follows from Eq. (5.24). For comparison, we have calculated D for these studies by using a value for r_p of 1×10^{-4} m, typical for the order of the particle radius of crushed coal used in adsorption or desorption experiments.

	CO_2	CH_4	Method	
	Diffusion coefficient $[m^2 s^{-1}]$	Diffusion coefficient $[m^2 s^{-1}]$		
This study	10^{-11} to 10^{-14}	10^{-12} to 10^{-13}	Finite difference model, dry coal	
	10^{-11} to 10^{-13}		Finite difference model, moist coal (first introduction)	
Nandi and Walker (1970) *		10^{-10}	Unipore model solution, Eq. (5.24)	
Smith and Williams (1984) *		10^{-13}	Unipore model solution, Eq. (5.24)	
Olague and Smith (1989)*		10^{-11} to 10^{-13}	Value for microporosity based on bidisperse model	
Mavor *et al.*(1990)		10^{-13}	Unipore model solution, Eq. (5.24)	
Clarkson and Bustin (1999b) *	10^{-11} to 10^{-13}		Value determined by $\frac{D}{{r_p}^2}\left(\frac{\phi}{\phi+SH}\right)$	Unipore model solution, Eq. (5.24), dry coal
		10^{-12} to 10^{-15}	where is porosity, S is pore surface area per unit bulk volume of coal	Unipore model solution, Eq. (5.24), dry coal
		10^{-12} to 10^{-14}	(m^2/m^3), and H is Henry's law constant (m^3/m^2)	Unipore model solution, Eq. (5.24), moist coal
Busch *et al.* (2004)	10^{-11}		Unipore model solution, Eq. (5.24)	
Cui and Bustin (2006) *	10^{-11} to 10^{-14}	10^{-14} to 10^{-15}	Value for microporosity based on bidisperse model	
Siemons *et al.* (2007)	10^{-9} to 10^{-12}		Slow rate determined by fitting procedure	
	10^{-8} to 10^{-10}		Fast rate determined by fitting procedure	
Saghafi *et al.* (2007)	10^{-9} to 10^{-10}	10^{-10}	Matching measured flux curve to Fickian theoretical curve	
Pone *et al.* (2009b)	10^{-12}		Slow rate determined by Gaussian method	
	10^{-6}		Fast rate determined by Gaussian method	
		10^{-7}	Gaussian method	
Kelemen and Kwiatek (2009) *	10^{-13} to 10^{-16}	10^{-14} to 10^{-15}	Unipore model solution, Eq. (5.24)	
Charrière *et al.* (2009)	10^{-12} to 10^{-13}	10^{-13}	Unipore model solution, Eq. (5.24), values T dependent	

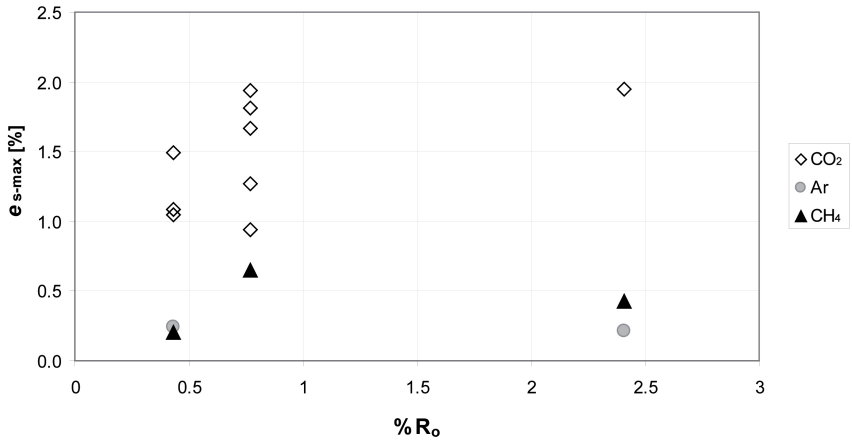

Figure 5.6: Maximum surface strain (e_{s-max}) versus rank expressed in terms of vitrinite reflectance R_0 (%).

because there are no samples were investigated with rank in the range 1-2% vitrinite reflectance, where the minimum is expected.

Similar reasoning can be followed to investigate the relation reported between rank and diffusion rates (Levine, 1993). The effective diffusion coefficient depends on the porosity in the micropores through (Olague and Smith, 1989):

$$D \approx \frac{D_i \phi_{micro}}{\tau} \tag{5.26}$$

where D_i is the intrinsic diffusion coefficient through the pore structure, ϕ_{micro} is the microporosity, and τ is the tortuosity factor for the coal pore network. Based on Eq. (5.26) and the rank dependency of microporosity describe above, a U-shaped relation was expected. Although the contours of such an U-shape are vaguely visible for the CO_2 experiments (Fig. 5.7), it is clear that the spread in data overprints any such relation. This spread is likely to be an expression of sample variability .To clarify possible rank effects in the materials studied in this paper, the dataset should be extended with coal samples of rank in the range 1-2% vitrinite reflectance.

5.4.3 Moisture dependence of diffusion

Inherent moisture constitutes an integral component of coal of all ranks and is one of the principal components of low rank coals (Levine, 1993). Experiments on the present Italian subbituminous and Polish bituminous coals by Van Bergen *et al*. (2009a) indicated that those coal samples swell as the result of water uptake, presumably through adsorption effects. A volumetric response due to water uptake or drying

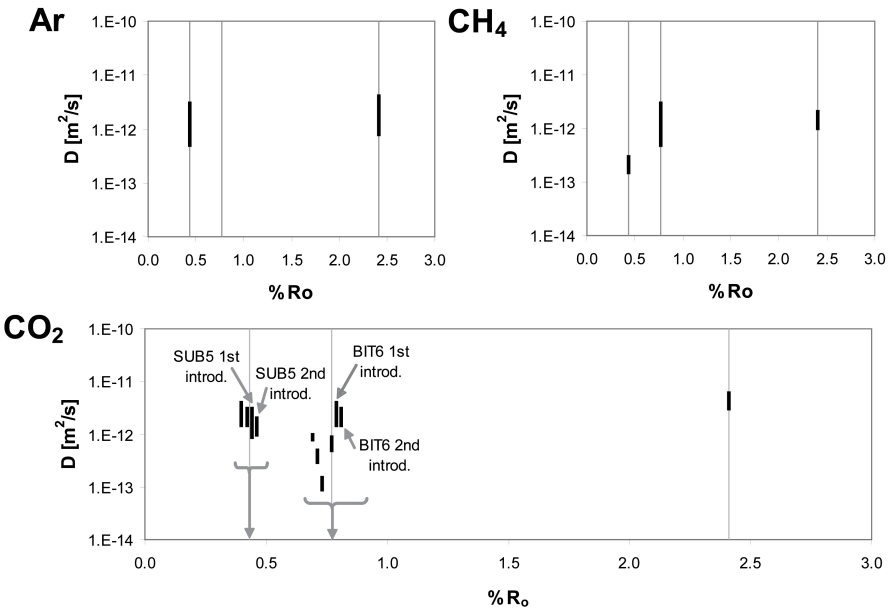

Figure 5.7: Ranges of diffusion coefficients resulting from the spherical model per coal for each gas.

has also been reported by others (Allardice and Evans, 1978; Kelemen and Kwiatek, 2009; Kelemen *et al*., 2006; Levine, 1993; Suuberg *et al*., 1993). Because swelling due to water adsorption is less than observed for CO_2 adsorption and since CO_2 and H_2O compete for the same sites (e.g. Joubert *et al*. (1974), Mavor *et al*. (1990), Seewald and Klein (1986)), moisturized coal samples should exhibit less swelling upon CO_2 exposure than (air) dried samples. However, this could not be confirmed in previous studies (Gruszkiewicz *et al*., 2009; van Bergen *et al*., 2009a), probably because of the large range of swelling values for dry coal samples. However, when CO_2 pressure is released from the samples in such experiments, it removes much of the moisture that is present in the coal, resulting in a shrinkage compared to the moisturized state before the introduction of CO_2. The individual bituminous coal samples all showed a larger swelling during the second introduction of the fluid, thus after removal of moisture, than during the first introduction. This drying effect is less marked for experiments with Ar and CH_4, because of the lower solubility of these gases in water, and vice versa.

Our moisturized anthracite sample (ANT5M) exhibited different behaviour than the moisturized bituminous coal. The anthracite revealed a shrinkage effect upon the uptake of water, which cannot be explained by the theories outlined above. The positive permanent strain remaining in experiment ANT4 (air dried coal exposed to CO_2) may therefore indicate removal of moisture, an opposite effect to that observed in subbituminous and bituminous coal. However, after the first cycle of CO_2 addition and release in experiment ANT5M (moisturized coal exposed to CO_2), the sample returned to its initial volume after moisturizing. The equilibrium strain after the second introduction of CO_2 was also almost the same (Fig. 5.3). This does not match with expectations, based on the idea that the release of the CO_2 would have removed the moisture from adsorption sites in the coal, which was expected to result in slight shrinkage of the coal compared to its initial moisturized state. A possible explanation could be that adsorption of moisture on adsorption sites in anthracite is reduced, because anthracite contains fewer hydrophilic adsorption sites, such as oxygen bearing functional groups, than bituminous coal. Competition between moisture and CO_2 for adsorption sites would therefore also be limited. Given the spread in values for the bituminous coal, the lower value for e_{s-max} (1.27%) compared to the air-dried sample (1.95%) may be attributable to sample variability rather than to the effect of moisture. At this stage, further research is required to provide an unambiguous explanation for this behaviour.

Turning to the kinetics of swelling, the rate of sorption-induced strain development is found to be significantly slower in moist samples compared with dried samples (Gruszkiewicz *et al*., 2009; Kelemen and Kwiatek, 2009). Water present in the coal, possibly in molecular clusters, impedes the entry to the pores of the coal (Krooss *et al*., 2002; Laxminarayana and Crosdale, 1999; Yee *et al*., 1993), which is therefore likely to delay diffusion into coal. Due to the large spread in diffusion coefficients obtained in our experiments, because of the earlier-mentioned variability in our samples, it is not possible to identify clear differences between the diffusion coefficients

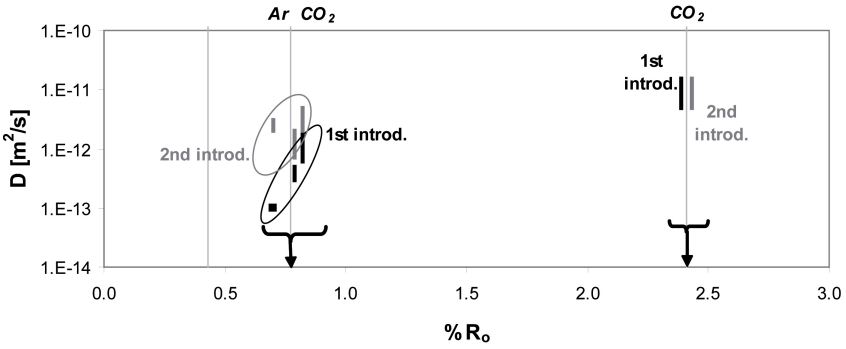

Figure 5.8: Modelled range of diffusion coefficients in the spherical model of the moisturized coal samples. No good range could be determined for the experiment with moisturized coal exposed to Ar.

of moisturized coal samples and those of air dried samples (Tab. 5.1, Fig. 5.7). However, per individual bituminous coal sample, there is a clear difference between the first and the second introduction of the CO_2 or Ar (Fig. 5.8). In our experiments, higher diffusion coefficients were obtained for the second introduction of the fluid, which suggests that drying enhances pore access. This is supported by the work of Gruszkiewicz *et al*. (2009), who report that water has no effect on adsorption rates for very finely crushed coal, and infer that water only affects the diffusion rate, but not the kinetics of adsorbate exchange at the adsorption sites. An alternative to pore blocking by water is a change in transport properties due to some chemical or other change of the coal. Allardice and Evans (1978) report that the collapsing and shrinking coal structure upon moisturization is associated with changes in physical and chemical properties that are reversible at high rank (Rees *et al*., 1939; Stansfield and Gilbart, 1932), but partly irreversible at low rank (Levine, 1993; Selvig and Ode, 1953). In our experiments, the coal structure already has undergone some strain during the first addition of gas. This could imply that the pores will open up more easily when gas is added for a second time allowing a higher diffusion coefficient.

The diffusion coefficients obtained here for the first and second exposures of the moisturized anthracite sample to CO_2 did not show this marked difference. This could suggest that moisture in anthracite does not block pore access. Taken into account the earlier observation that also the total swelling of the first and second introduction is comparable (Fig. 5.3), and that competition for adsorption sites between water and CO_2 is therefore probably limited, it appears that the effect of the presence and/or state of moisture (i.e. free or adsorbed) is different in anthracite compared to bituminous coal.

5.5 Conclusions

Experiments have been performed that involved the exposure at a pressure of ~ 8.0 MPa and a temperature of 40°C of block-shaped coal matrix fragments to CO_2, CH_4 and Ar in a see-through high-pressure cell under an optical microscope. Comparison between the observed swelling of the samples and simulation results by using a spherical model has led to the following conclusions:

- The present diffusion model provides a good fit to the data obtained for different rank coals, indicating that a simple unipore model can be used to describe the transport governed swelling of the coal matrix very well. The finite difference approximation corresponds very well to the unipore model solution based on work of Carslaw and Jaeger (1959) and Crank (1975) at the start of the diffusion process. However, whereas the unipore model solution can only be applied to fit data from the start of the diffusion process, our model provides a satisfactory fit until the end of the experiment. A more exact numerical solution would be desirable in future work, which includes all terms in Eq. (16).

- The good fit of the present diffusion model to our data is probably also related to the selection of a small matrix sample of bright coals where cleats and other microfractures, which can form a distinct second porosity in the system, are not present.

- The diffusion coefficients retrieved from fitting our model to our experimental data fall within the range of previously published literature values, indicating that swelling experiments can be used to determine transport properties of coal matrix material. Similarly, diffusion coefficients can be used to predict the development of swelling with time.

- No relation could be confirmed between the rank of the coal and the magnitude of swelling nor between diffusion coefficients and the rank of the coal. We recommend extending the data set to include samples with rank between 1 and 2% vitrinite reflectance, because a minimum in porosity and therefore in swelling and diffusion coefficient can be expected in this rank range.

- The effect of moisture on the rate of swelling seems to be larger for bituminous coal than for anthracite, which could be related to the lower content of hydrophilic sites in anthracite.

Acknowledgements

This study was undertaken as part of the Dutch national research programme CATO (on CO_2 Capture, Transport and Storage) programme, which is acknowledged for funding. Additionally, Shell International and TNO are acknowledged for co-funding and supporting this study through CATO. The laboratory experiments would have been impossible without the technical support of Peter van Krieken, Gert Kastelein,

and Eimert de Graaff who we gratefully thank. Ruud Schotting and Arie van de Berg are appreciatively acknowledged for their support on the finite difference model and the Fortran coding. Colin Peach is thanked for many fruitful discussions in the course of the study. The Central Mining Institute and the Brzeszcze mine in Poland, the Italian coal mining company Carbosulcis and Delft University of Technology are thanked for providing the coal samples.

Chapter 6

Stress-strain response of pre-compacted granular coal samples exposed to CO_2, CH_4, He and Ar

Frank van Bergen, Sander Hol & Chris Spiers

Abstract

The interaction between supercritical carbon dioxide and coal has been the subject of many studies in recent years. This paper reports two different types of swelling experiments, one on confined and one on unconfined samples of pre-pressed, crushed bituminous coal, performed at gas or fluid pressures up to 10 MPa and temperatures of around 40°C. These experiments confirm earlier observations of increased swelling of coal due to carbon dioxide adsorption compared with methane and argon. However, the experiments reveal a previously unrecognised swelling phenomenon. The swelling observed in the present samples is up to 3 times larger than that seen in block-shaped coal matrix fragments that have not been pre-compacted and is largely irreversible. We propose that pre-pressing led to permanent compaction of the internal pore structure of the coal matrix grains, decreasing the mean pore aperture and increasing the proportion of micropores. Introduction of CO_2 and CH_4 resulted in increased micropore adsorption which, through the associated surface forces developed within the micropores, led to a disjoining pressure effect that caused recovery of the pre-pressing-induced permanent strain. The higher affinity of micropores for CO_2 than for CH_4 adsorption, explains the markedly bigger effect of CO_2. After the recovery of the permanent strain was achieved, the samples seem to have exhibited a normal, reversible response to adsorption. We thus attribute the irreversible swelling effect seen in our experiments to the stress-history effect of pre-pressing. The findings of this study may be relevant for coals that have undergone deep burial

after formation, or for naturally stressed coals in tectonic zones, which may exhibit more swelling upon gas adsorption than expected from their reversible adsorption capacity.

Key words: swelling; carbon dioxide; methane; permanent strain, creep recovery

6.1 Introduction

Understanding the sorption of carbon dioxide (CO_2) and methane (CH_4) by coal and the associated swelling effects is of key importance to assessing the feasibility of using CO_2 to enhance the production of coalbed methane (ECBM). Many laboratory studies have shown that coal samples display swelling due to the uptake of gas (e.g. Day *et al*.(2008), Karacan (2007), Kelemen and Kwiatek (2009), Majewska *et al*.(2009), Mazumder *et al*. (2006b), Mazumder and Wolf (2008), Pone *et al*. (2009a), Robertson and Christiansen (2005a)). These studies also show that a larger volumetric change is observed for CO_2 sorption than for CH_4 sorption. Van Bergen *et al*. (2009a) recently investigated the swelling response of unconfined matrix blocks (~ 1 mm^3) of coal exposed to CO_2, CH_4 and argon (Ar) by means of microscopic observations performed in a high pressure optical cell. In the present paper, we report a parallel study undertaken to establish the response of confined matrix material in comparison with unconfined samples. In order to measure matrix response, rather than the more complex response of a larger sample including both matrix and cleats, we used pre-pressed aggregates of crushed and sieved coal powder, i.e. pressed granular aggregates, for both the confined and unconfined experiments. Pre-pressing of the homogenized samples at a fixed stress also allowed us to exclude microstructural variations and to fix the elastic properties of the samples, thus improving the reproducibility of volumetric measurements.

In the first part of this paper, the results of our experiments on confined samples are reported. In these experiments, the samples were loaded in a simple piston-cylinder apparatus, so as to maintain constant sample length upon addition of gas. The results showed a clear effect of pre-pressing on stress build-up due to the swelling response of the aggregates. The second part of the paper describes our experiments on unconfined samples, performed using the optical cell employed by Van Bergen *et al*. (2009a). These verify the effect of pre-pressing on swelling behaviour. Our results show that granular coal samples that are pre-compacted beyond there elastic limit recover part of their permanent strain as a result of gas adsorption. This may be relevant for understanding the swelling behaviour of intact coals that have undergone deep burial or tectonic loading after their formation.

6.2 Sample material and gases used

This study employed bituminous coal retrieved from mines in Poland and Germany. The material from Poland has been described in detail by Van Bergen *et al*. (2009a). It was taken in the form of bulk samples from Seam 364 at a depth of 640-740 m in the Brzeszcze coal mine, located in the Upper Silesian Basin of Poland. These vitrinite-dominated samples of Pennsylvanian age were passively dried, during storage at ambient conditions for 2-3 years before crushing and sieving . Their measured vitrinite reflectance was 0.77% $\pm$ 0.05.

The second bituminous coal used was mined in bulk from the Warndt-Luisenthal mine located in the Saar Basin in Germany and originates from Seam no. 1 (code 495). This material was again vitrinite dominated with a vitrinite reflectance value of 0.71% $\pm$ 0.05 as reported by Siemons and Busch (2007). This material was ground to a particle diameter below 3 mm before receipt, as described by Siemons (2007).

A sample of activated carbon was used for control experiments, in addition to the natural coal samples. The activated carbon (68% C) was manufactured by Alfa Aesar and delivered in a -20 to +50 mesh grain size fraction (0.30-0.85 mm), with a moisture content of 2 wt% and a 0.25 wt% dust fraction (dry basis).

The gases used in our experiments were high purity helium (grade 5, 99.999%), Argon (grade 5, 99.999%), CO_2 (grade 5, 99.999%) and CH_4 (grade 5.5, 99.9995%). As our experiments were conducted at 40°C, CO_2 was in the supercritical form while the helium (He), Ar and CH_4 were in the gaseous phase. For this reason all will be generally referred to as fluids.

6.3 Experiments on confined coal aggregates

These experiments consisted of piston-cylinder tests designed with the primary goal of measuring the development of axial stress in pre-compacted coal aggregate samples, constrained to undergo zero swelling strain after the addition of CO_2. The development of axial strain, after removal of the induced load from the sample, was also measured.

6.3.1 Sample preparation

In the present study, we aimed to investigate sorption-related, matrix-swelling behaviour, independently of effects on swelling and transport related to the coal's cleat system. To eliminate the cleat system from our coal samples, all coal samples and the activated carbon were ground and sieved into a range of grain size fractions. The 63-212 μm grain fraction of the natural coals and the activated carbon was selected for our experiments because the grain size was much finer than the average cleat spacing but large enough to preserve the (micro-)pore structure of the matrix. Enrichment of

inertinite and ash in the selected fraction compared to the bulk sample cannot be excluded, but is believed to be limited to a few percent only (*cf.*Busch *et al*. (2004); Cloke *et al*. (2002)) Prior to testing, samples of the chosen fraction were dehydrated in air by heating in an oven at 40°C for 2 days, followed by storage in a desiccator under an argon atmosphere at ambient pressure to prevent further oxidation.

6.3.2 Experimental method

Apparatus
A cylindrical stainless steel compaction vessel with an inner bore of 30 mm was used for the experiments. Granular samples placed in this vessel are confined laterally by the vessel walls and vertically by means of upper and lower loading pistons tipped with porous Monel plates of 1.5 mm in thickness (Fig. 6.1). Viton O-rings countersunk in the pistons ensure that the sample chamber is gas tight. The temperature of the sample was measured using a Type K thermocouple located inside the vessel wall. The vessel is heated by an external furnace connected to a Type K control thermocouple placed in the furnace windings. A process controller is used to regulate vessel and sample temperature to within ~ 1°C (Fig. 6.1). Gases or supercritical CO_2 are introduced into the sample chamber through a central bore in the top piston. A gas/fluid outlet at the base of the vessel allows sampling after the experiment.

To apply axial load, the vessel and piston assembly are placed in an Instron 1362 servo-mechanical loading frame with a static loading capacity of 100 kN. Given the inner diameter of the vessel of 30 mm, the system is capable of applying an axial stress up to 140 MPa. Applied axial force is measured external to the pressure vessel using the Instron's 100 kN load cell. The load cell has an total accuracy of $\pm$ 0.23 kN. Displacement of the top piston relative to the pressure vessel is measured with a high precision linear variable differential transformer or LVDT, with linearity error of 0.25% of full-scale (2 mm) and a repeatability of 0.01 μm. In the present experiments, the gas/fluid system was connected to two alternative gas supply sources, namely a He cylinder regulated at 1 MPa and a CO_2 cylinder regulated at 5.6 MPa. A nitrogen-backed pressure booster/separator was used to boost the gas supply pressure up to 10 MPa (Fig. 6.1). Gas/fluid pressure in the sample chamber was measured with a Jensen PE-type 0-50 MPa electronic pressure transducer located at the inlet to the top piston. This device has an accuracy of $\pm$ 0.05 MPa. During testing, the displacement, applied load, gas pressure and temperature were logged digitally (16 bit) and using an analogue chart recorder.

Experimental procedure
In setting up each experiment, individual 10 gram samples of the sieved coal or activated carbon powder were placed in the sample chamber of the one-dimensional stainless steel compaction vessel as shown in Fig. 6.1. The Instron testing machine was programmed to apply controlled loads or displacements to the top piston, or to keep the piston at a fixed position. All experiments were conducted at a fixed temperature of 40°C, well above the critical temperature of CO_2. After heating to 40°C,

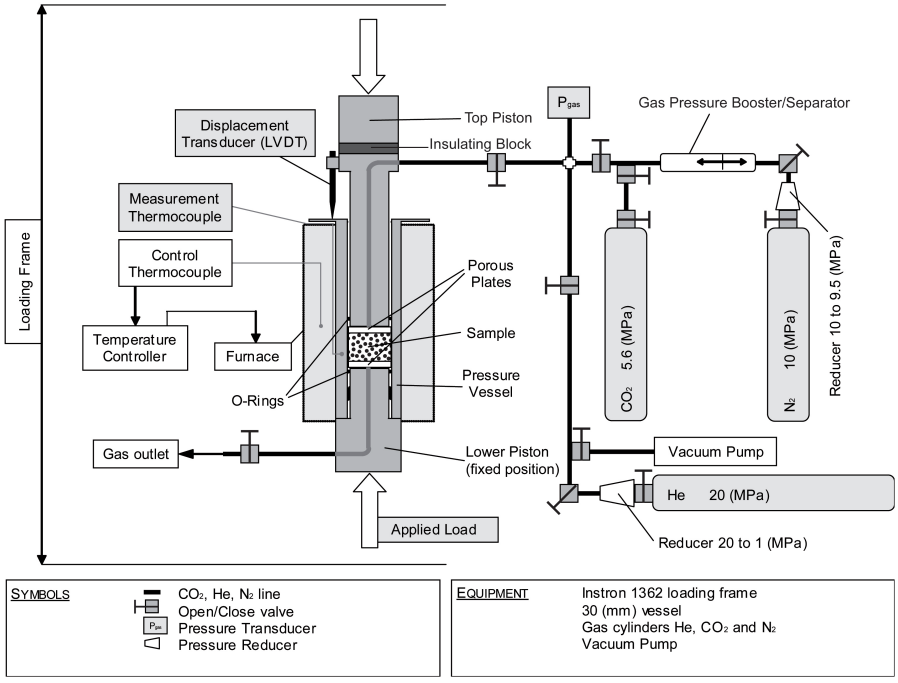

Figure 6.1: Experimental set-up

each experiment was initiated by evacuating and then pre-pressing the powdered sample, under vacuum, at a fixed axial stress of 65 MPa. This led to a more or less instantaneous compaction of ~ 30% followed by minor creep. The value of 65 MPa was chosen on the basis of manometric He porosimetry measurements performed on a sample of the 364 coal, which was progressively compacted at increasing applied stresses (5.7, 16.3, 34.1, 50.4, 67.4 and 83.6 MPa). In each of these steps, porosity was determined after creep ceased. The results showed a decrease in porosity from about 40% in the uncompacted sample to about 20% after compaction at 67.4 MPa. The application of higher axial stresses did not result in further porosity reduction.

When no further creep displacement could be measured after pre-pressing the samples at 65 MPa, i.e. after 1-2 days of compaction, the axial stress applied to the sample was reduced to about 0.3 MPa. This resulted in a small time-dependent expansion or rebound of the sample. After a few hours, no further expansion was measured. The permanent compaction strain of the sample at this point was again ~ 30% compared to its initial length. Prior to injecting CO_2 or He, the sample was re-evacuated. Each fluid/gas injection experiment was subsequently conducted in four stages. During the first and the third stages the sample volume was constrained, preventing it from swelling, while during the second and fourth stages the sample was unconstrained in the vertical direction.

Stage I: fixed volume measurements: At the start of this stage of the experiments, the Instron loading frame remained programmed to apply an axial stress of 0.3 MPa on the pre-pressed sample. The machine was then placed in position control mode, so that the loading piston was held at constant position, as measured by the Instron's internal LVDT. Under these conditions, the volume of the loaded sample is held constant, but for minor apparatus distortions associated with change in fluid pressure and axial load. The aim of this stage was measurement of the total axial stress exerted by the fluid and sample after the introduction of the fluid phase. The fluid, whether CO_2 or He, was introduced in two steps, first at a constant pressure of about 5.6 MPa and second at a constant pressure of about 9.5 MPa. During each stage, the effective axial stress changes caused by the sample response are represented by the difference between the total axial stress and the applied fluid pressure. The time between the first and the second introduction was variable, but was never longer than 15 minutes. The duration of the period between the second introduction of the gas and Stage II of the experiment, between 1 and 2 hours, varied per experiment. The fluid pressure was held constant at about 9.5 MPa during this entire period.

Stage II: vertically unconstrained measurements: The goal of this stage was the measurement of the uniaxial strain of the sample that developed after unloading. Directly after Stage I, the piston was therefore rapidly removed from contact with the sample, so that the volume of the sample was able to increase. After approximately 5 minutes, the piston was slowly brought down, in the direction of the sample. Motion of the piston was stopped directly upon re-contact with the sample, i.e. once the measured load began to increase. This usually occurred within 2-3 minutes. The

change in sample dimensions could then be determined from the new position of the piston. This remove-and-touch procedure was repeated at (irregular) intervals over a period of several hours to a day. Finally, the piston was positioned directly on top of the sample, using the remove-and-touch procedure, and the fluid was released from the sample through the gas outlet and captured for analysis using a gas chromatograph mass spectrometer (with the exception of one experiment). The vessel was then evacuated and the sample dimensions were measured using the remove-and-touch procedure. Uniaxial strain (e_l) developed during Stage II was calculated relative to the sample length (l_0) at the start of the experiment, i.e. after pre-pressing and evacuation and before the first introduction of the gas/fluid, using:

$$e_l(t) = 100 \times \frac{(l_t - l_0)}{(l_0)} \tag{6.1}$$

where l_t is the length of the sample at time t, taking extension positive.

Stage III: fixed volume measurements: The aim of this stage was to determine the repeatability of Stage I. First, the piston position was adjusted to apply a stress of 0.3 MPa on the sample, and then fixed. Fluid was next introduced in a pressure step to about 5.6 MPa, followed by a pressure step to about 9.5 MPa, in an identical procedure to that followed in Stage I.

Stage IV: vertically unconstrained measurements: This stage resembled Stage II and was intended to measure the uniaxial strain after unloading the sample for the second time. First, the piston was rapidly removed from the sample, followed by measurement of changes in the sample length with time using the remove-and-touch procedure over a period of several hours to a day. The piston was subsequently positioned to just touch the sample and the fluid pressure released through the gas outlet, but without taking further gas samples. The experiment was terminated by evacuation of the sample, followed by measuring its dimensions using the remove-and-touch procedure. Then, the vessel was flooded with air, disassembled from the Instron and the sample removed by gently pushing it out of the vessel using a hydraulic press. Strain development during Stage IV was calculated as in Stage II, taking the same value of l_0.

In total five experiments were executed: two experiments with CO_2 and 364 coal, one experiment with CO_2 and Warndt-Luisenthal (WL) coal and two control experiments. The first of the control tests was an experiment with CO_2 and activated carbon, while in the second control experiment a 364 coal sample was filled with He.

Corrections and uncertainties
The entire experimental set-up experiences dimensional distortion due to increasing axial stress and/or fluid pressure. Between 0 and 65 MPa axial stress, calibration tests performed using a stainless steel (Remanit 1.4122) dummy sample showed a non-linear relation between the applied stress and the externally measured piston displacement. Similarly, increasing the fluid pressure to 10 MPa led to a piston dis-

Table 6.1: Experiments on confined samples. Final stable pressure and stress values reached per experiment in Stage I, alongside the times taken to reach these stable values. AC represents the activated carbon control material. Both the fluid pressure and total applied stress in experiment C5 reached a maximum value in the first 1-2 minutes of Stage I, before decreasing to the stable values listed below. The stabilization times for experiment C5 represent the time taken to reach this final value.

			First P step				**Second P step**			
			Fluid Pressure		**Applied stress**		**Fluid Pressure**		**Applied stress**	
Experiment	Material	Fluid	Stable fluid P	Stabiliz. time fluid P	Stable applied stress σ	Stabiliz. time applied stress σ	Stable fluid P	Stabiliz. time fluid P	Stable applied stress σ	Stabiliz. time applied stress σ
			MPa	min	MPa	min	MPa	min	MPa	min
C1	364 coal	CO_2	5.77	1.29	11.40	15.00	9.32	1.40	14.30	17.00
C2	364 coal	CO_2	5.82	0	9.48	12.43	9.36	1.43	13.00	17.98
C3	WL coal	CO_2	6.02	0	9.42	6.16	9.62	33.85	13.56	51.68
C4	AC	CO_2	5.65	0	6.56	2.82	9.39	1.32	10.46	1.15
C5	364 coal	He	9.6	9.23	10.10	13.00	-	-	-	-

placement of ~ 0.2 mm relative to the top of the pressure vessel. These stiffness characteristics were described using sixth-order polynomials. All raw data were corrected for apparatus distortion using these polynomial functions. At maximum fluid pressure, dynamic friction between the o-rings on the top piston and the vessel was of the order of $\pm$ 0.5 kN. The effects of this led to underestimation of the axial stress on the sample by up to 0.35 MPa.

6.3.3 Results

The complete set of 5 experiments performed (C1-C5) and key data obtained in Stages I-III of these experiments are summarized in Tables 6.1- 6.3 respectively. The total axial stress and fluid pressure measured during the experiments are shown in Fig. 6.2.

The initial introduction of fluid into the sample chamber at ~ 5.6 MPa is seen in the initial rapid increase of the fluid pressure at the onset of Stage I. The later increase in fluid pressure to about 9.5 MPa during Stage I is also visible as a sharp step. Because the position of the piston was fixed in Stage I, these increases in the fluid pressure were associated with an increase in total measured axial stress. However, whereas the fluid pressure rapidly reached equilibrium, it generally took some time before the measured total stress stabilized, i.e. reached a steady value (see Tab. 6.1, Fig. 6.2).

During Stage I, stabilization of the total axial stress was reached within 6-15 minutes after the introduction of the CO_2, for the natural coal samples (experiments C1-3).

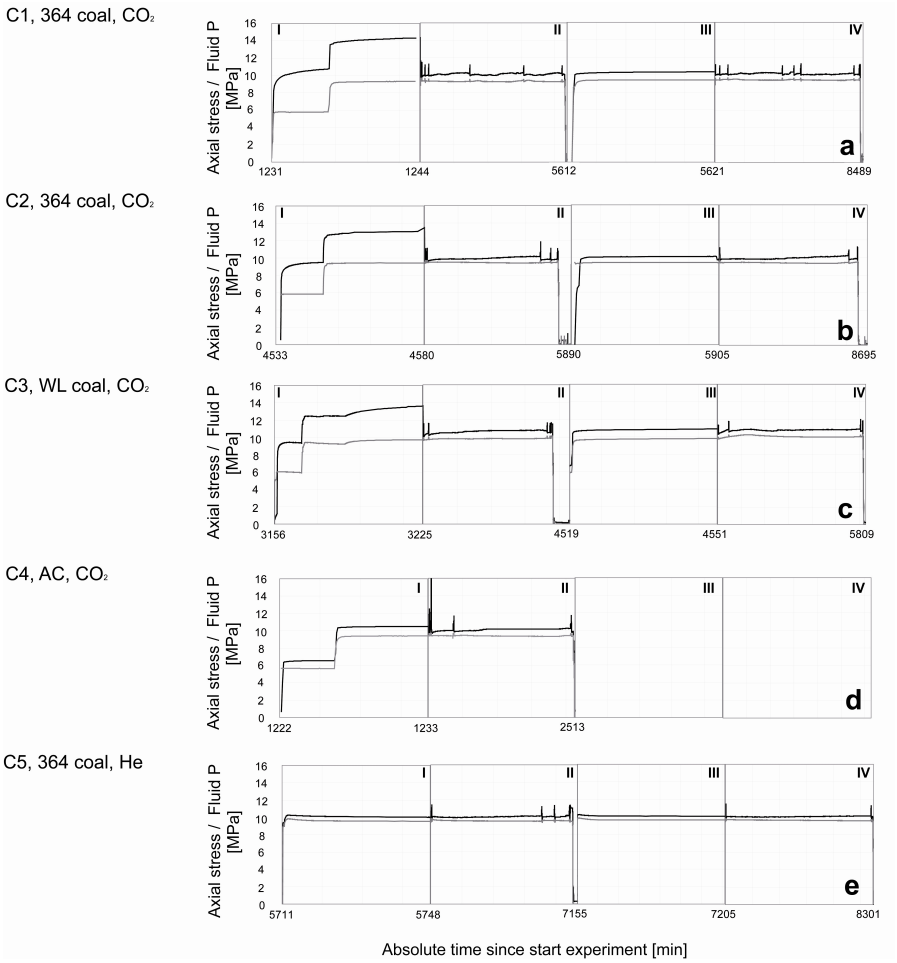

Figure 6.2: Total axial stress (black) and fluid pressure (grey) evolution during the experiments. Note that the absolute duration of the stages varied per experiment, but that the time scle in each experiment is linear. Stage I of the experiments was started after pre-compaction under vacuum at 65 MPa, load removal to 0.3 MPa and re-evacuation of the vessel. During Stage I the volume of the sample chamber was fixed with the piston in contact with the sample. Fluid was introduced in either two pressure steps of about 5.6 and 9.5 MPa, or, in the case of the experiment with He, in one step at about 9.5 MPa. The piston was periodically removed from the sample during Stage II and reapplied to determine any changes in sample length with time. The spikes in the applied stress curve indicate these temporary displacements of the piston. The sample was vented of fluid pressure and evacuated at the end of this stage. During Stage III the vessel volume was fixed again with the piston in contact with the sample, and fluid was introduced in one pressure step of about 9.5 MPa. In Stage IV, the piston was removed from the sample and the procedure of Stage II repeated.

In contrast, the stress stabilized within a shorter time in the control experiment using activated carbon and CO_2 (experiment C4, Tab. 6.1). In the control experiment with 364 coal and He (experiment C5), maximum values were rapidly reached, i.e. within 1-2 minutes for both total axial stress of (10.25 MPa) and fluid pressure (9.82 MPa). However, both subsequently decreased in the following 6-11 minutes until the stabilization values that are reported in Tab. 6.1 were reached. During Stage I, the measured stress was significantly ($\sim$ 3.5-4.9 MPa) higher than the fluid pressure for the natural coal samples with CO_2 (experiments C1-3), slightly higher ($\sim$ 1.1 MPa) for the experiment on activated carbon with CO_2 (experiment C4), and almost the same ($\sim$ 0.5 MPa higher) for the experiment on 364 coal with He (experiment C5).

The removal of load from the sample during Stage II of the experiments resulted in an immediate drop in the measured applied stress, followed by rapid stabilization at a value that approached, but remained slightly higher than, the fluid pressure of $\sim$ 9.5 MPa (Fig. 6.2). Small fluctuations in the data occurred when the piston was displaced during Stage II to measure sample length changes. The resulting strain values are given as a function of elapsed time in Tab. 6.2.

During Stage III, when the position of the piston was again fixed in contact with the sample, the fluid pressure and measured axial stress again increased when the fluid was introduced. Stabilization of the axial stress was established within 10 minutes. For the natural coal samples with CO_2 added (experiments C1-3), the difference between total stress and fluid pressure after stabilization was smaller ($\sim$ 0.7-0.9 MPa) than during Stage I (see Fig. 6.2, Tab. 6.3). The results of the experiment with 364 coal plus He (experiment C5) show that the difference between applied stress and fluid pressure was comparable for all experimental stages. The experiment with activated carbon (experiment C4) was terminated before Stage III.

During Stage IV, the immediate drop of applied stress and fluid pressure, when the piston was removed from the sample, was similar to that of Stage II. The calculated strain values are given versus elapsed time in Tab. 6.2.

Quantitative analysis of the gas that was released at the end of Stage II showed traces of hydrocarbons (mainly aliphatic compounds) in the case of the experiments on natural coal samples plus CO_2 (experiment C1-3), whereas these were absent from the control experiments on 364 coal plus He (experiment C5) and on activated carbon with CO_2 (experiment C4). Reduced sulphur compounds were detected in all experiments, but these were likely derived from rubber components in the apparatus and/or the containers used to store the retrieved gas.

When the samples were retrieved from the vessel after the experiments, the natural coal samples were fully cohesive, forming robust discs 30 mm in diameter and 15-17 mm in thickness. However, the activated carbon was still a loose powder.

Table 6.2: Strain data obtained during the different stages of the experiments on confined samples.

Exp	Material	Fluid	Stage	Time	Sample length	Strain
				min	mm	%
C1	364 coal	CO_2	vacuum	1231	15.71	0.00
			I	1231	15.83	0.76
			II	1260	16.46	4.76
			II	1295	16.44	4.65
			II	1386	16.46	4.76
			II	1496	16.47	4.84
			II	2719	16.48	4.90
			II	4322	16.50	5.03
			II-vac	5573	16.44	4.65
			II-vac	5603	16.43	4.61
			III	5613	16.57	5.47
			IV	5629	16.69	6.24
			IV	5712	16.67	6.14
			IV	5872	16.66	6.05
			IV	6926	16.67	6.10
			IV	7150	16.68	6.17
			IV	7282	16.67	6.14
			IV	8313	16.68	6.19
			IV	8416	16.68	6.17
			IV	8431	16.64	5.92
			IV-vac	8469	16.48	4.90
C2	364 coal	CO_2	vacuum	4519	16.01	0.00
			I	4535	16.13	0.75
			II	4605	17.01	6.28
			II	5615	17.06	6.55
			II	5706	17.01	6.25
			II	5766	17.02	6.31
			II-vac	5857	16.68	4.18
			III	5891	16.86	5.31
			IV	5911	17.01	6.28
			IV	7078	17.05	6.50
			IV	7155	17.03	6.37
			IV-vac	7172	16.75	4.62

Exp	Material	Fluid	Stage	Time	Sample length	Strain
				min	mm	%
C3	WL coal	CO_2	vacuum	3156	15.79	0.00
			I	3225	15.95	0.99
			II	3232	16.60	5.11
			II	4319	16.72	5.86
			II	4344	16.70	5.74
			II	4356	16.69	5.68
			II-vac	4515	16.40	3.86
			IV	4557	16.70	5.74
			IV	4645	16.73	5.93
			IV	5761	16.77	6.18
			IV	5780	16.76	6.12
			IV-vac	5815	16.48	4.34
C4	AC	CO_2	vacuum	1220	15.05	0.00
			I	1223	15.14	0.62
			II	1240	16.50	9.65
			II	1257	16.09	6.93
			II	1455	16.60	10.32
			II	2478	16.58	10.19
			II-vac	2510	15.92	5.80
C5	364 coal	He	vacuum	5711	16.16	0.00
			I	5711	16.29	0.80
			II	5758	16.24	0.49
			II	6813	16.30	0.86
			II	6934	16.29	0.80
			II	7078	16.29	0.80
			II	7084	16.28	0.74
			II-vac	7128	16.19	0.18
			III	7155	16.32	0.99
			IV	8284	16.30	0.84
			IV-vac	8298	16.24	0.47

Table 6.3: Experiments on confined samples. Final stable pressure and stress values reached per experiment in Stage III, alongside the times taken to reach these stable values. Both the fluid pressure and total applied stress in experiment C5 reached a maximum value in the first 1-2 minutes of Stage III, before decreasing to the stable values listed below. The stabilization times for experiment C5 represent the time taken to reach this final value.

			First P step			
			Fluid Pressure		**Applied stress**	
Experiment	Material	Fluid	Stable fluid P	Stabiliz. time fluid P	Stable applied stress σ	Stabiliz. time applied stress σ
			MPa	min	MPa	min
C1	364 coal	CO_2	9.40	1.88	10.34	7.02
C2	364 coal	CO_2	9.39	1.55	10.07	4.63
C3	WL coal	CO_2	9.67	4.79	10.72	4.19
C4	AC	CO_2	experiment terminated before Stage III			
C5	364 coal	He	9.64	7.47	10.08	7.47

6.3.4 Analysis of the confined coal data

Introduction of supercritical CO_2 or He into our samples under conditions of fixed piston position (near-fixed volume) led to an increase in fluid pressure. This produced an increase in the total axial stress measured. A consistent 1:1 correlation between total axial stress and fluid pressure was obtained for each experiment during Stages II and IV, where the piston was not in contact with the sample. This correlation is shown by the solid diagonal line drawn in Fig. 6.3a-e. The effect of the sample response to fluid injection upon the axial stress was evaluated by plotting the axial stress vs. fluid pressure data obtained in Stages I and III with respect to the correlation between total axial stress and fluid pressure established in Stages II and IV (Fig. 6.3a-e).

The control experiment on 364 coal with He (Fig. 6.3e) showed that throughout the experiment all changes in axial stress could be explained by changes in fluid pressure alone. As such, no sample effect could be measured. i.e. there was no tendency for swellling. However, the measured stress that ultimately developed during Stage I of the experiments on the natural coals with CO_2 and, though less pronounced, in the tests on the activated carbon, was higher than expected on the basis of the increase in fluid pressure. This effect can therefore be attributed to the sample, i.e. to constrained swelling of the samples. The time that was required for the total axial stress to stabilize was most likely related to the diffusion of the fluid into the individual coal grains of the samples. These grains will have had the tendency to swell, but because swelling was restricted to reducing the intergranular pore space, an increase in the stress exerted on the vessel walls and pistons occurred. This additional stress

was markedly higher for the natural coals tested with CO_2 (3.5-4.5 MPa) than for the activated carbon (1 MPa; see Fig. 6.3a-d). Remarkably, the stabilized additional stress remained constant when the fluid pressure was increased from 5.6 to 9.5 MPa during Stage I of all experiments on the natural coal samples (Fig. 6.3a-d).

The above tendency for the coal and activated carbon samples to swell upon addition of CO_2 was also demonstrated by the uniaxial volumetric expansion of the samples measured when the piston was removed from contact with the samples, during Stage II of the experiments at 9.5 MPa fluid pressure (Fig. 6.4). No expansion was measured in Stage II of the experiment on 364 coal with He, as expected from the lack of additional stress developed in this sample during Stage I. At the same time, however, there was no clear relation between the additional stress measured for the coal samples with CO_2 added during Stage I and the observed expansion in Stage II, i.e. highest additional stress was not related to the largest expansion (*cf.*Figures 6.3 and 6.4). Indeed, the largest strain was measured for the activated carbon sample with CO_2, although the additional stress developed in the sample during Stage I was limited. This may be related to the fact that the activated carbon remained a powder. After evacuating the sample at the end of Stage II, the natural coal samples with added CO_2 did not return to their initial dimensions, indicating a permanent increase in sample length of about 4% (Fig. 6.4). A permanent strain at the end of Stage II, of 5.8%, was also observed for the activated carbon powder sample (Fig. 6.4). By contrast, in experiment C5 on 364 coal plus He, the sampe did return more or less to its initial dimensions.

Introduction of the fluid during Stage III, when the sample volume was again constrained, did not lead to the development of an additional stress in any of the experiments. In this stage, the change in measured axial stress could be fully explained by the increase in fluid pressure (Fig. 6.3). Still, a volumetric increase was measured for the experiments with CO_2 when the piston was retracted from the sample during Stage IV (see Fig. 6.4). The total swelling was about the same as measured during Stage II. After evacuation at the end of Stage IV, the length of all samples was similar to that after evacuation at the end of the Stage II. This indicates that the volumetric expansion observed during Stage IV was fully reversible.

The methodology applied during Stages I and II and during Stages III and IV of the present experiments was similar. However, the response of our coal samples to introduction of the CO_2 was different in the second cycle (Stages III and IV) than in the first (Stages I and II). Our data indicate that the swelling of the samples during Stage II must be due to two different processes: one that led to a relatively large irreversible swelling and a second one that led to a smaller reversible swelling. During Stage IV only the process leading to the reversible swelling appeared to occur. This second process did not seem to be related to additional stress development under confinement, because this was not exhibited during Stage III. The additional stress measured during Stage I is therefore probably associated with the first process, i.e. that leading to the irreversible swelling.

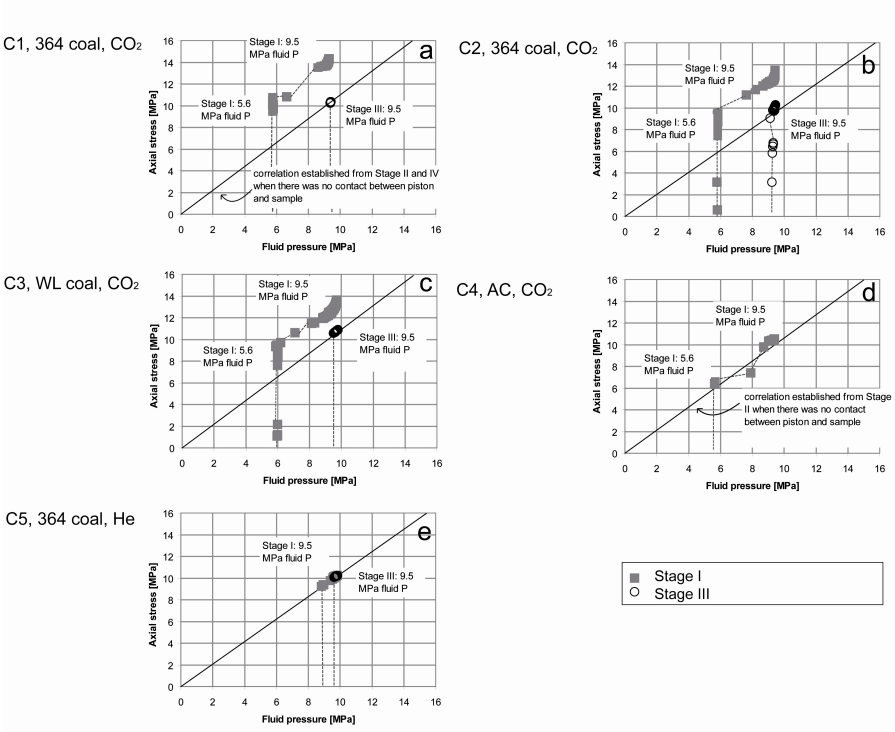

Figure 6.3: Total axial stress vs. fluid pressure measured during Stages I (grey squares) and III (open circles), plus the correlation between fluid pressure and applied stress as established during Stages II and IV, i.e. independently of sample behaviour (black line). Note that small differences in this correlation exist between the individual experiments. The continuous sequence of data obtained in Stages I and III, acquired every 5 seconds, is plotted as tied points. The plot for the experiment on 364 coal with He (e) shows that the measured stress can be fully explained by the fluid pressure. The axial stress measured in the second control experiment (d), with activated carbon, is slightly higher than expected from the fluid pressure, indicating that the sample exerts a stress on the piston. The other three experiments with the natural coal samples (a-c) show a similar but much larger stress response. During Stage I, a clearly higher stress is measured than can be expected from the fluid pressure, indicating that the sample has the tendency to swell but instead develops stress in its confined setting. However, when the procedure is repeated during Stage III, the measured stress can be fully explained by the fluid pressure, i.e. the sample does not exert additional stress on the piston.

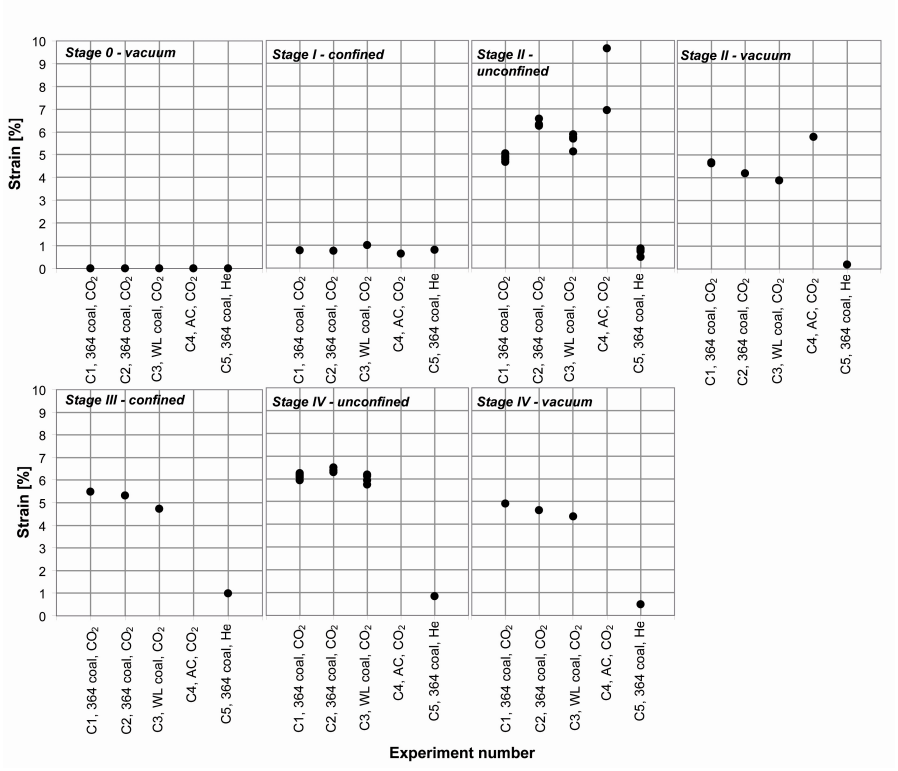

Figure 6.4: Axial strain measured during the different stages of the present experiments on confined samples. Note that strain is measured relative to sample dimensions after pre-pressing (see Eq. 6.1). The strain plotted in Stage I represents an apparent strain that reflects a small error in correcting for apparatus distortion. Two measured values (10.19 an 10.32%) during Stage II, unconfined, for activated carbon with CO_2 are not plotted in the figure.

By comparison with previous work on sorption of CO_2 (Ceglarska-Stefanska and Czaplinski, 1993; Day *et al*., 2008; Levine, 1996; Robertson, 2005a), the reversible swelling process observed in our experiments on coal was likely the result of the physical adsorption of the CO_2 on the coal surface, which led to swelling of the samples. The reversibility implies that both the adsorbent and adsorbate returned to their initial states once the pressure was released. However, the much larger irreversible swelling observed in our coal samples with added CO_2 is more difficult to explain. The presence of the hydrocarbons in the released gas after Stage II indicate extraction from the coal due to high-pressure CO_2. This extraction demonstrates that material was irreversibly removed from the solid coal phase (because the coal was evacuated at the start of the experiment). Extraction of hydrocarbons by supercritical CO_2 is a well-known phenomena attributed to its unusual physico-chemical properties, for example the gas-like high diffusivity, low viscosity, and lack of surface tension which facilitates penetration of supercritical CO_2 into small pores in the coal matrix (e.g. Amador-Hernandez and Luque De Castro (2000), Kolak and Burruss (2006) and Luque De Castro *et al*.(1994)). The extraction of hydrocarbons from the coal may have led to an alteration of the surface structure of the adsorbent, as for example suggested by Adamson and Gast (1997). At this stage, however, relating the observed irreversible swelling process to hydrocarbon extraction is purely speculative, also because no gas analyses were performed after Stage IV. Moreover, the gas analysed from experiment C4 using activated carbon and CO_2 did not show measurable hydrocarbon extraction, though a small additional stress during Stage I and an irreversible strain after Stage II were measured (Figures 6.3d and 6.4). It is more likely then, that the irreversible process was linked to compaction before the start of the experiment. This was further investigated in the set of experiments on unconfined coal aggregate samples described below.

6.4 Experiments on unconfined coal aggregates

In these experiments, the swelling behaviour of pre-pressed discs of granular coal was investigated by optically measuring their dimensional changes, following exposure to Ar, CH_4 or CO_2 under unconfined conditions, i.e. in an open chamber. The samples were pre-pressed in a similar manner to that employed in the confined experiments, but were much smaller in size.

6.4.1 Sample preparation

In the unconfined experiments, only the 364 coal was used. Bulk sample material was ground and sieved to obtain a granular coal fraction below 63 μm. Disc-shaped pellets with a diameter of 1.4 mm and a height of 0.8 mm were prepared from this powder using a manually driven hydraulic press and a cylindrical, stainless steel die. In this procedure, an axial stress of about 65 MPa was applied for 2 days or more in air at room temperature. Subsequently, the samples were unloaded for 12 to 24 hours

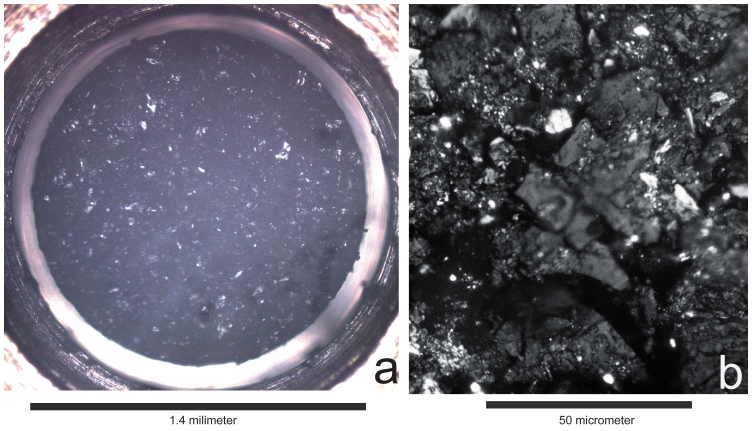

Figure 6.5: Optical images of the pressed coal discs used in the unconfined experiments. a) Entire sample viewed in the optical cell used to measure dimensional changes upon exposure to high pressure Ar, CH_4, and CO_2. b) Micrograph of sample surface, showing the individual grains. The bright spots in the picture are mostly pyrite grains.

before use. Therefore, apart from the much smaller size of the disc and the finer grain size, therefore, the samples were prepared in a manner resembling the pre-pressing stage of our experiments on confined samples. A smaller grain size was used to achieve a similar grain size to sample ratio. As in our confined experiments, maceral and/or ash fractionation due to sieving (Busch *et al.*, 2004; Cloke *et al.*, 2002) cannot be excluded, but is believed to be very limited.

6.4.2 Experimental method

The experiments were performed using the optical cell described in detail by Van Bergen *et al.* (2009a). This see-through, high-pressure cell consists of a pill-box-shaped stainless steel pressure vessel with top and bottom Pyrex windows. A titanium ring with an inner diameter of about 1.6 mm (Fig. 6.5a) placed coaxially between the windows acts as a sample holder. Unconfined samples placed within this ring are able to swell in all directions. The cell is connected to a gas supply system, which enables introduction of Ar, CO_2 or CH_4 at pressures up to 15 MPa, and is heated by PID-controlled heating elements embedded in the vessel body. During the full duration of each experiment, the cell was placed under a Leica DMRX optical microscope system to obtain digital images of the sample automatically, i.e. to monitor changes in sample surface dimensions. Digital images were acquired during the entire experiment, using an automatic sampling interval varying between 10 s (for the period immediately after the introduction of the gas) and 30 min (for approximately 1 h after release of the gas).

All experiments were performed at a pressure of about 8.0 MPa and temperature

of about 40°C: three with CO_2, one with Ar, and one with CH_4 (Tab. 6.4). Under these conditions, CO_2 is well above its supercritical point. In performing individual experiments, the sample was first placed in the cell, without evacuation. The temperature was then increased to the desired value and the chosen fluid or gas introduced at ~ 8.0 MPa. After a period of up to 28 hours, the gas pressure was released and the sample allowed to stand at atmospheric pressure (i.e. in an air environment) for periods of 30 minutes to 30 hours (Tab. 6.4). Changes in sample dimensions were monitored throughout by automatic image acquisition.

Data processing was performed following the method of Van Bergen *et al*(2009a). The 2-D surface dimensions of the sample were determined from the images taken at different stages of the experiment, using a network of distinctive marker points chosen in the surface of each sample. Two-dimensional surface strain (e_s), in percent, was calculated by comparing the surface dimensions per experimental stage (A_t) with those measured before the first addition of the gas (A_0), using

$$e_s(t) = 100 \times \frac{(A_t - A_0)}{(A_0)} \tag{6.2}$$

A best fit was made to the surface strain versus time data using a purely empirical hyperbolic function of the form:

$$e_s(t) = 100 \times \frac{(t \times e_{s-max})}{(t + t_{1/2})} \tag{6.3}$$

This yielded two parameters per exposure experiment, namely the maximum 2-D strain attained at equilibrium (e_{s-max}) and the half-saturation time ($t_{1/2}$), which is the time required to reach 50% of e_{s-max}. These parameters are used to describe our data. In the description of our results, an increase in size is taken as positive strain. For further details, see Van Bergen *et al* (2009a).

6.4.3 Results

As shown in Fig. 6.6 and Tab. 6.4, the single sample exposed to Ar (sample U1) exhibited a maximum surface swelling strain (e_{s-max}) of 0.38%. This was of the same order as the uncertainty in the measurement. For this sample, the data fit resulted in a negative value for the half saturation time $t_{1/2}$(Tab. 6.4), which therefore has no meaning. The strain measured after fluid release was slightly negative.

The experiments performed with CH_4 (samples U2 and U3) showed a swelling strain development in the sample of about 1.5%. In this case, $t_{1/2}$was also of the order of a few minutes (Fig. 6.6, Tab. 6.4). After a period of several hours of relaxation at atmospheric pressure, residual strains of +0.5% to 1% were measured.

The addition of supercritical CO_2 (samples U4-6) led to swelling strains of about 4.5-6.0%, i.e. to significantly higher values than for Ar or CH_4 (Fig. 6.6, Tab. 6.4). Half

Table 6.4: Overview of the experiments performed on unconfined coal aggregates and the parameters ($t_{1/2}$and emax) resulting from fitting of the hyperbolic function of Eq. 6.3 to the strain vs. time data obtained, including the correlation coefficient (R) of the fit to the data. The residual strain values (e_{s-eq}) measured at atmospheric pressure after the release of the gas/fluid are also listed. The strain data (in percent) could be determined with an absolute error in strain of ± 0.3%.

	Experimental conditions						**Experimental results**					
Exp.	**Coal Sample**	**Gas/ Fluid**	**P (MPa)**	**T (°C)**	**Duration of exposure to fluid at pressure P**	**Duration of subsequent relaxation at atm. pressure**	e_{s-max} [%]	e_{s-max}-error	$t_{1/2}$[min]	$t_{1/2}$-error	**R**	e_{s-eq}
U1	364	Ar	8.0±0.2	39.5±1.0	24.5 hrs	18.5 hrs	0.38	±0.02	-0.37	±0.77	0.75	-0.12
U2	364	CH_4	7.9±0.2	39.5±2.0	24 hrs	23.5 hrs	1.35	±0.04	2.16	±0.75	0.90	0.54
U3	364	CH_4	7.9±0.2	40.0±2.0	27.5 hrs	29.5 hrs	1.65	±0.03	3.22	±0.58	0.99	0.89 0.95 0.99
U4	364	CO_2	7.9±0.2	40.0±2.0	1hr 20min	45 min	4.79	±0.05	0.02	±0.01	0.99	4.15 3.78 3.68
U5	364	CO_2	8.0±0.2	40.0±2.0	1 hr 10min	30 min	4.62	±0.16	0.28	±0.33	0.99	3.02 2.42
U6	364	CO_2	8.0±0.2	40.0±2.0	20.5 hrs	24 hrs	5.84	±0.03	0.16	±0.04	0.99	2.95 2.87

of the maximum surface strain was reached within half a minute ($t_{1/2}$< 20 s). In this case, more than 50% of the maximum surface strain remained after fluid pressure release and equilibration at atmospheric pressure.

6.4.4 Analysis of the unconfined coal data

The results confirm the findings of Van Bergen *et al*. (2009a) and many previous workers (e.g. Day *et al*.(2008), Karacan (2007), Mazumder *et al*.(2006b), Mazumder and Wolf (2008), Robertson and Christiansen (2005a)) that the swelling strain developed during equilibration of coal with Ar is lower than seen using CH_4, and that the strains obtained using CH_4 are lower than obtained using CO_2. However, the swelling response to fluid addition in the present experiments on pre-pressed samples was much larger than for unconfined matrix blocks of the same 364 coal, as measured by Van Bergen *et al*. (2009a) using the same apparatus and pressure-temperature conditions (about 8.0 MPa and 40°C). Strain was detectable in the present experiment with Ar, whereas it was below detection in our previous work on matrix blocks. Similarly, the present experiments with added CO_2 showed swelling strain values in the range of 4.5-6% compared with 1.5-2% for CO_2 addition to matrix blocks. For CH_4, the present samples showed 1.5% strain compared with 0.65% measured for the blocks. For the matrix blocks, the ratio between the CH_4-strain and the CO_2-strain varied between 1/1.5 and 1/2.8 (van Bergen *et al*., 2009a), which is comparable to the ratios reported in the literature based on adsorption experiments (e.g. Hall *et al*. (1994), Puri and Yee (1990), Stevenson *et al*. (1991)). However, the ratio for the present coal samples falls between 1/3 and 1/4, which is clearly much lower. As the experimental conditions and coal starting material were very similar in the present experiments and in our previous work on matrix blocks (van Bergen *et al*., 2009a), we infer that there must be an effect of sample preparation, i.e. that the production of pre-pressed samples of crushed matrix material, with a fine, granular and porous structure, somehow changes the volumetric response of the constituent matrix grains compared with that of small, cleaved, matrix blocks.

A further notable difference between the present experiments on unconfined coal aggregates and those on matrix blocks reported by Van Bergen *et al*. (2009a) lies in the permanent strain that remained in the present experiments, after release of the gas/fluid pressure. It is assumed that, given the long period (0.5-24h) between gas release and strain measurement, the samples reached equilibrium with the atmosphere at the end of both sets of experiments. The final, permanent strain recorded will therefore be referred to as the equilibrium strain after gas release (e_{s-eq}). The present experiments with Ar showed a slightly negative value of e_{s-eq}(Tab. 6.4), which in view of the measurement error is effectively indistinguishable from zero. It thus appears that the strain developed in this experiment was reversible. In contrast, e_{s-eq} was significant in both the CO_2 and the CH_4 experiments (~ 2.5-4% and ~ 0.5-1%, respectively, see Tab. 6.4).

In the present tests, the difference between the maximum strain developed at equilib-

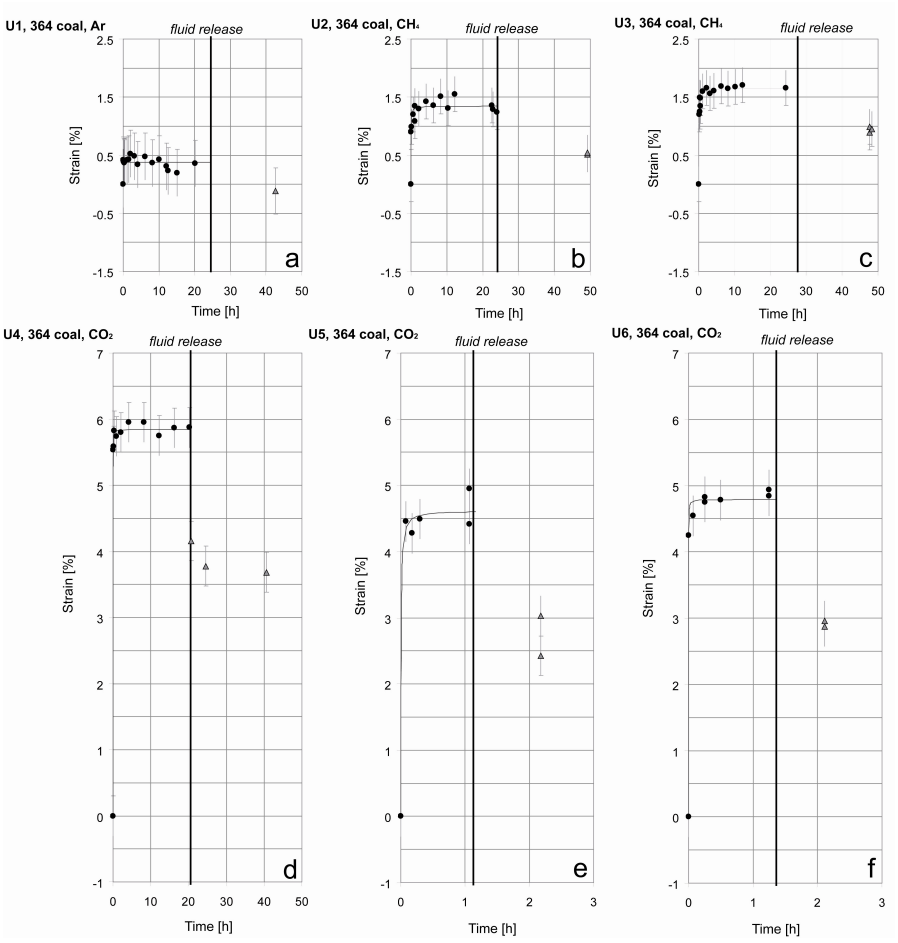

Figure 6.6: Development of strain with time in the unconfined experiments with Ar, CH_4 and CO_2 added at 7.9-8.0 MPa and 40°C. Fluid/gas pressure was applied at time=0 and removed at the time indicated by the bold vertical line. Note the different time-scales. Sample/experiment numbers are as indicated.

rium under pressure (e_{s-max}) and the permanent strain (e_{s-eq}) remaining after depressurization clearly constitutes a reversible strain. Remarkably, this reversible strain (i.e. e_{s-max} - e_{s-eq}) of about 2% for the CO_2 experiments (Tab. 6.4) is of the same order as the maximum strain reported for the matrix blocks, which was itself reversible (van Bergen *et al.*, 2009a). This observation is also valid for our CH_4 experiments, which showed a reversible strain of 0.6 and 1.0% compared to the 0.65% reported for matrix fragments by Van Bergen *et al.* (2009a). This clearly demonstrates general agreement between the reversible strain behaviour seen in the present coal aggregate samples and in matrix blocks, although detailed comparison is hampered by the differences in sample porosity.

Our data thus indicate that reversible swelling occurs in both matrix blocks and pre-pressed coal aggregates, while irreversible swelling occurs only in the aggregates. As mentioned before, it is well established in the literature that the reversible swelling of coal exposed to gases and fluids is related to the reversible process of physical adsorption (Ceglarska-Stefanska and Czaplinski, 1993; Day *et al.*, 2008; Levine, 1996; Robertson, 2005a). The development of irreversible strain implies that an additional process takes place in the pre-pressed aggregates. This process is most likely linked to the sample preparation, presumably to the compaction of the grains as neither the pores nor grain boundaries can contribute to strain. However, it must be emphasized that the amount of permanent strain (e_{s-eq}) developed was also clearly dependent on the fluid used in the experiment, being negligible for Ar and about 3-8 times higher for CO_2 than it was for CH_4. This suggests an effect of sample preparation that is somehow related to the adsorption phenomenon.

6.5 Discussion

We now proceed to integrate the results obtained in the confined and unconfined experiments reported in this paper. These experiments were executed under substantially different conditions, employing different sample grain sizes (63-212 μm vs. <63 μm), different sample sizes , different sample preparation details (pressing under vacuum or not), and different fluid pressures (5.6 and 9.5 MPa vs. 8.0 MPa). However, both types of experiment involved pre-pressing of an aggregate of coal grains in advance of the addition of gas or fluid. Both types of experiment showed unusually large swelling strains upon exposure to CO_2 and CH_4, which were mostly irreversible (i.e. permanent) once the samples were returned to equilibrium with the atmosphere. Permanent swelling could not be confirmed in pre-compacted granular coal samples in contact with He or Ar, because total sweling was generally too low to draw any conclusions.

The permanent strain response upon exposure to CO_2 or CH_4 which we report here is remarkable, because previous work on intact coal and on unpressed powder suggests reversibility of sorption/desorption and of the associated (much smaller) swelling effects (Ceglarska-Stefanska and Czaplinski, 1993; Day *et al.*, 2008; Levine, 1996;

Robertson, 2005a). To our knowledge, there is only one other reported case of partly irreversible strain development in an intact bituminous coal sample, from the Upper Silesian Basin, upon exposure to CO_2, which was attributed to disequilibrium in the experiments (Majewska *et al*., 2009). Our experiments on confined samples also showed that re-introduction of fluid, produced much lower, reversible strains, more consistent with conventional expectation from the literature. Taken together, these results point to two swelling processes operating in our pre-pressed samples:

1. A process leading to rapid development of large irreversible strains (or stresses). This process occurs only after the initial introduction of fluid, and must be somehow related to our sample preparation or pre-pressing procedure, but also to adsorption as it is affected by fluid/as type.

2. A process leading to strain (or stress) development that is reversible. This process is similar to that measured in unconfined samples, in conventional adsorption experiments, and probably related to reversible physical adsorption of the gas/supercritical fluid on the internal coal surface.

Earlier work by Hol *et al*. (2006) and Van Bergen *et al*. (2005) suggested that reversible and irreversible swelling of pre-pressed coal grains could be related to physical sorption and chemisorption, respectively. However, given the results of the present study, and that on matrix blocks by Van Bergen (2009a), it is more likely that the irreversible component is related to sample preparation than to chemisorption.

Turning now to the possible effects of grain size on the behaviour of our samples, studies of swelling of crushed coal using organic solvents have shown that particle size can have an effect on the observed swelling behaviour (Otake and Suuberg, 1997). This effect was attributed by Otake and Suuberg (1997) to variations in particle size distribution with changing mean grain size, rather than to a direct effect of mean particle size, i.e. to the tendency for small particles to pack into the interstitial spaces between larger grains. Although not investigated by Otake and Suuberg (1997), one could imagine that such grain packing effects could lead to permanent residual strains. However, this explanation is unsatisfactory for the behaviour seen in our experiments, because in our confined tests a grain size fraction was used with average narrow width.

A key observation in the present experiments is the clear difference in the response of the samples to the different fluids used. The effect was much more pronounced in the CO_2 experiments than for the other fluids. This implies that adsorption plays a major role and thus too the micropore surface of the coal, since this is the primary site of adsorption of high pressure CH_4 and CO_2 (Clarkson and Bustin, 1999a). The significantly greater permanent strain response of our samples to CO_2 compared with CH_4 suggests that preferential sorption of CO_2 occurred. This is consistent with the fact that CO_2 has both a larger adsorption affinity (energy) and a smaller kinetic diameter than CH_4 and can therefore diffuse into microporous coal matrix material more easily (Cui *et al*., 2004), reaching the smallest micropores not accessed by CH_4 (Melnichenko *et al*., 2009; Radlinski *et al*., 2009).

On the basis of the above, we infer that the irreversible swelling effect seen in the present experiments most probably reflects removal of permanent compaction strain imposed upon the coal grains during pre-compaction of our samples at 65MPa applied stress. During this pre-compaction stage of both the confined and unconfined experiments, the samples were compacted far beyond their elastic limit. Compaction occurred mainly instantaneously and partly via a minor creep response. The permanent compaction strains of ~ 30% imposed during this pre-pressing stage are far too large to be accommodated by interparticulate sliding alone, which means that compressive deformation or fracturing of the individual grains must have occurred. From acoustic emission measurements performed in a separate set of compaction tests at the same stress, we have shown that acoustic emission is virtually absent, so that microcracking is negligible. The implication is that the individual coal grains must have undergone permanent compressive deformation during pre-pressing. This would inevitably lead to permanent compaction of the internal pore structure of the coal matrix grains, decreasing the mean pore aperture and increasing the proportion of small diameter micropores ($4x10^{-10}$ - $2x10^{-9}$ m) relative to coarser mesopores. This would in turn lead to increased short range surface force interactions, i.e. disjoining pressure effects, upon introduction of gas or fluid into the enhanced micropore structure (e.g. Israelachvili (1992)). Indications for enhancement of the micropore structure is provided by the earlier mentioned preferential sorption-controlled swelling of CO_2 compared with CH_4.

We thus propose that introduction of CO_2, CH_4, and possibly of Ar and He into our pre-pressed samples, in the confined and unconfined experiments, resulted in increased micropore adsorption. The high affinity for adsorption, and the associated surface forces or disjoining pressure developed within the micropores, caused the coal grains to "undeform", i.e. caused recovery or removal of the pre-pressing-induced permanent strain. As mentioned earlier, an increase in microporosity will have a more pronounced effect on CO_2 adsorption than on CH_4 adsorption, thus explaining the bigger effect of CO_2. After recovery of the permanent strain was achieved, the samples seem to have exhibited a normal, reversible response to adsorption. We thus attribute the irreversible swelling effect seen in our experiments to the stress-history effect of pre-pressing. Against the background of this interpretation, our results imply that pre-loading of coal samples should be avoided in coal swelling experiments. Our results also point to an inevitable interaction between stress/strain and adsorption behaviour that poses interesting experimental challenges for the investigation of the sorption, swelling and transport properties of coal in a confined setting.

Extrapolation of our results to natural coal is complicated, as swelling of a powdered sample cannot be directly compared to swelling of a confined or even unconfined coal core, for a variety of reasons. These include the presence of cleats, homogenization of the lithotypes in the pulverisation process and moisture content (Mathews *et al.*, 2001; Pone *et al.*, 2009a; Siriwardane *et al.*, 2006). Still, our results give some

insight into the processes that occur when coal is stressed under in situ conditions. Our results show that granular coal samples that are compacted beyond their elastic limit can recover at least part of their permanent strain as a result of gas adsorption. This may be relevant for coals that have undergone deep burial after formation, or for naturally stressed coal in tectonic zones. These may exhibit more swelling upon gas adsorption in situ than expected on the basis of their adsorption capacity measured in conventional sorption tests on crushed coal. Permanent swelling effects may also be relevant for field operations in areas where stressed coal seams occur, specifically around the wellbore zone where coal fines resulting from drilling activities may exhibit large swelling, thereby decreasing reservoir accessibility.

6.6 Conclusions

We have performed experiments on both confined and unconfined samples of pre-pressed granular coal with the aim of investigating the effect of confinement on the stress-strain response of the samples exposed to CO_2, CH_4, He and Ar. Our principal findings can be summarized as follows.

Granular coal samples that are pre-compacted and subsequently brought into contact with CH_4 or CO_2 at 40°C and pressures between 5 and 10 MPa exhibit swelling effects. However, these are larger than generally seen in unpressed material. This swelling could not be confirmed for similar pre-compacted samples in contact with He or Ar because it was generally too small to quantify reliably.

The swelling behaviour caused by contact with CH_4 or CO_2 appears to be a combined effect of two processes. The first of the two processes leads to an irreversible swelling which is related to the initial compaction or pre-pressing of the sample, i.e. to its stress-history. This process occurs directly after first contact with the gas/fluid and cannot be discerned in repeat experiments. It is likely to be related to recovery of permanent compaction strain due to adsorption of fluid molecules and associated changes in surface forces occurring in the micro- and nanopores of the coal. The mean pore dimensions were probably reduced due to densification of the microstructure of the coal grains during sample preparation. As CO_2 has a higher affinity for small pores than CH_4, the coal samples exposed to CO_2 showed more recovery of permanent strain than those exposed to CH_4.

The second process (reversible swelling) is probably the result of reversible physical adsorption of the gas or fluid by the coal, in line with previous measurements of swelling and adsorption. Because the first process is related to the stress-history associated with sample preparation in the laboratory, it is not representative for natural swelling behaviour. Care should therefore be taken in the interpretation of lab experiments with comparable sample preparation steps and in extrapolation of results to field conditions. However, geological conditions at specific locations such as tectonically stressed areas, or a deep burial history, may have led to compaction of

coal beyond its elastic limit. Such coals may exhibit unexpectedly large, permanent swelling strains upon CO_2 injection that can not be explained by the material's reversible sorption capacity measured in conventional sorption experiments on loose powder.

Acknowledgements

This study was undertaken as part of the Dutch national research programme CATO on CO_2 Capture, Transport and Storage, which we gratefully acknowledge for funding. Additionally, Shell International and TNO are acknowledged for co-funding and supporting this study through CATO. The laboratory experiments would have been impossible without the technical support of Peter van Krieken, Gert Kastelein and Eimert de Graaff, who are gratefully acknowledged. Geerke Floor was invaluable in the execution of the optical experiments and is thankfully acknowledged. Colin Peach is thanked for many fruitful discussions in the course of the study. Harry Veld and Kathrin Reimer of TNO are acknowledged for their support and suggestions regarding coal characterization and gas analyses. The Central Mining Institute and the Brzeszcze mine in Poland and Karl-Heinz Wolf of Delft University of Technology are gratefully acknowledged for providing the coal samples.

Chapter 7

Synthesis, further research and recommendations for future field development

Frank van Bergen

7.1 Introduction

The main objective of this thesis has been the interpretation of observations from an enhanced coalbed methane (ECBM) field test with CO_2 injection through understanding gained from dedicated laboratory experiments. Most of the ECBM demonstration sites around the world operated to date, including RECOPOL, experienced permeability reduction in the targeted coal seam that were attributed to swelling of the coal as the result of CO_2 injection (Reeves, 2003; Shi *et al.*, 2008; Van der Meer and Fokker, 2003; Wong *et al.*, 2007). The present laboratory experiments therefore focused on understanding the development of swelling with time, and on the relationship between this and transport of the relevant gas or fluid phases through the coal. Managing the effect of swelling on injectivity and on transport through the cleat and matrix systems of coal seams, to the adsorption sites, will be one of the most critical factors determining the success of future ECBM operations. In this chapter, the results of the laboratory experiments conducted are evaluated in relation to the field observations, in the form of a synthesis of laboratory and field observations. The priorities for further research are then identified. Finally, the chapter (and thesis) is concluded with some general recommendations for the future implementation of ECBM as well as some more specific recommendations for ECBM in the Netherlands.

7.2 Synthesis: linking the experimental and field data

Under ECBM field conditions, an open system exists in which fluid transport, sorption-desorption, and coal swelling and shrinkage are coupled in a highly complex manner, with numerous processes taking place simultaneously. Three particular aspects of the system are highlighted and discussed below, as key factors in determining the progress of ECBM operations.

7.2.1 Matrix transport versus cleat transport

One of the main findings of the RECOPOL field experiment in Poland studied in this thesis was the early breakthrough of injected CO_2 in the production well (Chapter 2). This early initial breakthrough has been explained by a gravity driven (i.e. buoyant) override of the CO_2 over the denser water still present in the coal formation (Van Wageningen and Maas, 2007). Production of methane was therefore very limited because a) the reservoir pressure was maintained in the major part of the field due to injection, thereby preventing desorption of methane, and b) because the injected CO_2 did not come into contact with the coal matrix material between the cleats, so that desorption due to a reduction of CH_4 partial pressure did not take place. As more water was gradually produced from the reservoir, access of the injected CO_2 to the matrix should have increased, resulting in higher production rates of methane. However, this appeared not to be the case, as methane production rates remained low (Chapter 2). The most likely explanation for this is the low diffusion rate of methane into and through the coal matrix, as reported for the canister gas desorption tests on the coal cores (Chapter 2) and as measured experimentally in the laboratory (Chapters 4 and 5).

The low production rates of methane and the breakthrough of CO_2 observed in the RECOPOL test field indicate that, even when the injectivity problems were overcome, gas/fluid transport into the matrix micropores - where the CO_2 should adsorb - was limited. Because of the relatively high injection rates, much of the CO_2 thus bypassed the coal matrix before it could equilibrate (Fig. 7.1). Matrix transport therefore emerges as a crucial factor determining the performance of ECBM operations. The present laboratory experiments (Chapter 4 and 5) have provided a means to establish diffusion rates in coal, while simultaneously providing key information on the coal swelling behaviour (next section). In combination with coal data on characteristics such as cleat spacing, these rates can be used as valuable input for coal reservoir simulators, to adjust operational plans in ECBM field projects.

7.2.2 Injectivity decrease due to coal swelling

Loss of injectivity was experienced in the RECOPOL field experiment both before the hydraulic fracture treatment was performed but also afterwards, notably during periods when continuous injection was temporarily interrupted (Chapter 2). The decrease of injectivity was attributed to coal swelling, but this could not be proven

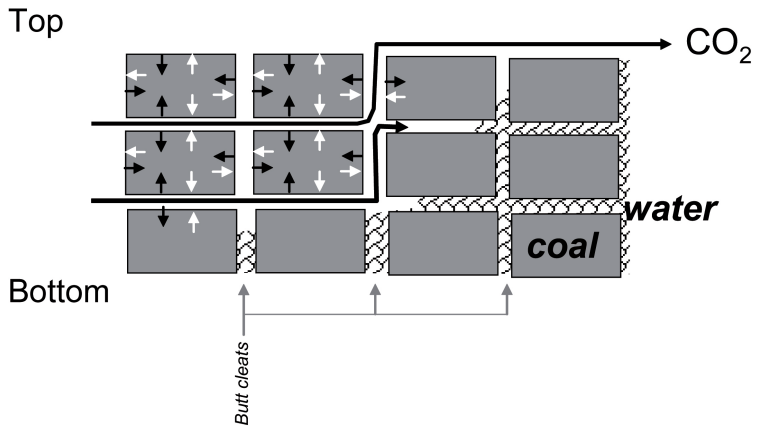

Figure 7.1: Schematic diagram of part of a coal seam showing the interpreted situation in the RECOPOL reservoir. The figure represents a view of the face cleat surface. Because the rate of transport of the CO_2 in the cleats (large arrows) is much faster than the transport into the matrix (small black and white arrows), much of the CO_2 by-passes the matrix before the CBM can be released. Also, buoyant gravity override of the formation water by the injected CO_2 will occur if the cleat system is still filled with water.

in the field (Chapter 2). Other possible explanations include clogging of the wellbore perforations or of the near-well zone by clays, precipitation of mineral scaling, and collapse of the cleat network around the well. Although such effects cannot be excluded, it can be inferred from the laboratory experiments on coal material from the RECOPOL site reported in this study (chapters 4, 5, and 6), and from those of Mazumder (2007), that coal swelling certainly played a role in the reduction of permeability in the RECOPOL test. To overcome this problem, there is a clear need for an operational strategy to control or avoid permeability loss due to coal swelling during ECBM operations. No firm strategy of this type yet exists. However, the laboratory experiments reported in this thesis can be considered as the first step towards the development of such a strategy, because a strategy can only evolve once the processes controlling swelling and associated self-stressing phenomena are understood and quantified.

7.2.3 The role of water

As mentioned above, the main impact of water in the RECOPOL reservoir, and probably in most ECBM reservoirs in bituminous coals, is the gravity override by CO_2 of the water present in the cleat system,. The present laboratory experiments have shown that water residing in the matrix micropores can also play a role in controlling performance in ECBM operations, because it can block access to part of the pore system and competes with CO_2 for adsorption in the micropores. Adsorption of moisture also leads to swelling of the coal matrix, whereas desorption results in shrinkage.

Once the water is removed from the cleats, for example by sweeping or flushing with CO_2, the moisture in the coal matrix may be released and shrinkage of the matrix may occur, also because of the desorption of methane. The use of CO_2 for drying of the coal in this way is advantageous, because water can dissolve to a significant extent in the CO_2 phase, though quantitative data on the uptake of water by CO_2 are scarse (Seo *et al.*, 2009). Such drying could potentially be very effective, especially when the pressure of the CO_2 is released from the coal and the CO_2 leaves the system, as seen in our experiments (Chapter 4 and 5) and during operations conducted in the RECOPOL field (Chapters 2 and 3). Active CO_2 flow will promote drying, because it will transport moisture towards the production well. The positive effect of drying on matrix diffusion rates seen in our experiments on moisturized coal samples (Chapter 4 and 5) will further promote CO_2-CH4 exchange, although the increased tendency for dry coal to swell may partly counteract the benefits of improved diffusion rates. Nevertheless, the effects of drying of the coal by injected CO_2 could explain the slight increase in injectivity, therefore permeability, that was observed during the period of continuous injection at the RECOPOL site (Chapter 2).

7.3 Further research

The present work has inevitably left some questions unanswered, as well as raising many new ones. In the following, some of the most important outstanding questions, new questions and experimental problems are identified and suggestions made for future ways to address them.

1. The coal-water-CO_2-CH_4 system is complex and much work is still required to comprehend all aspects of its behaviour and to predict the specific behaviour of coal and ECBM systems under in-situ conditions. We have shown that much can be learned from field observations, but it could well be that some of the results of the RECOPOL test are site-specific. This would hamper extrapolation of the results and conclusions of the field test in Poland to other basins. It must be emphasized that only a limited number of other field experiments have been realized to date under different geological and operational conditions, for example in Alberta, Canada (Gunter *et al.*, 1997; Gunter *et al.*, 1998), in Shanxi, China (Wong *et al.*, 2007), in Hokkaido, Japan (Yamaguchi *et al.*, 2005; Yamaguchi *et al.*, 2007), and in the San Juan Basin in New Mexico, U.S.A. ((Erickson and Jensen, 2001; Gunter *et al.*, 1998; Reeves and Schoeling, 2001; Schoeling and McGovern, 2000) and the technology is still far from mature. Further advances require additional field tests under geological conditions that differ from the tests operated to date, such as depth, burial history, coal composition and rank, and mineral matter in coal, taking into account the learning and experience of the field experiment reported here. This could lead to major steps forward if differences in performance can be explained in terms of differences in these geological conditions, thereby providing screening criteria for future ECBM projects.

2. The present optical cell experiments (Chapters 4, 5, and 6) have proven very useful for quantifying matrix swelling and diffusion. These experiments can be improved by developing automated identification of recognizable points on the digital images. Such points usually represent bright inertinite or pyrite particles embedded in a dark vitrinite background, which should enable automated identification. Automated processing eliminates any subjectivity of visual identification and would speed up the processing of individual experiments significantly. Reducing data acquisition and processing time in this way will enable rapid expansion of datasets on matrix swelling and diffusion properties of different coals.

3. The experiments reported in Chapters 4 and 5 have shown that, even for small matrix samples selected from a single block of coal the variability in equilibrium swelling and in the diffusion coefficient values obtained from the swelling response is quite large, suggesting significant variability in composition. To understand the effects of composition on matrix properties in optical experiments like the present, better coal characterization is needed, in terms of composition and texture for individual small samples. However, it should be recognized that a large number of experiments will be required to relate the measured differences in swelling, diffusion and other parameters to composition in a systematic way.

4. One of the objectives of the laboratory experiments described in Chapter 5 was to investigate dependence of the magnitude and rate of coal swelling on rank. This dependence could not be conclusively determined, because a) the variability of the samples obscured possible trends in the data, and b) bituminous coal samples with rank in the range of 1-2% vitrinite reflectance, with an expected minimum matrix porosity, were not investigated. Both magnitude and rate of swelling are expected to be lowest in this rank range. It is therefore recommended to measure the swelling and determine the diffusion coefficient of coal samples with a rank in the range of 1-2% vitrinite reflectance to investigate this possible minimum of swelling and swelling rate in this range.

5. As coal is laterally confined under in-situ conditions, there is clearly a need to investigate the swelling response of confined matrix samples on exposure to gas or fluid. Our experiments with confined, pre-pressed, granular samples were valuable because they revealed a new (permanent) swelling phenomena (see point 8 below). However, they appeared not to be representative for in-situ coal matrix because of the pre-pressing treatment before exposure to gas or fluid. New experiments need to be set-up to work with confined coal matrix samples. The main challenge of these experiments will be confinement of the small samples (< 1 mm), needed to exclude the cleats in the coal, in such a way that it is still possible to quantitatively measure changes in pressure, temperature and stress state.

6. Based on the results of this study, it was suggested in Chapters 4 and 5 that the presence or absence of moisture may play a role in future mitigation of swelling

in field operations. Removal of the water from the matrix may result in a slight permeability increase. It is difficult to quantify this effect, because the additional storage capacity of the matrix created by drying may result in additional swelling. The combined effect of swelling and shrinkage due to water removal by CO_2 needs to be further investigated.

7. Present and previous investigations have shown that, generally speaking, to achieve ECBM production in an effective way, a technical solution is required to prevent reduction of permeability and matrix transport due to coal swelling. A possible solution could be found via investigation of the impact of swelling and stress development in coal (cf. Chapter 6) on the transport properties of the coal, under confined conditions resembling the in-situ situation. For example, if the injected CO_2 would increase the brittleness of the coal, the coal would be more susceptible to hydraulic fracturing. Alternatively, rapid pressure cycling could potentially create fractures around enlarged boreholes via the rapid escape of the gas from the matrix, thereby increasing the matrix permeability and enhancing matrix transport.

8. The present experiments have shown that adsorption of CO_2 by (pre-pressed) granular coal under confined conditions leads to self-stressing, and to swelling under unconfined conditions. Because swelling and adsorption are related, it is therefore highly likely that confinement and associated stress have an effect on sorption capacity, as already mentioned in the literature (e.g. Pone *et al.* (2009a)). A constitutive equation relating these quantities is needed to improve modelling of the in-situ response of coal to CO_2 injection in terms of the spatial distribution of sorption stress-strain evolution and the effects of the latter on cleat transport properties.

9. Overcoming the low cleat permeability of the coal seams is generally considered key to the success of ECBM. Although this is true, it certainly is not the only factor of importance. Low cleat permeability of coal is likely to be related to compaction during the geological burial history. Such compaction will generally have affected the matrix also. It can therefore be expected that low cleat permeability is associated with slow matrix transport. However, from the matrix diffusion coefficients determined in our experiments (Chapter 5), it is clear that overcoming permeability problems (e.g. by hydraulic fracturing) does not overcome matrix transport problems. The suggested relation between low permeability and low matrix diffusion coefficient is important for predicting the ECBM potential of different coals and should be investigated further. Moreover, it is possible that low permeable coals exhibit larger swelling, hence larger self-stressing and associated permeability reduction effects, because of their deep burial, as described in Chapter 6.

10. The re-production of the injected CO_2 and CBM from the RECOPOL reservoir after a 1 year soaking period (Chapter 3) resulted in a gas composition that stabilized at 60% CH_4 and 40% CO_2. This composition could not be readily

explained (Chapter 3). However, it is important to gain an understanding of the in-situ processes that lead to this composition, because these processes determine the exchange of CO_2 for CH_4 in the coal matrix and thereby partly the success of the project. It is very well possible that the exchange of the CO_2 for CH_4 is controlled by the transport properties of the coal matrix and not by the sorption capacity of the coal. Counter diffusion of different species could offer a possible explanation. This should be further investigated in the laboratory. In general, the dataset should be expanded with experiments using gas mixtures, for example by presaturating samples with CH_4 before adding CO_2 at a higher pressure. Also, the effect of mixtures that include nitrogen would be interesting, as this could be one of the components of the injected gas if it comes from a power plant. Also, nitrogen is reported to have a positive effect on the permeability of coal seams (Shi *et al.*, 2008).

7.4 Recommendations for future ECBM field development

7.4.1 General recommendations

One of the main results of the development of the RECOPOL demonstration experiment described in Chapters 2 and 3, from an organizational point of view was the realization of the field experiment itself. Many issues were solved during the course of the project, in relation to technology, regulation and public acceptance and perception, that can serve as a blue-print for future development of on-shore CO_2 storage sites in Europe and beyond. Carbon dioxide injection rates of approximately 15 tonnes per day were achieved. The mass balance of the injected and produced CO_2 showed that the total volume of CO_2 produced was only a fraction of the amount that was injected (Chapter 3). It was concluded that most likely, the CO_2 was taken up by the coal and remained adsorbed to the coal. As mentioned already, coal matrix swelling due to the adsorption of CO_2 probably sealed the cleat system and the entire coal seam eventually.

These conclusions give confidence to the notion that CO_2 injected into coal remains fixed in-situ, so that, from this point of view, development of ECBM sites merits further attention. However, from a technical point of view, the RECOPOL results (Chapters 2 and 3) show that there are still many unresolved issues. These issues are expected to be relevant to other basins with similar low permeability coal, notably those of NW Europe but also many basins in China, for example. These issues will now be briefly considered, in the light of the results of the present laboratory experiments, not forgetting the uniqueness of each coal basin.

First, an important lesson learned from the RECOPOL field experiment was that injection into low permeability coal seams is not trivial. It was expected that a high injection pressure would overcome the low injectivity but this appeared not to be

the case. Flexibility in operational equipment and metering tools is therefore highly recommended in future ECBM operations. Understanding of the in-situ processes leading to swelling is also crucial in the planning phase of ECBM operations. Much can be learned about the swelling behaviour of the coal at a given site by numerical modelling studies (e.g. (Van Wageningen and Maas, 2007; van Wageningen *et al.*, 2009), but additional laboratory characterization of the swelling properties of the coal is highly recommended because it provides quantitative data on the extent and rate of coal matrix swelling. As explained under point 9 in Section 3, this characterization should address both cleat transport, involving cm or larger size samples, and matrix transport properties, involving mm scale samples. The experimental method developed and applied in this thesis to measure swelling and rate of swelling (chapter 4 and 5) is highly suitable for testing the matrix transport properties.

On the basis of these data, for implementation of ECBM at a given site, dedicated operational plans with optimized injection rates are required that take into account both the cleat and the matrix transport. Investigation of the role of a) mineral matter, which may enhance sorption kinetics (Radlinski *et al.*, 2009), and b) neighbouring strata, which may provide pathways of the gas or fluid to the coal outside the well zone, is also highly recommended. Such aspects were not covered in this thesis.

With regard to the scale of future ECBM projects, it should be anticipated in the development stage that the injection rates per well will be restricted due to limited permeability. Based on the results of the RECOPOL field experiment (Chapter 2 and 3), it is expected that the maximum injection rate in vertical wells in low permeability coal seams ($<$ 2mD) will be $\sim$ 100 tonnes per day (depending on well completion, cumulative coal thickness, etc.), or about 30,000 tonnes per well per year. To reach injection volumes similar to those anticipated for CO_2 storage projects in depleted gas fields or aquifers ($>$1Mt per well per year), many vertical wells will be required, which has to be taken into account in the spatial planning of the operation. Although technological solutions (e.g. horizontal/multi-lateral wells) may increase injection rates in ECBM projects, the application of ECBM for CO_2 storage seems unfavourable when alternative storage option are available nearby. However, if these alternatives are not available, as is the case in many coal basins worldwide, e.g. in large countries like India, South Africa and China (Fig. 7.2), the ECBM option might still prove attractive.

If, despite low injectivity and high well density,ECBM still emerges as an attractive storage option at a given site, it should be realized that, although CO_2 injection will enhance CH_4 production significantly (e.g. up to 2 times as much gas in the RECOPOL site, see Chapter 2), CO_2 injection is probably not sufficient to transform non-economic CBM production to economic production. As such, ECBM seems to be most feasible when it can be applied in an area with existing, thus commercial, CBM production. In this case, major investments in wells and infrastructure have already been made. ECBM would then be applied as a secondary production phase after regular CBM passes its peak gas production phase (Fig. 7.3c). This has three other major advantages: the coal reservoir is already dewatered before CO_2 injection, it is depres-

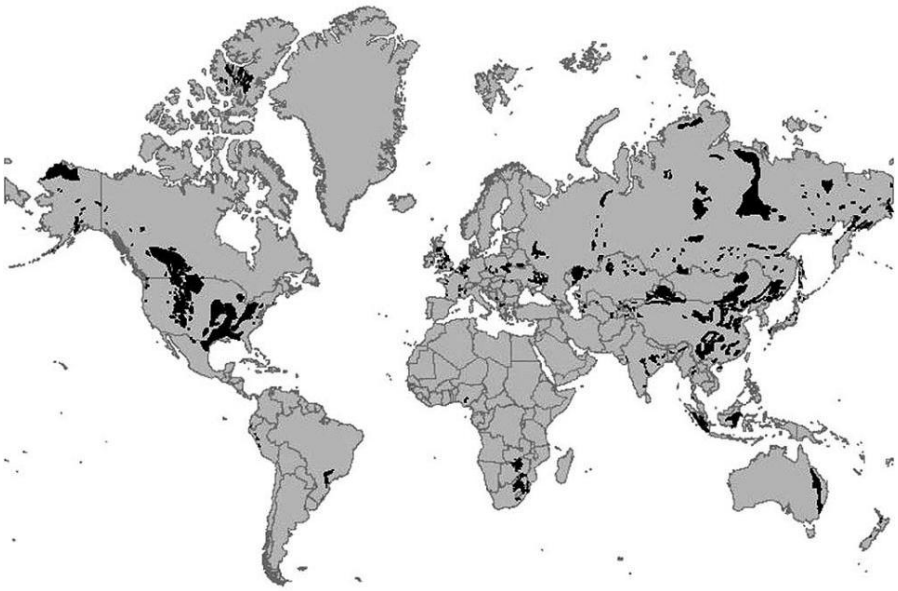

Figure 7.2: Distribution of major coal basins in the world (from Van Bergen *et al.* (2004), which hold estimated CBM volumes of the order of 83-263$\times 10^{12}$ m^3 (Boyer II and Qingzhao, 1998).

surized, and the quality of the gas is not affected by potential mixing with injected CO_2 during the primary production phase. The disadvantage of this approach is the long time it can take, possibly several years after the start of CBM production, before CO_2 injection starts. A tertiary phase in operations can be envisaged during which CBM production ceases while CO_2 is still being injected, making this a pure storage operation in this phase (Fig. 7.3d).

In conclusion, while worldwide coal holds an enormous volume of methane of the order of 83-263$\times 10^{12}$ m^3 (Boyer II and Qingzhao, 1998), this volume is not proven to be recoverable. For reference, the total, proven, world-recoverable reserves of natural gas are of the order of 170$\times 10^{12}$ m^3 (calculated at the end of 2002, World Energy Council (2004)). It is expected that CBM production will emerge throughout the world in the near future to exploit the CBM resources. This development also provides opportunities for ECBM, as a secondary production phase. The lower estimate of the global storage capacity in coal fields is 3-15 Gt and the upper estimate 200 Gt CO_2, compared to the vast potential storage medium for CO_2 of 675-900 Gt CO_2 for oil and gas fields (IPPC, 2005). However, the complexity of the response of coal to ECBM makes the implementation of large scale projects more complicated than other subsurface options, such as depleted gas fields. On the other hand, major regions of the world, like major parts of India, South Africa and China, have abundant unminable coal deposits but few alternative options for CO_2 storage, like depleted oil and gas fields. Even with its limitations, then, ECBM may become crucial in climate-

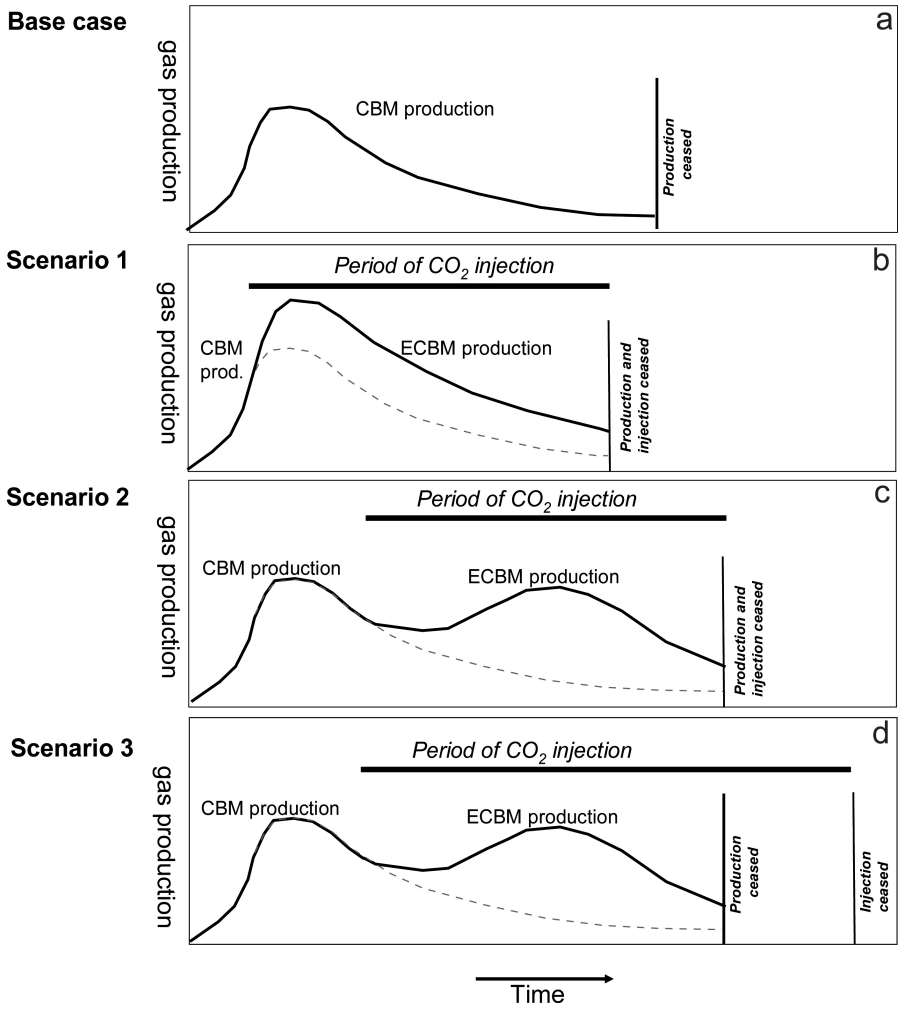

Figure 7.3: Different scenarios for future ECBM operations in combination with CBM. The base case a) represents the situation if CBM is produced without injection of CO_2. Scenario 1 (b) is often envisaged for storage in coal seams in unexplored coal basins, where CO_2 should be injected as early as possible to achieve emission reductions. Associated challenges with this scenario are the risk of an early breakthrough of the injected CO_2 in the CBM production wells, thereby decreasing the caloric value of the gas, and the need for high injection pressures to overcome the high fluid pressure in the reservoir that is not yet dewatered. These issues can be resolved in scenario 2, where the formation water and therefore the fluid pressure in the coal are already depleted. Additionally, the possible breakthrough of CO_2 is postponed until after the peak production when the majority of the high caloric CBM is already produced. Here, investments have been made during the primary CBM phase which do not need to be earned back from CO_2 operations. In scenario 3, there is a third phase of continued CO_2 injection. However, gas production is discontinued because of an uneconomically high CO_2 concentration after breakthrough.

friendly energy production in such regions in future.

7.4.2 Recommendations for the Netherlands

The subsurface of the Netherlands holds substantial volumes of coal, with estimates for bituminous and anthracite coal resources shallower than 1500 m between 4000 and 38 000 Mt in Limburg, the Peel and the Achterhoek areas (Van Bergen *et al.*, 2007). These volumes occur mainly in Late Carboniferous (Westphalian) deposits with a total original thickness of up to 3000 m. These sediments were deposited in a cyclic, river-dominated environment and have coal contents between 1.0 and 2.1 volume % (Van Buggenum and Den Hartog Jager, 2007). During the Saalian phase of deformation and uplift at the end of the Carboniferous, about 2000 m of Carboniferous strata were eroded away across large parts of what is now the Netherlands, leading to the current configuration of the Carboniferous subcrop below the basal Permian unconformity (Pagnier *et al.*, 1987; Van Buggenum and Den Hartog Jager, 2007). At present, the coal-bearing deposits are found above sea-level in the southernmost Netherlands and deepen northward to depths of more than 2 km across the majority of the country (Fig. 7.4). The rank of the coal is mainly bituminous; though anthracite occurs locally in South-Limburg.

Because conventional coal mining is economically not feasible in the Netherlands in the short term, other ways to use the nation's coal have been investigated, including the possibility of (E)CBM production. Fails (1996) established that the depositional setting and coal distribution of the Eastern Ruhr Basin (Fig. 7.4) are favourable for CBM. The coal basins in the Netherlands resemble the Eastern Ruhr Basin in the sense that the coal-bearing deposits are of the same age and the basins are located at a similar position with respect to the Variscan front. The feasibility of coalbed-methane production in the Netherlands still awaits the evaluation of the full-spectrum of production-related, technical and geological issues, as well as agreement on societal, environmental and economic aspects (NITG, 1999; Van Bergen *et al.*, 2007). Estimates for the theoretically recoverable volumes of coalbed methane shallower than 1500 m lie between 7 and 107×10^9 m^3 (Van Bergen *et al.*, 2007). Although these estimates for potential gas in place are based on scarse data available on coal gas content, due to lack of coal-mining activities in the Netherlands since 1974 and of coal exploration since 1985, it is unlikely that gas content will be the limiting factor for production. The many gas fields in the Netherlands sourced by the Westphalian show that the coal is highly gasprone and has significant gas generation potential. Some of the generated gas is likely to be retained by the coal, as isotherm measurements indicate methane sorption capacities of dry coals from the Achterhoek area of about 15 m^3/t (Krooss *et al.*, 2002). Indications of substantial gas content in coal seams in the Netherlands come from gas peaks logged during drilling of exploration wells for coal, and for gas when penetrating coal seams, and from reported methane release in the mines of South-Limburg (Stuffken, 1957).

Aside from gas content, it is likely that the production potential of the Dutch coal

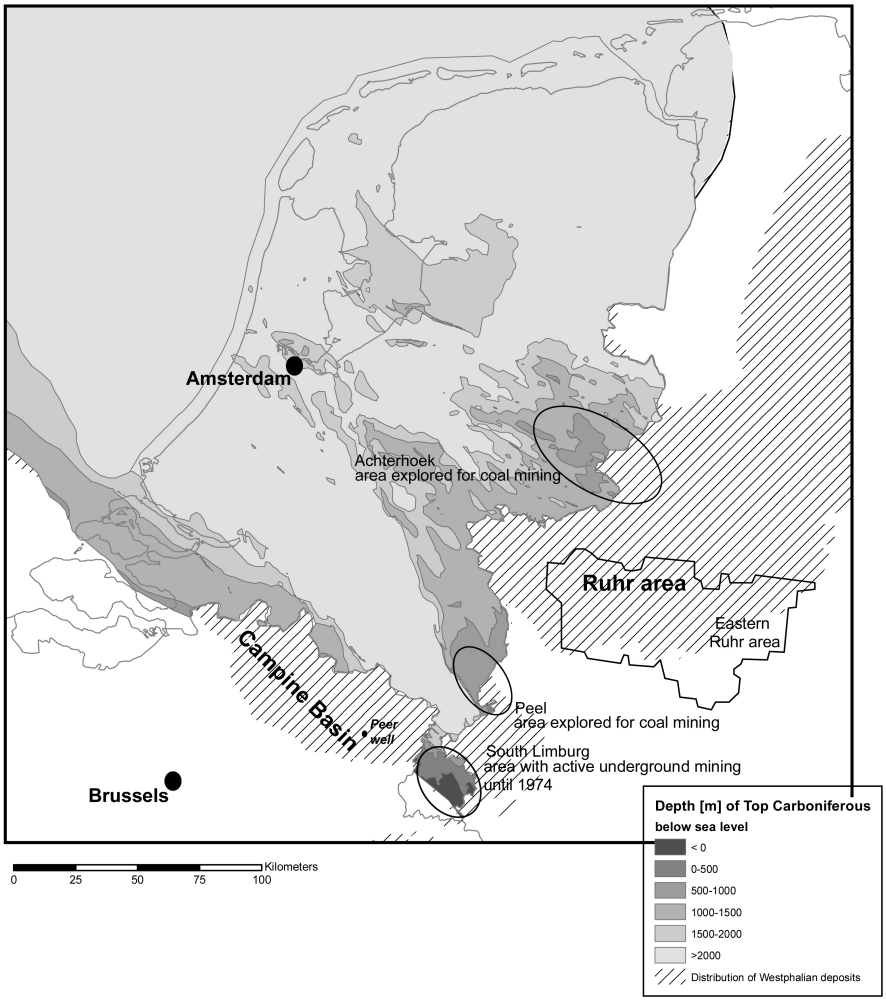

Figure 7.4: Depth map of the top of the Carboniferous sediments in the Netherlands. The distribution of the Westphalian deposits is indicated more schematically in bordering areas in Germany and Belgium.

basins will be determined by the local stress conditions. Local stress conditions in combination with the cleat orientation will determine the magnitude and anisotropy of the cleat permeability in the coal seam. The tectonic history and structural setting in the Netherlands is in general more complex than CBM producing basins in the United States. The Dutch basins are heavily faulted and locally also folding occurs, especially near the Variscan front (e.g. in South-Limburg). During the geological history of the Netherlands, most coal seams have been buried deeper than the present depth. This complex geological history has probably resulted in low permeability of the coal, possibly as low as 0.1 to 1 mDarcy at a depth of around 1000 m. This is based on the permeability measured in-situ in the Peer well in the Campine Coal Basin in Belgium, the only well drilled and tested for CBM production in the proximity of the Netherlands. The permeability of this coal was less than 1 mDarcy in Westphalian A and B seams at depths between 850 and 1250 m, i.e., which is about 450 m less than their maximum paleo-burial depth (Wenselaers *et al.*, 1996).

As described in Section 3, it is likely that due to this deep burial in the geological past the matrix transport potential of Dutch coals is also low. The matrix diffusion coefficients could well be as low as those determined in this study (Chapter 5) for the bituminous coal in Poland, because these coals were also buried deeper then their current position in their past (McCants *et al.*, 2001). Probably, the highest permeability and diffusion coefficients will be found where tectonic stresses were limited, thus away from the Variscan front. Additionally, given the results reported in Chapter 6, it should be evaluated whether deep burial of the Dutch coals has resulted in matrix compaction beyond the elastic limit. In that case, additional swelling upon the injection of CO_2 may result from strain recovery, as discussed in Chapter 6. Local stress conditions are also important for the applicability of well stimulation techniques, such as hydraulic fracturing, and horizontal drilling. The application of horizontal drilling techniques may be limited by the fact that coal seams in the Netherlands are mostly relatively thin, with seams in excess of 50cm thickness generally being between 80 and 100 cm. These thicker seams are often distantly spaced (~ 20-100m). However, at specific locations the conditions for production are better, with individual coal-layer thicknesses reaching up to 3-3.5 m (Van Bergen *et al.*, 2007).

Apart from stress state, the water content and hydrological conditions play an important role in determining the feasibility of ECBM, primarily because of the required pressure decrease in the coal seam, which is governed by hydrological recharge potential. The importance of this is shown by the production history of the aforementioned Peer well in the Campine Basin in northeastern Belgium, where only a limited amount of CH_4 was produced because of inflow of water into the well. This flow was too high to reduce the pressure sufficiently for substantial CH_4 desorption (Wenselaers *et al.*, 1996). Identifying recharge areas and subsurface flow paths would therefore be of major importance for delineating prospective coalbed methane plays in the Netherlands. This is also important for identifying possible late-stage bacterial methanogenesis, which may add additional methane to the coal (Van Bergen *et al.*, 2007). However, the general high salinity of formation water in the Carboniferous

deposits in the Netherlands does not indicate recharging with meteoric water, probably due to the sealing of the coal-bearing sequences by thick clay covers. A secondary aspect of the role of water that may be relevant for coal seams in the Netherlands is its impact on the volume of the coal and the diffusion rates of gas or supercritical fluid, as identified in Chapters 4 and 5 and discussed in Section 4.1.

It is recommended in section 4.1, that CO_2 storage in subsurface coal should be considered if conventional CBM production proved to be feasible. Based on the potential gas content and an assumed exchange ratio of 2-4 between CO_2 and CH_4, determined from adsorption studies, estimates of the adsorption storage potential of coal seams shallower than 1500 m are reported to be between 39 and 594 Mt of CO_2 (Hamelinck *et al*., 2001; Van Bergen *et al*., 2000; Van Bergen *et al*., 2007). These figures are already an overestimation, because due to infrastructural, societal and environmental constraints, it will be impossible to exploit all investigated areas (Van Bergen *et al*., 2007). Furthermore, these values are of limited use because the actual storage potential will depend on the expected injectivity and transport of CO_2 with time to the adsorption sites in the coal. Clearly, if CBM production appears to be feasible, it is likely that permeability and matrix transport properties are also satisfactory for ECBM. The main issue for CO_2 injection would then be to gain understanding of the swelling behaviour. For the Dutch coals, with a mainly bituminous rank, significant swelling can be expected as shown by the results of Chapters 4 and 5 of this thesis. Similar to ECBM locations worldwide, a specific operational strategy will be needed to cope with the swelling, as discussed in section 4.1.

In conclusion, ECBM in the Netherlands offers theoretically significant capacity for storage of CO_2, but the actual capacity will be determined, from a technical point of view, by the ease or difficulty of transport of the CO_2 from the well to the micropores in the coal matrix of the coal seam. Because cleat permeability and matrix diffusion coefficients are not expected to be high, taking into account the current absence of CBM infrastructure and noting the availability of alternative storage options such as depleted gas fields, it is likely that future application of ECBM in the Netherlands will be restricted to areas with relatively shallow coal seams that have access to relatively inexpensive CO_2. The most promising areas are likely to be those areas with a nearly pure source of CO_2 on top of the coal seam, as for example investigated for South-Limburg (Van Bergen *et al*., 2003a). However, future developments, like the installation of pipelines for CO_2 transport near coal fields, may widen the options.

Acknowledgements

Parts of this synthesis chapter are based on two publications: Van Bergen *et al*. (2007) and Van Bergen *et al*. (2009b). Elsevier and the Royal Netherlands Academy of Arts and Sciences are acknowledged for granting the permission to reprint parts of these publications. Co-authors of these publications, Henk Pagnier, Peter van Tongeren, Pawel Krzystolik, Niels van Wageningen, Bart Jura, Jacek Skiba and Pascal Winthae-

gen are gratefully thanked for their interactions and contributions to these papers.

Bibliography

Adamson, A., & Gast, A. (1997). *Physical Chemistry of Surfaces, 6th edition*. Wiley-Interscience Publications, ISBN 0-471-14873-3.

Allardice, D., & Evans, D. (1978). Moisture in coal. In C. Karr (Ed.) *Analytical methods for coal and coal products*, vol. 1, (pp. 247–262).

Amador-Hernandez, J., & Luque De Castro, M. (2000). On-line detection for supercritical-fluid extraction. *Journal of Biochemical and Biophysical Methods*, *43*(1-3), 329–343.

Anderson, R., Hall, W., Lecky, J., & Stein, K. (1956). Sorption studies on American coals. *Journal of Physical Chemistry*, *60*, 1548–1558.

Ayers Jr., W. (2002). Coalbed gas systems, resources, and production and a review of contrasting cases from the San Juan and Powder River basins. *American Asssociation of Petroleum Geologists Bulletin*, *86*, 1853–1890.

Beamish, B., & Gamson, P. (1993). Sorption behaviour and microstructure of Bowen Basin coals, Coalseam Gas Research Institute, James Cook University. Tech. rep., CGRI TR 92/4.

Besserer, G., & Robinson, D. (1973). Refractive indices of ethane, carbon dioxide and isobutane. *Journal of Chemical and Engineering Data*, *18*(2), 137–140.

Bielicki, R., Perkins, J., & Kissell, F. (1972). Methane diffusion parameters for sized coal particles. Tech. rep., US Bureau of Mines Report of Investigations #7697.

Boyer II, C., & Qingzhao, B. (1998). Methodology of coalbed methane resource assessment. *International Journal of Coal Geology*, *35*(1-4), 349–368.

Burruss, R. (2003). CO_2 adsorption in coals as a function of rank and composition: A task in usgs research on geologic sequestration of CO_2. In *Presentation on the Second International Forum on Geologic Sequestration of CO_2 in Deep, Unmineable Coalseams (Coal-Seq II)*. Washington DC, March 6 and 7, 2003, www.coal-seq.com (accessed March 2006).

Busch, A., Alles, S., Gensterblum, Y., Prinz, D., Dewhurst, D., Raven, M., Stanjek, H., & Krooss, B. M. (2008). Carbon dioxide storage potential of shales. *International Journal of Greenhouse Gas Control*, *2*(3), 297–308.

Busch, A., Gensterblum, Y., & Krooss, B. (2003). Investigation of preferential sorption behaviour of CO_2 and CH_4 on coals by high pressure adsorption/desorption experiments with gas mixtures. In *Proceedings of the International Coalbed Methane Symposium 2003*. University of Alabama, Tuscaloosa (USA), CD-ROM.

Busch, A., Gensterblum, Y., Krooss, B. M., & Littke, R. (2004). Methane and carbon dioxide adsorption-diffusion experiments on coal: upscaling and modeling. *International Journal of Coal Geology*, *60*(2-4), 151–168.

Bustin, M., Cui, X., & Chikatamarla, L. (2008). Impacts of volumetric strain on CO_2 sequestration in coals and enhanced CH_4 recovery. *American Association of Petroleum Geologists Bulletin*, *92*(1), 15–29.

Bustin, R., & Clarkson, C. (1998). Geological controls on coalbed methane reservoir capacity and gas content. *International Journal of Coal Geology*, *38*, 3–26.

Carslaw, H., & Jaeger, J. (1959). *Conduction of heat in solids*. New York City: Oxford University Press.

Ceglarska-Stefanska, G., & Czaplinski, A. (1993). Correlation between sorption and dilatometric processes in hard coals. *Fuel*, *72*(3), 413–417.

Charrière, D., Pokryszka, Z., & Behra, P. (In press). Effect of pressure and temperature on diffusion of CO_2 and CH_4 into coal from the Lorraine basin (France). *International Journal of Coal Geology*.

Clarkson, C., & Bustin, R. (1996). Variation in micropore capacity and size distribution with composition in bituminous coal of the Western Canadian Sedimentary Basin. *Fuel*, *75*, 1483–1498.

Clarkson, C., & Bustin, R. (2000). Binary gas adsorption/desorption isotherms: effect of moisture and coal composition upon carbon dioxide selectivity over methane. *International Journal of Coal Geology*, *42*, 241–271.

Clarkson, C. R., & Bustin, R. M. (1999a). The effect of pore structure and gas pressure upon the transport properties of coal: a laboratory and modeling study. 1. Isotherms and pore volume distributions. *Fuel*, *78*(11), 1333–1344. 0016-2361 doi: DOI: 10.1016/S0016-2361(99)00055-1.

Clarkson, C. R., & Bustin, R. M. (1999b). The effect of pore structure and gas pressure upon the transport properties of coal: a laboratory and modeling study. 2. Adsorption rate modeling. *Fuel*, *78*(11), 1345–1362.

Cloke, M., Lester, E., & Belghazi, A. (2002). Characterisation of the properties of size fractions from ten world coals and their chars produced in a drop-tube furnace. *Fuel*, *81*(5), 699–708.

Crank, J. (1975). *The Mathematics of Diffusion*. Oxford University Press.

Crosdale, P., & Beamish, B. (1993). Maceral effects on methane sorption by coal. In J. Breston (Ed.) *New Developments in Coal Geology, A Symposium*, (pp. 95–98).

Crosdale, P., & Beamish, B. (1995). Methane diffusivity at South Bulli (NSW) and central (Qld) collieries in relation to coal maceral composition. In R. Lama (Ed.) *International Symposium-cum-Workshop on Management and Control of High Gas Emissions and Outbursts*, (pp. 363–367).

Crosdale, P., Beamish, B., & Valix, M. (1998). Coalbed methane sorption related to coal composition. *International Journal of Coal Geology*, *35*, 147–158.

Cui, X., Bustin, M., & Chikatamarla, L. (2007). Adsorption-induced coal swelling and stress: implications for methane production and acid gas sequestration into coal seams. *Journal of Geophysical Research*, *112*(B10202), 1–16.

Cui, X., & Bustin, R. (2006). Controls of coal fabric on coalbed gas production and compositional shift in both field production and canister desorption tests. *Society of Petroleum Engineers Journal Paper 89035-PA*, *Volume 11*(1, March), 111–119.

Cui, X., Bustin, R. M., & Dipple, G. (2004). Selective transport of CO_2, CH_4, and N_2 in coals: insights from modeling of experimental gas adsorption data. *Fuel*, *83*(3), 293–303.

Day, S., Fry, R., & Sakurovs, R. (2008). Swelling of Australian coals in supercritical CO_2. *International Journal of Coal Geology*, *74*(1), 41–52.

De Jager, J., & Geluk, M. (2007). Petroleum geology. In T. Wong, D. Batjes, & J. De Jager (Eds.) *Geology of the Netherlands*, (pp. 241–264).

Dreesen, R., Bossiroy, D., Swennen, R., Thorez, J., Fadda, A., Ottelli, L., & Keppens, E. (1997). A depositional and diagenetic model for the Eocene Sulcis coal basin of SW Sardinia. *Geological Society, London, Special Publications*, *125*, 49–75.

Durucan, S., Ahsanb, M., & Shi, J. (2009). Matrix shrinkage and swelling characteristics of European coals. *Energy Procedia*, *1*(1), 3055–3062.

Eddy, G., Rightmire, C., & Byrer, C. (1982). Relationship of methane content of coal rank and depth: Theoretical vs. observed. *SPE/DOE 108000*, (pp. 117–119).

Erickson, D., & Jensen, J. R. (2001). CO_2 sequestration in an unminable coalbed - San Juan Basin, Colorado, USA. In D. Williams, B. Durie, P. McMullan, C. Paulson, & A. Smith (Eds.) *Proceedings of the Fifth International Conference on Greenhouse Control Technologies*, (pp. 589–592).

Ettinger, I., Eremin, I., Zimakov, B., & Yanovskaya, M. (1966). Natural factors influencing coal sorption properties. I. Petrography and sorption properties of coals. *Fuel*, *45*, 267–275.

Fails, T. (1996). Coalbed methane potential of some variscan foredeep basins. In R. Gayer, & I. Harris (Eds.) *Coalbed Methane and Coal Geology. Geological Society Special Publication 109*, (pp. 13–26).

Faiz, M., Aziz, N., Hutton, A., & Jones, B. (1992). Porosity and gas sorption capacity of some eastern Australian coals in relation to coal rank and composition. In *Coalbed Methane Symposium*, (pp. 9–15).

Freudenberg, U., Lou, S., Schlüter, R., Schütz, K., & Thomas, K. (1996). Main factors controlling coalbed methane distribution in the ruhr district, germany. In R. Gayer, & I. Harris (Eds.) *Coalbed Methane and Coal Geology. Geological Society Special Publication 109*, (pp. 67–88).

Gamson, P., Beamish, B., & Johnson, D. (1993). Coal microstructure and micropermeability and their effects on natural gas recovery. *Fuel*, *72*, 87–99.

Gamson, P., Beamish, B., & Johnson, D. (1996). Coal microstructure and secondary mineralization: their effect on methane recovery. In R. Gayer, & I. Harris (Eds.) *Coalbed Methane and Coal Geology. Geological Society Special Publication 109*, (pp. 165–179).

Gan, H., Nandi, S. P., & Walker Jr, P. L. (1972). Nature of the porosity in american coals. *Fuel*, *51*(4), 272–277.

Goodman, A., Campus, L., & Schroeder, K. (2005a). Direct evidence of carbon dioxide sorption on Argonne Premium coals using attenuated total reflectance - Fourier Transform Infrared Spectroscopy. *Energy and Fuels*, *19*, 471–476.

Goodman, A., Favors, R., Hill, M., & Larsen, J. (2005b). Structure changes in Pittsburgh no. 8 coal caused by sorption of CO_2 gas. *Energy and Fuels*, *19*, 1759–1760.

Goodman, A. L., Favors, R. N., & Larsen, J. W. (2006). Argonne coal structure rearrangement caused by sorption of CO_2. *Energy Fuels*, *20*(6), 2537–2543.

Gruszkiewicz, M. S., Naney, M. T., Blencoe, J. G., Cole, D. R., Pashin, J. C., & Carroll, R. E. (2009). Adsorption kinetics of CO_2, CH_4, and their equimolar mixture on coal from the black warrior basin, west-central alabama. *International Journal of Coal Geology*, *77*(1-2), 23–33.

Gunter, W. D., Gentzis, T., Rottenfuser, B. A., & Richardson, R. J. H. (1997). Deep coalbed methane in alberta, canada: a fossil resource with the potential of zero greenhouse gas emissions. *Energy Conversion and Management*, *38*(supplement), S217–S222.

Gunter, W. D., Wong, S., Cheel, D., & Sjostrom, G. (1998). Large CO_2 sinks: Their role in the mitigation of greenhouse gases from an international, national (Canadian) and provincial (Alberta) perspective. *Applied Energy*, *61*, 209–227.

Gutierrez-Rodriguez, J. A., Purcell, R. J., & Aplan, F. F. (1984). Estimating the hydrophobicity of coal. *Colloids and Surfaces*, *12*, 1–25.

Hall, F., Zhou, C., Gasem, K., Robinson Jr., R., & Yee, D. (1994). Adsorption of pure methane, nitrogen, and carbon dioxide and their binary mixtures on wet Fruitland coal. In *Society of Petroleum Engineers Eastern Regional Conference and Exhibition, Paper no. 29194*, (pp. 329–344).

Hamelinck, C., Faaij, A., Ruijg, G., Jansen, D., Pagnier, H., Van Bergen, F., Wolf, K.-H., Barzandji, O., Bruining, H., & Schreurs, H. (2001). Potential for CO_2 sequestration and enhanced coalbed methane production in the Netherlands. Tech. Rep. report no. 2ECBM01.01.

Harpalani, S. (2005). Gas flow characterisation of Illinois coal. ICCI Project No. 03-1/7 1B-2. Final. Tech. rep.

Harpalani, S., & Chen, G. (1995). Estimation of changes in fracture porosity of coal with gas emission. *Fuel*, *74*(10), 1491–1498.

Harpalani, S., & Chen, G. (1997). Influence of gas production induced volumetric strain on permeability of coal. *Geotechnical and Geological Engineering*, *15*, 303–325.

Harpalani, S., & Schraufnagel, R. (1990). Shrinkage of coal matrix with release of gas and its impact on permeability of coal. *Fuel*, *69*(May), 551–556.

Hol, S., van Bergen, F., Spiers, C., & Peach, C. (2006). Volumetric behaviour of coal due to CO_2 and effects on stress. In V. Pavlovic, & L. Thomas (Eds.) *Proceedings of 6th European Coal Conference*, (pp. 281–290).

IEA (2008). *World Energy Outlook 2008*.

IPPC (2005). *IPPC Special Report on Carbon Dioxide Capture and Storage. Prepared by Working Group III of the Intergovernmental Panel on Climate Change*. Cambridge university Press, Cambridge, United Kingdom and New York, NY, USA.

Israelachvili, J. (1992). *Intermolecular and Surface Forces*. London: Academic Press Limited.

Iwai, Y., Amiya, M., Murozono, T., Arai, Y., & Sakanishi, K. (1998). Drying of coals by using supercritical carbon dioxide. *Ind. Eng. Chem. Res.*, *37*(7), 2893–2896.

Iwai, Y., Koujina, Y., Arai, Y., Watanabe, I., Mochida, I., & Sakanishi, K. (2002). Low temperature drying of low rank coal by supercritical carbon dioxide with methanol as entrainer. *The Journal of Supercritical Fluids*, *23*(3), 251–255.

Jahediesfanjani, H., & Civan, F. (2006). Effect of resident water on enhanced coal gas recovery by simultaneous CO_2/N_2 injection. In *SPE Annual Technical Conference*, (pp. 1–18). San Antonio, Texas, USA.

Joubert, J., Grein, C., & Bienstock, D. (1974). Effect of moisture on the methane capacity of american coals. *Fuel*, *53*, 186–191.

Karacan, C. O. (2003). Heterogeneous sorption and swelling in a confined and stressed coal during CO_2 injection. *Energy and Fuels*, *17*(6), 1595–1608.

Karacan, C. O. (2007). Swelling-induced volumetric strains internal to a stressed coal associated with CO_2 sorption. *International Journal of Coal Geology*, *72*(3-4), 209–220.

Karacan, C. O., & Mitchell, G. D. (2003). Behavior and effect of different coal microlithotypes during gas transport for carbon dioxide sequestration into coal seams. *International Journal of Coal Geology*, *53*(4), 201–217.

Kędzior, S. (2002). The influence of tectonic factor on methane bearing capacity in chosen areas of the Upper Silesian Coal Basin. In J. Jureczka, & M. Podemski (Eds.) *Proceedings of the IV European Coal Conference*, (pp. 143–148). Polish Geological Institute Special Papers 7.

Kelemen, S., & Kwiatek, L. (2007). Physical properties of dry block Argonne Premium bituminous coal related to CO_2, CH_4 and N_2 adsorption, paper no. 0711. In *Int. Coalbed Methane Symp.*. Tuscaloosa (AL), USA.

Kelemen, S. R., & Kwiatek, L. M. (2009). Physical properties of selected block Argonne Premium bituminous coal related to CO_2, CH_4, and N_2 adsorption. *International Journal of Coal Geology*, *77*(1-2), 2–9.

Kelemen, S. R., Kwiatek, L. M., Siskin, M., & Lee, A. G. K. (2006). Structural response of coal to drying and pentane sorption. *Energy and Fuels*, *20*(1), 205–213.

Kim, A. (1977). Estimating methane content of bituminous coalbeds from adsorption data. Tech. Rep. of Investigations 8245, United States Department of the Interior, Bureau of Mines.

Kissell, F., & Bielicki, R. (1972). An in-situ diffusion parameter for Pittsburgh and Pocahontas No. 3 coalbeds. Tech. rep.

Kolak, J., & Burruss, R. (2006). Geochemical investigation of the potential for mobilizing non-methane hydrocarbons during carbon dioxide storage in deep coal beds. *Energy and Fuels*, *20*, 566–574.

Kotas, A. (1994). *CBM Potential of the USCB, Poland*. Polish Geological Institute.

Krooss, B., Busch, A., Gensterblum, Y., Wolf, K., Bruining, H., Mazumder, S., Bossie-Codreanu, D., & Kobiela, Z. (2005). Laboratory results and data integration for the RECOPOL project. Tech. rep.

Krooss, B., Van Bergen, F., Gensterblum, Y., Siemons, N., Pagnier, H., & David, P. (2002). High-pressure methane and carbon dioxide adsorption on dry and moisture-equilibrated pennsylvanian coals. *International Journal of Coal Geology*, *51*, 69–92.

Lama, R., & Bodziony, J. (1996). Outburst of gas coal and rock in underground coal mines. r.d. lama and associates, wollongong: 499 pp. Tech. rep.

Lamberson, M., & Bustin, R. (1993). Coalbed methane characteristics of Gates Formation coals, northeastern British Columbia: Effect of maceral composition. *American Association of Petroleum Geologists Bulletin*, *77*, 2062–2076.

Larsen, J. W. (2004). The effects of dissolved CO_2 on coal structure and properties. *International Journal of Coal Geology*, *57*(1), 63–70.

Laxminarayana, C., & Crosdale, P. (1999). Role of coal type and rank on methane sorption characteristics of bowen basin, australia coals. *International Journal of Coal Geology*, *40*, 309–325.

Levine, J. (1993). Coalification: the evolution of coal as source rock and reservoir rock for oil and gas. In B. Law, & D. Rice (Eds.) *Hydrocarbons from coal: American Association of Petroleum Geologists Bulletin Studies in Geology 38*, (pp. 39–77).

Levine, J. (1996). Model study of the influence of matrix shrinkage on absolute permeability of coal bed reservoirs. In R. Gayer, & I. Harris (Eds.) *Coalbed Methane and Coal Geology. Geological Society Special Publication 109*, (pp. 197–212).

Levine, J., Johnson, P., & Beamish, B. (1993). High pressure microgravimetry provides a viable alternative to volumetric method in gas sorption studies on coal. In *Proceedings 1993 International Coalbed Methane Symposium University of Alabama, Tuscaloosa (USA)*, (pp. 187–195).

Levy, J., Day, S., & Killingley, J. (1997). Methane capacity of Bowen Basin coals related to coal properties. *Fuel*, *74*, 1–7.

Luque De Castro, M., Valcárcel, M., & Tena, M. (1994). *Analytical supercritical -fluid extraction*. Heidelberg: Springer.

Majewska, Z., Ceglarska-Stefanska, G., Majewski, S., & Zietek, J. (2009). Binary gas sorption/desorption experiments on a bituminous coal: Simultaneous measurements on sorption kinetics, volumetric strain and acoustic emission. *International Journal of Coal Geology*, *77*(1-2), 90–102.

Marecka, A., & Mianowski, A. (1998). Kinetics of CO_2 and CH_4 sorption on high rank coal at ambient temperatures. *Fuel*, *77*(14), 1691–1696.

Mares, T. E., Radlinski, A. P., Moore, T. A., Cookson, D., Thiyagarajan, P., Ilavsky, J., & Klepp, J. (2009). Assessing the potential for CO_2 adsorption in a subbituminous coal, Huntly Coalfield, New Zealand, using small angle scattering techniques. *International Journal of Coal Geology*, *77*(1-2), 54–68.

Mathews, J., Karacan, O., Halleck, P., Mitchell, G., & Grader, A. (2001). Storage of pressurized carbon dioxide in coal observed using X-ray tomography. In *First National Conference on Carbon Sequestration*. Washington, DC.

Mavor, M., & Gunter, W. (2006). Secondary porosity and permeability of coal vs. gas composition and pressure. *Society of Petroleum Engineers Reservoir Evaluation and Engineering*, *Paper 90255 Volume 9*(2, April), 114–125.

Mavor, M., Owen, L., & Pratt, T. (1990). Measurement and evaluation of coal sorption isotherm data. In S. o. P. Engineers (Ed.) *SPE 65th Annual Technical Conference and Exhibition*, vol. SPE 20728, (p. 157170). New Orleans (LA), USA.

Mazumder, S. (2007). *Dynamics of CO_2 in coal as a reservoir*. Ph.D. thesis, Delft University of Technology.

Mazumder, S., Bruining, J., & Wolf, K. (2006a). Swelling and anomalous diffusion mechanisms of CO_2 in coal. In *2006 International Coalbed Methane Symposium*, (p. 17). University of Alabama, Tuscaloosa (USA), CD-ROM, Paper 0601.

Mazumder, S., Karnik, A., & Wolf, K. (2006b). Swelling of coal in response to CO_2 sequestration for ECBM and its effect on fracture permeability. *Society of Petroleum Engineers Journal Paper 97754-PA*, *Volume 11*(3, September), 390–398.

Mazumder, S., Plug, W., & Bruining, H. (2003). Capillary pressure and wettability behavior of coal-water-carbon dioxide system. In *SPE Annual Technical Conference*, (pp. 1–10). Denver, Colorado, U.S.A.

Mazumder, S., van Hemert, P., Bruining, J., Wolf, K. H. A. A., & Drabe, K. (2006c). In situ CO_2-coal reactions in view of carbon dioxide storage in deep unminable coal seams. *Fuel*, *85*(12-13), 1904–1912.

Mazumder, S., & Wolf, K. H. (2008). Differential swelling and permeability change of coal in response to CO_2 injection for ECBM. *International Journal of Coal Geology*, *74*(2), 123–138.

McCants, C., Spafford, S., & Stevens, S. (2001). Five-spot production pilot on tight spacing: Rapid evaluation of a coalbed methane block in the Upper Silesian Coal Basin, Poland. In *Proceedings of the International Coalbed Methane Symposium 2001*, (pp. 193–204). University of Alabama, Tuscaloosa (USA).

McElhiney, P. G. Y. G., J.E., & McCartney, J. (1993). Reservoir engineering aspects of coalbed methane. In B. Law, & D. Rice (Eds.) *Hydrocarbons from coal. American Asssociation of Petroleum Geologists Bulletin Studies in Geology 38*, (pp. 361–372).

McKee, C., Bump, A., & Koenig, R. (1988). Stress-dependent permeability and porosity of coal and other geologic formations. Society of Petroleum Engineers Formation Evaluation. (pp. 81–91).

Melnichenko, Y. B., Radlinski, A. P., Mastalerz, M., Cheng, G., & Rupp, J. (2009). Characterization of the CO_2 fluid adsorption in coal as a function of pressure using neutron scattering techniques (SANS and USANS). *International Journal of Coal Geology*, *77*(1-2), 69–79.

Moffat, D., & Weale, K. (1955). Sorption by coal of methane at high pressure. *Fuel*, *34*, 449–462.

Nandi, S., & Walker, P. (1964). The diffusion of nitrogen and carbon dioxide from coals of various ranks. *Fuel*, *43*, 385–393.

Nandi, S., & Walker, P. (1970). Activated diffusion in coal. *Fuel*, *49*, 309–323.

Nandi, S., & Walker, P. J. (1966). Diffusion of argon from coals of different rank. In R. Gould (Ed.) *Coal Science*, (pp. 379–385). American Chemical Society.

Nandi, S. P., & Walker Jr, P. L. (1975). Activated diffusion of methane from coals at elevated pressures. *Fuel*, *54*(2), 81–86.

Nelson, E., & Walker, P. (1961). Some techniqus for investigating the unsteady state molecular flow of gas through a microporous medium. *J. Appl. Chem.*, *11*, 358–364.

Nishino, J. (2001). Adsorption of water vapor and carbon dioxide at carboxylic functional groups on the surface of coal. *Fuel*, *80*(5), 757–764.

NITG (1999). *Geological Atlas of the Subsurface of the Netherlands (1 : 250 000). Explanation to Map Sheet XV: Sittard-Maastricht*. Netherlands Institute of Applied Geoscience - TNO.

Olague, N. E., & Smith, D. (1989). Diffusion of gases in American coals. *Fuel*, *68*, 1378–1381.

Otake, Y., & Suuberg, E. M. (1997). Temperature dependence of solvent swelling and diffusion processes in coals. *Energy and Fuels*, *11*, 1155–1164.

Ottiger, S., Pini, R., Storti, G., Mazzotti, M., Bencini, R., Quatrocchi, F., Sardu, G., & Deriu, G. (2006). Adsorption of pure carbon dioxide and methane on dry coal from the Sulcis Coal Province (SW Sardinia, Italy). *Environmental Progress*, *25*(4), 355–364.

Pagnier, H., Pestman, P., & Van Tongeren, P. (1987). Recent coal exploration in the Netherlands. In J. Martin, & S. Barone (Eds.) *Proceedings 13th Annual Underground Coal Gasification Symposium*, vol. METC 88-6095, (pp. 151–162). Laramie, WY: US Department of Energy.

Pagnier, H., van Bergen, F., Krzystolik, P., Skiba, J., Jura, B., Hadro, J., Wentink, P., De-Smedt, G., Kretzschmar, H.-J., Fröbel, J., Müller-Syring, G., Krooss, B., Busch, A., Wolf, K.-H., Mazumder, S., Bossie-Codreanu, D., Choi, X., Grabowski, D., Hurtevent, D., Gale, J., Winthaegen, P., Van der Meer, B., Kobiela, Z., Bruining, H., Reeves, S., & Stevens, S. (2005a). Field experiment of ECBM-CO_2 in the upper silesian basin of poland (recopol). In M. Wilson, T. Morris, J. Gale, & K. Thambimuthu (Eds.) *Proceedings of the Seventh International Conference on Greenhouse Gas Control Technologies*, (pp. 1391–1397). Vancouver (Canada): Elsevier, Vol. II-Part 1.

Pagnier, H. J. M., Van Bergen, F., Kreft, E., Van der Meer, L. G. H., & Simmelink, H. J. (2005b). Field experiment of ecbm-CO_2 in the upper silesian basin of poland (recopol). In *Society of Petroleum Engineers paper SPE 94079, 14th Europec Biennial Conference, CD-ROM, paper P258*, (p. 3).

Palmer, I., & Mansoori, J. (1996). How permeability depends on stress and pore pressure in coalbeds: a new model. *Society of Petroleum engineers Paper SPE 36737, Proc. of the 71st Annual Techn. Conf., Denver (Co)*, (pp. 557–564).

Palmer, I., & Mansoori, J. (1998). How permeability depends on stress and pore pressure in coalbeds: A new model. *Society of Petroleum Engineers Reservoir Evaluation and Egineering*, *Paper SPE 52607*(December 1998), 539–544.

Pan, Z., & Connell, L. (2007). A theoretical model for gas adsorption-induced coal swelling. *International Journal of Coal Geology*, *69*, 243–252.

Pashin, J. (1998). Stratigraphy and structure of coalbed methane reservoirs in the United States: an overview. *International Journal of Coal Geology*, *35*, 207–238.

Pashin, J., Carroll, R., Groshong, J., R.H., Raymond, D., McIntyre, M., & Payton, J. (2004). Geologic screening criteria for sequestration of CO_2 in coal: quantifying potential of the Black Warrior coalbed methane fairway, Alabama: Final technical report, U.S. Department of Energy, National Technology Laboratory, contract DE-FC26-00NT40927. Tech. rep.

Pashin, J., & Hinkle, F. (1997). Coalbed methane in Alabama: Alabama Geological Survey Circular 192: 71 pp. Tech. rep.

Pashin, J., & McIntyre, M. (2003). Temperature - pressure conditions in coalbed methane reservoirs of the Black Warrior basin: implications for carbon sequestration and enhanced coalbed methane recovery. *International Journal of Coal Geology*, *54*, 167183.

Patching, T., & Mikhal, M. (1986). Studies of gas sorption and emission on Canadian coals. *CIM Bulletin*, *79*, 104–109.

Pekot, L., & Reeves, S. (2002). Modelling coal matrix shrinkage and differential swelling with CO_2 injection for enhanced coalbed methane recovery and CO_2 sequestration applications. Tech. rep.

Pitman, J., Pashin, J., Hatch, J., & Goldhaber, M. (2003). Origin of minerals in joint and cleat systems of the Pottsville Formation, Black Warrior basin, Alabama: implications for coalbed methane generation and production. *American Association of Petroleum Geologists Bulletin*, *87*, 713–731.

Plug, W. J., Mazumder, S., Bruining, H., Siemons, N., & Wolf, K. H. A. A. (2006). Capillary pressure and wettability behavior of the coal water carbon dioxide system at high pressures. In *2006 International Coalbed Methane Symposium*, (p. 15). University of Alabama, Tuscaloosa (USA), CD-ROM, Paper 0601.

Pone, J. D. N., Halleck, P. M., & Mathews, J. P. (2009a). Methane and carbon dioxide sorption and transport rates in coal at in-situ conditions. *Energy Procedia*, *1*(1), 3121–3128.

Pone, J. D. N., Hile, M., Halleck, P. M., & Mathews, J. P. (2009b). Three-dimensional carbon dioxide-induced strain distribution within a confined bituminous coal. *International Journal of Coal Geology*, *77*(1-2), 103–108.

Prinz, D., & Littke, R. (2005). Development of the micro- and ultramicroporous structure of coals with rank as deduced from the accessibility to water. *Fuel*, *84*(12-13), 1645–1652.

Prinz, D., Pyckhout-Hintzen, W., & Littke, R. (2004). Development of the meso- and macroporous structure of coals with rank as analysed with small angle neutron scattering and adsorption experiments. *Fuel*, *83*, 547–556.

Puri, R., & Yee, D. (1990). Enhanced coalbed methane recovery. In *65th Annual Technical Conference of the Society of Petroleum Engineers*, vol. paper 20732, (pp. 193–202). New Orleans: Society of Petroleum Engineers.

Radlinski, A. P., Busbridge, T. L., Gray, E. M. A., Blach, T. P., & Cookson, D. J. (2009). Small angle X-ray scattering mapping and kinetics study of sub-critical CO_2 sorption by two Australian coals. *International Journal of Coal Geology*, *77*(1-2), 80–89.

Rees, O., Reed, F., & Land, G. (1939). A study of the equilibration method of determining moisture in coal for classification by rank. Tech. rep.

Reeves, S. (2003). Coal-seq project update: Field studies of ECBM recovery / CO_2 sequestration in coal seams. In J. Gale, & Y. Kaya (Eds.) *Proceedings of the Sixth International Conference on Greenhouse Gas Control Technologies, Vol. II*, (pp. 557–562). Kyoto (Japan): Pergamon Press.

Reeves, S., & Schoeling, L. (2001). Geological sequestration of CO_2 in coal seams: reservoir mechanisms field performance, and economics. In D. Williams, B. Durie, P. McMullan, C. Paulson, & A. Smith (Eds.) *Proceedings of the Fifth International Conference on Greenhouse Control Technologies*, (pp. 593–598).

Reeves, S., Taillefert, A., Pekot, L., & Clarkson, C. (2003). The Allison Unit CO_2 - ECBM pilot: A reservoir modeling study. Tech. rep., Department of Energy Topical Report. 56 p. excl. appendix.

Robertson, E., & Christiansen, R. (2005a). Measurement of sorption-induced strain. In *2005 International Coalbed Methane Symposium*, (pp. 1–15).

Robertson, E., & Christiansen, R. (2005b). Modeling permeability in coal using sorption-induced strain data. In *2005 SPE Annual Conference and Technical Exhibition*, (pp. 1–10).

Rodrigues, C., & Lemos de Sousa, M. (2002). The measurement of coal porosity with different gases. *International Journal of Coal Geology*, *48*, 245–251.

Ryan, B. (1992). An equation for estimation of maximum coalbed methane resource potential. In *British Columbia Ministry of Energy, Mines, and Petroleum Resources, Geological Fieldwork 1991, Paper 1992-1*, (pp. 393–396).

Saghafi, A., Faiz, M., & Roberts, D. (2007). CO_2 storage and gas diffusivity properties of coals from Sydney Basin, Australia. *International Journal of Coal Geology*, *70*(1-3), 240–254.

Saulsberry, J., Schafer, P., & Schraufnagel, R. (1996). A guide to coalbed methane reservoir engineering. In *Gas Research Institute Report*.

Schoeling, L., & McGovern, M. (2000). Pilot test demonstrates how CO_2 injection enhances coalbed methane recovery. *Petroleum Technology Digest*, *September 2000*, 14.

Scott, A. (2002). Hydrogeologic factors affecting gas content distribution in coal beds. *International Journal of Coal Geology*, *50*, 363–387.

Scott, A., Kaiser, W., & Ayers, J., W.B. (1994). Thermogenic and secondary biogenic gases, San Juan basin, Colorado and New Mexico Implications for coalbed gas producibility. *American Association of Petroleum Geologists Bulletin*, *78*, 1186–1209.

Seewald, H., & Klein, J. (1986). Methansorption an steinkohle und kennzeichnung der porenstruktur. *Glckauf-Forschungshefte*, *47*(3), 149–156.

Selvig, W., & Ode, W. (1953). Determination of moisture-holding capacity (bed moisture) of coal for classification by rank. Tech. rep.

Seo, M., Kim, Y., Kang, J., & Lee, C. (2009). Solubility of water in carbon dioxide containing gas hydrate, abstract. In NIST (Ed.) *Seventeenth symposium on thermophysical properties*. Boulder, Co, USA.

Shi, J., & Durucan, S. (2005). Gas storage and flow in coalbed reservoirs: Implementation of a bidisperse pore model for gas diffusion in a coal matrix. *Society of Petroleum Engineers Paper 84342-PA, SPE Reservoir Evaluation and Engineering*, *Volume 8*(2, April), 169–175.

Shi, J.-Q., Durucan, S., & Fujioka, M. (2008). A reservoir simulation study of CO_2 injection and N_2 flooding at the Ishikari coalfield CO_2 storage pilot project, Japan. *International Journal of Greenhouse Gas Control*, *2*(1), 47–57.

Siemons, N. (2007). *Carbon Dioxide Transport and Retention in Coal*. Ph.D. thesis, Technische Universiteit Delft.

Siemons, N., Bruining, H., Castelijns, H., & Wolf, K.-H. (2006). Pressure dependence of the contact angle in a CO_2-H2O-coal system. *Journal of Colloid and Interface Science*, *297*(2), 755–761.

Siemons, N., & Busch, A. (2007). Measurement and interpretation of supercritical CO_2 sorption on various coals. *International Journal of Coal Geology*, *69*(4), 229–242.

Siemons, N., Wolf, K.-H. A. A., & Bruining, J. (2007). Interpretation of carbon dioxide diffusion behavior in coals. *International Journal of Coal Geology*, *72*(3-4), 315–324.

Siriwardane, H., Haljasmaa, I., McLendon, R., Irdi, G., Soong, Y., & Bromhal, G. (2009). Influence of carbon dioxide on coal permeability determined by pressure transient methods. *International Journal of Coal Geology*, *77*(1-2), 109–118.

Siriwardane, H., Smith, D., & Gorucu, F. (2006). Shrinkage and swelling of coal during coal bed methane production or geologic sequestration of carbon dioxide. In *International Coalbed Methane Symposium*. University of Alabama, Tuscaloosa, AL.

Smith, D., & Williams, F. (1982). Diffusion models for gas production from coals. *Fuel*, *61*, 261–265.

Smith, D., & Williams, F. (1984). Diffusional effects in the recovery of methane from coalbeds. *Society of Petroleum Engineers Journal SPE 10821*, *October*, 529–535.

Span, R., & Wagner, W. (1996). A new equation of state for carbon dioxide covering the fluid region from the triple-point temperature to 1100 K at pressures up to 800 MPa. *J. Phys. Chem. Ref. Data*, *25*, 1509–1596.

St. George, J., & Barakat, M. (2001). The change in effective stress associated with shrinkage from gas desorption in coal. *International Journal of Coal Geology*, *45*, 105–113.

Stach, E., Mackowsky, M.-T., Teichmüller, M., Taylor, G., Chandra, D., & Teichmüller, R. (1982). *Stach's Textbook of Coal Petrology, 3rd edn*. Berlin: Borntraeger.

Stansfield, E., & Gilbart, K. (1932). Moisture determination for coal classification. *AIME transactions*, *101*, 125–143.

Stevens, S. H., Kuuskraa, V., Spector, D., & Riemer, P. (1999). CO_2 sequestration in deep coal seams: Pilot results and worldwide potential. In B. Eliasson, N. Reimer, & P. Wokaun (Eds.) *Proceedings of the Fourth International Conference on Greenhouse Gas Control Technologies*, (pp. 175–180).

Stevenson, M., Pinczewski, W., Somers, M., & Bagio, S. (1991). Adsorption / desorption of multicomponent gas mixtures at in-seam conditions. In *Society of Petroleum Engineers Asia-Pacific Conference, Perth, Australia*, vol. Paper 23026, (pp. 741–756).

Stuffken, J. (1957). *De mijngasafgifte van kolenlagen (in Dutch)*. Ph.D. thesis, Technische Hogeschool Delft.

Sun, Y., Shekunov, B., & York, P. (2003). Refractive index of supercritical CO_2-ethanol solvents. *Chem. Eng. Comm.*, *190*, 1–14.

Suuberg, E. M., Otake, Y., Yun, Y., & Deevi, S. C. (1993). Role of moisture in coal structure and the effects of drying upon the accessibility of coal structure. *Energy and Fuels*, *7*(3), 384–392.

Taylor, G., Teichmüller, M., Davis, A., Diessel, C., Littke, R., & Robert, P. (1998). *Organic Petrology*. Berlin: Gebrüder Borntraeger.

Unsworth, J. F., Fowler, C. S., & Jones, L. F. (1989). Moisture in coal: 2. Maceral effects on pore structure. *Fuel*, *68*(1), 18–26.

Van Bergen, F., Gale, J., Damen, K. J., & Wildenborg, A. F. B. (2004). Worldwide selection of early opportunities for CO_2-enhanced oil recovery and CO_2-enhanced coal bed methane production. *Energy*, *29*(9-10), 1611–1621.

Van Bergen, F., Hol, S., Spiers, C., & Peach, C. (2005). Chemical interaction between CO_2 and coal under high pressure. In *International Coal-Sequestration Workshop*.

Van Bergen, F., Pagnier, H., Damen, K., Faaij, A., & Ribberink, J. (2003a). Feasibility study on CO_2 sequestration and Enhanced CBM production in Zuid-Limburg. Tech. rep.

Van Bergen, F., Pagnier, H., David, P., & Krooss, B. (2000). Inventory of potential volumes of methane extraction and carbon dioxide storage in coallayers in the Dutch subsurface. TNO contribution to the "Feasibility study of combined coalbed methane production and carbon dioxide storage in the Netherlands. Tech. rep.

Van Bergen, F., Pagnier, H., & Krzystolik, P. (2006). Field experiment of enhanced coalbed methane-CO_2 in the upper Silesian basin of Poland. *Environmental Geosciences*, *13*(3), 201–224.

Van Bergen, F., Pagnier, H., Van der Meer, L., Van den Belt, F., Winthaegen, P., & Krzystolik, P. (2003b). Development of a field experiment of ecbm in the upper silesian coal basin of poland (recopol). In *Proceedings of the International Coalbed Methane Symposium 2003*, (p. 8). University of Alabama, Tuscaloosa (USA), CD-ROM, Paper 0320.

Van Bergen, F., Pagnier, H., & Van Tongeren, P. (2007). Peat, coal and coalbed methane. In T. Wong, D. Batjes, & J. De Jager (Eds.) *Geology of the Netherlands*, (pp. 265–282). Amsterdam: Royal Netherlands Academy of Arts and Sciences.

Van Bergen, F., Pagnier, H. J. M., Van der Meer, L. G. H., Van den Belt, F. J. G., Winthaegen, P. L. A., & Westerhoff, R. S. (2003c). Development of a field experiment of CO_2 storage in coals seams in the Upper Silesian Basin of Poland (RECOPOL). In J. Gale, & Y. Kaya (Eds.) *Proceedings of the Sixth International Conference on Greenhouse Gas Control Technologies, Vol. II*, (pp. 569–574).

Van Bergen, F., Spiers, C., Floor, G., & Bots, P. (2009a). Strain development in unconfined coals exposed to CO_2, CH_4 and Ar: Effect of moisture. *International Journal of Coal Geology*, *77*(1-2), 43–53.

Van Bergen, F., Winthaegen, P., Pagnier, H., Krzystolik, P., Jura, B., Skiba, J., & Van Wageningen, N. (2009b). Assessment of CO_2 storage performance of the enhanced coalbed methane pilot site in kaniow. *Energy Procedia*, *1*(1), 3407–3414.

Van Buggenum, J. M., & Den Hartog Jager, D. (2007). Silesian. In T. Wong, D. Batjes, & J. De Jager (Eds.) *Geology of the Netherlands*, (pp. 241–264).

Van der Meer, B., & Fokker, P. (2003). The injectivity of coalbed CO_2 injection wells. In *Proceedings of the International Coalbed Methane Symposium 2003*, (p. 6). University of Alabama, Tuscaloosa (USA), CD-ROM, Paper 0319.

Van Krevelen, D. (1993). *Coal; Topology, physics, chemistry, constitution; Third edition*. Elsevier.

Van Wageningen, W., & Maas, J. (2007). Reservoir simulation and interpretation of the Recopol ECBM pilot in Poland, paper no. 0702. In *2007 International Coalbed Methane Symposium, Tuscaloosa, AL., May 21-25, 2007*.

Van Wageningen, W., Wentinck, H., & Otto, C. (2009). Report and modeling of the MOVECBM field tests in Poland and Slovenia. *Energy Procedia*, *1*(1), 2071–2078.

Viete, D. R., & Ranjith, P. G. (2006). The effect of CO_2 on the geomechanical and permeability behaviour of brown coal: Implications for coal seam CO_2 sequestration. *International Journal of Coal Geology*, *66*(3), 204–216.

Walker, P. L., Verma, S. K., Rivera-Utrilla, J., & Davis, A. (1988). Densities, porosities and surface areas of coal macerals as measured by their interaction with gases, vapours and liquids. *Fuel*, *67*(12), 1615–1623.

Ward, C. R. (1984). *Coal geology and coal technology*. United States: Blackwell Scientific Publications, Inc.,Palo Alto, CA.

Wenselaers, P., Dusar, M., & Van Tongeren, P. (1996). Steenkoollaag methaangaswinning in het Kempisch kolenbekken Het proefproject te Peer. Ministerie van de Vlaamse gemeenschap, afdeling Natuurlijke Rijkdommen en Energie (Brussel): 67 pp. Tech. rep.

Wolf, K.-H., Hijman, R., Barzandji, O., & Bruining, J. (1999). Laboratory experiments and simulations on the environmentally friendly improvement of coalbed methane production by carbon dioxide injection. In *Proceedings of the 1999 International Coalbed Methane Symposium. Tuscaloosa, AL, May 3-7*, (pp. 279–290).

Wong, S., Gunter, W. D., & Gale, J. (2001). Site ranking for CO_2enhanced coalbed methane demonstration pilots. In D. Williams, B. Durie, P. McMullan, C. Paulson, & A. Smith (Eds.) *Proceedings of the Fifth International Conference on Greenhouse Gas Control Technologies*, (pp. 531–536).

Wong, S., Law, D., Deng, X., Robinson, J., Kadatz, B., Gunter, W., Jianping, Y., Sanli, F., & Zhiqiang, F. (2007). Enhanced coalbed methane and CO_2 storage in anthracitic coals - Micro-pilot test at South Qinshui, Shanxi, China. *International Journal of Greenhouse Gas Control*, *1*, 215–222.

World Energy Council (2004). *2004 Survey of Energy Resources*. Elsevier, 20th ed.

Yalcin, E., & Durucan, S. (1991). Methane capacities of zonguldak coals and the factors affecting methane adsorption. *Mining Science and Technology*, *13*(2), 215–222.

Yamaguchi, S., Ohga, K., Fujioka, M., & Muto, S. (2005). Prospect of CO_2 sequestration in the Ishikari coal field, Japan. In *7th Int. Conf. on Greenhouse Gas Control Technologies, September 5-9, 2004.*. Vancouver, BC, Canada.

Yamaguchi, S., Ohga, K., Fujioka, M., & Nako, M. (2007). History matching on micropilot tests of CO_2 sequestration and ECBM in the Ishikari Coal Field. *Journal of the Japan Institute of Energy*, *86*(2), 80–86.

Yee, D., Seidle, J., & Hanson, W. (1993). Gas sorption on coal and measurement of gas content. In B. Law, & D. Rice (Eds.) *Hydrocarbons from coal: American Association of Petroleum Geologists Bulletin Studies in Geology 38*, vol. AAPG studies in Geology 38.

Yi, J., Akkutlu, I. Y., Karacan, C. O., & Clarkson, C. R. (2009). Gas sorption and transport in coals: A poroelastic medium approach. *International Journal of Coal Geology*, *77*(1-2), 137–144.

Summary

Carbon capture and storage (CCS) is considered a key technology to reduce world-wide emissions of carbon dioxide (CO_2), alongside other measures such as increasing energy efficiency and the use of renewables. One option for carbon capture coupled with underground storage is to inject CO_2 into subsurface coal beds. When combined with simultaneous production of coalbed methane (CBM) naturally present in the coal, this process is referred to as enhanced coalbed methane production (ECBM). The term "enhanced coalbed methane" is used because the injected CO_2 improves the production of CBM compared to standard production without CO_2. However, ECBM is not yet a well-established, mature technology. Although several theoretical studies have illustrated the potential of the process, world-wide only a handful of demonstration sites have been realized to date.

Demonstration projects are essential for testing the applicability of the ECBM technique under field conditions. The first part of this thesis (Chapters 2 and 3) is therefore concerned with reporting the results of the first field test in Europe, the so-called RECOPOL test. The main aim of this test was to investigate the technical and economic feasibility of ECBM under conditions commonly encountered in European coal fields of Carboniferous age. Within the RECOPOL project an existing coalbed methane well was cleaned up, repaired and put back into production (May 2004) to establish a baseline output. A new injection well was then drilled 150 m away from the production well. Initial injection of CO_2 took place in August 2004, in three seams of Carboniferous age in the depth interval between 900 and 1250 m. Several actions were taken to establish continuous injection, which was eventually achieved in April 2005, after stimulation of the reservoir by hydraulic fracturing. In May 2005, approximately 12-15 tonnes per day were injected in continuous operations. Compared to the baseline production level, methane output increased significantly due to the injection activities. About 760 tons CO_2 were injected into the reservoir from August 2004 to June 2005. During this period, breakthrough of the injected CO_2 was established, resulting in the production of about 10% of the injected CO_2. The storage performance of the reservoir was assessed in the follow-up period after the injection. This involved evaluating whether the injected CO_2 was adsorbed onto the coal or whether it was still present as a free phase in the pore space, by back-producing the injected CO_2 together with CBM from the reservoir.

The injection well was used for this purpose, as the production well had to be abandoned for permitting reasons. Based on the experience gained from the production well, these back production operations showed that whereas the gas production rates were as expected, water production was remarkably low. This may be related to permeability issues or, alternatively, to a drying effect of the CO_2 within the reservoir. In addition, the recovered gas composition showed a predominance of CO_2 over CH_4 during the gas release stage, which changed gradually into a predominance of CH_4 over CO_2 during the production phase, approaching a composition of 60% methane and 40% CO_2 during the last phase of production. This indicates that the exchange of CH_4 and CO_2 is more complex than often envisaged based on adsorption studies. Based on these studies, it can be expected that CO_2 molecules are exchanged for CH_4 molecules in the coal, due to a higher sorption affinity of the CO_2 and due to an increased partial CO_2 pressure in the gas/fluid phase in the reservoir. This would lead to an steady increase with time of the concentration of CH_4 and a decrease of CO_2 in the produced gas instead of the observed stabilization of the concentrations. After removal of the pump, the pressure in the reservoir returned to its original value. As the total mass of CO_2 produced was only a fraction of the amount that was injected (68 tonnes of the 760 tonnes injected), it was concluded that 692 tonnes of CO_2 was taken up by the coal and remains currently adsorbed.

Two important observations were made during the field operations. First, it was found that the injection well experienced a reduction of injectivity into the coal seam with time, sometimes leading to operational difficulties. This reduction is considered to be caused by permeability reduction due to swelling of the coal that was exposed to CO_2 within the reservoir. The second observation was the low production rate of CBM in the production well, which is interpreted as an indication of slow diffusion in the coal matrix. Production of gas from the injection well, after modification into a production well, also pointed towards low diffusion coefficients of the coal matrix. Based on these results from the field test, it is concluded that understanding the transport of the gas/fluid through the coal, including the effects of diffusion and the development of swelling with time, is key to determining the success of future ECBM sites.

The second part of the thesis (Chapters 4-6) is therefore dedicated to laboratory investigations of the swelling behaviour of the coal matrix, and its dependency on coal rank, moisture content, and stress state or confinement. Two types of experiments were performed. The first type of experiment (Chapter 4 and 5) involved measurements of strain development with time at 8 MPa and 40°C performed on unconfined (subbituminous, bituminous and anthracite) block-shaped coal matrix fragments of about 1.0-1.5 mm^3, exposed to carbon dioxide, methane and argon, using a high-pressure-temperature, see-through, optical cell located under a microscope. Both air dried and moisturized samples were used.

The experimental results confirmed different swelling behavior in coals exposed to different substances: carbon dioxide leads to higher strain than methane, while ex-

posure to argon leads to very little swelling. Another result followed from the development and application of a spherical diffusion model (Chapter 5), under the assumption that the kinetics of swelling are governed by transport properties of the coal matrix, characterized by a single valued (uniform) diffusion coefficient (unipore model). The model showed good correspondence with the so-called unipore model solution often applied to the start of the diffusion process, and provides a satisfactory fit to the experimental data up to the point where equilibrium is reached. Effective diffusion coefficient values obtained by fitting our model to the data are within the range of previously published literature values, indicating that the swelling experiments can be used to determine the diffusive transport properties of the coal matrix. Rank effects on diffusion were expected but could not be discerned.

The present experiments on moisturized samples (Chapters 4 and 5) seem to confirm the role of moisture as a competitor for adsorption sites. Adsorption of water could also explain the observed swelling due to water uptake at atmospheric pressure. A re-introduction of carbon dioxide, after intermediate gas release, results in higher strains which indicate a drying effect of the carbon dioxide on the coal. Furthermore, it was found that moisture that is present in the coal matrix decreases the diffusion rate, probably by blocking access to part of the pore network. This effect seems to be larger for bituminous coal than for anthracite, although it cannot be explained at present. The results of this study show that the role of water can not be ignored if one wants to understand the fundamental processes that are taking place in enhanced coalbed methane operations.

The second type of experiment reported here involved measuring stress-strain development in confined, pre-pressed samples of granular bituminous coal, at gas or fluid pressures up to 10 MPa and temperatures of around 40°C. These experiments were performed using a 1-D compaction vessel plus axial loading frame, and revealed a previously unrecognized swelling effect, up to 3 times larger than seen in coal samples that are not pre-compacted, and largely irreversible. We propose that pre-pressing led to permanent compaction of the internal pore structure of the coal matrix grains, decreasing the mean pore aperture and increasing the proportion of micropores. Introduction of CO_2 and CH_4 therefore resulted in increased micropore adsorption which, through the associated surface forces developed within the micropores, led to a disjoining pressure effect that caused recovery of the pre-pressing-induced permanent strain. The higher affinity of micropores for CO_2 than for CH_4 adsorption, explains the markedly bigger effect of CO_2 over CH_4. After the recovery of the permanent strain was achieved, the samples seem to have exhibited a normal, reversible response to adsorption. We thus attribute the irreversible swelling phenomenon to a stress-history effect of pre-pressing. This effect may be relevant for coals that have undergone deep burial after formation, or for naturally stressed coal in tectonic zones.

The thesis is concluded with a synthesis (Chapter 7) which draws together the results of both the field and laboratory tests, and with recommendations. It is inferred that

ECBM offers possibilities for storing CO_2 underground, but this will require that several conditions are met. These include the lack of alternative storage options, such as depleted gas fields, and the existence of a CBM industry with a relatively large number of wells in the area. Still, if these criteria are met, implementation of ECBM remains challenging because of the complex behaviour of the coal reservoir upon exposure to CO_2, such as swelling of the coal. It is therefore recommended that future research should focus on investigating this behaviour, through both field and laboratory experiments. This future research will provide better screening criteria for site selection for ECBM operations and measures to cope with the low matrix diffusion and decreasing permeability due to matrix swelling. Solutions may be provided by optimized injection strategies and pre-drying of the coal by the CO_2.

Samenvatting (Summary in Dutch)

Afvang en opslag van koolstofdioxide wordt, samen met andere maatregelen zoals het verbeteren van de efficiëntie van het energieverbruik en het gebruik van alternatieve energiebronnen, beschouwd als een essentiële technologie om de wereldwijde uitstoot van koolstofdioxide (CO_2) te reduceren. Eén van de mogelijkheden voor ondergrondse opslag van CO_2, na afvang, is de injectie van CO_2 in ondergrondse steenkoollagen. Indien dit gecombineerd wordt met gelijktijdige productie van koolbedmethaan (CBM, afkorting van het Engelse "coal bed methane") dat natuurlijk aanwezig is in de steenkool, wordt dit proces "gestimuleerde productie van koolbedmethaan", ofwel ECBM (afkorting van het Engelse "enhanced coal bed methane"), genoemd. De term "gestimuleerde productie van koolbedmethaan" wordt gebruikt aangezien het geïnjecteerde CO_2 de productie van CBM verbeterd ten opzichte van de standaard manier van produceren zonder CO_2. ECBM is echter nog geen uitontwikkelde technologie. Hoewel er verschillende theoretische studies zijn uitgevoerd die het potentieel van het proces hebben geïllustreerd, is er tot nog toe wereldwijd slechts een beperkt aantal demonstratie projecten gerealiseerd.

Demonstratie projecten zijn essentieel om de toepasbaarheid van de ECBM techniek te testen onder de omstandigheden in het veld. In het eerste gedeelte van dit proefschrift (Hoofdstukken 2 and 3) worden daarom de resultaten beschreven van de eerste veldtest in Europa, de zogenoemde RECOPOL test. Het voornaamste doel van deze test was het onderzoeken van de technische en economische haalbaarheid van ECBM onder de omstandigheden die in het algemeen worden aangetroffen in Europese kolenvelden uit het Carboon. In het kader van het RECOPOL project is een bestaande koolbedmethaan put opgeknapt, gerepareerd en terug in productie gebracht (mei 2004) om de baseline productie te bepalen. Een nieuwe injectieput is vervolgens geboord op 150 m afstand van de productieput. De eerste injectie van CO_2 vond plaats in augustus 2004, in drie steenkoollagen van Carboon ouderdom op een diepte tussen de 900 and 1250 m. Verschillende acties zijn ondernomen om een continue injectie te bereiken. Dit is uiteindelijk gelukt in april 2005, na een stimulatie middels een hydraulisch gecreëerde breuk in het reservoir. In mei 20005 werd er onder continue injectie ongeveer 12-15 ton per dag geïnjecteerd.

Als gevolg van de injectie nam de productie van methaan significant toe vergeleken met de baseline productie. In de periode van augustus 2004 tot juni 2005 is er ongeveer 760 ton CO_2 geïnjecteerd in het reservoir. In deze periode is de doorbraak van de CO_2 gerealiseerd, wat resulteerde in de productie van ongeveer 10% van het geïnjecteerde CO_2. Het functioneren van het reservoir is geëvalueerd in de periode na de injectie. Deze evaluatie hield in dat er gekeken is naar aanwijzingen dat het geïnjecteerde CO_2 geadsorbeerd was aan de steenkool of dat het nog als een vrije fase in de porieruimte aanwezig was. Deze aanwijzingen werden gevonden door middel van het terugproduceren uit het reservoir van het geïnjecteerde CO_2 samen met CBM. De injectieput werd voor dit doel gebruikt, aangezien de productieput moest worden verlaten in verband met aflopende vergunningen. Op basis van de ervaring met de productieput bleek uit de terugproductie dat, terwijl de gasproductie snelheden volgens verwachting waren, de water productie aanmerkelijk lager was dan verwacht. Mogelijk was dit gerelateerd aan de permeabiliteit of aan een drogingseffect van het CO_2 in het reservoir. Daarnaast had het geproduceerde gas in het begin een hogere concentratie aan CO_2 ten opzichte van methaan (CH_4). Dit veranderde in de loop van de tijd geleidelijk naar een hogere CH_4 concentratie. De compositie van het gas bestond aan het eind van de productie uit 60% CH_4 and 40% CO_2. Dit was een indicatie dat de uitwisseling van CH_4 voor CO_2 complexer is dan vaak wordt aangenomen op basis van adsorptiestudies. Op basis van deze studies kan men verwachten dat CO_2 moleculen uitgewisseld worden voor CH_4 moleculen in de kool, wegens een hogere sorptie affiniteit van het CO_2 en wegens een toegenomen partiële CO_2 druk in de gas/vloeistof fase in het reservoir. Dit zou moeten leiden tot een geleidelijke toename in de tijd van de concentratie van CH_4 en een afname van CO_2 in het geproduceerde gas in plaats van de geobserveerde stabilisatie van de concentraties. Na verwijdering van de pomp keerde de druk in het reservoir terug naar de oorspronkelijke waarde. Aangezien de totale massa van het CO_2 dat is geproduceerd slechts een fractie was van de hoeveelheid CO_2 dat was geïnjecteerd (68 ton van de geïnjecteerde 760 ton), is er geconcludeerd dat 692 ton CO_2 is opgenomen door de steenkool en geadsorbeerd is.

Twee belangrijke observaties kwamen voort uit de veldactiviteiten. Ten eerste was er de afname van de injectiviteit in de steenkoollaag in de tijd in de injectieput. Dit leidde soms tot operationele problemen. Deze afname werd geacht te worden veroorzaakt door een afname van de permeabiliteit door zwelling van de kool in het reservoir. De tweede observatie was de lage productie snelheid van CBM in de productieput. Dit is geïnterpreteerd als een aanwijzing voor trage diffusie in de steenkool matrix. De gasproductie van de injectieput, nadat deze was veranderd in een productieput, wees ook op lage diffusie-coëfficiënten voor de kool matrix. Op basis van de resultaten van de veldtest is daarom geconcludeerd dat het begrip van het transport van de gas/vloeistof door de steenkool, inclusief het effect van diffusie en van de koolzwelling in de tijd, cruciaal is voor het succes van toekomstige ECBM projecten.

Het tweede gedeelte van dit proefschrift (Hoofdstukken 4-6) is daarom gewijd aan

laboratorium studies naar het zwelgedrag van de steenkool matrix en de afhankelijkheid van de inkoling, vochtgehalte en de spanning op en de insluiting van het monster. Twee soorten experimenten werden uitgevoerd. Het eerste type (Hoofdstuk 4 and 5) betrof metingen aan de ontwikkeling van zwelling in de tijd bij een druk van 8 MPa en een temperatuur van 40°C op niet ingesloten, blokvormige steenkool (subbitumineuze steenkool, bitumineuze steenkool en antraciet) matrix fragmenten van ongeveer 1.0-1.5 mm^3. Deze werden blootgesteld aan koolstofdioxide, methaan en argon, waarbij gebruik werd gemaakt van een hoge-druk-hoge-temperatuur, doorkijk optische cel gepositioneerd onder een microscoop. Zowel luchtgedroogde als bevochtigde monsters zijn gebruikt.

De experimentele resultaten bevestigden verschillen in het zwelgedrag voor steenkool blootgesteld aan verschillende substanties: koolstof dioxide leidt tot grotere vormverandering dan methaan, terwijl blootstelling aan argon leidt to zeer beperkte zwelling. Een ander resultaat volgde uit de ontwikkeling en toepassing van een sferisch diffusie model (Hoofdstuk 5), onder de aanname dat de kinetiek van zwelling wordt bepaald door de transport eigenschappen van de kool matrix, gekenmerkt door een enkelwaardige (uniforme) diffusie coëfficiënt (uni-porie model). Het model liet goede overeenkomsten zien met de zogenoemde "unipore model solution"die vaak wordt toegepast voor het begin van het diffusieproces. Het leverde een toereikend resultaat, dat goed kon worden vergeleken met de experimentele data, tot op het punt waar evenwicht werd bereikt. De waarden voor de effectieve diffusie coëfficiënt verkregen door aanpassing van het model aan de data, vielen binnen de range van eerder gepubliceerde literatuur waarden. Dit gaf aan dat de zwelling experimenten gebruikt kunnen worden om de diffusieve transport eigenschappen van de kool matrix te bepalen. Een effect van inkoling op de diffusie werd verwacht, maar kon niet worden afgeleid.

De experimenten op bevochtigde monsters (Hoofdstukken 4 and 5) leken de rol van vocht als mededinger voor adsorptie plekken te bevestigen. Adsorptie van water zou ook de zwelling van de kool door de opname van water bij atmosferische druk kunnen verklaren. Her-introductie van koolstof dioxide, na het tussentijds aflaten van gas, resulteerde in grotere vormverandering. Dit was een aanwijzing voor een drogingseffect van het koolstof dioxide op de steenkool. Daarnaast werd gevonden dat vocht aanwezig in de kool matrix tot een afname van de diffusie snelheden leidt, waarschijnlijk door het blokkeren van de toegang tot een deel van het porie netwerk. Dit effect leek groter te zijn voor bitumineuze steenkool dan voor antraciet, al kan dit momenteel niet verklaard worden. De resultaten van deze studie toonden aan dat de rol van water niet buiten beschouwing kan worden gelaten als men de fundamentele processen wil begrijpen die plaats vinden tijdens de toepassing van gestimuleerde productie van koolbedmethaan.

Het tweede type experiment dat hier worden gerapporteerd betrof metingen van de ontwikkeling van spanning en vormverandering ("stress-strain") aan ingesloten, geperste monsters van granulaire bitumineuze steenkool, na toevoeging van gas of

vloeistof bij een druk tot 10 MPa en een temperatuur van rond de 40°C. Deze experimenten werden uitgevoerd door gebruik te maken van een 1-D compactie vat plus een axiaal beladings frame. Ze onthulden een tot dusver onbekend zwellingseffect, tot 3 maal groter dan voor kool monsters die niet vooraf werden gecompacteerd. Daarnaast was het zwellingseffect grotendeels onomkeerbaar(ïrreversibel"). De onderzoekerd opperen dat het vooraf persen heeft geleid tot een permanente compactie van de interne porie structuur van de kool matrix korrels, waarbij de gemiddelde porie apertuur afnam en het aandeel van microporiën toenam. De introductie van CO_2 en CH_4 resulteerde derhalve in een toegenomen adsorptie in de microporiën. Dit leidde, door de geassocieerde oppervlakte krachten die in de microporiën werden ontwikkeld, tot een ontkoppelend druk effect dat resulteerde in een herstel van de permanente vormverandering veroorzaakt door het vooraf persen. De grotere affiniteit van de microporiën voor adsorptie van CO_2 dan voor adsorptie van CH_4 verklaart het opmerkelijk grotere effect van CO_2 in vergelijking met CH_4. Na het herstel van de permanente vormverandering laten de monsters een normale, reversibele adsorptie reactie zien.
Daarom wordt het fenomeen van irreversibele zwelling toegeschreven aan het effect van de spanningshistorie. Dit effect kan van belang zijn voor steenkool die een diepe begraving hebben ondergaan na vorming, of voor steenkool die in de natuur onder spanning staan in tektonische zones.

Het proefschrift wordt afgesloten met een synthese (Hoofdstuk 7) die de resultaten van zowel de veldtest als de laboratorium experimenten integreert en aanbevelingen bevat. Het wordt verondersteld dat ECBM mogelijkheden biedt voor ondergrondse opslag van CO_2 maar dat dit specifieke voorwaarden vereist. Deze voorwaarden omvatten de afwezigheid van alternatieve opslagmogelijkheden, zoals gedepleteerde gasvelden, en het bestaan van een CBM-industrie met een relatief groot aantal putten. Desalniettemin, mocht er aan deze voorwaarden worden voldaan dan blijft de toepassing van ECBM een uitdaging wegens het complexe gedrag van het steenkool reservoir onder blootstelling aan CO_2, zoals de koolzwelling.
Het wordt daarom aangeraden dat toekomstige studies zich richten op verder onderzoek naar dit gedrag, door voortzetting van zowel veld- als laboratoriumexperimenten. Dit toekomstig onderzoek zal betere screening criteria opleveren voor de selectie van locaties voor ECBM toepassingen en maatregelen om met langzame matrix diffusie en afnemende permeabiliteit door matrix zwelling om te gaan. Oplossingen worden mogelijk geboden door geoptimaliseerde injectie-strategieën en het vooraf drogen van de kolen door de CO_2.

Curriculum Vitae

Frank van Bergen was born on February 11, 1974 in Woerden (The Netherlands). After finishing secondary school at College De Klop in Utrecht he started his study Geology at Utrecht University in 1992. During his study he switched to Geochemistry and completed the study with two research projects. The first project involved an environmental geochemical study to surface waters in Espirito Santo (Brazil). The second project was executed during an internship at TNO in their former office in Heerlen and involved a study to the petroleum geology and geochemistry of the West Netherlands Basin. Following this internship, Frank has joined TNO in Haarlem in 1998 where he has been involved in projects related to CO_2 storage. Parallel, he has been working on petroleum systems in the Netherlands and internationally from 1998 onwards. Also, Frank has worked on geochemical studies for geothermal energy projects and the evaluation of the geochemical intergrity of the geological CO_2 storage complex.

Several projects enabled Frank to build expertise on the specific topic of CO_2 storage in subsurface coal. From 1998 to 2003 he has worked on an inventory of Coalbed Methane and CO_2 storage potential in coal in the Netherlands. From 1999 to recent he has also worked on several European projects related to CO_2 storage, both in coal as in other geological media. These projects included a European Thermie B project on coal gas, the GESTCO project (Geological Storage Options for CO_2), the CO2GEONET project, and the ADEMA project for the ECCS. Also, Frank completed in 2002 a study called PEACS for the International Energy Agency Greenhouse Gas R & D Programme, which aimed at a world-wide inventory of early opportunities for EOR and ECBM. Frank could do much research work, including laboratory studies, in the scope of the national CATO-project (2004-2008). He had a major involvement in the RECOPOL project, from the acquisition in 2001 to the co-ordination of the project from 2002-2005. RECOPOL was a demonstration project of CO_2 storage in coal in the Silesian Basin in Poland. In the follow-up project MOVECBM (2006-2008) he was involved in the field operations in Poland and acted as work package leader coordinating the activities in China. Currently (2009-2010), he is project leader of Chinese-Dutch cooperation on the evaluation of the feasibility for ECBM applications in China.
Frank has attended the major international congresses worldwide on the subject of CO_2 storage and has presented several papers on these occasions, many as invited

speaker on the subject of ECBM. He has been project leader for several projects that were executed for government and industry.
The work on CO_2 storage in coal in projects executed for TNO enabled Frank to start a parallel PhD study at Utrecht University from the beginning of 2003 onwards. This resulted in the current thesis, completed in 2009.

Publications

- van Balen, R. T.; **Van Bergen, F.**; De Leeuw, C.; Pagnier, H.; Simmelink, H.; Van Wees, J. D.; Verweij, J. M. (2000). *Modelling the hydrocarbon generation and migration in the West Netherlands Basin, the Netherlands.* Geologie en Mijnbouw / Netherlands Journal of Geosciences, 79, (1), 29-44.

- Hamelinck, C. N.; Faaij, A. P. C.; Turkenburg, W. C.; **Van Bergen, F.**; Pagnier, H. J. M.; Barzandji, O. H. M.; Wolf, K.-H. A. A.; Ruijg, G. J. (2002).*CO_2 enhanced coalbed methane production in the Netherlands.* Energy, 27, 647-674.

- Krooss, B. M.; **Van Bergen, F.**; Gensterblum, Y.; Siemons, N.; Pagnier, H. J. M.; David, P. (2002). High-pressure methane and carbon dioxide adsorption on dry and moisture-equilibrated Pennsylvanian coals. International Journal of Coal Geology, 51, 69-92.

- **Van Bergen, F.**; Gale, J.; Damen, K. J.; Wildenborg, A. F. B. (2004). *Worldwide selection of early opportunities for CO_2-enhanced oil recovery and CO_2-enhanced coal bed methane production.* Energy, 29, (9-10), 1611-1621.

- Damen, K.; Faaij, A.; **Van Bergen, F.**; Gale, J.; Lysen, E. (2005). *Identification of early opportunities for CO_2 sequestration - worldwide screening for CO_2-EOR and CO_2-ECBM projects.* Energy, 30, (10), 1931-1952.

- **Van Bergen, F.**; Pagnier, H.; Krzystolik, P. (2006). *Field experiment of enhanced coalbed methane-CO_2 in the upper Silesian basin of Poland.* Environmental Geosciences, 13, (3), 201-224.

- **Van Bergen, F.**; Pagnier, H. J. M.; Van Tongeren, P. C. H. (2007). *Peat, coal and coalbed methane.* In Geology of the Netherlands, Wong, T. E.; Batjes, D. A. J.; De Jager, J., Eds. Royal Netherlands Academy of Arts and Sciences: Amsterdam; pp 265-282.

- C. Hofstee, C., Seeberger, F., Orlic, B., Mulders, F., **Van Bergen, F.**; Bisschop, R. (2008). *The feasibility of effective and safe carbon dioxide storage in the De Lier gas field.* First Break, 26, (1), 53-58.

- Wolf, K.-H. A. A.; **Van Bergen, F.**; Ephraim, R.; Pagnier, H. (2008). *Determination of the cleat angle distribution of the RECOPOL coal seams, using CT-scans and image analysis on drilling cuttings and coal blocks.* International Journal of Coal Geology, 73, (3-4), 259-272.

- **Van Bergen, F.**; Krzystolik, P.; van Wageningen, N.; Pagnier, H.; Jura, B.; Skiba, J.; Winthaegen, P.; Kobiela, Z. (2009). *Production of gas from coal seams in the Upper Silesian Coal Basin in Poland in the post-injection period of an ECBM pilot site.* International Journal of Coal Geology, 77, (1-2), 175-187.

- **Van Bergen, F.**; Winthaegen, P.; Pagnier, H.; Krzystolik, P.; Jura, B.; Skiba, J.; van Wageningen, N. (2009). *Assessment of CO_2 storage performance of the Enhanced Coalbed Methane pilot site in Kaniow.* Energy Procedia, 1, (1), 3407-3414.

- **Van Bergen, F.**; Spiers, C.; Floor, G.; Bots, P. (2009). *Strain development in unconfined coals exposed to CO_2, CH_4 and Ar: Effect of moisture.* International Journal of Coal Geology, 77, (1-2), 43-53.

- Van Wees, J. D.; **Van Bergen, F.**; David, P.; Nepveu, M.; Beekman, F.; Cloetingh, S.; Bont, D. (2009). *Probabilistic tectonic heat flow modeling for basin maturation: Assessment method and applications.* Marine and Petroleum Geology, 26, (4), 536-551.

- Kombrink, H.; Leever, K. A.; Van Wees, J.-D.; **Van Bergen, F.**; David, P.; Wong, T. E. (2008). *Late Carboniferous foreland basin formation and Early Carboniferous stretching in Northwestern Europe: inferences from quantitative subsidence analyses in the Netherlands.* Basin Research, 20, 377-395.

- Tambach, T. J.; Mathews, J. P.; **Van Bergen, F.** (2009). *Molecular Exchange of CH_4 and CO_2 in Coal: Enhanced Coalbed Methane on a Nanoscale* . Energy & Fuels, 23, (10), 4845-4847.

Dankwoord/Acknowledgements

Zoals velen voor mij begin ik dit dankwoord aan het eind van mijn proefschrift met de opmerking dat ik het alleen niet zou hebben kunnen realiseren. Dit is in mijn geval zeker geen loze opmerking, aangezien het voor mij zonder hulp absoluut onmogelijk zou zijn geweest dit naast mijn dagelijkse werkzaamheden af te ronden.
Met name het werk in het laboratorium is zeer intensief en tijdrovend geweest en ik ben daarom heel veel dank verschuldigd aan Sander, Geerke, Pieter en Philip die mij veel werk uit handen hebben genomen. Ik vond het bijzonder om experimenten uit te voeren met zulke verschillende karakters en heb met jullie allemaal met veel plezier samengewerkt. Doordat jullie met een verse blik en ieder vanuit een andere achtergrond naar mijn onderzoek hebben gekeken en bijgedragen, hebben jullie mij scherp gehouden en is de inhoud van het onderzoek werkelijk verbeterd. De experimenten zouden ook onmogelijk zijn geweest zonder de technische ondersteuning, maar zeker ook de creativiteit, van Peter, Gert en Eimert. Ondanks dat jullie mij soms maanden niet in het laboratorium zagen, stonden jullie direct weer voor mij klaar wanneer ik met een verzoek op de stoep stond, waarvoor dank. Colin has always been around with creative solutions when needed and has been crucial for the success of the laboratory experiments. Many thanks for all your input during last years. Alhoewel ik onder andere omstandigheden mijn proefschrift heb afgerond, heb ik altijd met veel plezier promotieperikelen besproken met de andere promovendi in mijn omgeving: Iwan, Allard, Henk, Suzanne, Reinier, Emilia en Sander, bedankt!

I have been able to write the first chapters of this thesis because of my direct involvement in the field tests in Poland. In my role of responsible person for the data collection I have had the opportunity to be the first to process and interpret these data, which resulted in chapters 2 and 3. Although I have written these chapters, it is impossible to consider these interpretations completely independent from the often lively discussions within the project, many times on the field site. I would like to acknowledge all those involved on behalf of the organisations that participated in the RECOPOL and MOVECBM projects, as listed in the acknowledgement section of chapters 2 and 3. Special thanks go out to Pawel, Jacek and Bartek for their role in the success of the project. In the context of the project (and related data), you have not always made life easy for me, but I am pretty sure I returned the favour. On a personal level, I highly value the friendship we developed during my many visits to

Poland. Enkelen van de partners wil ik vanwege hun betrokkenheid bij zowel RECOPOL/MOVECBM als bij het werk binnen CATO in het bijzonder bedanken voor de prettige samenwerking: Karl-Heinz Wolf van de TU Delft en Pablo Tejera Cuesta, Jos Maas en Niels van Wageningen van Shell.

Binnen TNO heb ik altijd kunnen rekenen op steun en expertise van vele collegae, die hiermee zeker hebben bijgedragen tot de afronding van het proefschrift. Zonder iemand te kort te doen wil ik met name noemen Petra, die al jaren over mijn schouder mee kijkt en altijd goed is voor een vrolijk gesprek, Pascal en Rob, op wie ik altijd kan rekenen om als klankbord te functioneren, Bert, vanwege zijn nuchtere inbreng, Tjirk en Tim, vanwege hun verfrissende inbreng, en Harry en Kathrin, die altijd klaar staan voor de analyses en met kennis over steenkool. Een speciaal dankwoord gaat uit naar Henk Pagnier, met wie ik de afgelopen jaren intensief heb samengewerkt. Dankzij onze verschillende persoonlijkheden hebben wij elkaar zeer goed aangevuld bij de realisatie van de veldtest en ondanks deze verschillen hebben wij altijd voldoende raakvlakken gevonden om op een zeer prettige manier samen te werken en een goede vriendschap op te bouwen. Ik ben de tel kwijt geraakt van de keren dat wij naar Polen en andere plekken in de wereld zijn gegaan, maar "never a dull moment". Heel erg bedankt voor het vertrouwen in de afgelopen jaren en de ondersteuning vanuit TNO. De organisatie TNO heeft mij in staat gesteld om naast mijn werkzaamhden te promoveren, waarvoor hartelijk dank. Daarnaast ben ik TNO dank verschuldigd voor het mede-financieren van de drukkosten van dit proefschrift.

I am really owing gratitude to my promotor Chris Spiers. Chris, you always seemed to have more confidence in the positive outcome of this thesis than I had, which really made the difference because you pushed me in the right directions when needed. I hope that we can continue our cooperation in the next years (. . . I'll promise to stay away from the poro-elastics . . .).

Alhoewel het lastig is om de precieze rol van ouders, schoonouders, familie en vrienden te specificeren bij de afronding van dit proefschrift is het voor mij overduidelijk dat ik zonder hen dit proefschrift niet had kunnen realiseren. Jullie verzorgden voor mij de afleiding van mijn dagelijkse beslommeringen en zorgen, waardoor ik mij weer beter op de promotiewerkzaamheden kon storten. Dankzij jullie liefde, vertrouwen, en vriendschap kon en kan ik vrij functioneren. Ik vind het fantastisch dat ik tijdens de verdediging van het proefschrift wordt bijgestaan door mijn broer en zus als paranimfen.
Tot slot zijn daar Vicky en mijn kinderen. Lieve Mirre en Kalle, ik heb vaak gehoord dat het wel lastig moet zijn om naast het vaderschap te promoveren maar ik denk dat ik juist door jullie aanwezigheid deze promotie tot een goed einde heb weten te brengen. Jullie geboortes zijn de belangrijkste gebeurtenissen uit mijn leven en hebben mij daarmee het juiste perspectief geboden voor afronding van de promotie. Vick, het is een feest om al die jaren bij jou te zijn. Mijn promotie is voor mij best een belasting geweest, maar heeft op ons nauwelijks invloed gehad. Met een last minder kan het alleen maar beter worden! Love U.

Appendix A

Data processing

A selection of pictures obtained during the swelling experiments was loaded in Adobe Photoshop. The selection of pictures was chosen arbitrary with increasing time steps towards the end of the experiment as the sample approached steady state. Five points (that could easily be distinguished on the basis of distinct colour and geometry) in each selected picture were identified. These points were selected close to the boundary of the coal sample. The lengths of all 10 lines between these 5 points were calculated. By comparing the lengths between the points on the coal sample, no correction was required for a possible shift or rotation of the sample. Also, through this approach the edges of the sample were not relevant.

Using these 10 lines results in the determination of linear strain in multiple directions. For each of these line lengths, the linear strain was calculated with equation A.1.

$$e_l(t) = 100 \times \frac{(l_t - l_0)}{(l_0)} \tag{A.1}$$

where:
e_l = linear strain (%)
t = time (min)
l_0 = initial length of a line (m)
l_t = length of a line at t (m)

To obtain the strain values in percentages, the strain value obtained by equation 1 is multiplied by 100 %. The average was calculated for the line lengths and for the ten values of linear strain. From this average line lenght the value of the surface strain could be approached by Eq.(A.2).

$$e_s(t) = 100 \times \frac{(A_t - A_0)}{(A_0)} \tag{A.2}$$

where:

e_s = surface strain (%)
t = time (min)
A_0 = initial surface area (= $l_0 \cdot l_0$) (m^2)
A_t = surface area at t (m^2) (= $l_t \cdot l_t$)

Substituting equation A.1 into equation A.2 results in equation A.3, from which the surface strain can be determined by the average linear strain. This is a similar methodology as Robertson and Christiansen (2005a) used to calculate 3D strains from coal swelling experiments.

$$\begin{aligned} e_s(t) &= \frac{(A_t - A_0)}{(A_0)} = \frac{(l_t \cdot l_t - l_0 \cdot l_0)}{(l_0 \cdot l_0)} \\ &= \frac{((l_t - l_0)(l_t + l_0))}{(l_0 \cdot l_0)} = e_l(t) \cdot \frac{l_t + l_0}{l_0} \\ &= e_l(t) \cdot \frac{l_t - l_0 + 2l_0}{l_0} = e_l(t) \cdot \left(\frac{l_t - l_0}{l_0} + 2\right) \\ &= e_l(t)^2 + 2e_l(t) \end{aligned} \tag{A.3}$$

Uncertainty in the determination may arise due to the pixel size, heterogeneity, sharpness of the pictures etc. The uncertainties in the data processing were calculated by performing the strain determination 5 times independently for the same picture. The uncertainty was defined as 2 times the standard deviation.

Comparison between the squared linear strain to measured surface strain indicated a good correlation (Fig. A.1). The surface strain was measured by calculating the surface area between the five points that were identified on the photographs from different time steps.
In order to interpret and compare the data of different experiments, a hyperbolic equation was used to fit the experimental data of surface strain development with time (equation A.4). Equation A.5 was used for the second and third CO_2 addition to take into account a different starting strain value at the beginning of a subsequent gas addition.

$$e_s(t) = e_{s-max} \cdot \frac{t}{(t_{1/2} + t)} \tag{A.4}$$

$$e_s(t) = y_0 + e_{s-max} \cdot \frac{t}{(t_{1/2} + t)} \tag{A.5}$$

where:
e_{s-max} = maximum linear strain (%)
$t_{1/2}$ = half saturation time (s or min)
y_0 = strain value at the beginning of the second or third introduction of gas (%)

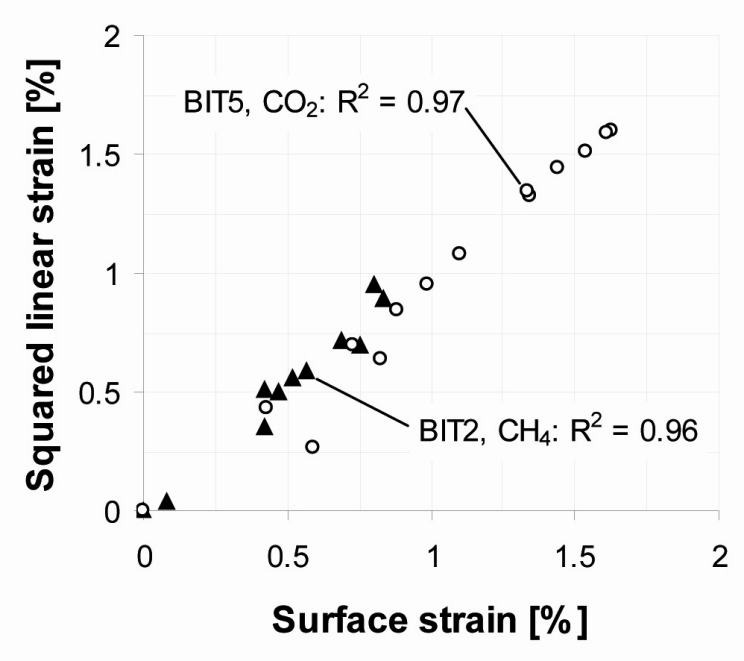

Figure A.1: Correlation between surface strain and squared linear strain as determined from one experiment with CH_4 and one with CO_2.

The hyperbolic data fit resembles a Langmuir adsorption equation. However, there is no physical basis for this resemblance with strain replacing adsorption and time replacing pressure.

Appendix B

Conservation of mass during diffusion in a spherical particle

In the model, the flux passing outward through any spherical surface within the particle is given in mol/s by:

$$f = J \cdot 4\pi \cdot r^2 \tag{B.1}$$

Substituting J from Eq. (5.8) provides:

$$f = -4\pi \cdot r^2 \frac{DC}{RT} \cdot grad\mu = -4\pi \cdot r^2 \frac{DC}{RT} \cdot \frac{\partial \mu}{\partial r} \tag{B.2}$$

The rate of change of concentration at any point (r, t) is determined by considering the conservation of mass in a spherical shell around the inner sphere with radius r and volume V. The thickness of the shell is ∂r. Conservation of mass states that any change in mass is due to the flux of matter through the surface of the inner sphere. The difference in inward and outward flux for the inner sphere is given by

$$\delta f = f(r) - f(r + \delta r) \tag{B.3}$$

Where $f(r)$ is the inward flux and $f(r + \delta r)$ the outward flux. The inward flux is negative since the outward direction is stated to be positive. The increase in concentration within the shell per unit time is therefore given by

$$\frac{\delta C}{\delta t} = \frac{-\delta f}{V} \tag{B.4}$$

where V is the shell volume $4\pi r^2 \delta r$. Hence,

$$\frac{\delta C}{\delta t} = \frac{-1}{4\pi r^2} \cdot \frac{\delta f}{\delta r} \tag{B.5}$$

which in the limit of $\delta r, \delta t \to 0$ results in

$$\frac{\partial C}{\partial t} = \frac{-1}{4\pi r^2} \cdot \frac{\partial f}{\partial r} \tag{B.6}$$

This yields, by incorporating Eq. (A2)

$$\frac{\partial C}{\partial t} = \frac{-1}{4\pi r^2} \cdot \frac{\partial}{\partial r}\left[-4\pi \cdot r^2 \frac{DC}{RT} \cdot \frac{\partial \mu}{\partial r}\right] \tag{B.7}$$

which can be rewritten as:

$$\begin{aligned} \frac{\partial C}{\partial t} &= \frac{D}{RTr^2} \cdot \frac{\partial}{\partial r}\left(r^2 C \frac{\partial \mu}{\partial r}\right) \\ &= \frac{D}{RTr^2}\left[r^2\left\{C\frac{\partial^2 \mu}{\partial r^2} + \frac{\partial \mu}{\partial r} \cdot \frac{\partial C}{\partial r}\right\} + C\frac{\partial \mu}{\partial r} \cdot 2r\right] \end{aligned} \tag{B.8}$$

Taking

$$\frac{\partial C}{\partial t} = \frac{\partial C}{\partial \mu} \cdot \frac{\partial \mu}{\partial t}, \text{or} \frac{\partial \mu}{\partial t} = \frac{\partial C}{\partial t} \cdot \frac{\partial \mu}{\partial C} \tag{B.9}$$

and

$$\frac{\partial C}{\partial r} = \frac{\partial C}{\partial \mu} \cdot \frac{\partial \mu}{\partial r} \tag{B.10}$$

and substituting Eq. (5.6) leads in combination with Eq. (B.8) to:

$$\frac{\partial \mu}{\partial t} = \frac{\partial C}{\partial t} \cdot \frac{RT}{C} = D\left[\frac{\partial^2 \mu}{\partial r^2} + \frac{1}{RT} \cdot \left(\frac{\partial \mu}{\partial r}\right)^2 + \frac{2}{r} \cdot \frac{\partial \mu}{\partial r}\right] \tag{B.11}$$